Belemnite Palaeo-proxies and Dating of Mesozoic Carbonates

Qiong Li

Department of Earth Sciences

UCL

A thesis submitted to University College London

in the Faculty of Mathematics and Physical Sciences

for the degree of:

Doctor of Philosophy (PhD)

Earth Sciences

April 2011

I, Qiong Li confirm that the work presented in this thesis is my own. Where information has been derived from other sources, I confirm that this has been indicated in the thesis.

Signed _____

Date _____

Abstract

This PhD project contains two related parts, both linked by a study of belemnites. The first part is to test the validity and quality of belemnite palaeo-environmental proxies, and the second to investigate the feasibility of U-Pb dating of Mesozoic carbonates.

In the first part, a wide range of well-preserved Mesozoic belemnites was analyzed for bulk stable isotope and trace element compositions, so as to access species-specific effects on compositions and to evaluate belemnite palaeo-proxies (notably $\delta^{18}O$, $\delta^{13}C$, Mg/Ca and Sr/Ca) as palaeo-temperature indicators. Then, high-resolution profiles of trace elements (Mg, Ca, Sr, Na, etc.) were obtained from those best-preserved specimens by electron microprobe and laser ablation-ICP-MS, and compared with the bulk analysis for a better understanding of intro-rostral variations. Results of four different belemnite polulations with differing ages and from differing stratigraphic levels show that Mg/Ca ratios in bulk analysis neither correlate with $\delta^{18}O$ within one single species nor within one belemnite population. Mg/Ca is therefore not considered as a palaeo-temperature indicator for belemnites. Variations in Mg profiles along belemnite cross-sections are then interpreted to likely reflect the changes of ontogeny and growth rate. Part two is to apply U-Pb dating method to Mesozoic belemnites and other carbonates. An innovative approach of dating carbonates in deep time has been developed, using both laser-ablation MC-ICP-MS and isotope dilution measurements; and ages with the highest achieveable precision (±1%) and accuracy for Mesozoic calcite cements from three separate ammonites have been produced.

Part I contains chapters 1 to 8. Chapter 1 gives a brief account of belemnites (e.g. the morphology, biogeography, palaeo-proxies and palaeo-ecology) and problems that need addressing in belemnite studies; and chapters 2-8 then focus on the geochemistry (isotopic ratios and elemental compositions) of belemnites from four different Mesozoic stratigraphic levels of Europe (Pliensbachian of Yorkshire, Toarcian of Dorset, Callovian of Oxfordshire and Valangigian of Vergol, SE Fance). Part II only contains chapter 9 which presents the U-Pb dating work of a range of Mesozoic carbonate samples.

Acknowledgements

I would first and foremost like to express my great thanks to my principal supervisor, Professor John McArthur, for his guidance, support, and encouragement throughout the period of this PhD. The conversations and meetings with him always brought me with fresh ideas and plans to take my work forward. I have also learned through his teaching never to be afraid of errors but to find solutions. I could not have asked for more in a supervisor like him.

This PhD project was funded by two overseas scholarships at UCL and NIGL of British Geological Survey. I would particularly like to thank my second supervisor Professor Randy Parrish at NIGL, not only for providing me with the funding and lab facilities for sample dating, but also for his great contributions on my data scrutinizing and his enthusiastic support in writing scientific papers. His care to my work and life has kept me going through so many difficult times. I would also like to thank Dr Matt Horstwood, Dr Steve Noble and Vanessa Pashley for their assistance in radioactive isotope analyses and data processing. My particular thanks also go to Professor Melanie Lang and Hilary Sloane for arranging and running stable isotope analyses of my belemnite samples very quickly. The whole NIGL team has brought me an open and international working environment that I have enjoyed with my heart.

I am grateful to Professor Tim Atkinson for revising this thesis and his contributions to our submitted paper based on some work in this PhD research. I would also like to thank Dr Wolfgang Muller for his support during profiling elemental concentrations at Royal Holloway; and Tony Osborn and Dorinda Ostermann for their help during chemical and isotopic analyses at UCL. Jim Davy at UCL and Hank Sombroek at Birkberk are also thanked for help with thin/thick section making. I would especially like to thank my best friend Bethan Hallett who was working with me in the same office over the past three years. Her solid friendship and company have kept me working hard in many late evenings.

Last but not least, I would like to thank my family especially my husband Dr Yongliang Sun, who was supporting me overwhelmingly throughout my PhD. His

patience, love and willingness to look after our family have ensured me a comfortable home to work and relax. And finally, I would love to dedicate this thesis to my coming baby girl. She might even read it one day!

Contents

List of Figures

List of Tables

Part I:

Testing Belemnite Palaeo-proxies

Chapter 1 Introduction

Part I of this PhD thesis is regarding to the study of the geochemistry of Mesozoic belemnites. Chapter 1 of Part I explains in detail the perspectives of belemnites that have been well-studied, such as morphology, taxonomy, biogeography, belemnite geochemistry and its use as a paleothermometer. It then discusses the problems that have been encountered in the study of belemnites and need addressing. For example, although temperature estimates for Jurassic and Cretaceous seas supplied by the isotopic composition ($\delta^{18}O$) of low-Mg belemnite calcite have been widely accepted, recent publications show that belemnite isotopic records are noisy and scattered. The complexity in belemnite compositions, such as inter-species and intra-rostral variations, brings uncertainties in belemnite palaeotemperture reconstructions. Meanwhile, the poor knowledge of the belemnite palaeo-ecology and ontogeny has also hampered the interpretation of their $\delta^{18}O$ signals. This chapter compares belemnites with its modern analogue (e.g. cuttlefish *Sepia*), and gives a general picture of the lifestyle of belemnites.

This chapter also outlines the main objectives in Part 1 of this PhD thesis: 1) to investigate and specify the species difference in the composition of collected belemnite populations; 2) to test the validity of the presently used belemnite palaeo-proxies at species level; and 3) to understand the ontogeny of belemnites.

On the other hand, U-Pb dating of carbonates was explored on the best-preserved Mesozoic belemnites and other carbonates. The sample preservation assessment of the least-altered belemnites is provided in Chapter 3. The introduction of U-Pb methodology and dating work are separately presented in chapter 9 in the second part of this thesis, in order to keep the structure of this thesis clear.

1.1 Belemnite morphology

1.1.1 The structure and terminology

Belemnites are an extinct group of marine cephalopods, similar to the modern squid in body structure and related to modern cuttlefish. A reconstruction of the belemnite body is shown below in Fig. 1.1 a. The body is assumed to consist of three parts: the front pro-ostracum, the middle phragmocone and the posterior rostrum. The commonly preserved part of a belemnite is the rostrum, which is the bullet-shaped inner shell in the back of the body; the structure of the rostrum is shown in Fig. 1.1 b.

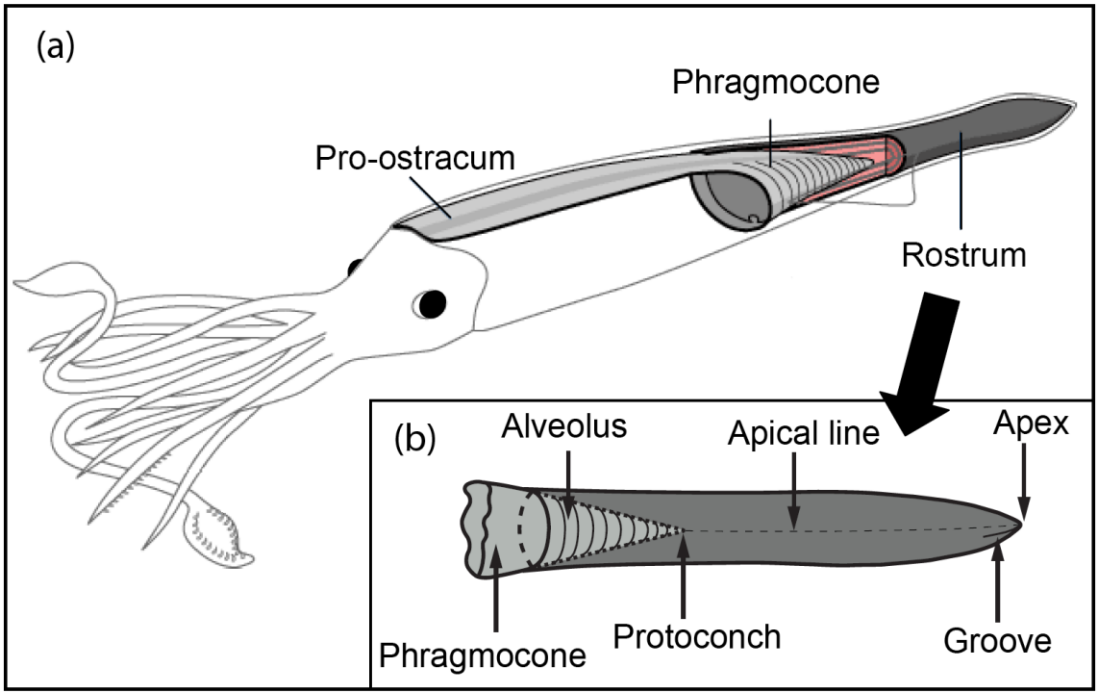

Fig. 1.1. a) The reconstructed body structure of belemnite organism, showing the three parts of a belemnite body: the front pro-ostracum, the middle phragmocone and the posterior rostrum; and b) Shell morphology of schematized rostrum and part of fractured phragmocone. Diagram a) is modified from http://www.ucmp.berkeley.edu/taxa/inverts/mollusca/cephalopoda.php.

Belemnite morphology has been discussed by many authors (e.g. Saelen, 1989; Doyle, 1990). The soft part of a belemnite is rarely preserved and thus is still vaguely known. The phragmocone is the part that connects with the rostrum in belemnite structure. It is conical-shaped and sitting in a conical chamber known as the alveolus (Fig. 1.1 b). Successive chambers added to the phragmocone in life led to more layers of the rostrum being formed. Phragmocones are very fragile, and the anterior part of them is usually missing. The rostrum, however, is of the most

significance in belemnite systematics. It is composed of the 6 elements listed in Table 1.1:

Table 1.1 The components and descriptions of a belemnite rostrum.

	Elements	Descriptions
BELEMNITE ROSTRUM	Alveolus	A conical region at the anterior of the rostrum that houses phragmocone (Fig. 1.1 b).
	Radial structure	A radiating arrangement of calcite crystals growing within a rostrum (Fig. 1.2 a)
	Apical line	The axis of the rostrum that marks the trajectory of the apex during successive growth stages (Fig. 1.1 b).
	Growth intervals & boundaries	The successive calcite growth increments reflected on a cross-section are termed 'growth intervals'; and the thin layers between the growth intervals are the 'growth boundaries' (Fig. 1.2 b).
	Apex	The most posterior part of the rostrum (Fig. 1.1 b). Very few species have an extension from apex called epirostrum (Fig. 1.3).
	Grooves	Depressions, found as paired dorso-lateral apical grooves, ventral or alveolus groove, and lateral lines on the rostral flanks (Fig. 1.1 b & Fig. 1.3).

(a) the radial structure of calcite crystals (b) Growth intervals & boundaries

Fig. 1.2 (a) The clear, dark brown calcite crystals showing a radial arrangement in a half transverse section of a belemnite specimen, also shown in the middle of this graph is the protoconch; (b) Dark growth intervals and light growth boundaries in between on a cross-section of a belemnite specimen. The light colored lines are cracks.

1.1.2 Belemnite growth pattern

The circular growth pattern of a belemnite rostrum was first noticed as ‘laminae pelucidae’ and ‘laminae obscurae’ by Müller-Stoll (1936), which refer to the layers of successive growth increments of clear calcite and the obscure growth boundaries between them. Saelen (1989) used the term ‘growth ring’ or ‘growth line’ for both the ‘laminae pelucidae’ and ‘laminae obscurae’, as being primary structures resulting from growth of belemnites. Since then, growth rings are confusingly used to refer to either calcite growth increments (Wierzbowski and Joachimski, 2009), or the growth boundaries between them in belemnites (Podlaha *et al.*, 1998).

The growth laminae in the skeletons of many marine organisms (including bivalves, corals, gastropods and cephalopods), however, were separately termed as growth increments of calcite layers and growth rings which separate the growth increments (Schone *et al.*, 2005). This devision is herein adapted, but the terms slightly modified, to describe the growth structure in belemnite rostrum. The two separate types of bands are termed here *‘growth intervals’* and *‘growth boundaries’*. *Growth intervals* are the primary calcite layers precipitated shortly after ingestion of food and present a radial structure of clear light brown calcite crystals. *Growth boundaries*, on the other hand, are thin layers between growth intervals and are considered as zones of weakness subject to alteration. They were black organic films laid during the gaps when growth was halted or retarded. They were originally very thin and sharp, but after the death of the animal, they gradually decayed producing reducing environments appealing to diagenetic fluids containing high Mg (and/or Mn, Fe). The secondary calcite bands (Fig. 1.2 b) precipitated from the diagenetic fluids therefore inherited high Mg (and/or Mn, Fe). The colour, thickness and form of the growth boundaries depend on the chemistry of diagenetic fluids and preservation degree of the sample. High degree of diagenetic alteration can thicken and emphasize growth boundaries.

1.1.3 Belemnite differentiation characteristics

The rostra of belemnites are common and readily preserved in Mesozoic strata, and the relatively simple morphology allows easy recognition. The taxonomy of belemnites in the British Jurassic sequences has a long history of study. For example,

Philips (1865) first described a range of Jurassic taxa from across Britain, including some Dorset Lower Lias species; Lang (1928) gave a very detailed taxonomic revision and the stratigraphical range of 26 nominal species of Pliensbachian belemnites found within the Belemnite Marls on the Dorset coast. Lang's work is still largely accepted, but has been refined by Doyle (2003), and some of his taxa were found to be no more than ontogenetic or sexual variations. Doyle (1990, 2003) also made a comparison between the Dorset Pliensbachian belemnites and the Yorkshire Toarcian taxa. Another useful classification study of belemnites of similar age was in Germany by Schumann (1974). According to these authors' descriptions, the terms and characters that are of great importance for belemnite differentiation at generic and species level are:

Shape: Although belemnite rostra are generally bullet-shaped (Fig. 1.1 b), there are actually three basic morphotypes shown in Fig. 1.3: cylindrical, conical and hastate. The shape of whole rostra is usually expressed by description of outline (dorsal or ventral view) and profile (side view). The outline is always symmetric whereas the profile can be either symmetric or asymmetric (Fig. 1.3).

Transverse section: also called cross section, it shows the shape of the surface perpendicular to the apical line. The cross-sections of belemnites are described as (laterally) compressed or (dorso-ventrally) depressed, and generally circular, elliptical, pyriform or subquadrate (Fig. 1.3).

Grooves: Grooves are of great importance at generic and higher levels. Two types of grooves have been defined: apical and alveolar grooves (Fig. 1.3). The former is confined or originates from the apex and the later from the alveolar region. Also present in belemnites are fine lateral depressions called lateral lines (Doyle, 1990).

There are other features employed to identify belemnites, such as the depth of penetration of the alveolus and the epirostrum (Fig. 1.3), but they are less commonly used and hence not explained here. The belemnite specimens from four stratigraphic levels in this study have all been identified at species level, and their descriptions are provided in the chapter of that specific belemnite population.

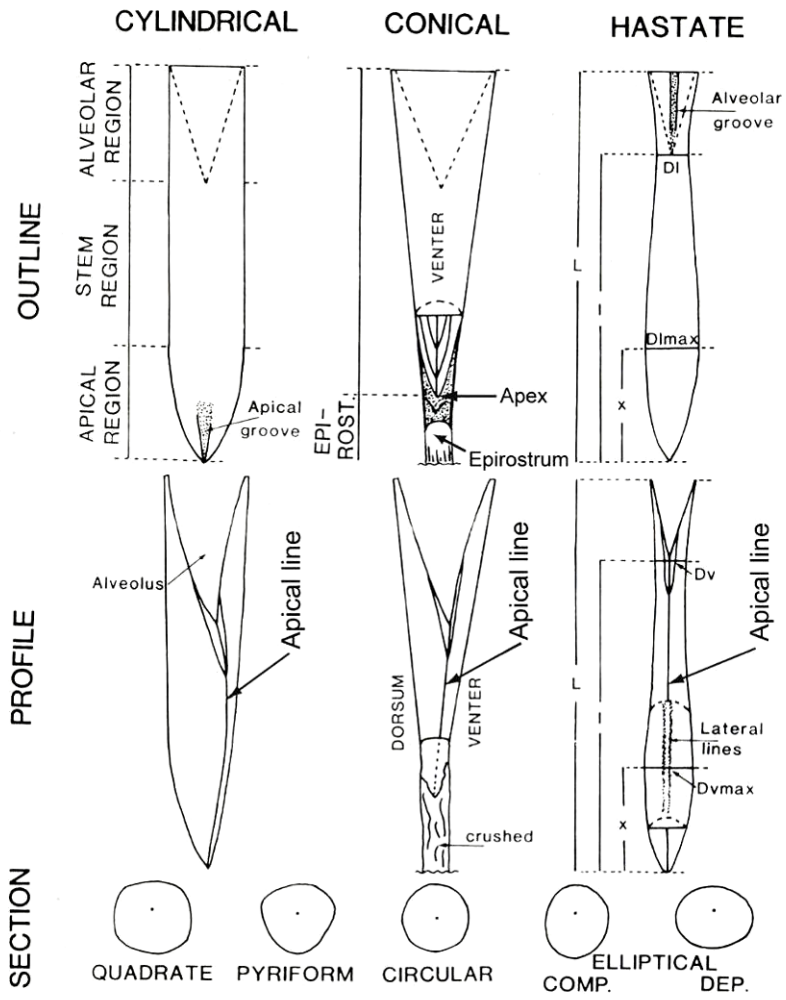

Fig. 1.3 Morphological terms measurements in the descriptions of belemnite genera and species. Epirost – Epirostrum; COMP. – compressed, DEP. – depressed; L – the length of a whole belemnite; I- the distance between the base of alveolus to the tip of the apex; X- the distance between where the max diameter is to the apical tip; DI – the diameter on a dorsol-ventral cross-section at the base of alveolus, DV is perpendicular to DI; DImax and DVmax are the maximal diameters on dorsal-ventral and lateral corss-sections, respectively. Diagram is from Doyle, (1990).

1.2 Belemnite biostratigraphy

Early studies of belemnites focused on taxonomy, geographical distribution and evolution, with the attempt of investigating the utility of belemnite biostratigraphical correlation. The biogeography of Jurassic – Cretaceous belemnites have been reviewed adequately, and the development of belemnite provinciality (e.g. Boreal and Tethyan realms) largely understood (Doyle, 1987, 1992; Christensen, 1996). Belemnites have been used as biostratigraphical index fossils for Jurassic and Cretaceous sequences (Lang *et al.*, 1928; Stoyanova-Vergilova, 1977; Christensen,

1990; Doyle, 1990; Mutterlose, 1990; Doyle and Bennett, 1995; Combémorel, 1997); however, the utility of belemnite biozonation is limited because species endemism and diachroneity of belemnites are problematic for correlation between realms and continents. Therefore, only the palaeo-geographical distribution of belemnites is discussed here.

Belemnites probably occurred initially in Hettangian (199.6-196.5 Ma) of early Jurassic in Europe (Doyle, 1987). During the Late Pliensbachian to Toarcian (~183.0 Ma) interval, belemnites developed many species and became widespread. By Middle Jurassic time, the Boreal and Tethyan Realms were exhibited, and a distinct Arctic province with endemic genera within the Boreal Realm had emerged and remained endemic until the Late Jurassic. During the Middle-Late Jurassic, the Boreal faunas were dominated by *Cylindroteuthid* genera that belong to the *Belemnitina* group (those possessing apical grooves). In contrast, the Tethyan Realm, extending from the Tethyan Ocean southwards circum to Gondwana, was populated largely by *Hibolithes* that belong to *the Belemnopseina* group (those with alveolar grooves).

The Boreal-Tethyan pattern continued through the Early Cretaceous, when the genus *Acroteuthis* became predominant in Boreal and Atlantic provinces, and the Tethyan genus *Hibolithes* invaded into Boreal and Arctic zones (e.g. England, northern Germany and Greenland). In the late Early Cretaceous, *Oxyteuthididae* genera with aspect of both *Belemnitina* and *Belemnopseina* morphologies then replaced the *Acroteuthis-Cylindroteuthid* assemblage in the Northern Hemisphere. In Aptian, a new entirely endemic, austral belemnite fauna (*Dimitobelidae*) developed and by the end of the Cenomanian, the Tethyan Realm cannot be identified in terms of belemnite evidence alone. The bipolar pattern was established in the latter part of the Early Cretaceous, with *Belemnitellidae* restricted to northern Europe, Greenland and North America and *Dimitobelidae* restricted to the Austral Realm, and lasted until belemnites became extinct at the Cretaceous/Tertiary boundary (Dutton *et al.*, 2007).

1.3 Belemnite palaeo-proxies

Well-preserved belemnites are presumed to retain the primary stable isotope (C,O and Sr) content (Urey *et al.*, 1951; Stevens and Clayton, 1971; Jones *et al.*, 1994a;

Jones *et al.*, 1994b) and trace element (e.g. Mg/Ca) compositions (Berlin *et al.*, 1967; Yasamanov, 1981) of the ambient water and offer a partial window into the geochemistry of the Jurassic and Cretaceous oceans (Saelen *et al.*, 1996; Podlaha *et al.*, 1998; Veizer *et al.*, 1999; Gröcke *et al.*, 2003; Wierzbowski, 2004; Rosales *et al.*, 2004a,b; van de Schootbrugge *et al.*, 2005; McArthur *et al.*, 2007a,b). The studies that focus on different aspects of belemnite geochemistry are listed in Table 1.2, and discussed separately in the following sections.

Table 1.2 Studies of different aspects of belemnite geochemistry.

Aspects	Contents	Literature
Belemnite isotopic compositions	$\delta^{18}O$ & $\delta^{13}C$	*Urey, 1951;* *Wierzbowski, 2002, 2004;* *Van de Schootbrugge et al,2005;*
	$\delta^{18}O$, $\delta^{13}C$ & species	*Spaeth et al., 1971;* *Stevens and Clayton, 1971;* *Saelen, 1996;* *Podlaha et al., 1998;* *Price and Sellwood, 1997;* *Price et al., 2000;* *Price & Mutterlose, 2004 ;* *Mutterlose et al.,2010;*
Trace elements & isotopic compositions	$\delta^{18}O$ & trace element (El/Ca)	*McArthur et al., 2000;* *Gröcke et al., 2003;* *Rosales, 2004a,b;* *Nuun & Price, 2010;*
	$\delta^{18}O$, El/Ca & species	*Bailey et al, 2003;* *McArthur et al., 2007a,b;* *Wierzbowski & Joachimski, 2009;* *Wierzbowski and Rogov, 2010.*

1.3.1 Belemnites palaeotemperature indicator: $\delta^{18}O$

The oxygen isotopic composition ($\delta^{18}O$) of marine biogenic calcite is presumed to reflect calcification temperature, salinity and the isotopic composition of the seawater. Belemnite $\delta^{18}O$ was first employed as a palaeo-thermometer by Urey *et al.* (1951) using the palaeotemperature equation developed in Epstein *et al.* (1951). The Jurassic belemnite in his study was judged well-preserved, not by modern well-acknowledged standards, but based on the simple petrographic observation of compact belemnite structure and the optical features of the calcite crystals in the rostrum. However, their belemnite looks apparently altered (see Figure 1 in Urey *et al.* (1951) in present geologists' eyes because the growth rings (a sign of alteration) are clearly visible and domains of materials which likely show alteration were sampled. Their interpretation of cyclical isotopic signatures in terms of seasonal temperature variations is therefore questionable, and the $\delta^{18}O_{belemnite}$ data may actually suggest a diagenetic origin for that cyclicity.

Three pre-requirements of using $\delta^{18}O_{belemnite}$ derived palaeotemperatures are: 1) equilibrium fractionation of oxygen isotopes is achieved between belemnites and the ambient water; 2) belemnite rostra must be well-preserved to be able to retain the primary palaeo-environmental signals; 3) the isotopic composition of the original sea water should be known (Spaeth *et al.*, 1971; Stevens and Clayton, 1971). For the second condition, the diagenetic alteration can be well-constrained through the application of combined petrographic, cathodoluminescence and elemental analyses. After removing the exterior and the innermost apical line which are well-known as the altered areas (Berlin *et al.*, 1967; Stevens and Clayton, 1971), fragments of specimens are considered the least altered when showing clear calcite under ×10 magnification with non-luminescence and low Fe (<100ppm) and Mn (<30 ppm) contents. It is, nevertheless, difficult to identify vital effects (biological fractionation) and species-specific effects since belemnites are extinct. It is presumed that belemnites may have probably achieved equilibrium fractionation in oxygen isotopes with the ambient seawater, according to the study of their modern analogue cuttlefish (Rexfort and Mutterlose, 2006). Meanwhile, the $\delta^{18}O$ of the seawater ($\delta^{18}O_{sw}$) in which belemnites once lived is hard to accurately assess, an assumption of $\delta^{18}O_{sw}$ of -1‰ SMOW for ice-free oceans (Shackleton and Kennet, 1975; Pirrie and Marshall,

1990a) has been suggested and widely used. However, the theory of ice-free Mesozoic oceans has been challenged (e.g. Price, 1999; Miller *et al.*, 2005). Also, from the chemical studies on modern Pacific and Atlantic oceans, the surface seawater $\delta^{18}O$ values are known to shift with latitude by 2 ‰ (Hoefs, 2009). The Mesozoic oceanic $\delta^{18}O$ might vary similarly; and hence an assumed average value of -1‰ SMOW is certainly not representative for a wide range of palaeo-latitudes. This poor knowledge of the past oceanic oxygen isotopic composition then brings more uncertainty to the use of belemnite $\delta^{18}O$ as palaeotemperature indicator. To sum up, the $\delta^{18}O$ of belemnites can be influenced by many other factors than temperature, and therefore is far more complicated than just reflecting the original palaeotemperatures.

In the researches on belemnite isotopic compositions, many authors presumed that their studied belemnites were well-preserved and had recorded the primary signal, using sample screening criteria that are not up to modern standards (e.g. Stevens and Clayton, 1971; Saelen *et al*., 1996; Price and Sellwood, 1997; Wierzbowski, 2002, 2004). Meanwhile, vital effects were ignored, and inter-species differences and intra-rostral variations in belemnite isotopic composition mostly not analyzed (e.g. Saelen *et al.*, 1996; Podlaha *et al.*, 1998; McArthur *et al.*, 2000; Bailey *et al.*, 2003; Gröcke *et al.*, 2003; Rosales *et al.*, 2004a; Pirrie *et al.*, 2004; Wierzbowski, 2004). It is then difficult to establish whether or not the spread in belemnite $\delta^{18}O$ reflects real signals of temperature change. Finally, the shifts in belemnite $\delta^{18}O$ ratios were too literally transferred to absolute temperature values (e.g. Price and Sellwood, 1997; Wierzbowski, 2002, 2004). By analogy with its modern analogue cuttlefish, belemnite species were likely to have lived a mobile life, with different species experiencing differing ranges of temperatures and salinities over their individual lifetime (Rexfort and Mutterlose, 2006; McArthur *et al.*, 2007b; Mutterlose *et al.*, 2010). It is therefore better to look at the temperature ranges and trends in belemnites. On the other hand, the calculated absolute temperatures can vary with using differing assumptions of seawater isotopic compositions and palaeotemperature equations. The significance of these effects, however, would be much smaller in the temperature changes and trends. Consequently, belemnite isotopic compositions are very complicated, and the sole use of belemnite oxygen isotopic temperatures has limitations.

1.3.2 Trace elements & $\delta^{18}O$: the combined palaeo-proxies

In addition to $\delta^{18}O$, the relation between belemnite elemental composition (usually expressed as Element/Ca ratios or El/Ca) and calcification temperature has drawn much attention. Mg in modern marine biogenic calcareous skeleton (e.g. foraminifera, echinoids and barnacles) has shown a strong linear relationship with temperature, with high Mg/Ca ratios associated with warmer seawater temperature and low ratios cooler temperature (Chave, 1954). Mg/Ca ratios in belemnites were first used to obtain palaeotemperatures by Berlin *et al.,* (1967) and Yasamanov, (1981). Based on these early studies, the potential use of Mg/Ca ratios in belemnites as new geochemical proxies for oceanic temperature was proposed and followed by a few authors (e.g. Bailey *et al.,* 2003; McArthur *et al.,* 2007a).

If the El/Ca ratios in belemnites reflect mainly temperature, whilst belemnite $\delta^{18}O$ reflects temperature, salinity and ice volume of the ambient sea water, a good correlation between El/Ca ratios and $\delta^{18}O$ in biogenic calcite would be expected. Such covariance was demonstrated in a few populations of undifferentiated Pliensbachian-Toarcian (early Jurassic) belemnites from Yorkshire of the UK (McArthur *et al.,* 2000; Bailey *et al.,* 2003) and in northern Spain (Rosales *et al*., 2004a, b); and Valanginian belemnites from SE Vergol (McArthur *et al.,* 2007a). This leads to the combined use of elemental and isotopic compositions as a tool to estimate palaeotemperatures and test for the isotopic composition of Jurassic oceans where belemnites lived and migrated.

For example, using both Mg/Ca ratios and $\delta^{18}O$ data of belemnites, cool and saline waters in the northwest European epi-continental sea in the late Pliensbachian, followed by warmer and fresher waters in the early Toarcian time, have been suggested (Bailey *et al*., 2003). These sequential events likely contributed to the plausible density stratification of the water column that finally triggered the Early Toarcian regional oceanic anoxic event (T-RAE). Another example is to use belemnite $\delta^{18}O$ and the palaeotemperatures derived from belemnite Mg/Ca ratios to calculate the oxygen isotopic compositions of the seawater between Berriasian and Hauterivian time of SE France and Spain. Using the estimated $\delta^{18}O$ of the seawater, the global climate changes in the interval from Valanginian to Hauterivian were hypothesized, with cooling period starting in Lower Valanginian, followed by the

presence of variable amounts of polar ice in the Upper Valanginian to Lower Hauterivian before the global warming across the Early/Late Hauterivian boundary (McArthur *et al.*, 2007a).

The above applications, however, will only be valid if Mg/Ca ratios in belemnites are solely temperature-dependent, or the temperature-dependence of Mg/Ca in belemnites can be quantified when influences other than temperature exist. However, whether or not belemnite Mg/Ca ratios can be affected by other factors, such as species-specific fractionation, hasn't been systematically tested. Also, temperature-dependence of trace elements in belemnite calcite is still poorly quantified because belemnites are extinct. Another unsolved question is whether the correlation holds true for a single belemnite species, or belemnites in general, or just these particular populations. With our increasing understanding on the complexity and species difference in belemnite composition, it is also worthwhile trying to understand whether the current interpretation of belemnite compositions in terms of palaeo-environment is valid at species level. This PhD hence aims to address these problems.

Moreover, Sr/Ca has been suggested as a better palaeotemperature indicator than Mg/Ca for Toarcian belemnites, since Sr/Ca correlates well with $\delta^{18}O$ but Mg/Ca doesn't in two Toarcian belemnite species (*Acrocoelites vulgaris* and *Acrocoelites subtenuis,* McArthur *et al*., 2007b). There are, however, not enough data to address the temperature sensitivity of Sr in biogenic and inorganic calcite. Mg and Sr are unlikely to have equal temperature-dependence, according to current understanding of temperature-dependence of trace elements in modern biogenic calcite (Bailey *et al*., 2003). This difference has been noticed in the differing variation patterns of these elements within specimens of Toarcian belemnites of McArthur *et al.,* (2007b). Further studies on variable belemnites are therefore required to test whether Sr/Ca can be used as a palaeotemperature proxy.

1.3.3 Belemnite $\delta^{13}C$

The carbon isotopic composition of belemnites through time is thought to reflect changes in the carbon cycle that can be linked to changes in oceanic productivity and atmospheric CO_2 (Podlaha *et al.*, 1998; Kump and Arthur, 1999; Wierzbowski, 2002). C-isotope excursions in the profiles of belemnite $\delta^{13}C$ against stratigraphic levels in

Jurassic-Cretaceous period are of great interest. Negative C-isotope excursions have been largely associated with upwelling of deep-ocean water rich in isotopically light carbon derived from the decomposition of organic matter (Wierzbowski, 2004), whereas the positive excursions interpreted as a result of elevated burial rate of large amount of isotopically light organic matter into marine sediments (Jenkyns and Clayton, 1997; Wierzbowski, 2004), which could occur during transgressions when sea level and shelf area increase (Price *et al.*, 2000; Price and Mutterlose, 2004), or during volcanism that increases the carbon dioxide in atmosphere and leads to enhanced weathering and nutrient supply to oceans (Lini *et al.*, 1992; van de Schootbrugge *et al.*, 2000). However, besides the external drivers of carbon isotope excursions, there seem to be internal reasons (e.g. vital/species-specific effects) for the occurrence of these spikes. For example, the broad positive $\delta^{13}C$ excursion that predates the Toarcian regional oceanic anoxic event (T-RAE) witnesses short-returns to near-normal isotopic values. These small negative excursions suggest the instability and local origin of the broad spike (McArthur *et al*., 2000). Species analysis has shown that not all species yield the C-isotope spike in this interval (McArthur *et al*., 2007b). Consequently, species effects have to be removed when interpreting belemnite C-isotope spikes in terms of environmental changes.

1.4 Problems to address

1.4.1 Inter-species differences in belemnite composition

Large scatter of isotopic values (around 3 to 4‰ spread in both $\delta^{18}O$ and $\delta^{13}C$) was observed in the bulk analysis of undifferentiated contemporaneous Jurassic and Cretaceous belemnites (Podlaha *et al*., 1998). These authors attributed the isotope oscillating to diagenetic alteration, changes of the environmental conditions of belemnite habitats (e.g. temperature and salinity variations); and the variations in palaeo-productivity within the water column where they dwelled. The scatter, nevertheless, may at least partically result from biological fractionation (i.e. species or genera effects) since isotopic disequilibrium in biological carbonates is commonly observed (McConnaughey, 1989a; 1989b). However, early belemnite researchers didn't speculate biological fractionation to be a dominant factor to influence belemnite isotopic values (e.g. Saelen *et al.*, 1996; Podlaha *et al.*, 1998), and very

few studies have been done at species or generic level to actually address the species differences in belemnite compositions; therefore the topic remains only partially understood.

A few studies that specify belemnite species are summarized below: Price & Sellwood, (1997) found that two Oxfordian – Tithonian (Late Jurassic) belemnite genera (*Hibolites* & *Belemnopsis*) from Falkland Plateau at high palaeo-latitudes (55-60˚S) possess similar isotopic values and alike narrow isotopic ranges, which seemed to imply no species effects. However, scatter in compositions is seen in the two species of Toarican (Early Jurassic) belemnites deposited in a geological instant of time, *Acrocoelites vagaris* and *Acrocoelites subtenuis* (McArthur *et al*., 2007b) with the former having a narrow compositional range that has little overlap with the widespread isotopic and elemental values of the latter. These differences in compositions may suggest both differing living habitats and biological fractionation (or species specific fractionation) as potential causes. Inter-species differences in belemnite composition have also been observed between two belemnite species (*Hibolithes beyrichi* and *H. hastatus*) from the Bathonian of central Poland (Wierzbowski and Joachimski, 2009) and a few Callovian - Oxfordian belemnite genera from Russia (Wierzbowski and Rogov, 2010).

Accordingly, belemnite species are likely to possess different compositions, reflecting the differing living habitats during lifetime, coupled with different biological fractionation. The scatter in belemnite record can therefore result from species-differing habitats, different biofractionation and climate changes. It is now considered inappropriate to interpret belemnite data solely in terms of palaeotemperature without taking the other two effects into account. Because much of the literature on belemnites hasn't realized the importance of species effects in the study of belemnite geochemistry and palaeo-ceanography, this PhD aims to investigate and specify the species difference in the composition of collected belemnite populations, and test the validity of the presently used belemnite palaeo-proxies at species level.

1.4.2 Intra-rostral variations

Published data on the isotope and elemental composition of belemnites are predominantly derived from bulk rostra samples, which are assumed to be homogeneous in composition. However, belemnites were likely mobile in a life span of at least 1-3 years (Rexfort and Mutterlose, 2006; Wierzbowski and Joachimski, 2009); and the successive growth increments of calcite in a single belemnite should preserve in their compositions ontogenetic changes of their inhabited niches. There are only few studies on investigating the intra-rostral variations in composition within an individual belemnite. For example, McArthur *et al*., (2007a) interpreted the variations in El/Ca concentrations (Mg/Ca, Sr/Ca and Na/Ca), seen over scales from <50 µm to several hundred µm within a rostrum of Toarcian (early Jurassic) belemnites, as reflecting changes in temperature and depth in their habitats during growth. The intra-rostral variations are different for different elements in different species, showing effects of differing biofractionation and temperature change during ontogeny. In addition, analysis at 50 µm spacing across the rostra of four *Dimetobelid* belemnites from the Upper Cretaceous reveals variations of ~2 ‰ in $\delta^{18}O$ and $\delta^{13}C$, with maxima occurring towards the rim (Dutton *et al*., 2007). However, white growth boundaries with secondary calcite, a sign of alteration, are present between the dark growth intervals of well-preserved calcite (Fig. 2 in Dutton *et al*., 2007). The diagenetic alteration may have magnified the amplitude of isotopic variations within a rostrum, and hence the palaeo-depth of their habitat and climate seasonity interpreted from isotopic variations. Moreover, high- and low-amplitude variations in isotope and elemental concentrations are seen at a resolution of 100 µm across two Bathonian (Middle Jurassic) belemnite rostra from Poland (Wierzbowski and Joachimski, 2009); their specimens, however, are poorly preserved: growth boundaries, seen as thin, white bands of secondary calcite in Fig. 2 and 10 in Wierzbowski and Joachimski (2009), clearly show alteration. The alteration compromises the quality of this study and brings doubts to the interpretation of $\delta^{18}O$ values of the two species as reflecting originally low palaeotemperatures (10 °C and 6 °C) of their living environments.

Therefore, for the study of intra-rostral variations in belemnite composition, sample preservation is critical. The least altered specimens are the key to minimize the

overprints of marine diagenesis or recrystallization on isotopic values. Meanwhile, alteration is known to be most severe in the alveolar region and apical line of a rostrum, which even occurs in specimens with overall high preservation; hence these areas should be excluded when interpreting the isotopic range within a belemnite rostrum. Further studies are required on the compositional ranges in the least altered regions within well-preserved rostra; so as to quantify the amplitude of these variations, assess the range of environmental settings belemnites once dwelled in during their life, and finally to evaluate to what degree internal compositional variations can potentially contribute to the scatter in belemnite records.

1.4.3 The palaeo-ecology of belemnites

Previous studies on belemnites discussed above have been mostly pursued from a geochemical perspective whereas neglecting the palaeo-ecological and ontogenetic factors that might have influences on belemnite shell calcification and hence isotopic compositions. In order to understand the paleoecology and ontogeny of belemnites, it is necessary to compare belemnites with modern marine taxa that are closely related to them. The reconstructions of belemnites show strong resemblance to one group of Coleoidea – squid; however, during evolution, squid has lost the inner shell that existed in belemnites, leaving the cuttlefish *Sepia*, the only group of Coleoidea that retains a calcareous internal shell, as the available object for comparison.

1.4.3.1 Bioecology

Life style: The life styfe of cuttlefish has been well-known for many years. The cuttlefish *Sepia officinalis* (*S. officinalis*) is a marine nectobenthic shallow-water dweller on the coast of Atlantic Ocean and in the Mediterranean Sea, living in a depth range of 1-200 m and commonly migrating up to a few hundred kilometers horizontally during their lifespan (Rexfort and Mutterlose, 2006). The lifestyle of belemnites, however, is still vaguely understood. By analogy with cuttlefish *S. officinalis*, belemnite species were likely to be nektonic-nektobenthic and lived over a range of depths, temperatures and salinities in the shelf seas of Jurassic and Cretaceous time. However, the recent study of Barremian belemnites obtained from laminated black shales by Mutterlose *et al.* (2010) seem to support the view of a consistent, stable nektonic life like that of teuthids.

Ontogeny: While *S. officinalis* are considered to grow isometrically (with the same growth rate) in their life span, belemnites likely grew allometrically with the differential growth rates of the rostra (Rexfort and Mutterlose, 2006). This hypothesis on belemnite ontogeny is supported by our findings within a population of over 250 belemnite specimens of a single species that adult belemnites have larger diameter to length (D/L) ratios than juveniles and that specimens with the same length can have variable D/L ratios (details are provided in Chapter 6). The allometric growth of adult belemnites might reflect metabolic changes during ontogeny, which may possibly influence the calcite precipitation and isotopic composition of the rostra. Therefore, belemnites cannot be easily and simply compared to *S. officinalis* regarding to ontogeny and its effects.

Life span: *S. officinalis*, like all other modern coleoids, normally has a life span of 1 to 2 years, but can live up to 5 years. The life expectancy for belemnites is more difficult to judge. The growth intervals of belemnite rostra have been used to estimate the life span of Bathonian belemnite specimens from Poland, assuming the growth intervals representing daily increments of calcite layers (Wierzbowski and Joachimski, 2009). The estimated life span of 1.5 to 2 years seems to be comparable to that of modern coleoids.

1.4.3.2 Palaeo-environment

The stable isotope composition of *S. officinalis* has shown some implications for understanding belemnite palaeo-environmental conditions. Oxygen isotopes in the cuttlebone of cultured *S. officinalis* appear to achieve equilibrium fractionation with the surrounding water and show no shifts in response to ontogenetic changes. Rexfort and Mutterlose (2006) found a nearly 4‰ internal variation in $\delta^{18}O$ of a wild *Sepia* specimen from German North Sea and transferred the shift in $\delta^{18}O$ to a temperature range of 18 °C during its mobile life. However, Dutton *et al* (2007) and Wierzbowski and Joachimski (2009) have reported a variation of only ~2‰ in $\delta^{18}O$ across a belemnite rostrum. If the equilibrium fractionation in oxygen isotopes was achieved between belemnites and the ambient water, as we see in *Sepia*, the smaller variation in belemnite $\delta^{18}O$ may suggest that either belemnites had less wide habitats than cuttlefish *Sepia* or changes in ontogeny and/or salinity during belemnite growth may have affected the $\delta^{18}O$ values. Such influences, although difficult to measure,

should not be as large as temperature effects. So a shift of 2‰ in $\delta^{18}O$ would roughly reflect a temperature change of ~7-8 °C. If belemnites live in modern oceans, for example, the modern North Sea, such temperature variations would require a depth range of a couple of hundred meters (Appendix A - B). Belemnites possibly migrated through the thermocline down to the cold water. However, the 2‰ intro-rostral shift of $\delta^{18}O$ is deduced from a few less well-preserved specimens in Dutton *et al* (2007) and Wierzbowski and Joachimski (2009); more complete analyses are therefore required to look for the possible variation range of $\delta^{18}O$ within a rostrum and hence the temperature and depth ranges of belemnites' living habitats.

Chapter 2 Samples and Methodology

This chapter contains first a brief description of belemnite samples collected in this PhD study. Details of each sample population are provided in chapters 4 – 7. It then explains in detail the methods used for belemnite analyses. Specimens were carefully examined, prepared and then analyzed for microstructure, isotopic and elemental compositions.

2.1 Samples

In order to pursue the aims of this study, extensive collections of belemnites were made. Belemnite samples were obtained from four stratigraphic intervals (Table 2.1) from the UK and France. Specimens from each interval are termed here a belemnite population (Table 2.1) and were identified to species level. Over 550 specimens belonging to ~30 species were herein analysed.

Table 2.1 The four belemnite polulations obtained in this study.

Interval	No. of specimens	No. of species/genera	Location
Pliensbachian	100	10	Charmouth to Seatown, Dorset, UK.
Toarcian	58	10	Saltwick Bay, Whitby, Yorkshire coast, UK.
Callovian	335	2	Kings Dyke, Whittlesey, UK.
Valanginian	62	5	Vergol, SE France.
Total	**555**	**27**	

2.2 Sample preparation of belemnites

Prior to chemical and isotopic analysis, the dorso-ventral and lateral diameters were measured at the base of alveolus of belemnite rostra. This is to see whether, after analysis, there was any correlation between size and composition of belemnites. Specimens were sectioned from near the base of the alveolus into slabs perpendicular

to the apical line (Fig. 2.1). The slabs of the best-preserved specimens (shown as the cross-section in Fig. 2.1) were then made into polished resin mounts or thick sections for multi-element concentration analysis within a rostrum with electron microprobe and laser ablation ICP-MS. The front slabs were used for this purpose unless they are less well-preserved than the back slabs. This is because they are closer to the base of alveolus, and hence provide more ontogenetic information. Meanwhile, thin sections of a few highly preserved belemnite specimens were also made for the observation of the microgrowth patterns in well-preserved belemnite rostra.

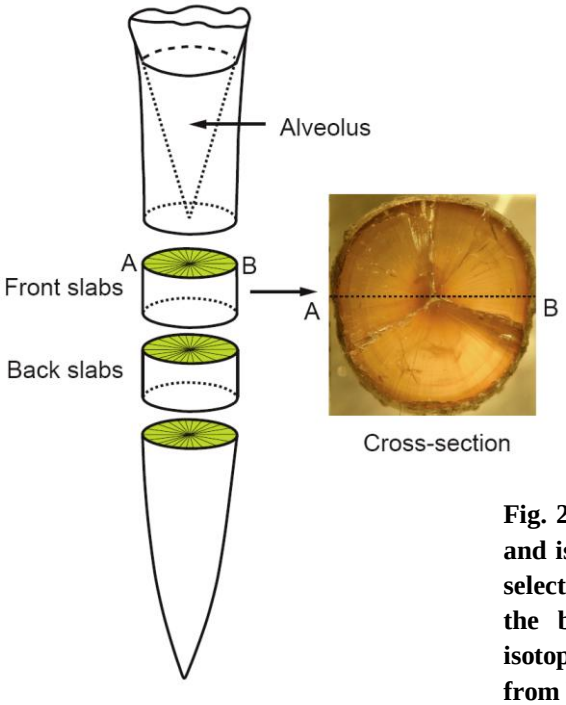

Fig. 2.1 Belemnite rostrum slabs cut for chemical and isotopic analyses. The front slabs are usually selected for intra-rostral element analysis, and the back slabs for bulk chemical and stable isotope measurements. The diagram is modified from Wierzbowshi, *et al*. (2009).

For the remaining of the sectioned specimens, the altered areas (the alveolus region and the apical line) and the apex were removed using diamond cutting tools, or 10% hydrochloric acid for very small samples. The fragments were broken into pieces at mm size, briefly immersed in 1.2 molar hydrochloric acid to remove the dust, and picked in alcohol under the microscope (shown as pellucid, light brown bits in Fig. 2.2). Then, the picked bits were washed in ultrapure water, and dried in a clean cupboard for bulk stable isotope and chemical analysis. These bits thus represent mixed materials from the back slab of each belemnite.

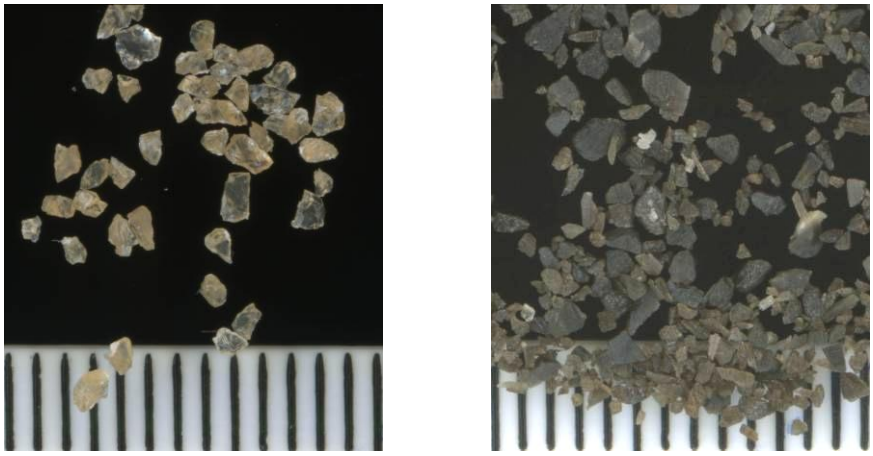

a) Clear, well-preserved belemnite calcite bits b) Cloudy, altered belemnite calcite bits

Fig. 2.2. a) Picked well-preserved, clear, light brown belemnite fragments for analysis, and b) unpicked altered, cloudy, dark brown calcite bits. The scale in the pictures is mm.

2.3 Visual preservation judgement and microstructure analysis by SEM

The fragments of each belemnite sample were judged visually under the microscope for the preservation degree, each specimen was given a visual preservation index. A few visually clean belemnites were examined for the microstructure, using the S-3600N scanning electron microscope (SEM) at University of Leicester. The operating conditions were as follows: Scan was by a S-3600N SEM with an accelerating voltage of 15 kv, normal lens and mono colour mode. Broken sections of five visually well-preserved belemnites were coated with gold before being scanned. Acid etched (by 5% HCl for 2 minutes) and unetched samples were compared to see the topographical difference between their surfaces. Images were taken at ×300 to ×4700 magnifications in order to see the surface structure clearly.

2.4 Bulk sample analysis

For bulk analysis, picked sample fragments were measured for carbon and oxygen isotopic compositions with a VG Optima mass specrometer at NIGL and a Delta GASBENCH at UCL; and for trace elements (Ca, Mg, Na, Sr, S, Fe, Mn and Ba) with ICP-AES at Royal Holloway and UCL.

2.4.1 Stable isotope analysis

Toarcian belemnite samples from Yorkshire were measured for stable isotopes ($\delta^{13}C$ and $\delta^{18}O$) by a Delta GASBENCH connected to a ThermoFinnegan Delta +XP continuous flow isotope ratio mass spectrometer (CF-IRMS) at the Bloomsbury Environmental Isotope Facility, UCL. Around 1 mg of each ground sample powder was first reacted with one droplet of 10% H_2O_2 to remove organic matter, evaporated using a droplet of acetone and dried in an oven at 60 ℃ overnight. Next, samples and standard vials were fixed in a temperature-regulated block at 45 ℃ for stable isotope measurements. A continuous stream of He was used to remove the air in the vials, and 8 droplets of phosphoric acid were then added in each carbonate sample to ensure complete reaction. Isotopic values ($\delta^{13}C$ and $\delta^{18}O$) are reported as per mil relative to the VPDB scale. Analytical precision, estimated using within-run standards and repeat analyses of NBS19 over runs, was better than 0.05‰ for $\delta^{13}C$ and 0.1‰ for $\delta^{18}O$.

For Pliensbachian, Callovian and Valanginian belemnite specimens, the stable isotope analyses of bulk samples were conducted at NIGL, British Geological Survey, Keyworth, Nottingham, using the method provided by Professor Melanie Leng, and with the help of Catherine Jex, Hilary Sloane and Tanya Knowles. The picked least-altered fragments (e.g. the clearest calcite without visual cloudiness under 10 × magnification) of samples with low visual preservation index (VPI ≤ 3) were ground in agate and 10 mg of powder sample was reacted with anhydrous phosphoric acid *in vacuo* overnight at a constant 25 °C. The CO_2 liberated was separated from water vapour under vacuum and collected for analysis. Measurements of bulk samples were made on a VG Optima mass spectrometer. Overall analytical reproducibility for these samples was better than 0.1‰ for $\delta^{13}C$ and $\delta^{18}O$ (2σ). Isotope values ($\delta^{13}C$, $\delta^{18}O$) are reported as per mil (‰) deviations of the isotopic ratios ($^{13}C/^{12}C$, $^{18}O/^{16}O$) calculated to the VPDB scale using a within-run laboratory standard calibrated against NBS standards.

In both methods, some altered samples with high VPI (= 4 or 5) were analyzed along with the well-preserved ones for comparison and assessing the effect of alteration on composition.

2.4.2 Trace element measurement

Around 20 mg of picked bits of each sample (at ~1 mm in size) were dissolved in 10 ml 2% HNO_3 and analyzed for Ca, Ba, Mg, Na, S, Fe, Mn and Sr with ICP-AES at the Department of Geography of Royal Holloway and at UCL. Duplicates were run between batches to estimate the reproducibility of the analyses, which was better than 4% for Ca, Mg and Sr, but more changeable for other elements. Within each batch, samples were measured with repeated analyses of acid blanks and three standards that cover the compositional ranges of samples. The final reported data were blank- and drift-corrected. The mean of all blank measurements within a run was used for blank-correction of all samples in the run due to their stability, whereas the drift correction was made using the top standard (containing the highest elemental concentrations) and applied regionally to the interval that each two top standards cover.

2.5 Intro-rostral analysis

Intra-rostral profiles of isotopic and elemental compositions were obtained on polished cross – sections of belemnite rostra. The purpose of doing so is to compare with the bulk analysis, and also get a better understanding of the relationship between intro-rostral variations in composition and changes in living habitats during growth. Microsamples were obtained from one polished longitudinal section and analyzed for stable isotopes whereas elemental analysis was made on polished cross-sections with electron microprobe and laser ablation ICP-MS.

2.5.1 Microsampling and stable isotope analysis within a rostrum

Microsampling was performed at Bloomsbury Environmental Isotope Facility (BEIF), UCL, using a New Wave Research micromill. A clean polished longitudinal section of a belemnite was sampled at ~500µm steps along growth lines. The width of microsampling interval was ~250µm. After each drilling, the resulting powder was immediately transferred to a valve for later analysis, and the surface of the section cleaned using a dust sprayer to prevent cross-contamination. Forty subsamples were collected and measured for carbon and oxygen isotopes using a Delta GASBENCH mass spectrometer in the Bloomsbury Environmental Isotope

Facility (BEIF) at UCL. Isotope values are reported as per mil relative to VPDB. Precision was estimated using a within-run laboratory standard calibrated against NBS-19 and was better than 0.1‰ for $\delta^{13}C$ and $\delta^{18}O$.

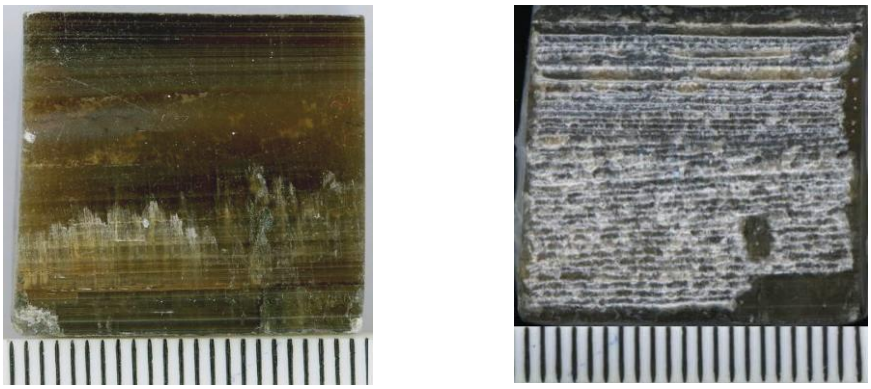

a) Original longitudinal section b) Microsampled longitudinal secion

Fig. 2.3 Pictures of the original and the microsampled same longitudinal section of *C. pusoziana* specimen Bed 13-49a. The scale is mm.

2.5.2 Multi-element analysis by Electron microprobe

The electron microprobe analysis was done on polished cross-sections with carbon coating at UCL, using a Jeol JXA-8100. The operating conditions were 50 kv accelerating voltage with a beam current of 2.5×10^{-8} mA, and a beam diameter varying from 10 to 80 µm, depending on the size of the sections. Two radial traverses were analyzed on each cross section, starting from rim to centre to rim again, for Ca, Mg, Na, Sr, S, Mn, Fe (and/or Ba) concentrations.

2.5.3 Multi-element analysis by LA-ICP-MS

2.5.3.1 Operating Conditions

Analytical traverses cross radial sections of belemnites were made for multi-element analysis by RESOM-50 laser-ablation inductively coupled plasma mass spectrometer (LA-ICP-MS) at Royal Holloway University of London. The operating conditions were as follows: ArF excimer (193nm) laser-ablation system (RESOlution M-50, Resonetics LLC, USA) was coupled to a two-volume laser-ablation cell (Laurin Technic, Australia), and this LA unit was connected to an Agilent 7500ce/cs

quadruple ICP-MS. The diameter of the laser spot varies from 44 to 57 μm and the laser repetition speed from 2 to 0.4 mm/sec, depending on the diameter of the sample. The coupled ICP-MS Agilent 7500ce/cs was operated at a RF power of 1250 W. The dwell time is 20 ms for most measured isotopes. NIST 612 was used as a reference glass to bracket sample analysis. Pre-ablation was done to clean the mount surface before scanning.

2.5.3.2 Data Acquisition, Processing And Reduction

On each section, I analysed two traverses carefully selected along the least altered regions for laser ablation (the two black lines in Fig. 2.4**).** The measured isotopes of 14 elements are ^{23}Na, ^{25}Mg, ^{43}Ca, ^{55}Mn, ^{57}Fe, ^{66}Zn, ^{85}Rb, ^{88}Sr, ^{89}Y, ^{138}Ba, ^{140}Ce, ^{208}Pb, ^{232}Th and ^{238}U. Data were collected in 7 runs, each of which contains 2 to 3 sample analyses bracketed by paired analyses of reference NIST 612. The laser repetition rate was kept 10 Hz for most samples and was 15 Hz for the last run. This gives 1/3 higher intensity to analysed elements in the last run than previous runs, but does not affect the concentrations as the samples and standard NIST 612 were run in the same condition. Although ^{55}Mn and ^{57}Fe were interfered with ^{40}Ar^{15}N and ^{40}Ar^{17}Omolecules from the carrying gas, data of both Fe and Mn look good enough for the purpose of indicating alteration. Fe concentration was subtracted by 200 ppm because the data clearly show a baseline of 200 ppm introduced by mass interference. The final processed Fe and Mn data are plotted along with other elements in the multi-element profiles of belemnite sections.

The first step in data reduction is background correction. The gas background was stable for all measured elements other than Na, and therefore their net intensity was obtained from the subtraction of mean background during each run. For Na, gas background drifted downwards by 8% on average within one run and by 60% from the first to the last run. This is because the LA-ICP-MS was tuned in the beginning with several short analyses of standard NIST 612 which has abundant Na and therefore provided a Na reservoir around the plasma before sample measurements. In the process of running belemnite samples with much lower elemental contents (apart from Ca), the LA-ICP-MS was gradually being flushed and the gas background was reducing. In order to minimize the uncertainty in data reduction, local gas

background correction was applied to Na. This means the data points were only subtracted by the mean of the gas background that brackets them.

The concentration of a certain element is derived from the equation in (Longerich *et al.*, 1996) which can be rewritten in the following formula:

$$C^{x}_{sample} = C^{r}_{sample} \times \frac{C^{x}_{std}}{C^{r}_{std}} \times \frac{i^{x}_{sample}}{i^{r}_{sample}} \times \frac{i^{r}_{std}}{i^{x}_{std}} \quad (2\text{-}1)$$

Here, C is concentration, i the intensity of ICPMS, and std the external standard. x is the unknown element and r the reference element (or internal standard). For our analysis, NIST 612 was used as external standard and Ca in the samples acts as an internal standard. The above equation was applied in samples with known Ca concentration. Since these samples are among the best-preserved ones that have ever been analyzed, the concentration of Ca (40.08%) in pure calcite was assumed to be C^{r}_{sample}. In the parts where lower Ca is found, such as the altered rim and centre, approximate concentration values are given simply by scaling the mean of the intensity and concentration of each element given by the equation. Those low Ca areas are only used to mark the boundary of the altered and pristine calcite; the absolute concentration is of no consequence. The elemental concentrations, other than elemental/Ca ratios (El/Ca), are plotted in the graphs because the concentrations are derived from the internal standard Ca in equation (2-1), and thus represent El/Ca ratios here.

2.5.4 Method validation

One polished section (Pliensbachian sample 7-37 S3 of *P.cuspidatus*) were analyzed chemically by electron microprobe after LA-ICP-MS analysis for comparison. One microprobe traverse was on the LA track and another short path perpendicular to the LA track (Fig. 2.4). Ca, Mg, Na, S, Sr, Fe and Mn were measured, using electron microprobe JXA-8100, with a spot diameter of 10µm and a step interval of 3µm. This work is to check the validity of both methods and whether there is any effect from LA on concentrations along the LA track.

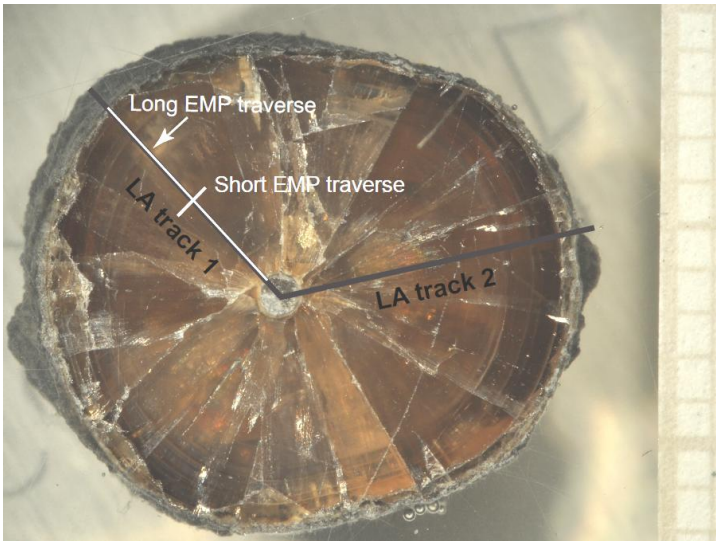

Fig. 2.4 The electron microprobe traverses (white lines) and LA tracks (black lines) of *P. cuspidatus* sample 7-37 S3. The scale on the right is mm.

Chapter 3 Sample Preservation

Diagenetic alteration changes the stable isotope (C and O) and elemental compositions (El/Ca) in biogenic carbonate, such as belemnites (Veizer, 1974; Podlaha *et al.*, 1998; McArthur *et al.*, 2007b); it is therefore important to select for analysis the well-preserved samples or parts of samples. To achieve this aim, various methods of assessing the degree of preservation of belemnites have been tried prior to isotopic and elemental measurements. Firstly, a number of belemnite thin sections were observed for microgrowth patterns of pristine calcite under microscope; then the calcite fragments from the least altered regions of each belemnite specimen are visually judged in alcohol bath under the microscope according to their optical features and a visual preservation index (VPI) ranging from 1 (the least altered) to 5 (completely altered) is given to each sample; finally a few visually well-preserved specimens with VPI ≤ 3 were scanned by SEM to evaluate the optical criteria. The samples with low visual preservation degree (VPI ≤ 3) in this study are proved to be the well-preserved with SEM examination, and therefore are selected for isotopic and elemental analysis to minimize the effect of diagenetic alteration on their compositions.

3.1 Belemnite thin section observation

The microstructure of belemnite rostra is discernible in petrographic thin-sections. Cross-sections of well-preserved belemnites show predominant concentric regions of pristine, colorless calcite crystals when viewed under plane polarized light. The growth boundaries are poorly defined in most of the least altered specimens; but are accentuated by diagenesis in specimens showing small degree of alteration (e.g. Fig. 3.1 c). These growth boundaries are thin, sharp and dark, so probably contain black organic matter rather than diagenetic precipitates. Even in well-preserved belemnites, small areas around the centre (the apical line area), the exterior and the fractures are usually stained by dark-colored minerals (e.g. iron oxides and/or organic matter) and sometimes with secondary cloudy calcite. Small inclusions are occasionally visible inside calcite crystals (Fig. 3.1 f). Belemnite calcite suffers from brittleness, so fractures and cracks are commonly noticeable. Small fractures can occur between crystal boundaries, or cut the crystals into concentric arcs; and long fractures can cut

through a section along its diameter. These fractures may be caused by stress during diagenetic burial.

The calcite crystals, with the form of prisms, are densely packed and grow radially towards the rim of a section under the cross polars (Fig. 3.1 here and p173-174 in Scholle and Ulmer-Scholle, 2003). These calcite prisms are not interrupted by the growth boundaries, as reported in Dunca *et al.* (2006). The calcite prisms can be thin and long fibres (e.g. Fig. 3.1 a, b), or large and bulky columns (e.g. Fig. 3.1 c). A calcite prism can attain sizes up to the radius of the rostrum, though it's usually fractured by parallel cracks perpendicular to its growth direction. In this case the boundary between two prisms would be straight and sharp (e.g. Fig. 3.1 f). It can also be short with irregular edges, with other calcite aggregates growing on the edge of it, so producing uneven interfaces and jagged boundaries between crystals (Fig. 3.1 d, e). This competitive growth pattern may suggest grain-coarsening probably driven by diminished solubility due to energetic reasons (Podlaha *et al.*, 1998), or imply a change in growth rate due to the change of energy available during growth.

All calcite crystals are radiating from the centre, so they reflect different optical orientations and extinction at 90°. No cleavages and lamellar twinning are observed in the calcite prisms, and no recrystallization is found to have taken place in the well-preserved specimens. The dense structure of belemnite rostra is therefore the reason for preventing the intense diagenetic alteration.

Table 3.1 Microstructure features of different belemnite species under a minocular microscope.

Species (no.)	Form of calcite crystals	Growth bands	Fractures
Cylindroteuthis pusoziana (3)	Fibrous or columnar crystals radiating from the centre and attaining sizes up to the radius of the guard.	Growth bands are very thin and poorly defined in the least altered specimens, but are accentuated in specimens with slight alteration.	Long fractures along the diameter of the section, small fractures within and between calcite crystals that cut the large radiating crystals into concentric arcs.
Passaloteuthis cuspidatus	Short radial calcite crystals with irregular	Growth bands barely seen, except for the middle and	Small fractures near the rim cutting crystals perpendicular to the

Species (no.)	Form of calcite crystals	Growth bands	Fractures
(2)	edges and boundaries.	the very exterior.	growth direction.
Nannobelus Acutus (2)	Fibrous to columnar, irregular grain boundaries. Inclusions are seen in calcite crystals.	Visible close to the apical line and rim. Growth bands are not circular, but look squeezed around the centre in one specimen (7-41S3).	Long radial fracture and small fractures (close to rim) perpendicular to the growth direction of calcite crystals.
Passoloteuthis elongata (1)	Not as well-preserved as others, calcite crystals look dirty but still show radial structure. Contamination (e.g. dark minerals) and inclusions are seen. Calcite prisms can obtain a size up to the radius of the section.	Not discernible, a couple of thin bands are visible very close to the rim.	Small and long fractures all over the section.
Bairstowius junceus (1)	Mostly large columnar calcite crystals up to the size of the radius, sharp and straight boundaries between crystals. Short calcite prisms are also seen. Inclusions filling small cavities.	Hardly seen.	Small fractures perpendicular to the growth direction of calcite crystals.
Hastites Spadixari (1)	Radial calcite crystals grow either up to the size of the radius, or aggregate showing irregular interfaces and boundaries between crystals.	Thin and dark growth bands are visible in the middle part, whereas thick growth bands seen in the middle and outer parts.	Few small fractures present in the outer part of the section.
Hastites Stonebarroensis (2)	Calcite crystals grow similar to *H.spadixari*	Growth bands are only barely seen around the apical line.	Radial fractures are well-developed, and small cracks are very common near the rim.

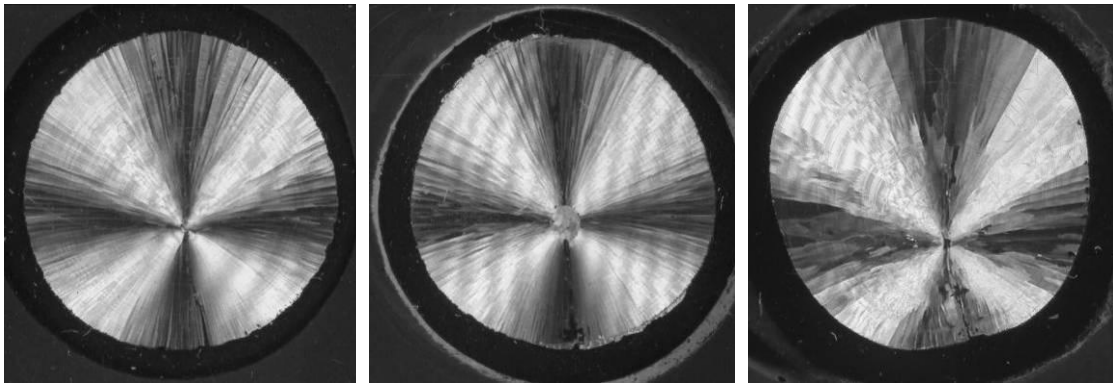

(a) 1S 61 (b) 2S 72 (c) 2S 116

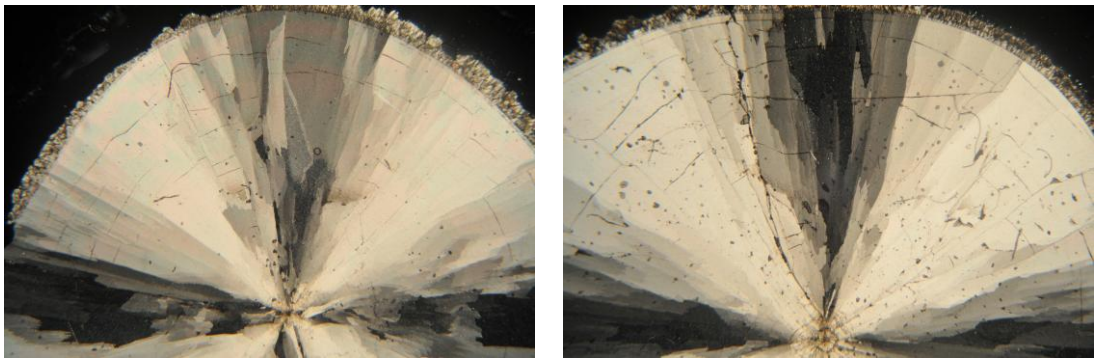

(d) 7-17 S3 (e) 7-33 S3

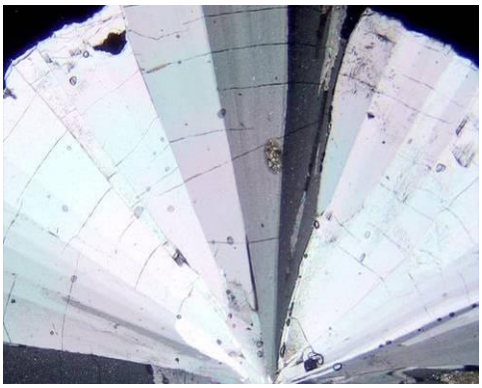

(f) 7-38 S3

Fig. 3.1 Belemnite thin sections under cross-polarized light. The fibrous calcite crystals are shown in specimens (a) 1S 61 and (b) 2S 72 of species *C. pusoziana*, while (c) 2S 116 of the same species show more columnar crystals form; (d) 7-17 S3 and (e) 7-33 S3 of species *P. cuspidatus* reflect bulky columnar calcite crystals aggregates growing on the edge of each other radially towards the exterior, uneven interfaces and jagged boundaries between these crystals are discernible, the actual width of the picture is 7 mm; (f) 7-38 S3 of species *B. junceus* shows calcite prisms with a size up to the radius of the rostrum, the actual length from left to right is 5 mm.

3.2 Visual preservation degree

A visual preservation index (VPI) ranking from 1 (essentially unaltered) to 5 (completely altered) is given to each belemnite specimen in order to evaluate the

effect of diagenetic alteration. When viewed under 10× magnification, sample fragments ranked 1 to 3 preserve large proportion of clearest calcite fragments without visual cloudiness, whereas fragments of samples with higher rankings (VPI = 4-5) are dominantly composed of cloudy calcite. The clearest calcite bits of samples rated 1 to 3 were hence picked for analysis to minimize the effects of diagenetic alteration, with some of higher rankings that were analyzed to compare unaltered with altered samples. The VPIs of specimens in this study are summarized in Table 3.2, and can also be found in Appendix C – F.

Table 3.2 Summary of VPI data of each belemnite population in this PhD study.

Percentage of specimens / Sampling interval	Visual preservation index (VPI)			
	VPI = 1	**VPI = 2**	**VPI = 3**	**VPI = 4**
Pliensbachian	34.7 %	45.7 %	19.6 %	0 %
Toarcian	6.0 %	36.0 %	44.0 %	14 %
Callovian	34.5 %	55.2 %	10.3 %	0 %
Valanginian	5.3 %	36.8 %	57.9 %	0 %

3.3 Belemnite microstructure

A few visually judged well-preserved specimens (VPI < 3) were then examined to reflect the microstructure of the unaltered belemnites, using a scanning electron microscope (SEM). The scanned sample sections are listed in Table 3.3.

Table 3.3 Samples selected for SEM analysis

Sample No.	Species	Biostra. Age	VPI
2S30	*C. pusoziana*	Callovian	2
Bed 13/46	*C. pusoziana*	Callovian	1
D08 7/3 S2	*P. elongata*	Pliensbachian	1
D08 118/2	*A. gabrier*	Pliensbachian	1
D08 120/8	*P. cupidatus*	Pliensbachian	1

SEM pictures show very solid dense calcite structure of belemnite rostrum (Fig. 3.2). The calcite is likely to be pristine and no secondary fractures are found to cut the original crystals. The etched and unetched sections of *P. elongata* sample D08 7/3 S2 were both analyzed to see the topographical difference between them. The unetched section of D08 7/3 S2 shows solid pristine calcite with no holes or fractures or banding at ×3700 magnification (Fig. 3.2 a), whilst the etched surface reveals small holes at magnification of ×2300 (Fig. 3.2 b). This may suggest that tiny holes are subject to being recognizable at high magnification on etched surfaces and may be created by acid etching. Sections of specimens 2S30 (*C.pusoziana*) and D08 118/2 (*A. gabrier*) were also acid-etched. Tiny holes again are visible on both surfaces (Fig. 3.2 d & f), and thin growth boundaries are present close to the edge of the section of 2S30. The picture of 2S30 does not look uniform due to the contrast and brightness adjusting problem when imaged. Meanwhile, radial arrangement of pristine calcite crystals is clearly visible on section D08 118/2 at a magnification of ×1000. The other two unetched sections (Bed 13/46 and D08 120/8) repeatedly show very dense calcite crystals with no banding (Fig. 3.2, c & e). The broken surfaces of calcite crystals in D08 120/8 give a false image that crystals are cut by secondary fractures.

SEM results indeed reflect the morphology of well-preserved belemnites which preserve dense calcite crystals in radial arrangement and poorly-defined growth boundaries. These findings apparently contradict the interpretation of well-defined circular structure, the ‘laminae pelucidae’ and ‘laminae obscurae’ as being primary structure resulting from growth of belemnites (Saelen, 1989). The ‘laminae obscurae’ observed in his altered samples is actually the alteration-thickened growth boundaries.

3.4 Summary of preservation assessment

Both thin section observation and SEM examination show that well-preserved belemnites contain predominantly pristine calcite growing radially within a rostrum and reflect poorly defined growth boundaries, though small-scaled alteration occur around the centre (the apical line area), the exterior and the fractures.

The visual preservation assessments (or the VPIs) are confirmed by SEM analysis and therefore are applied to all belemnite samples prior to chemical analysis. Specimens with VPI rated 1 to 3 are proved to retain pristine calcite microgrowth structure of belemnite rostra, so chosen for the compositional analysis. Finally, the compositional data of these selected samples of each of the four belemnite populations present in chapter 4 to 7 were further constrained by the chemical criterion (Fe <100 ppm and Mn < 30ppm) proposed in chapter one, so as to eliminate the overprint of alteration on composition.

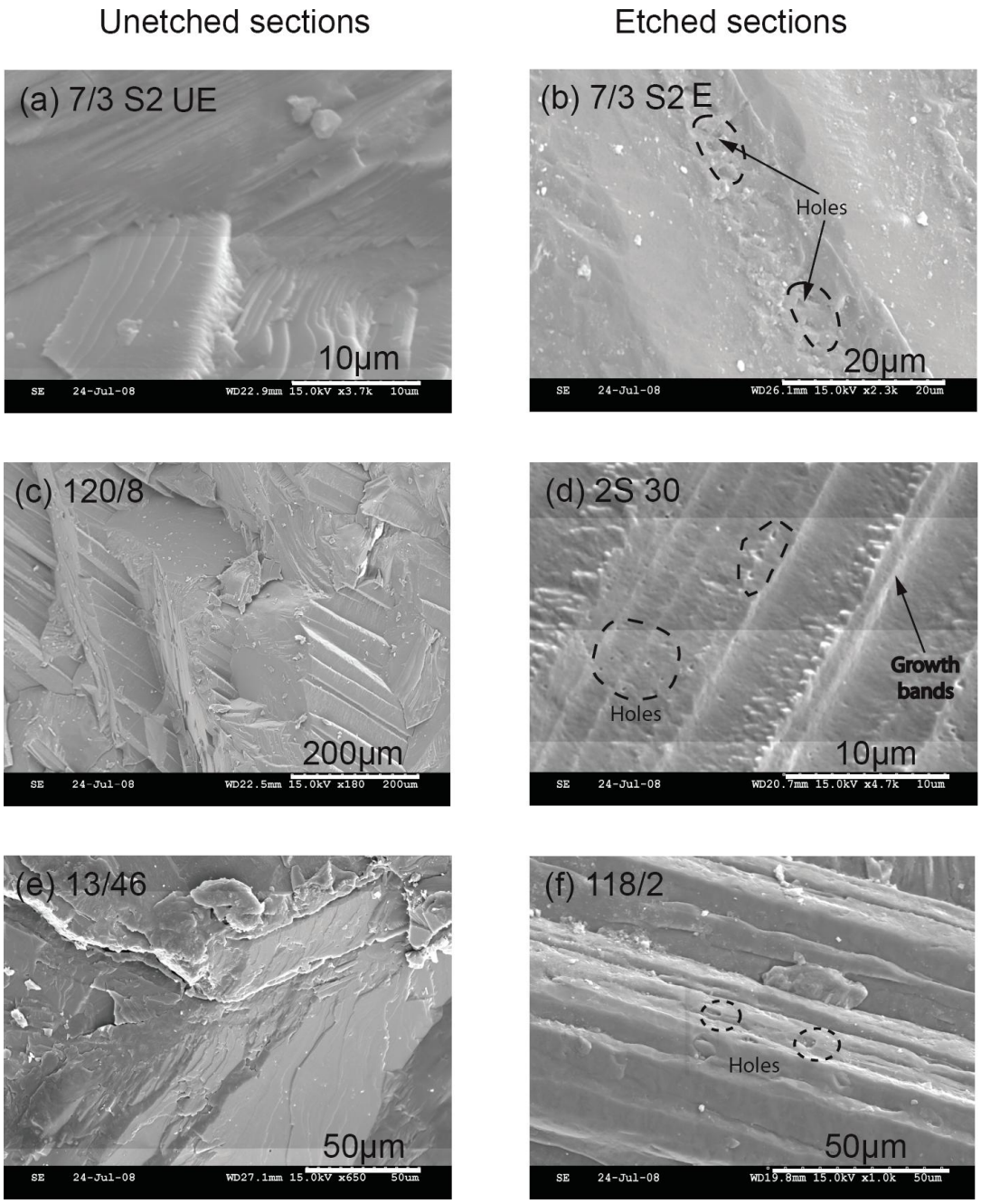

Fig. 3.2 SEM images of well-preserved belemnite fragments, (a) the alveolar part of the *Passaloteuthis elongata* (7/3 S2) at magnification ×3700; (b) The stem part of the same *Passaloteuthis elongata* (7/3 S2) at magnification of ×2300; (c) *Passaloteuthis cupidatus* (120/8), ×180; (d) *C.pusoziana* (2S30): acid-etched transverse section at very high magnification (×4700); (e) *C.pusoziana* (Bed 13/46): a longitudinal fragment without acid etching, magnification (×650); (f) *Angecoteuthis gabrier* (118/2) at magnification of ×1000. UE-Unetched; E-etched.

Chapter 4 Pliensbachian Belemnites from Dorset

The objective of this chapter is first to investigate the complexity of the compositions of Pliensbachian belemnites from Dorset, such as compositional variations within a single specimen, between specimens of a single species and between species; then to demonstrate the lifestyles and living habitats of different species; and finally to evaluate palaeo-proxies in them.

The compositional profiles within a belemnite rostrum were obtained by both laser-ablation ICP-MS (LA) and electron microprobe (EMP). Both methods were validated through obtaining LA and EMP profiles on the same radial traverse of the same sample. The method comparison indicates that LA and EMP both give comparable data of Ca, Mg and Na, but the former produces more reliable Sr, Fe and Mn profiles than the later. Accordingly, LA profiles were picked for the interpretation of intra-rostral variations. Meanwhile, bulk chemical data of belemnites are comparable to intro-rostral data. The smaller variations in elemental composition between specimens of a species than the intra-rostral variations are likely due to the homogenization of large sample volumn in bulk analysis.

4.1 Introduction

In the UK, numerous Pliensbachian belemnites occur on the coast of Dorset and Yorkshire. The stratigraphy and palaeontology of the Pliensbachian belemnites from Dorset has been well-documented by Lang *et al*. (1928), and those of Yorkshire by Doyle, (2003). For Yorkshire belemnites, the stable isotope and trace element concentrations ($\delta^{13}C$, $\delta^{18}O$, Mg/Ca, Sr/Ca and Na/Ca) have been used as palaeo-proxies to deduce the palaeotemperature and palaeo-salinities through Toarcian times (McArther *et al*., 2000; Bailey *et al*., 2003; van de Schootbrugge *et al*., 2005; McArthur *et al*., 2007b). Pliensbachian belemnites of Dorset, on the other hand, are prominently noticeable for higher degree of preservation than contemporaneous Yorkshire ones, but less widely sampled and little work has been done to investigate their geochemical features. The Pliensbachian belemnites here preserve great species variety, which therefore enables the study on differences in compositional ranges between species. These specimens are also the best-preserved ones among all the

collections of this PhD study. They hence should retain closely the primary signal of the geochemistry of the Pliensbachian seas of the UK. The investigation of the geochemistry of these belemnites will potentially refine the current understanding of belemnite palaeo-proxies.

4.2 Sampling

Samples were collected from the Pliensbachian sedimentary rocks from Charmouth to Seatown on the coast of Dorset, UK (Fig. 4.1). The biostratigraphy and lithostratigraphy of the section sampled is well-documented (Lang *et al.*, 1928; Hesselbo and Jenkyns, 1995) and summarized in Table 4.1. Specimens came from the top of Belemnite Marls and the base of the overlying Green Ammonite Beds. The sampling interval is between the *masseanum* Subzone of *Prodactylioceras ibex* Zone and the *maculatum* Subzone of *Prodactylioceras davoei* Zone. In the Belemnite Marls, belemnites were sampled from unweathered rock at 2 sites: bed 118 c-d (2.1-2.2 m below the Belemnite Stone) and bed 120 d-e (between the Belemnite Stone and the Belemnite Bed). Samples were not taken from the rich belemnite accumulation of the Belemnite Bed or the Belemnite Stone because those from the two beds were judged visually to be poorly preserved. The remaining samples were collected from the Bed 7 (5-30 cm above the Belemnite Stone) at the bottom of the Green Ammonite Beds. The bed numbers are taken from Lang *et al*. (1928) and Hesselbo and Jenkyns (1995).

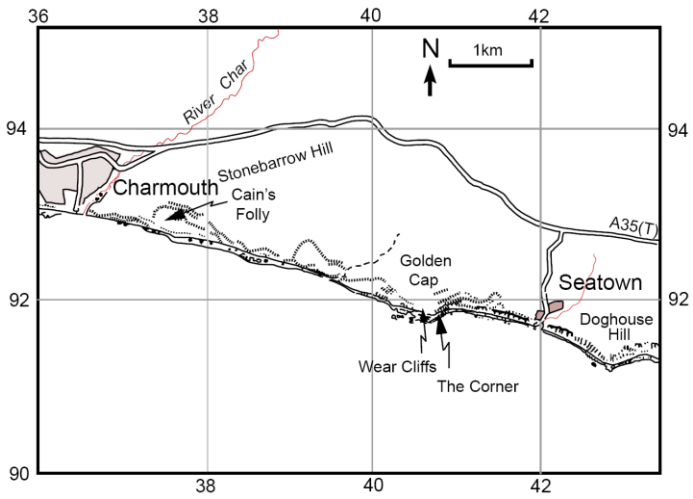

Fig. 4.1 The simplified map of sampling area- Charmouth to Seatown on the coast of Dorset, UK.

The genera and species of each belemnite were identified, with initial guidance from Peter Doyle. Five genera and ten species are present, and their characteristics and pictures are provided in Table 4.2 and Fig. 4.2. Only six species were collected in sufficient numbers (e.g. species with ≥ 6 specimens) for studying intra- and inter-rostral compositional variations within and between species. They are (with numbers of specimens in parenthesis): *Passaloteuthis cuspidatus* (37), *Nannobelus acutus* (30), *Bairstowius junceus* (10), *Passaloteuthis elongata* (7), *Hastites spadixari* (6) and *Hastites stonebarroensis* (6). Polished cross–sections of belemnites representatives from each of the above species have been made to investigate the intra-rostral variations in composition.

a). *P. cuspidatus* 7/3 S3

b). *B. junceus* 7-38 S3

c). *P. elognata* 7-29 S3

d). *N. acutus* 7/6 S3

e). *H. spadixari* 7/68 S3

f) *H. stonebarreonsis* 7/83 S3

Fig. 4.2 Typical specimens of the studied species from Pliensbachian of Dorset, UK. Scale is in mm and cm. Apex missing for *B.junceus* and *P.elognata*.

Table 4.1 The biostratigraphy and lithostratigraphy of the *ibex* to *davoei* Biozones on the Charmouth to Seatown section of Dorset coast, UK. The beds from which samples were collected are in highlighted in bold. *P. davoei - Prodactylioceras davoei*; *P. ibex - Prodactylioceras ibex.* The bed numbers are from Lang *et al.* (1928) and Hesselbo and Jenkyns (1995).

Stage	Zone	Subzone	Formation	Bed No.	Lithology	D (cm)
PLIENSBACHIAN (PART)	*P. davoei* *(part)*	*maculatum* *(part)*	Green Ammonite Beds (base)	**7**	**Light-colored, silty and less calcareous mudrocks.**	**108**
	P. ibex *(part)*	*luridum*	Belemnite Marls (top)	121	The Belemnite Stone, hard, pale-grey, nodular limestone.	6
		valdani		**120 d-e**	**Greyish-black friable marl**	**27**
				120 c	The Belemnite Bed, dark greypyritic and friable, organic rich mudstone, with abundant belemnites and bivalves.	5
				120 a-b	Pyritic Marls, with small smooth nodules of iron sulphide distributed (120 a) and capped by a layer of larger similar nodules (120 b).	30
				119	Brown marly shales, with impersistent lenticles of crinoid-limestone at the top.	101
				118 d	**Upper darker Marls, top part, bluish-grey marl.**	**46**
		masseanum		**118 c**	**Upper darker Marls, middle part, bluish-grey marl.**	**76**

Table 4.2 The description of the collected Pliensbachian belemnite genera from Dorset. Pictures of the typical specimens of species analyzed in this study are provided below in Fig. 4.2.

Genera	Species	No.	Description
Passaloteuthis	*cuspidatus*	37	Medium to large cylindriconical rostra, quadrate to circular transverse sections, paired dorso-lateral grooves at apex and poorly-defined lateral lines.
	elongate	7	
	apicicurvata	2	
	stonebarrowensis	2	
Hastites	*spadixari*	6	Small sized, slender and hastate rostra form, subcircular transverse section, triple lateral lines, and lack of apical grooves.
	stonebarroensis	6	
Bairstowius	*junceus*	10	Medium sized, elongate, specular to feebly hastate rostra, compressed cross-sections, no apical grooves, and triple lateral-lines.
Nannobelus	*acutus*	30	Small to medium cylindriconical rostra with pyriform, subquadrate or oval traverse sections, sharp apex, and poorly defined short apical lines.
Angeloteuthis	*uriel*	3	Short cylindrical to cylindriconical rostra with rounded apex, quadrate transverse sections and distinctively flattened flanks, no apical grooves, but triple lateral lines and broad furrows.
	gabrier	3	
Total		**106**	

Note: Small size refers to a length < 5cm and medium size is between 5 and 10cm.

4.3 Results

4.3.1 Belemnite section observation

All cross-sections (Fig. 4.3 – 4.9) were highly polished, but broken surface crystals and fractures (shown in white colour) are visible close to the edge of many sections (*e.g.* Fig. 4.3 b). On each section, large areas of clear primary calcite are perserved,

but regions around the apical line and the perimeter are often filled with cloudy secondary calcite (e.g. Fig. 4.4 a, Fig. 4.6 a) and/or stained with dark colored minerals (*e.g.* Fig. 4.9), which are possibly iron and manganese oxides and/or iron sulphides because cross-sectional profiles of Fe and Mn show high peaks present in these regions. Between growth intervals, growth boundaries are visual, and appear as dark or white, thin or thick, complete or incomplete bands in variable specimens. In samples with high preservation, growth boundaries are barely seen (Fig. 4.3 a, Fig. 4.5 b), or occur as thin bands (complete or imcomplete) towards the exterior of the cross-sections (Fig. 4.3 b). In contrast, they occur as thick bands (dark or white) in cross-sections showing variable degrees of alteration (Fig. 4.7, Fig. 4.9 c). The two specimens of *H. stoneberroensis* (7-70 S3 and 7-86 S3) and one of *H.spadixara* (7-84 S3) show resembling ring patterns, characterized by three prominent bands appearing in the inner, middle and outer areas of the rostrum (Fig. 4.9).

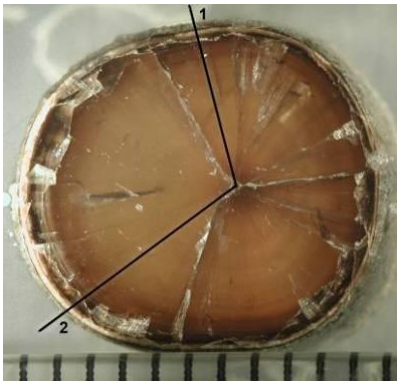

(a) 7-35 S3

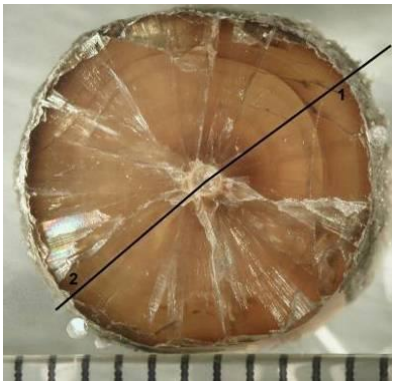

(b) 7-74 S3

Fig. 4.3 Polished cross-sections of *P. cuspidatus* specimens (a) 7-35 S3 and (b) 7-74 S3. The Numbers 1 and 2 stand for the 2 laser ablation tracks. The scale is mm.

(a) 7-37 S3

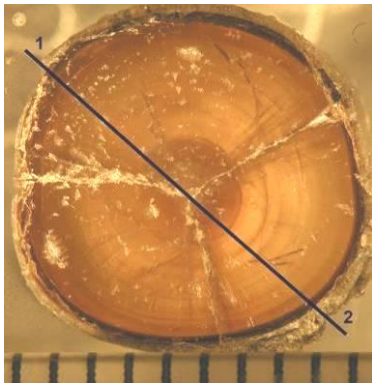

(b) 7-72 S3

Fig. 4.4 (a) *P. cuspidatus* specimen 7-37 S3 and (b) *N. acutus* specimen 7-72 S3. Scale is mm.

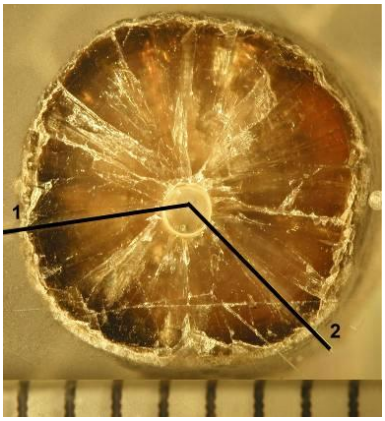

7-61 S3

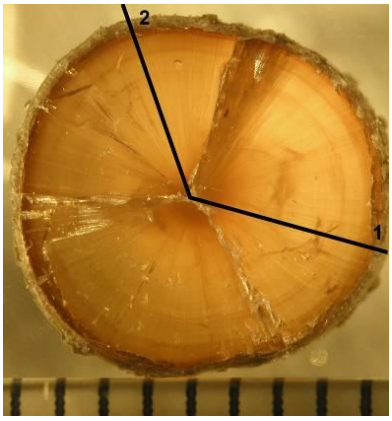

7-71 S3

Fig. 4.5 *N. acutus* specimen (a) 7-61 S3 and 7-71 S3.

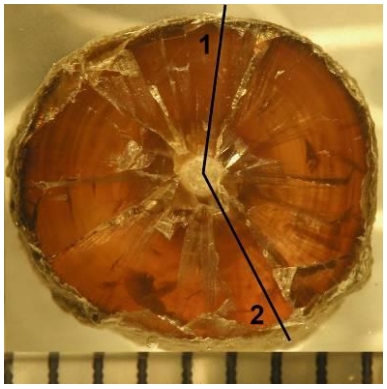

(a) 7-38 S3

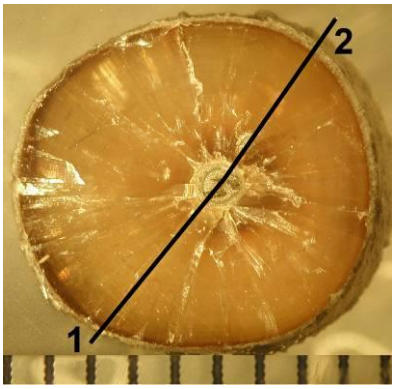

(b) 7-39 S3

Fig. 4.6 *B. junceus* specimens 7-38 S3 and 7-39 S3. Cloudy secondary calcite is filled in the round apical line area in the centre of specimen 7-38 S3.

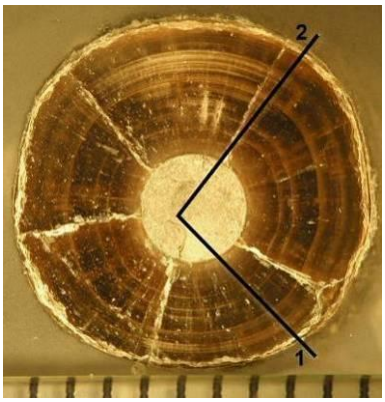

(a) 7-27 S3

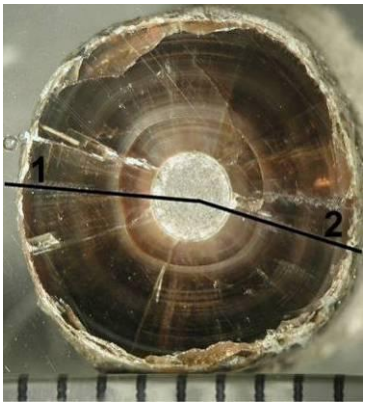

(b) 7-29 S3

Fig. 4.7 *P. elongata* specimens 7-27 S3 and 7-29 S3. Diagenetic infills are seen in the centre (the alveolus) of the two sections.

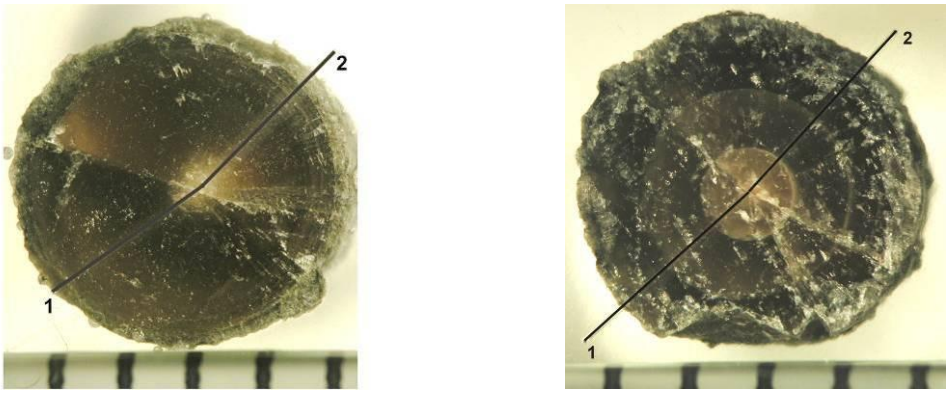

(a) 7-68 S3 (b) 7-84 S3

Fig. 4.8 *H. spadixari* specimens 7-68 S3 and 7-84 S3.

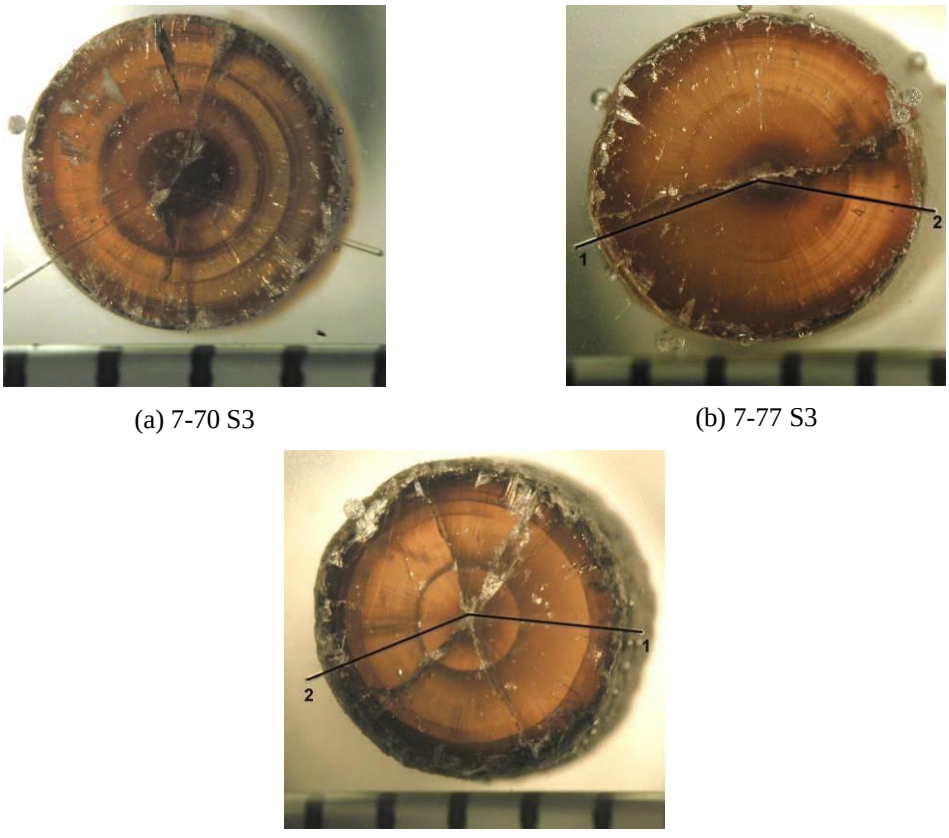

(a) 7-70 S3 (b) 7-77 S3

(c) 7-86 S3

Fig. 4.9 *H. stonebarroensis* specimens (a) 7-70 S3, (b) 7-77 S3 and (c) 7-86 S3. The apical line, thick growth bands and the edge of the sections are stained with dark-colored minerals.

4.3.2 Laser ablation profiles of different species

Cross-sectional profiles of multi-elements at a resolution of 57 µm are shown in Fig. 4.10 to 4.33. Fourteen elements were analyzed for each cross-section. They are Ca, Na, Mg, Sr, Fe, Mn, Zn, Ba, Rb, Y, Ce, Pb, Th and U (see Fig. 4.10). The profiles of

Mg, Na and Sr are used for the interpretation of belemnite ontogeny and potential species differences; whereas Fe and Mn indicate alteration, with Ba and Zn anomalies being supplementary alteration indicators. The remaining elements, including Rb, Y, Ce, Pb, Th and U give less indicative signals of alteration than Fe and Mn, hence are of no use in this study. They are only plotted in one specimen of *P. cuspidatus* (7-37 S3,) to show the above reason (Fig. 4.10).

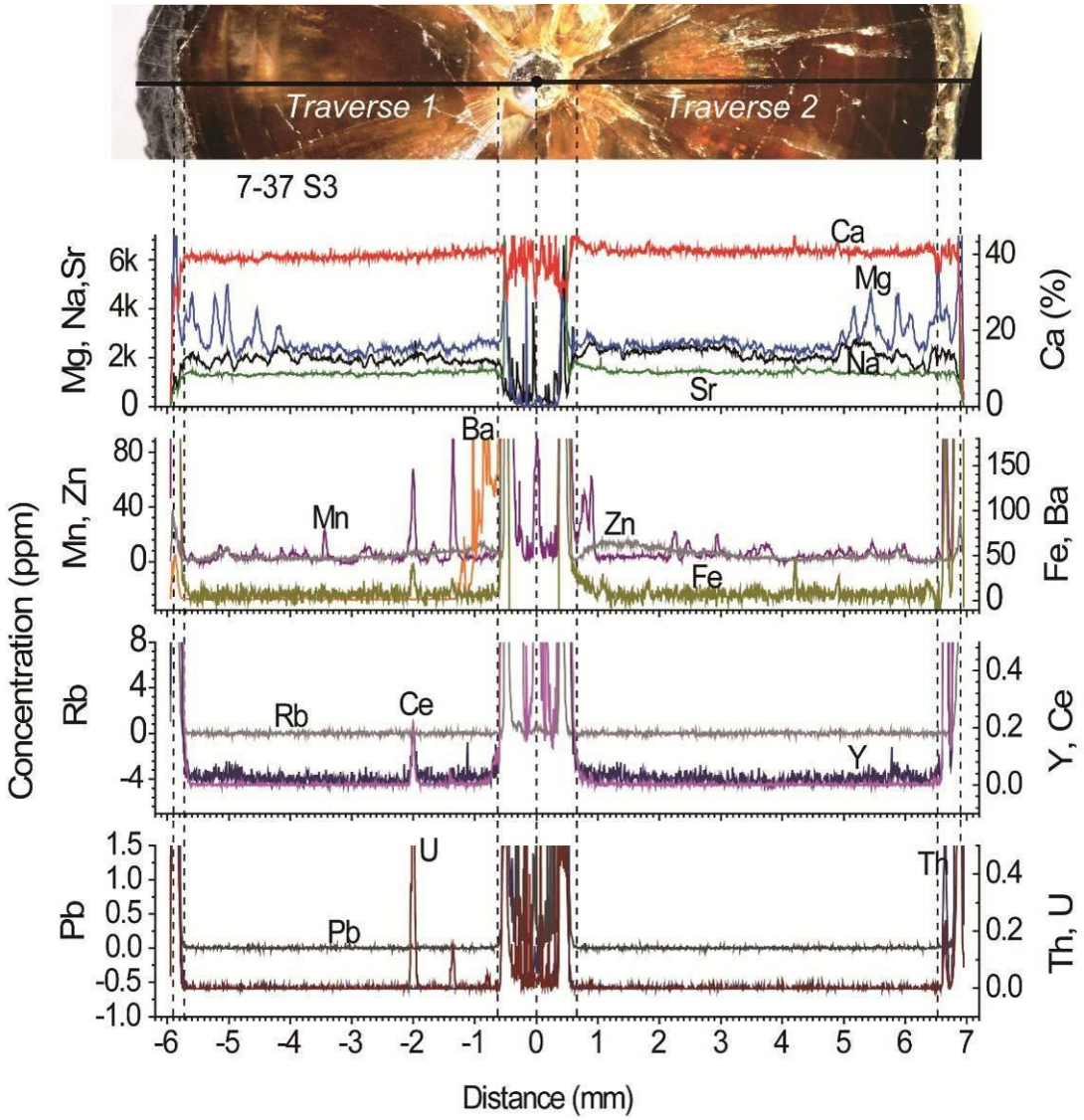

Fig. 4.10 Multi-elemental profiles (Ca, Na, Mg, Sr, Mn, Fe, Zn, Ba, Rb, Y, Ce, Pb, Th, and U) of *P. cuspidatus* specimen 7-37 S3 obtained by LA-ICP-MS. The two laser ablation traverses are shown in the picture on the top. They are not on one line. The real positions of them on the sample section are shown in Fig. 4.4 (a). Altered areas of the rim and apical line (central canal) of the belemnite section are enclosed within dotted lines and are not used in palaeotemperature reconstructions. X axis means the distance to the centre of the apical line (which is marked as the 0 mm).

Different elements show differing variations in amplitudes and patterns in cross-sectional profiles of an individual specimen. For example, Ca concentration is essentially flat in the large unaltered parts of the cross-sections of specimens in five species. Mg possesses the highest-amplitude variations (from 2000 to 6000 ppm) while Sr gives the smoothest concentration profiles varying from 1000 to 2000 ppm (*e.g.* Fig. 4.10). Meanwhile, similarities in the radial trends of elemental concentration profiles are noticeable between specimens within a species and between species, although differences occur in their compositional ranges. Among specimens of *P. cuspidatus, N. acutus, B. junceus, H. stonebarroensis* and *H. spadixari*, profiles of Mg show similar overall radial trends, so do Sr and Na profiles of them. Magnesium profiles reflect a decrease from near the centre to the middle part of the rostra and then an increase towards the edge in most specimens of the above species. This trend is termed as a bowl-shaped pattern. It is very prominent in most specimens of *P. cuspidatus* and *N. acutus* (Fig. 4.20 to Fig. 4.24), one specimen of *H. stonebarroensis* and one of *H. spadixari* (Fig. 4.27 & Fig. 4.28); less distinct in the two specimens of *B. junceus* (so called plate-shaped pattern, see Fig. 4.25 & Fig. 4.26), and is coupled with two Mg peaks in the remaining three specimens of *H. stonebarroensis* and *H. spadixari* (Fig. 4.29 to Fig. 4.31). Undulations in Na are commonly present in these specimens, and parallel the Mg variations. Sr generally decreases smoothly from the apical line to the rim across the sections of specimens in all five species. Na shows similar overall decreasing trend outwards as Sr does in *N. acutus, B. junceus, H. stonebarroensis* and *H. spadixari* specimens.

Concentrations of Mn, Zn and Ba are typically low in the unaltered parts of the sections in specimens of *P. cuspidatus, N. acutus, B. junceus, H. stonebarroensis* and *H. spadixari*. Mn is generally <20 ppm, but occasionally spikes to >100 ppm, especially close to the apical line, over a scale of 50-250 μm (e.g. Fig. 4.10, Fig. 4.21, Fig. 4.22, Fig. 4.25, Fig. 4.26 & Fig. 4.31). Manganese may overestimate alteration, with the evidence being that these Mn peaks appear to have no influence on Mg, Sr and Na in the concentration profiles of many specimens, such as 7-74 S3 (Fig. 4.21) and 7-61 S3 (Fig. 4.22). Zinc in *B. junceus* specimens has a constant low concentration (~2 ppm) in the clear calcite regions, and rises slightly in the high Mn area near the apical line; whereas *P. cuspidatus* and *N. acutus* specimens show continuous increase of Zn inwards to ~15 ppm near the apical line. The abnormal Zn

peaks (up to 45 ppm of Zn) of *N. acutus* specimen 7- 61 S3 line up with the Mn peaks (Fig. 4.22). Zinc in genus *Hastites* specimens (*H.stonebarroensis* and *H.spadixari*) shows an increase to over 100 ppm towards the centre (Fig. 4.28). Zinc (and sometimes Ba) profiles in three *Hastites* specimens are parallel to Mg trends, though on a lower scale (Fig. 4.29 to Fig. 4.31). Concentration of Ba is generally around 2 ppm, but Ba spikes occur in *P.cuspidatus* 7-74 S3 (Fig. 4.21) and *B. junceus* 7-39 S3 (Fig. 4.26). Extremely high concentration of Ba near apical line of *P. cuspidatus* specimen 7-37 S3 tripped the detector and cause a termination of measurement (Fig. 4.10). Barium in *N. acutus* samples follow the decreasing trend seen in their Zn profiles (Fig. 4.22 to Fig. 4.24).

As to *P.elongata* specimens, the incompleteness of the two sections (7-27 S3 and 7-29 S3) makes it difficult to interpret the radial trends in elemental profiles. Sodium and Sr in both samples decrease outwards to the middle, and then increase gradually towards the exterior, but Mg undulates and does not show the major trend seen in other species (Fig. 4.32 & Fig. 4.33). Many Mn peaks occur across the section and are parallel with Mg and Zn peaks at different scales in specimen 7-27 S3, which seems to have higher concentrations of Na, Mg, Sr, Mn and Zn than the less altered specimen 7-29 S3.

4.3.3 Electron microprobe traverses

Electron microprobe data of specimen 7-37 S3 are plotted in Fig. 4.11 to Fig. 4.16. High Mg and low Ca are common near the apical line and the edge of the section in Fig. 4.11. More Mg spikes appear in the cloudy calcite regions (e.g. 4000-5000 µm) of the section than the well-preserved clear calcite areas (*e.g.* the region between 2000 and 3000 µm in Fig. 4.11). The thin and white growth boundaries line up with Mg peaks. A sharp increase in Ca by 2% around 1340 µm and a drop in Ca to 33% at 800 µm before it flattens near the apical line are noticeable.

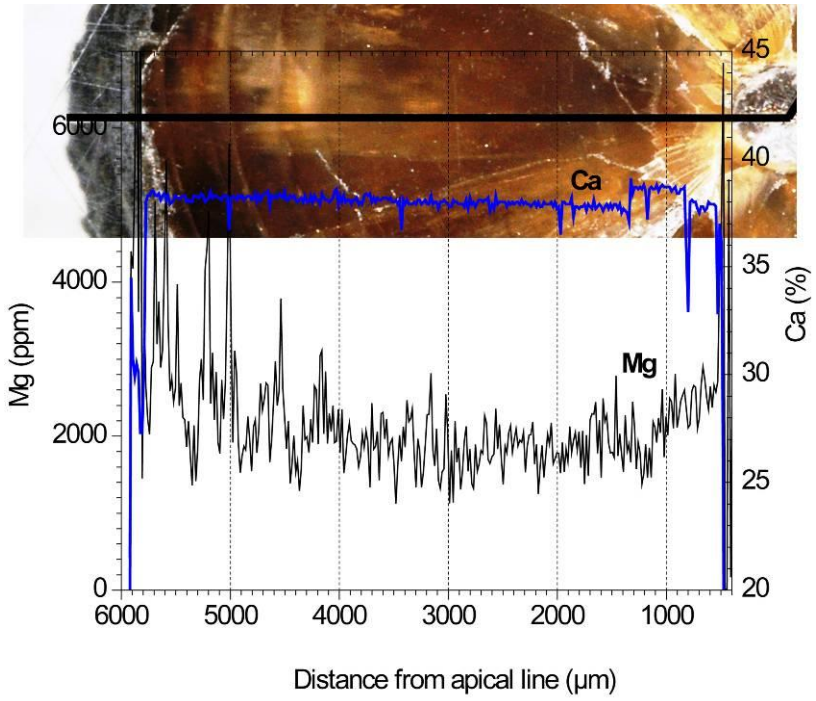

Fig. 4.11 Concentrations of Ca and Mg along traverse 1 of specimen 7-37 S3 by microprobe analysis. X axis shows the distance to the centre of the apical line (marked as zero in LA profiles).

A multi-element profile by electron microprobe along traverse 1 of specimen 7-37 S3 (Fig. 4.4 a), with a spot size of 10 µm and 8 µm step interval, is shown in Fig. 4.12. Magnesium decreases outwards to the middle of the transverse where it starts increasing and undulating severely towards the rim, this radial trend of Mg is already seen in the laser ablation (LA) profile of the same traverse. The concentration of Na is more stable than Mg, and varies in a narrow range of 1500-2000 ppm. Sr profile is very noisy, even the smoothed Sr curve using 5-spots average fluctuates between 1400 and 2500 ppm. There is no clear major radial trend seen in Sr. The profile of S shows large discrepancy with that of Fe, but good similarity to Mg profile.

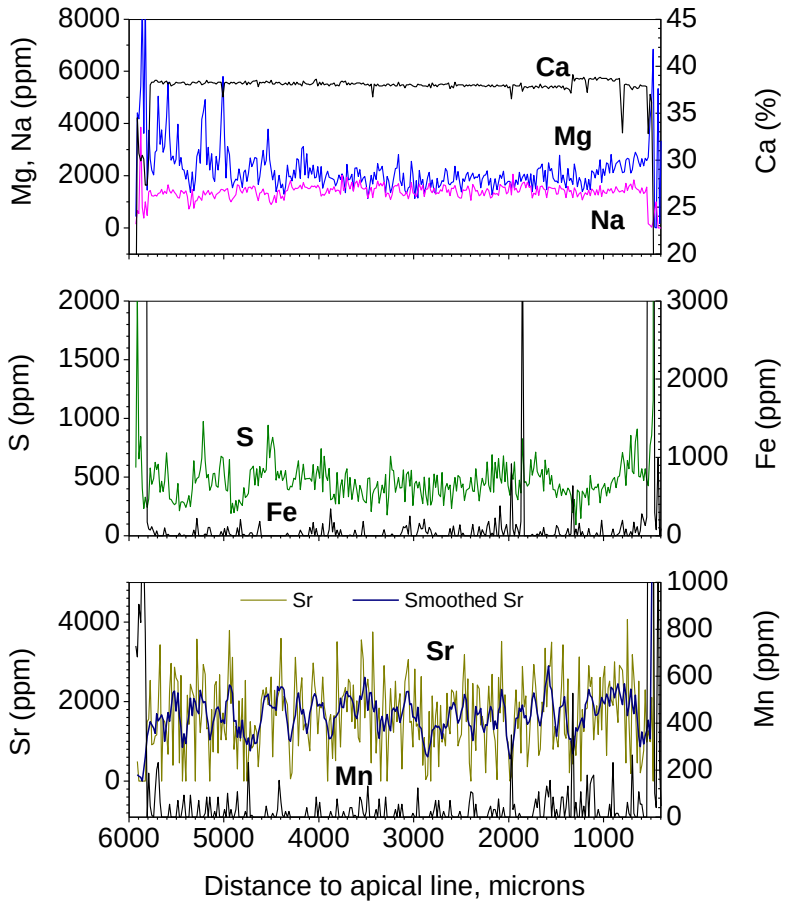

Fig. 4.12 Multi-element profiles obtained by electron microprobe along traverse 1 of *P.cuspidatus* specimen 7-37 S3. The smoothed Sr curve is plotted using five-spot averages.

Electron microprobe profiles of multi-elements along a short path perpendicular to the long traverse are plotted in Fig. 4.13. Concentrations in the traverse (shown as a red dashed box in Fig. 4.13) are similar to those in areas outside it. Only Na shows a decline of 1000 ppm in the red box, but the elemental compositions on each side of the track do not show any noticeable difference. These suggest that the high energy LA analysis has no effect on element concentrations in and on both sides of the traverse.

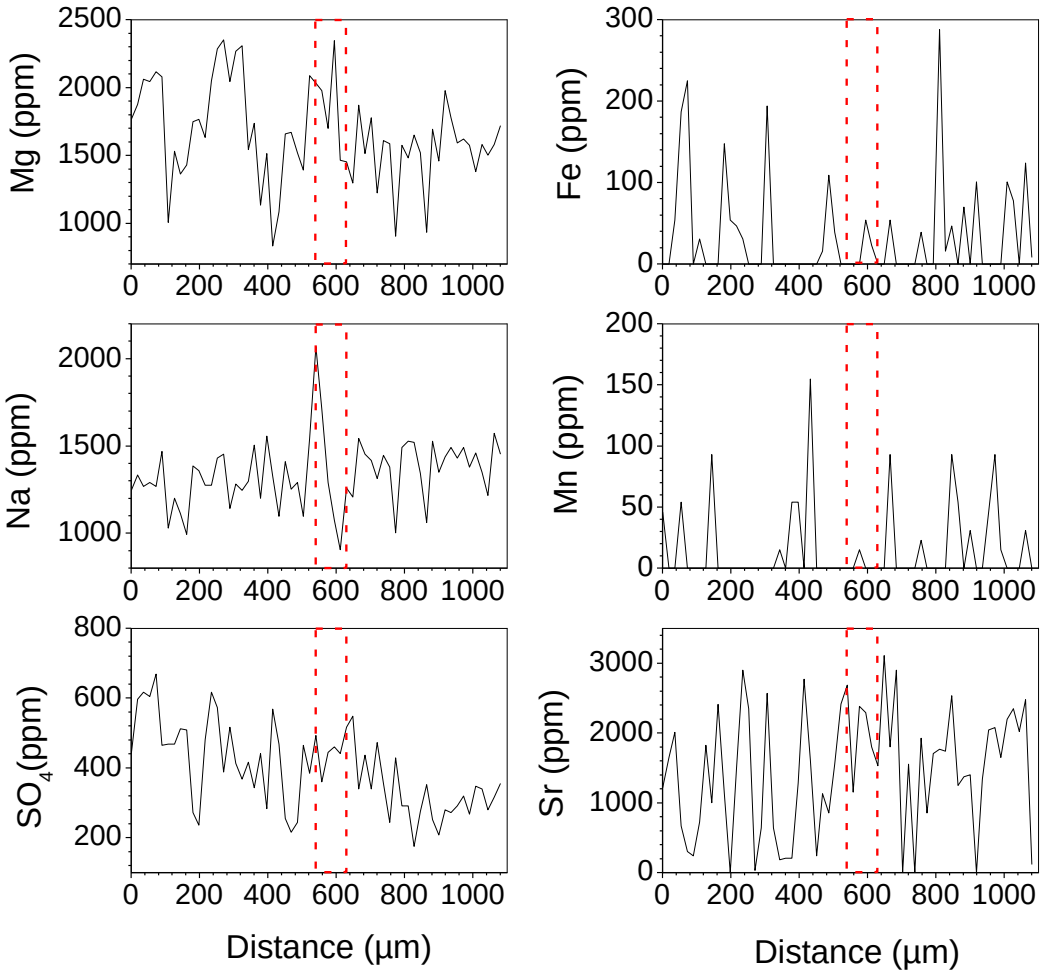

Fig. 4.13 The electron microprobe profiles of multi-elements in sample 7-37 S3 along a short path perpendicular to the long traverse 1. The red hollow boxes mark the area in traverse 1.

Fig. 4.14 The short electron microprobe path shown in white color. The two black lines mark the two radial traverses.

4.3.4 Comparison between LA and EMP profiles

Multi-element profiles by LA-ICP-MS and EMP along the same traverse of specimen 7-37 S3 are shown in Fig. 4.15. Profiles of Ca, Mg and Na show good comparability and similar radial trends between the two approaches, although LA profiles seem to give slightly higher concentration values. EMP profile of Sr and the smoothed Sr curve (pruned of short-ranged anomalies constituting 3-5 analyses) undulate highly, whereas the Sr profile of LA analysis is smooth and stable. The signals of Fe and Mn from EMP analyses are much noiser and higher than LA results.

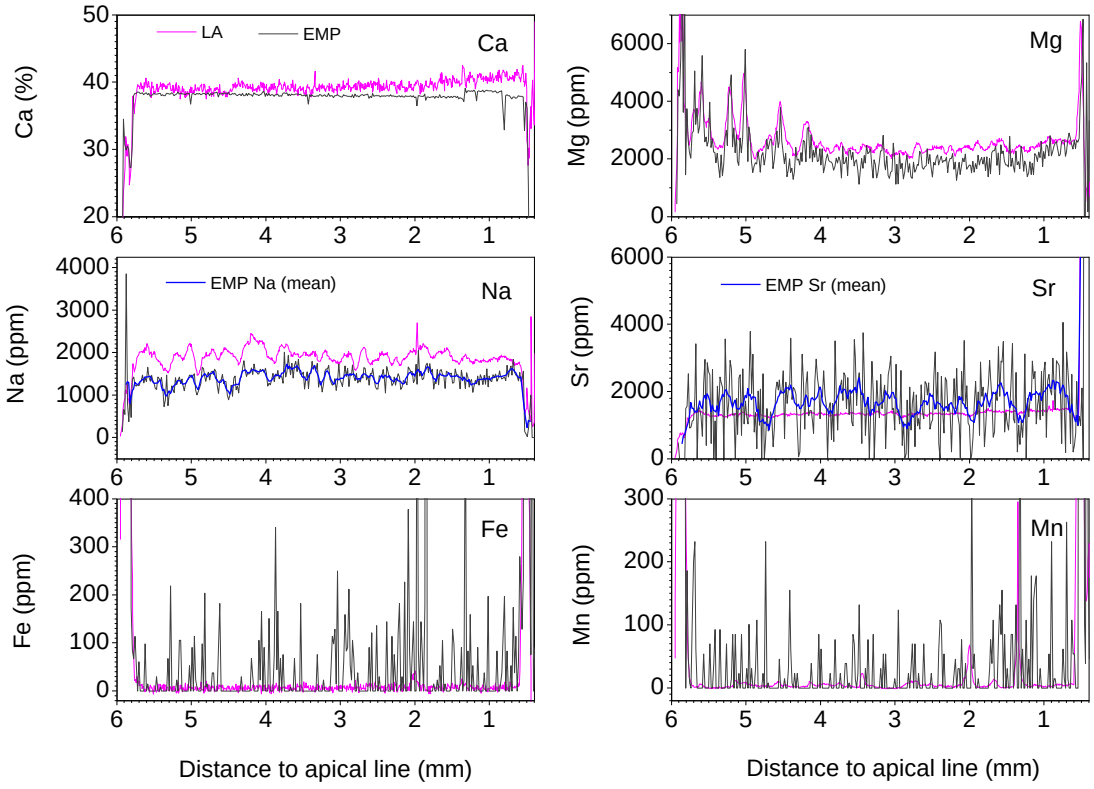

Fig. 4.15 Concentration profiles of sample 7-37 S3 by LA-ICP-MS and electron microprobe. LA – laser ablation, EMP – electron microprobe. The blue curves give 5-spot averages of the electron microprobe data.

For S, the LA profile of S intensity was compared with the EMP profile of S concentration because the running standard NIST 612 during LA measurements has no published value of its S concentration that can be used to calculate S content in samples (see equation (2-1) in chapter 2). The two profiles are broadly comparable, and line up better in the inner half than the outer half of the sample section. A big

difference between them lies in the interval of 4.2 to 5.6 mm, in which the intensity peaks line up with concentration troughs (Fig. 4.16).

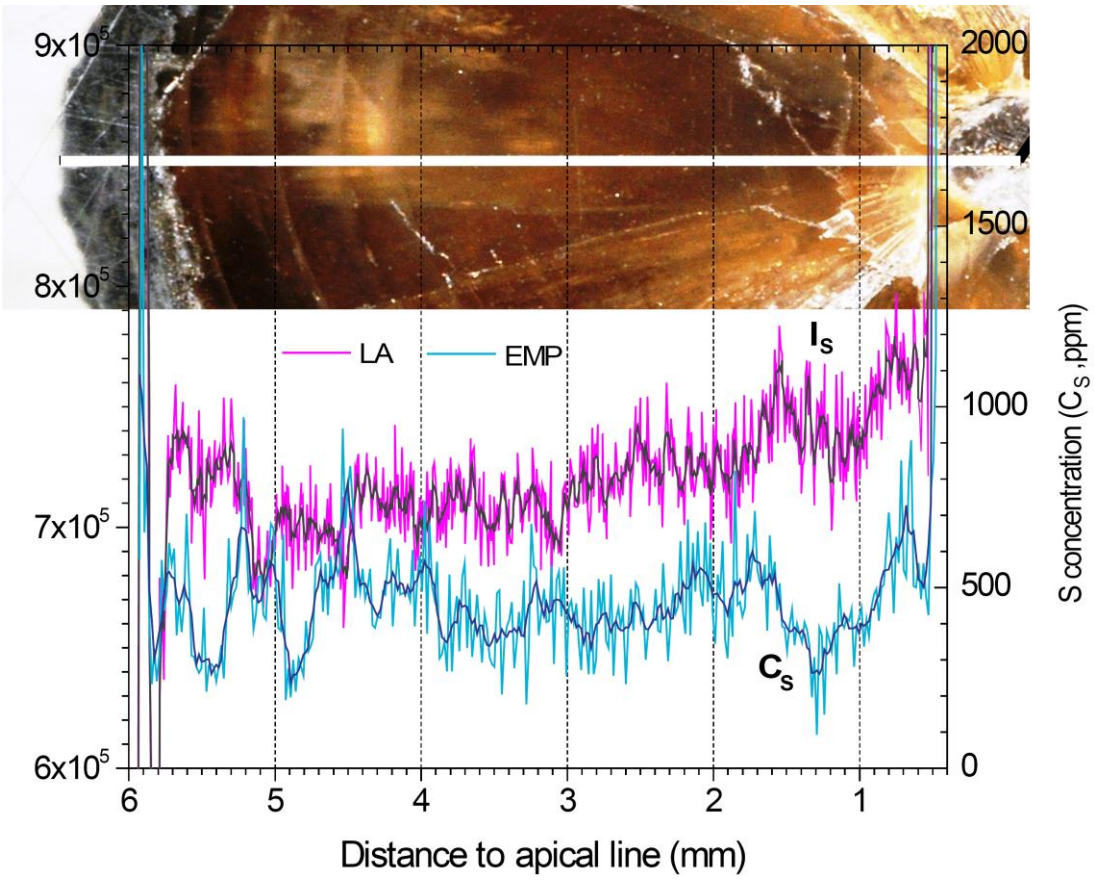

Fig. 4.16 The comparison of intensity profile of S obtained from LA-ICP-MS (LA) with S concentration profile produced by electron mirco-probe (EMP) along traverse 1. I_S – Intensity of sulphur, C_S – Concentration of sulphur. Smoothed curves are 5-spot averages of S intensity and concentration.

4.3.5 Bulk chemical analysis

The data of elemental and isotopic compositions of picked fragments of Pliensbachian belemnites are presented in Fig. 4.17 to Fig. 4.19 and Appendix C. Most samples contain < 30 ppm Fe and < 20 ppm Mn (Fig. 4.17). The content of S varies from 140 to 1400 ppm, and Ba ranges from 1 to 4 ppm. No correlation is seen between S and Fe (Fig. 4.17).

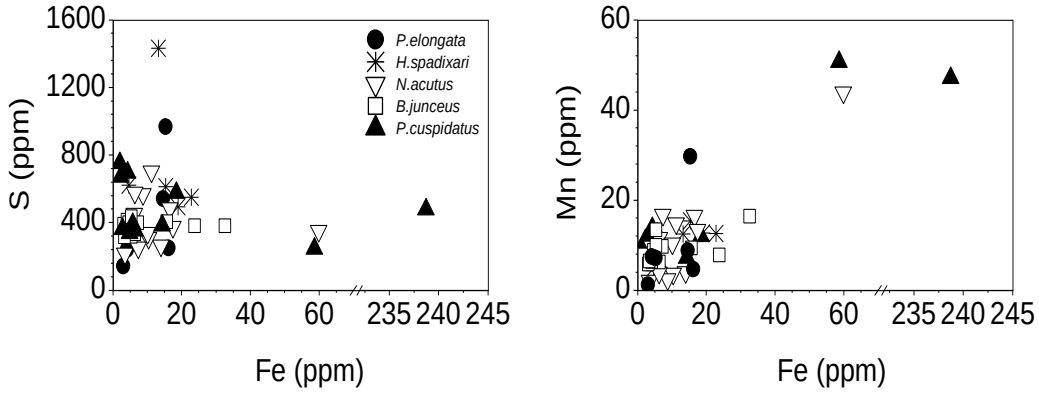

Fig. 4.17 Crosss-plots of concentrations of Fe against S, and Fe vs. Mn in the Pliensbachian belemnites from Dorset.

The isotopic ratios of specimens vary from -0.73 to +3.36 ‰ in $\delta^{13}C$ and from -2.00 to -0.48 ‰ in $\delta^{18}O$ (‰), respectively. The isotopic compositions do not differ much between species. The variations in $\delta^{13}C$ are much larger than in $\delta^{18}O$, and there are no clear correlation between $\delta^{13}C$ and $\delta^{18}O$ (Fig. 4.18). Specimens of *P. cuspidatus* tend to have higher $\delta^{13}C$ whereas *N. acutus* specimens seem to be lower in $\delta^{13}C$; but their $\delta^{18}O$ overlaps. The other three species (*B. junceus*, *P. elongata* and *H. spadixari*) fall in the composition areas of the above two species. They reflect less compositional variations and overlap with each other (Fig. 4.18).

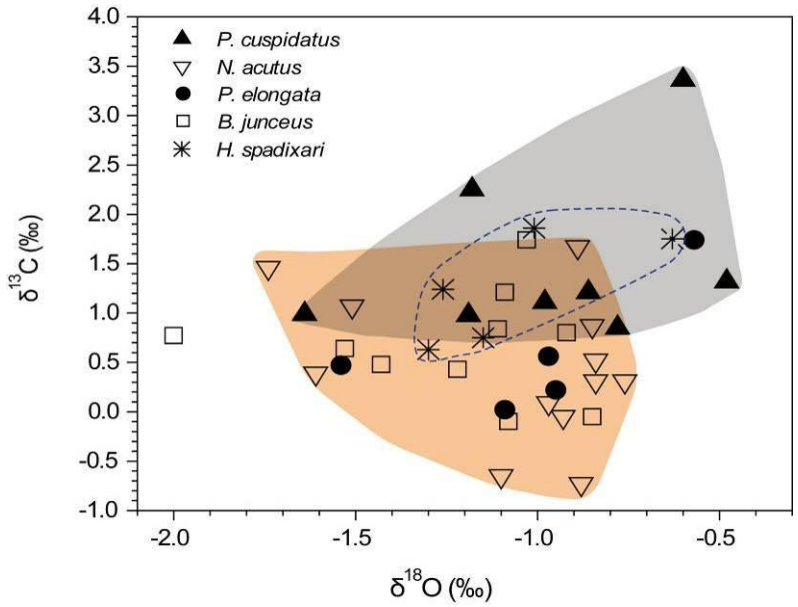

Fig. 4.18 Isotopic compositions of 5 belemnite species of Pliensbachian age from Dorset. The compositional ranges of *P.cuspidatus* and *N. acutus* are highlighted in grey and orange. The composition of *H. spadixari* specimens fall in the dashed area.

For elemental composition, specimens of *P. elongata* and *B. junceus* show a slightly wider spread of Na/Ca, Mg/Ca and Sr/Ca ratios, whereas specimens of *P. cuspidatus* and *N. acutus* appear to have narrower ranges of elemental compositions; and the variations of Na/Ca, Mg/Ca in *H. spadixari* fall in between (Fig. 4.19). *P. cuspidatus* likely possesses higher Na/Ca and Sr/Ca, whereas most of *P. elongata* specimens give lower Mg/Ca. For all the five species, Mg/Ca ratios do not reflect a significant correlation with $\delta^{18}O$, and neither do Sr/Ca values. Na/Ca correlates well with Sr/Ca ($r = 0.67$, $n = 46$ and $P < 0.001$, Fig. 4.19).

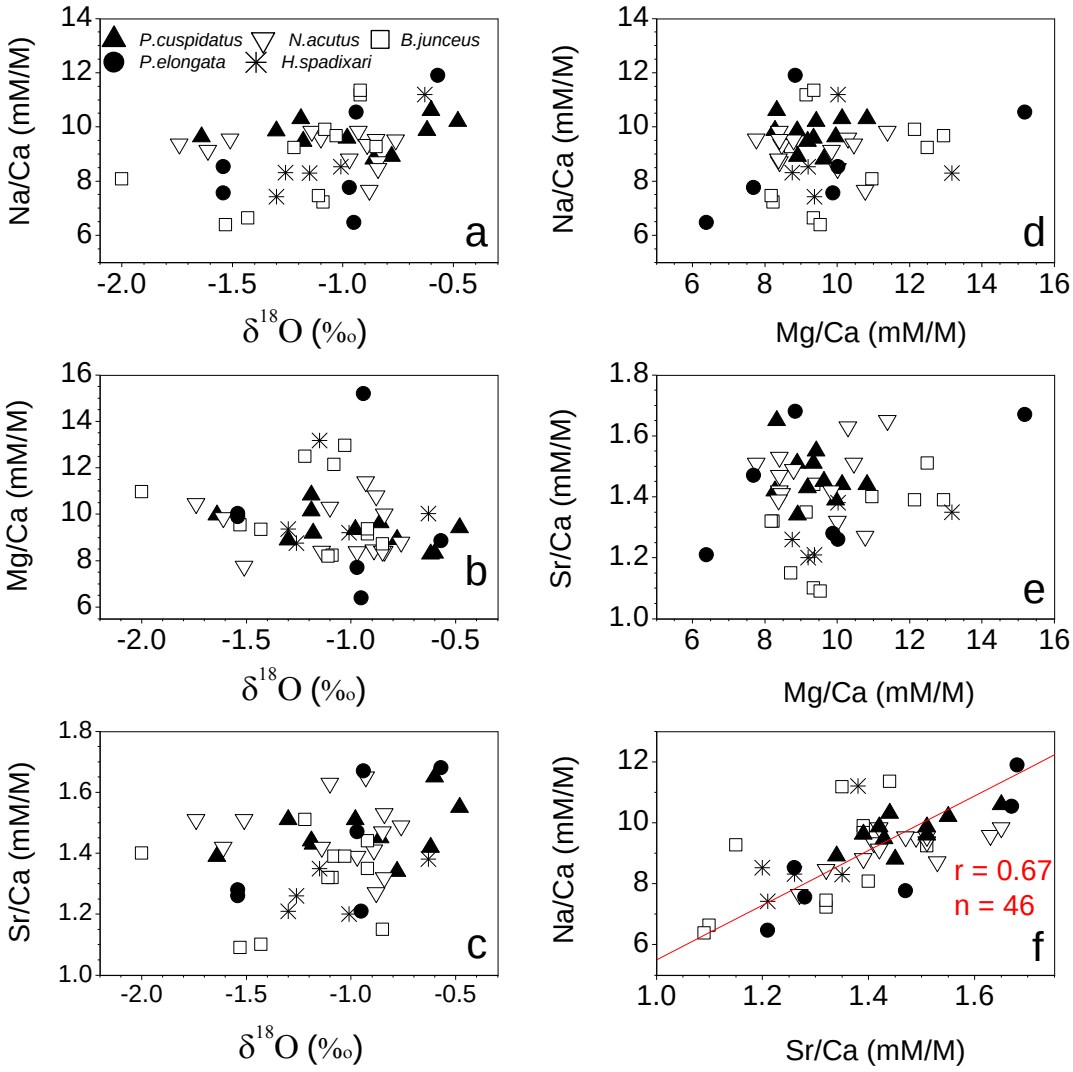

Fig. 4.19 Cross-plots of elemental and isotopic compositions. The reduced major axis (RMA) regression lines of all the data are present in graphs f.

4.4 Discussion

4.4.1 Methodology validation

In order to interpret the belemnite data properly, the two analytical methods (laser ablation and electron microprobe) used to obtain cross-sectional profiles of concentrations in belemnites are validated first in Fig. 4.15. Radial profiles of elements, obtained by electron microprobe (EMP) and LA-ICP-MS, were compared for a specimen of *P. cuspidatus* (7-37 S3). The LA data of Ca are slightly higher than EMP values and reflect a small increase from edge to core, whereas EMP Ca profile remains flat in most areas of the section. This is probably due to the calibration and sensitivity difference between the two instruments. The big jump of Ca around 1340 µm was caused by the drift-correction of the electron beam which gradually went off the track during the analysis, and the large drop at 800 µm is likely to reflect a surface fracture near the apical line. When taking the above explanation into account, Ca concentrations from LA and EMP agree well. For Mg and Na, the microprobe traverses present same variation patterns and major trends to the LA data, and the only difference between the two methods is that LA tends to give higher values. Considering that the beam size of LA is 5 times larger than that of EMP, the higher LA signals may be caused by larger analysis volume. Accordingly, both methods work well for Ca, Mg and Na.

Since Sr in these belemnites (~1000 ppm) is around the detect limit of electron microprobe, the big noise in EMP profile is no surprise. As to Fe and Mn, the high peaks of Fe and Mn in EMP profiles reflect very small-scale alteration that is averaged and cannot be shown in large analysis volume taken by LA. However, the purpose of measuring Fe and Mn is to indicate alteration areas, rather than alteration spots, so the less noisy LA data surely serve this purpose better. Therefore, LA analysis is more indicative for Sr, Fe and Mn in this study.

For S, electron microprobe is more sensitive than LA. The disagreements between them (Fig. 4.16) are likely to be attributed to differing analysis resolution and mass interference encountered in LA-ICP-MS. The double oxygen ($^{16}O^{18}O$) in the plasma of LA-ICP-MS has the same mass as sulphur ^{34}S, thus impairing the precision of measurements of ^{34}S intensity. Also, different standards and calibrations are used in

the two methods; strict comparability between the two profiles would therefore not be expected.

The method comparison has proved that LA works well for all the above elements except S, and is especially better for Sr, Fe and Mn than EMP. So, in the following sections, the LA profiles of major elements Ca, Mg, Na, Sr and trace elements Fe, Mn (and Zn) are the focus in the discussion sections.

4.4.2 Sample preservation and alteration

4.4.2.1 Alteration Indicators

The elements incorporated into the belemnite calcite structure can be divided into two phases (Table 4.3). Among all the measured elements (apart from Ca), Na, Mg, and Sr are in the structural phase as they are able to substitute for Ca in the calcite crystal structure. The detrital phase includes Mn, Fe, Rb, Y, Ce, Pb, Th, U, which are insoluble and form solid contaminant particles absorbed in altered areas of belemnite rostra. Mn^{2+} and Fe^{2+} also substitute for Ca^{2+}, but they are mobile only under post-oxic or anoxic conditions and so indicate alteration. Zinc and barium are likely to appear in both structural and detrital phases, so can indicate either structural substitution of calcium or small-scale detrital contamination. Low concentrations of Ba (<2 ppm) in the well-preserved parts of many rostra suggests that it is present dominantly as structural substitution of Ca, but the occasional Ba spikes reflect that Ba also occurs as barite inclusions at a fine scale of <20 µm (Fig. 4.21 & Fig. 4.26).

Table 4.3 Elements and the formation in belemnite calcite.

Phases	Elements	Formation
Structural	Ca, Na, Mg, Sr, SO_4^{2+} ?	Na_2CO_3, $SrCO_3$, $CaMg(CO_3)_2$
Detrital	Mn, Fe, Rb, Y, Ce, Pb, Th, U	FeS_2, MnO_2, RbO_2 , CeO_2
Both	Zn, Ba	$ZnCO_3$, ZnS_2, $BaSO_4$

In the elemental profiles (e.g. Fig. 4.10, Fig. 4.12 & Fig. 4.20), concentration anomalies are common at the rim and apical line. Mn and Fe are picked to indicate alteration in this study. Although marine invertebrates contain Fe as a metabolizable

element, high concentration of Fe (>30 ppm) and Mn (>10 ppm) in living organisms are toxic (Miramand and Bentley, 1992); and therefore the excessive Fe and Mn should come from diagenetic fluids after the death of marine animals. Mn and Fe peaks present at the exterior and apical line should then indicate they are diagenetically altered areas. Therefore, only areas in between are taken into account when discussing radial variations in composition and major radial trends in elemental profiles.

Manganese and iron reflect different alteration conditions. Manganese refers to alteration under Mn-reducing conditions which precedes Fe-reduction. So, Mn and Fe peaks do not necessarily coexist in LA profiles. Yttrium and Ce were found to show the major alteration signals that were also obtained from Mn and Fe, but at much smaller magnification due to their low environmental abundance relative to Fe and Mn. Their concentrations in belemnites are only around sub-ppm level in well-preserved parts and no higher than a few ppm in altered regions. They are only supplementary alteration indicators to further support Fe and Mn signals. Lead (Pb), Th and U and Rb are of no use for defining alteration areas. This is because the first three elements show extremely low-amplitude variations and Rb has flat signals.

4.4.2.2 Growth Boundaries

Concentric growth boundaries are visible in many cross sections, particularly near the rim and/or core where alteration has taken place. The variations in colour, thickness and form of the growth boundaries are not species-specific, but depend on the chemistry of diagenetic fluids and preservation degree of the samples. Diagenetic fluids containing high Mn and/or Fe can darken the precipitated secondary calcite bands in growth boundaries; and high degree of alteration can also thicken growth boundaries (*e.g. H. stonebarroesis* 7-86 S3 in Fig. 4.9).

4.4.2.3 Small-scaled Alteration in Well-preserved Parts of a Rostrum

Manganese peaks reveal alteration over scales from 50 to a few hundred µm in the largely clear calcite areas of most specimens. Small to large scale alteration implied by Mn seems to mildly affect the concentrations of Na, Mg and Sr (*e.g.* Fig. 4.10 to Fig. 4.21). Local alteration is also indicated by the fine-scale spikes in Zn and Ba

profiles in specimens of *P. cuspidatus*, *N. acutus*, *B. junceus* and *P. elongata*. These peaks probably indicate inclusions of diagenetic sulphide (e.g. ZnS_2) and barite ($BaSO_4$). This study shows that small scale alteration occurs even in well-preserved belemnites, which should be considered when interpreting concentrational variations within belemnite rostra.

4.4.2.4 Sample Preservation

The LA and EMP analyses confirm that belemnites in this study contain large proportion of pristine areas in their rostra, but are altered along the apical line, concentric growth boundaries and on the exteriors. The conclusions are supported by: 1) calcium shows a constant concentration along most part of the profile on a belemnite section, indicating a high degree of preservation of pure calcite; and 2) low concentrations of alteration indicators (e.g. Fe, Mn and possibly Ba) and typical major elemental (Na, Mg, Sr) compositions along most the regions of the sections demonstrate that the specimens are little altered. Hence, the geochemical signals they preserve should retain closely the primary palaeo-environmental conditions of their living niches.

4.4.3 Belemnite Mg profiles: In comparison to foraminiferal Mg/Ca

The Mg profiles, although at different variation degree, show a radial trend of 'high – low – high' Mg variation (termed a bowl-shaped pattern) in 5 of the analyzed 6 species, *P. cuspidatus*, *N. acutus*, *B. junceus*, *H. stonebarroensis* and *H. spadixari* (Fig. 4.20 to 4.33). Magnesium signals (or Mg/Ca ratios) are not considered to only reflect calcification temperature for these samples because the Mg/Ca ratios of them from bulk analysis do not show a significant correlation with $\delta^{18}O$ values (shown in Fig. 4.19 b and explained later in 4.4.5.3). In order to properly interpret belemnite Mg profiles in terms of lifestyle, belemnite Mg/Ca is compared with that of modern calcifying organism foraminifera, which have been intensively studied for Mg/Ca seawater thermometry and controls on their Mg/Ca composition.

Although temperature is well-known as a primary control on Mg/Ca ratios in biogenic calcite (Chave, 1954), for example, in foraminifera (Lea *et al.*, 1999), culturing experiments show that the foraminiferal Mg/Ca temperature dependency is

species-specific; depth, seawater PH or carbonate ion composition, and salinity might also influence shell Mg/Ca (Lea *et al.*, 1999; Eggins *et al.*, 2004; Russell *et al.*, 2004; Huber, 2008).

High resolution profiles of Mg/Ca in foraminiferal *Orbulina universa* (*O. universa*) indicate that the amplitude of Mg/Ca variations within individual foramilifers would require improbably, large changes in habitat depth that extend well below acceptable habitat for *O. universa*, and that the Mg/Ca deduced calcification temperature range during growth exceeds the maximum temperature range within the euphotic zone habitat of *O. universa* (Eggins *et al.*, 2004). Therefore, factors additional to temperature must control the Mg/Ca ratios in *O. universa*. Changes in the biological activity of foraminifera (specifically the symbiont photosynthesis and respiration) are shown in theoretical models to modify the seawater PH at the surface of planktonic foraminifera, which then causes the change in calcite saturation state and thus the change of calcification rate in *O. universa* (Spero, 1988; Rink *et al.*, 1998; Wolf-Gladrow *et al.*, 1999; Eggins *et al.*, 2004). It is also conceivable that Mg/Ca composition in foraminifers could be influenced by variations in light intensity with latitude, season; and/or depth within the euphotic zone, or variations in the vitality of foraminifers and their algal symbionts and impact on photosynthetic activity and respiration (Eggins *et al.*, 2004).

A number of foraminiferal species (e.g. *Globigerinoides sacculifer, G. conglobatus, Orbulina universa, Neogloboquadrina pachyderma, N. dutertrei and Globorotalia* spp.) are known to deposit an additional layer of calcite on the outside surface of their shells (e.g. Be *et al.*, 1983; Hamilton *et al.*, 2008). The calcite crust is associated with the transition from normal ontogeny to the reproductive phase of these species at the end of their life cycle and is called gametogenic calcite. Calcification can occur under varying environmental and physiological conditions as a foramenifer matures and slowly sinks across different depths in its photic zone habitat range. Ontogenetic calcification occurs throughout the lifespan of a species, whereas gametogenic calcification occurs following the cellular structure reorganization at the very end of its life cycle over a short period of time, and so is totally biologically controlled. The two calcite phases would surely reflect different calcification rates and geochemistry (e.g. isotopic and elemental compositions).

Foraminifera ontogenetic Mg/Ca seems to suggest a connection between Mg/Ca variations and changes in ontogeny and growth rates that may be associated with aging or sinking into deep water. In comparison to foraminifera, Mg/Ca composition in belemnites is also likely to be affected by factors other than temperature. Belemnites were likely to be nektonic-nektobenthic and lived over a few hundred meters of depths in the shelf seas of Jurassic and Cretaceous time. Mg/Ca ratios in belemnites are species-dependant and changes in the metabolic activities during ontogeny might also change the calcification rate (or growth rate) in belemnites. The Mg profiles of belemnites may reveal changes in ontogeny (e.g. metabolic activities) and the growth rate that may be associated with migration and changes in their living habits. The 'high – low – high' Mg trend is then speculated to reflect a life style that involves a fast length-growing in early ontogeny, a follow-up slow growth in adolescence-adulthood, and then a quick fattening adulthood associated with physiological maturity.

4.4.4 Compositional profiles within and between species: Mg, Na & Sr

The elemental profiles (Fig. 4.10, Fig. 4.20 - Fig. 4.33) show variation patterns along two transverses, each of which covers the area between the edge/rim and the centre/core. The edge is the exterior of a cross-section. It is not well-preserved, but clearly identified by high Mg peaks. The centre is the round apical line area that shows distinct alteration signals (e.g. extremely low Ca but high Mn, Fe, etc.) from the adjacent areas. In this section, the radial trend of the profiles is discussed because the two traverses on a sample section show similar compositional variation patterns for each element.

The profiles of Na, Sr and Mg show different variations and radial trends in each species. This may be because the sensitivity of the three elements to temperature changes and/or alteration is different; this may also show differing bio-fractionation on different elements (McArthur *et al.*, 2007b). The detailed comparison of compositional profiles (mainly Mg/Ca, Na/Ca and Sr/Ca) at species division is provided, and the possible reasons for these differences discussed beow.

4.4.4.1 For P. cuspidatus

For *P. cuspidatus,* magnesium in two specimens (7-35 S3 in Fig. 4.20 and 7-74 S3 in Fig. 4.21) shows a mid-rostral minimum, but the trend is not seen in the third specimen (7-37 S3 in Fig. 4.10). Samples 7-35 S3 and 7-74 S3 are believed to preserve in substantial parts the original geochemical features of the seawater they once lived in; and the radial pattern of a mid-rostral Mg minimum then implies a lifestyle through ontogeny, including a fast growing early life, a slow growing middle period and finally an increased growth that may be associated with physiological maturity for reproduction.

The third *P. cuspidatus* specimen 7-37 S3 show that Mg is smooth and flat along the inner 2/3 of the transverse but undulates intensively in the outer 1/3 of the rostrum (Fig. 4.10). Over a scale of ~ 50 μm, the Mg peaks line up well with the optically light bands of growth boundaries in the section, but no Mn and Fe spikes appear to match them (Fig. 4.10). The light coloured bands are composed of secondary calcite precipitated from diagenetic fluids that had no Fe to form dark coloured minerals (such as Fe oxide or/and pyrite). The lack of noticeable Fe peaks in the corresponding positions from the concentration profiles confirms the above explanation. The Mg wiggles near the rim in sample 7-37 S3 are likely related to the diagenetic alteration in the zones of growth boundaries. The big difference in Mg between 7-37 S3 and the other two samples cannot be reasonably interpreted due to the missing of the very tiny area of apical line. It may be attributed to the difference in the fine scale preservation degree or a gender difference. As Na undulations are seen to follow Mg variations generally well, the high undulations in Na close to the rim of 7-37 S3 should have the same origin of Mg ones.

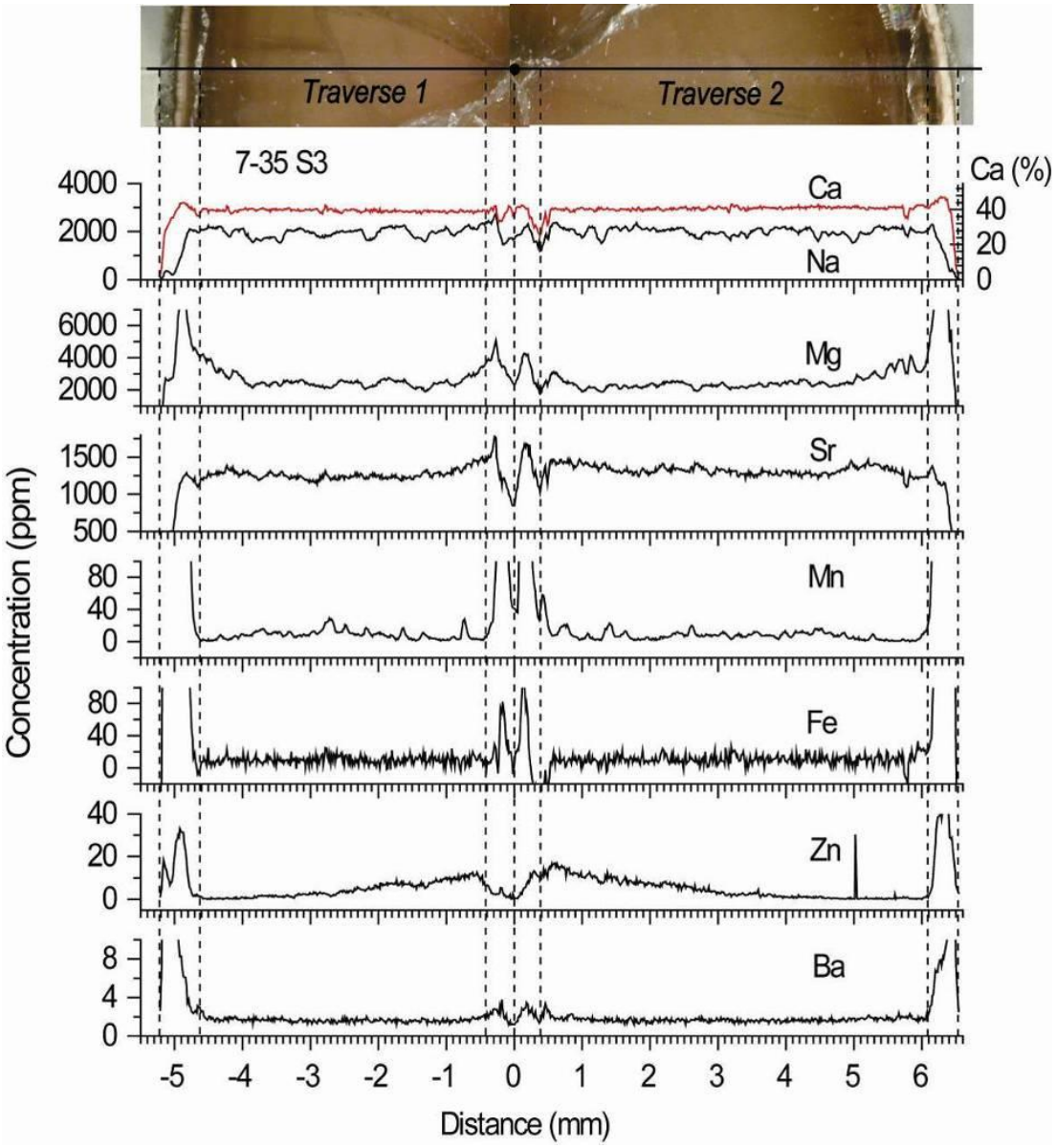

Fig. 4.20 Multi-elemental profiles (Ca, Na, Mg, Sr, Mn, Fe, Zn and Ba) of *P. cuspidatus* specimen 7-35 S3 obtained by LA-ICP-MS. The areas enclosed within the dotted lines are altered regions; and therefore, are excluded in palaeotemperature reconstructions.

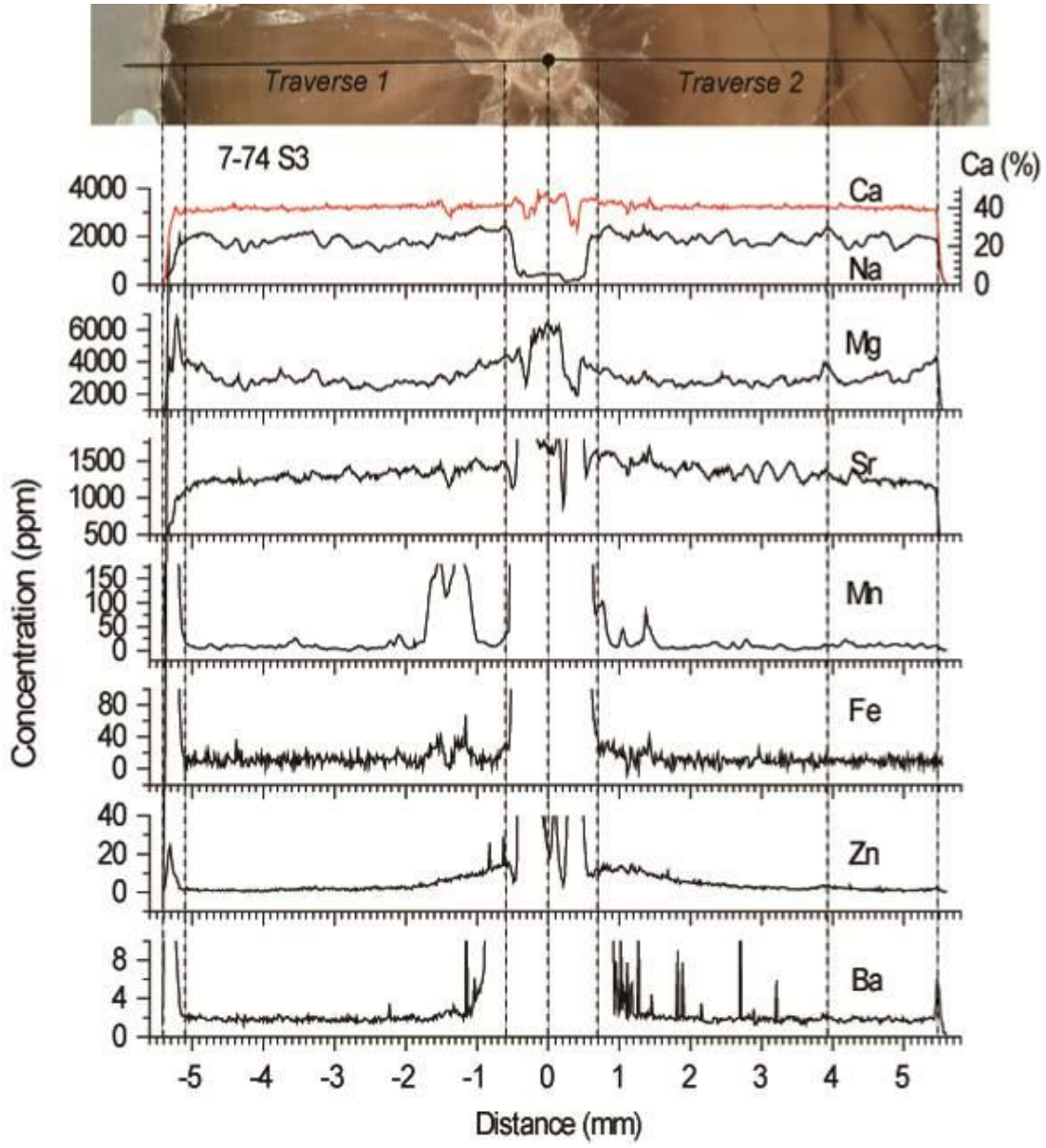

Fig. 4.21 Multi-elemental profiles (Ca, Na, Mg, Sr, Mn, Fe, Zn and Ba) of *P. cuspidatus* specimen 7-74 S3 obtained by LA-ICP-MS.

4.4.4.2 For N. acutus

Sample 7-71 S3 and 7-72 S3 both display low Mg in the middle and high Mg close to the core and the edge (Fig. 4.23 to Fig. 4.24), whilst 7-61 S3 shows a flat Mg pattern along most of the traverse and an increase in the outer part (Fig. 4.22). This is simply because the innermost part of ~ 0.8mm (Fig. 4.22) is missing on this section. Mg profiles in many specimens indicate that it is always the innermost 1/4 to 1/3 part of the rostra that witnesses a sharp increase towards the cetnre. Had the section been cut at the base of alveolus, it would have preserved the beast's

childhood and shown the resembling bowl-shaped trend in Mg as seen in 7-71 S3 and 7-72 S3. Mg profiles of them show less pronounced bowl patterns than those of *P.cuspidatus* specimens, and are thought to likely represent smaller ontogenetic changes and narrower migratory ranges than *P. cuspidatus*.

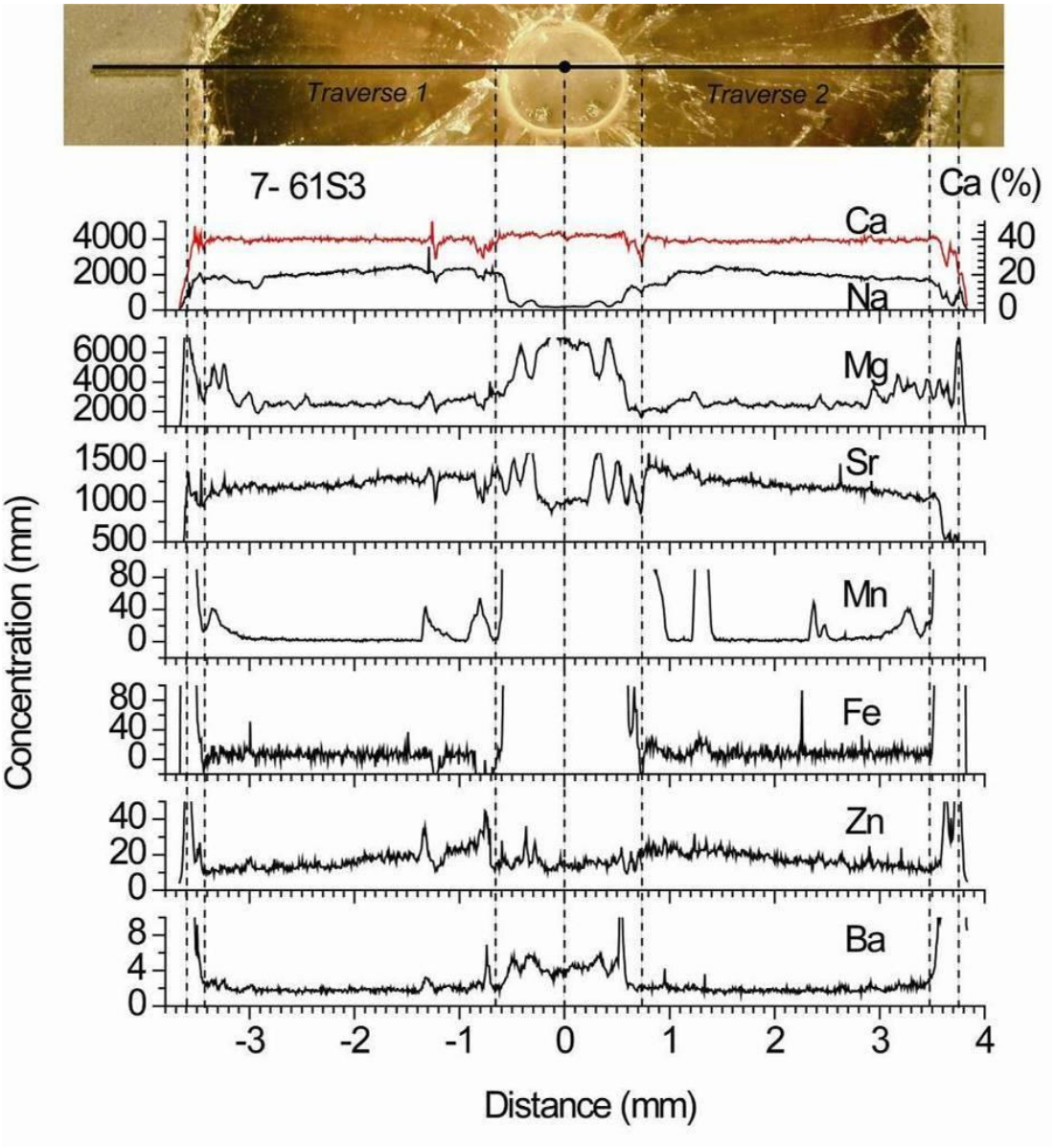

Fig. 4.22 Multi-elemental profiles (Ca, Na, Mg, Sr, Mn, Fe, Zn and Ba) of *N. acutus* specimen 7-61 S3 obtained by LA-ICP-MS. The section is not cut at the base of the alveolus, so a round alveolar area, not a small spot of protoconch (see Fig. 1.1 for belemnite body structure), is shown in the picture.

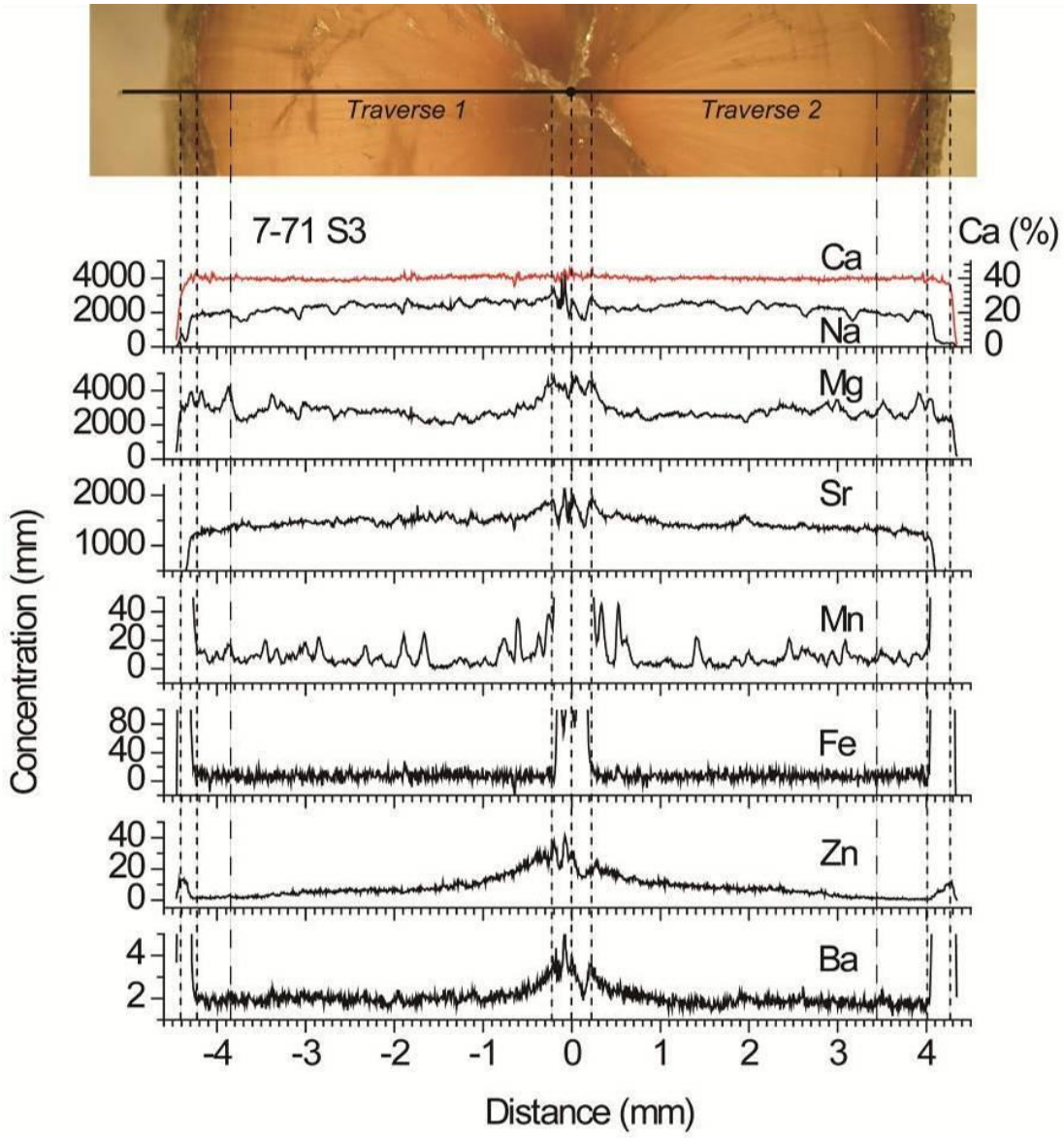

Fig. 4.23 Multi-elemental profiles (Ca, Na, Mg, Sr, Mn, Fe, Zn and Ba) of *N. acutus* specimen 7-71 S3 obtained by LA-ICP-MS. Long-dashed lines mark the visible rings in the cross-section of the specimen.

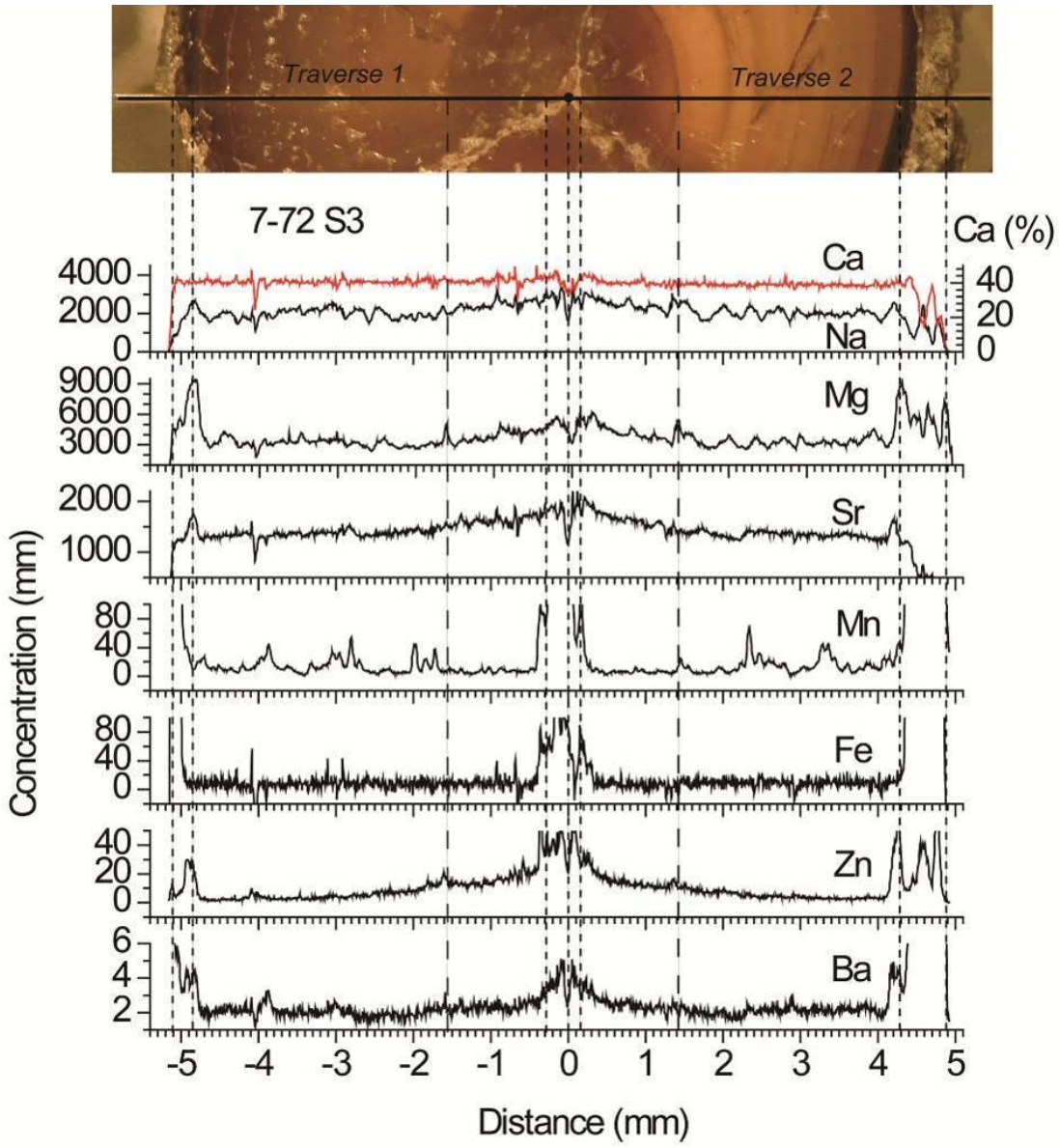

Fig. 4.24 Multi-elemental profiles (Ca, Na, Mg, Sr, Mn, Fe, Zn and Ba) of *N. acutus* specimen 7-72 S3 obtained by LA-ICP-MS. Long-dashed lines mark the visible rings in the specimen.

4.4.4.3 For B. junceus

The two cross-sections were sliced slightly above the base of the alveolus, so a small rounded alveolar area is present (Fig. 4.6). Despite that the innermost part (theoretically recording the chemistry of the early ontogeny) is missing, each traverse section can still provide the most of the information relevant to growth.

In the non-altered regions of the profiles, the shallow plate-shaped radial trend of Mg profiles (Fig. 4.25 & Fig. 4.26), seems to suggest that these two *B. junceus* specimens experienced limitted changes in growth rate and living habits during

ontogeny, but more complete sections of *B. junceus* samples are needed for testing their real life style. The abnormal troughs of Na and Sr close to the apical line area line up with Mn and Fe peaks, reflecting small effect of alteration in cracks on them over a scale of 200 µm (Fig. 4.25 & Fig. 4.26).

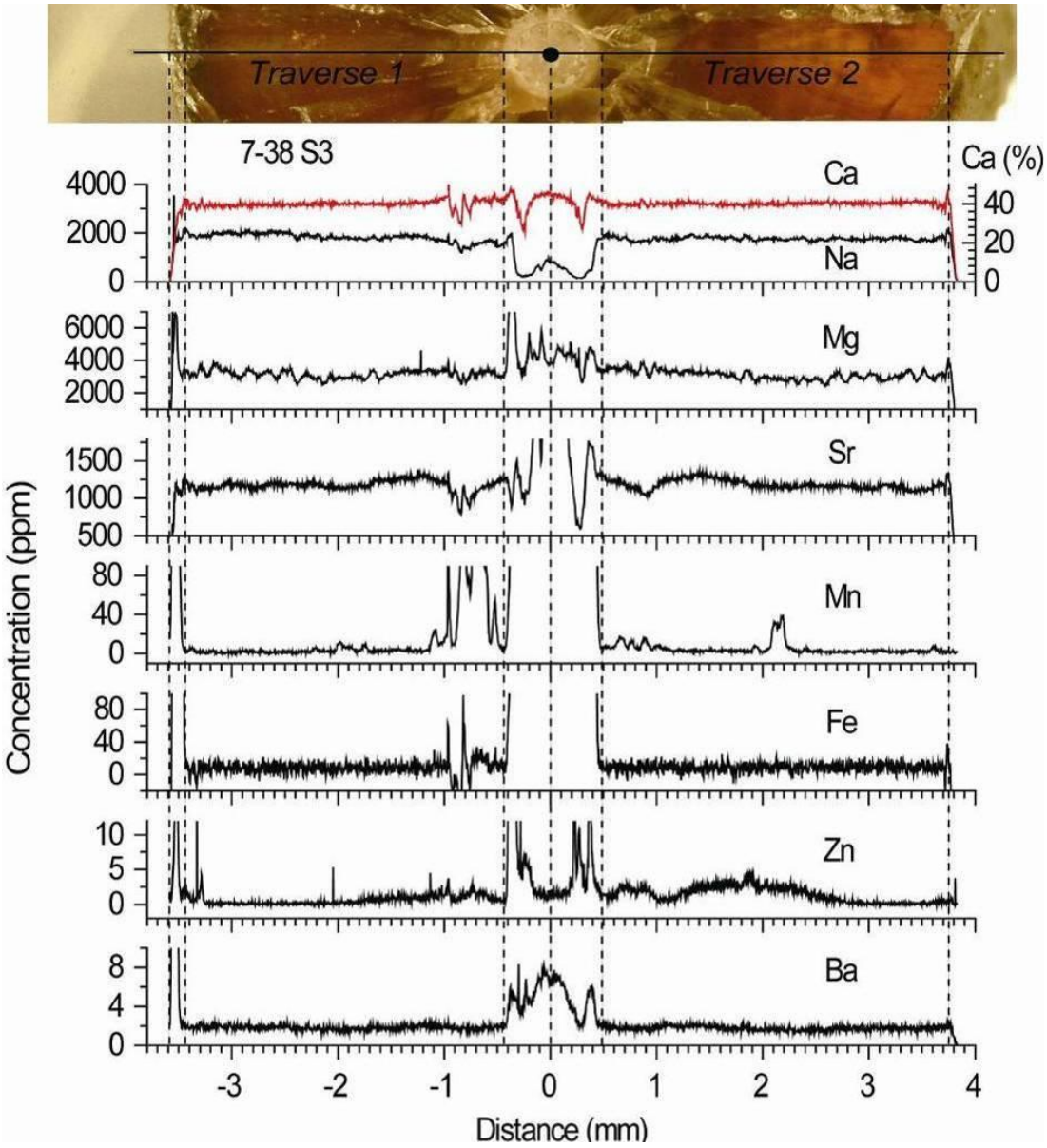

Fig. 4.25 Multi-elemental profiles (Ca, Na, Mg, Sr, Mn, Fe, Zn and Ba) of *B. junceus* specimen 7-38 S3 obtained by LA-ICP-MS.

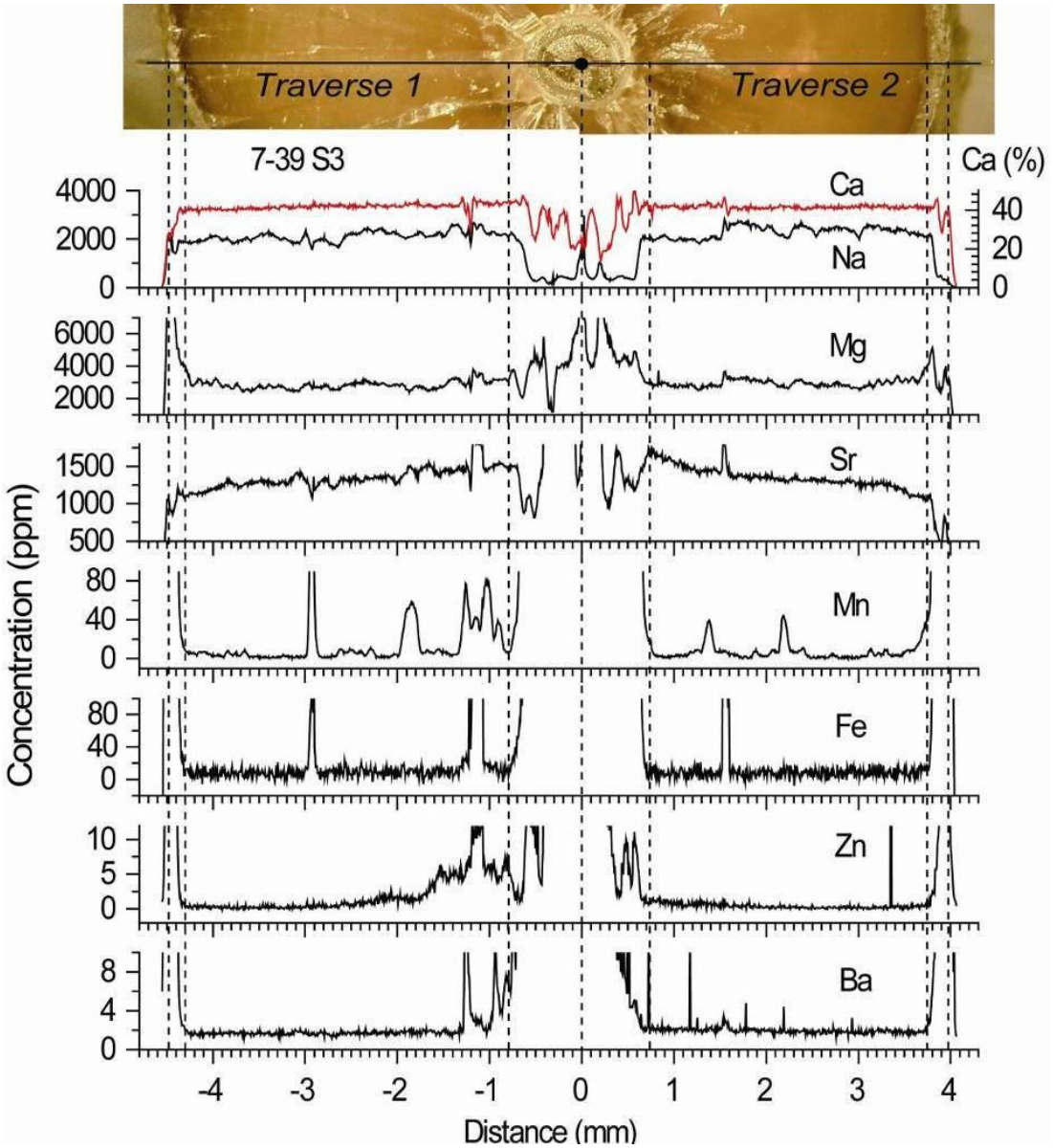

Fig. 4.26 Multi-elemental profiles (Ca, Na, Mg, Sr, Mn, Fe, Zn and Ba) of *B. junceus* specimen 7-39 S3 obtained by LA-ICP-MS.

4.4.4.4 For genus Hastites

For all the specimens of genus *Hastites*, the inner 1/3 area (commonly bounded by the inner growth boundary) of the sections witnesses greater increases in Na, Mg, Sr (and /or Zn and Ba) inwards than the outer parts of a cross-section. These belemnites had presumably grown very fast and continued precipitating growth increments of calcite when they were juveniles (probably living in warm shallow water where energy and nutrition were good for growth). This is very similar to modern cuttlefish. Thereafter, they migrated laterally or vertically, and grew at a slower pace perhaps due to the shortage of food and energy. The change of growth pace is reflected by

the change of optical continuity between the inner fast and outer slow growth regions on cross sections (e.g. Fig. 4.29 - Fig. 4.31).

The two species *H. stonebarroensis* and *H. spadixari* of genus *Hastites* both present bowl-shaped Mg profiles, but with some complexity and variations between specimens. For specimens of *H. spadixari* (7-68 S3, Fig. 4.27) and *H. stonebarroensis* (7-77 S3, Fig. 4.28), the bowl-shaped Mg concentration pattern is very similar to that seen in species *P. cuspidatus* and *N. acutus*. The Mg signal of later life is possibly overprinted by mild diagenetic alteration which gives small Mg peaks on top of the primary signal.

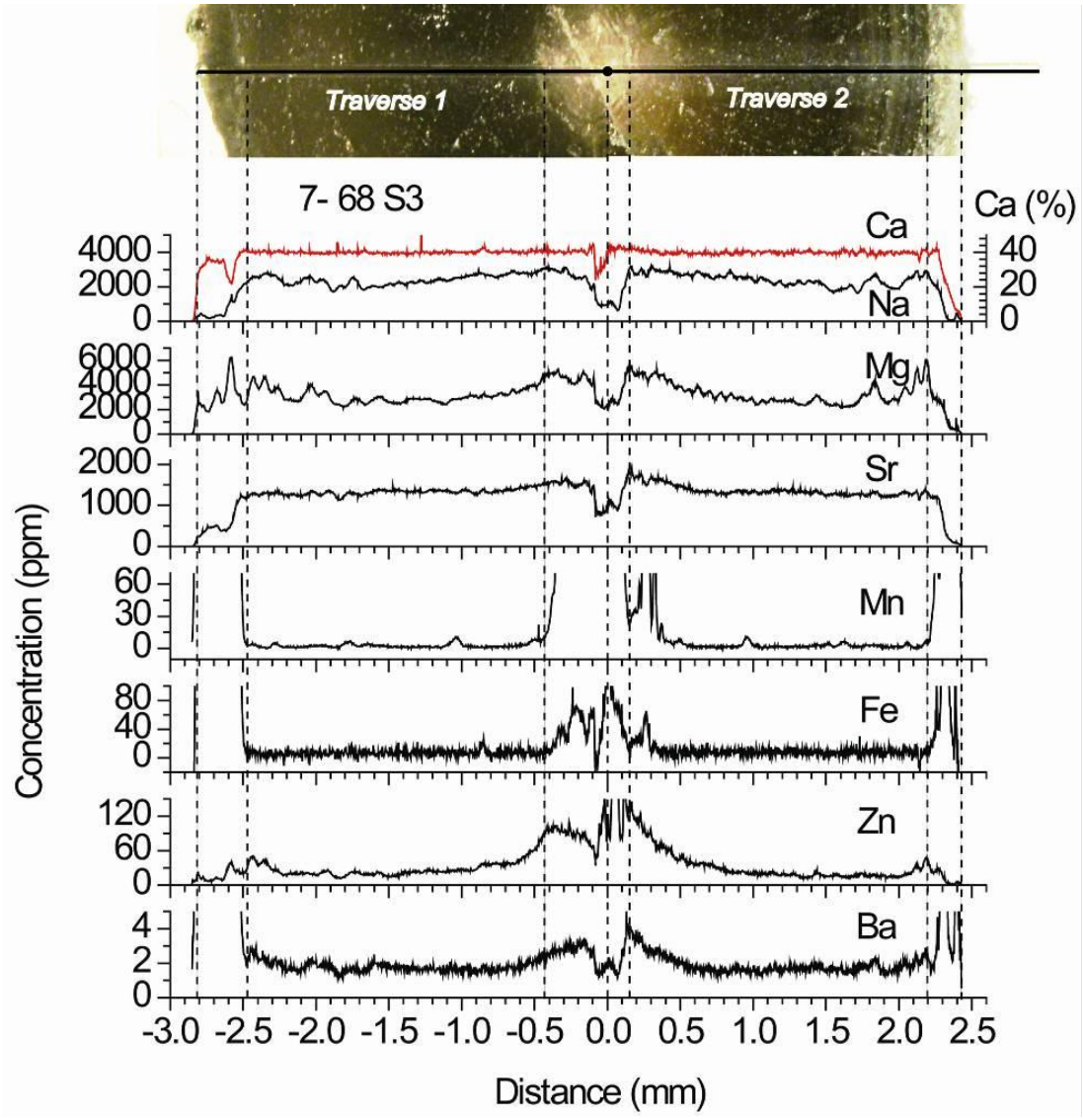

Fig. 4.27 Multi-elemental profiles (Ca, Na, Mg, Sr, Mn, Fe, Zn and Ba) of *H. spadixari* specimen 7-68 S3 obtained by LA-ICP-MS. The white circle marks the centre of the apical line (0 mm). The dotted lines mark the edge, centre and areas with low Mn.

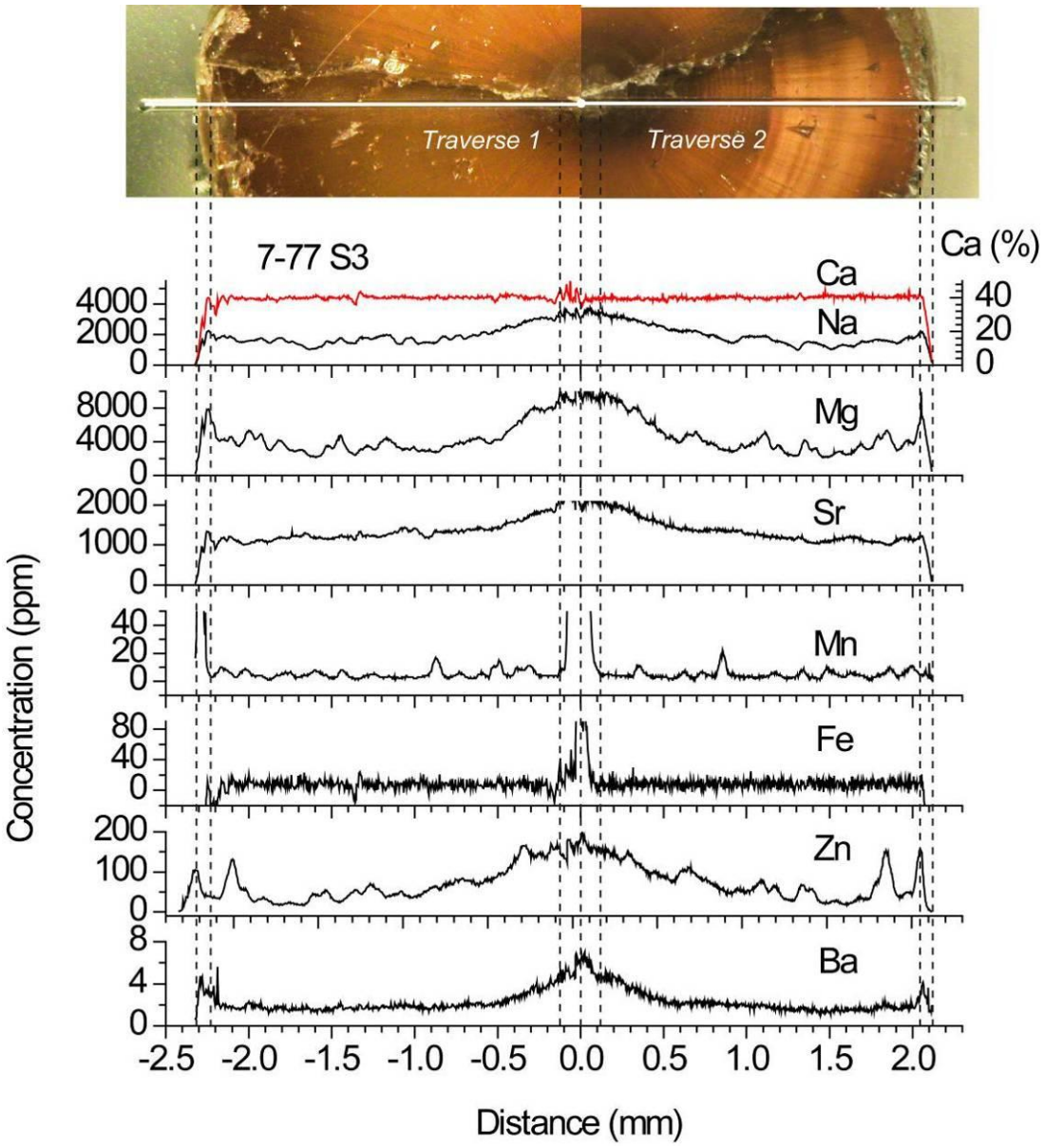

Fig. 4.28 Multi-elemental profiles (Ca, Na, Mg, Sr, Mn, Fe, Zn and Ba) of *H. stonebarroensis* specimen 7-77 S3 obtained by LA-ICP-MS.

On the other hand, specimens 7-86 S3 and 7-70 S3 (Fig. 4.29 & Fig. 4.30) of *H. stonebarroensis* and 7-84 S3 of *H. spadixari* (Fig. 4.31) are prominently characterized by distinct Mg peaks present in the inner, middle and outer parts of the cross-sections. In sample 7-86 S3, the inner Mg peak (peak 1) lines up with the growth boundary between two optically continual growth intervals, but no Fe and ~20ppm Mn present at the peak. The middle small Mg peak (peak 2 matches) neither a growth boundary nor Mn and/or Fe peaks; and the outer Mg peak (peak 3) only lines up with the outer growth boundary. Therefore, Mg peaks 2 and 3 are considered as real signals whereas peak 1 is likely to show the alteration effect.

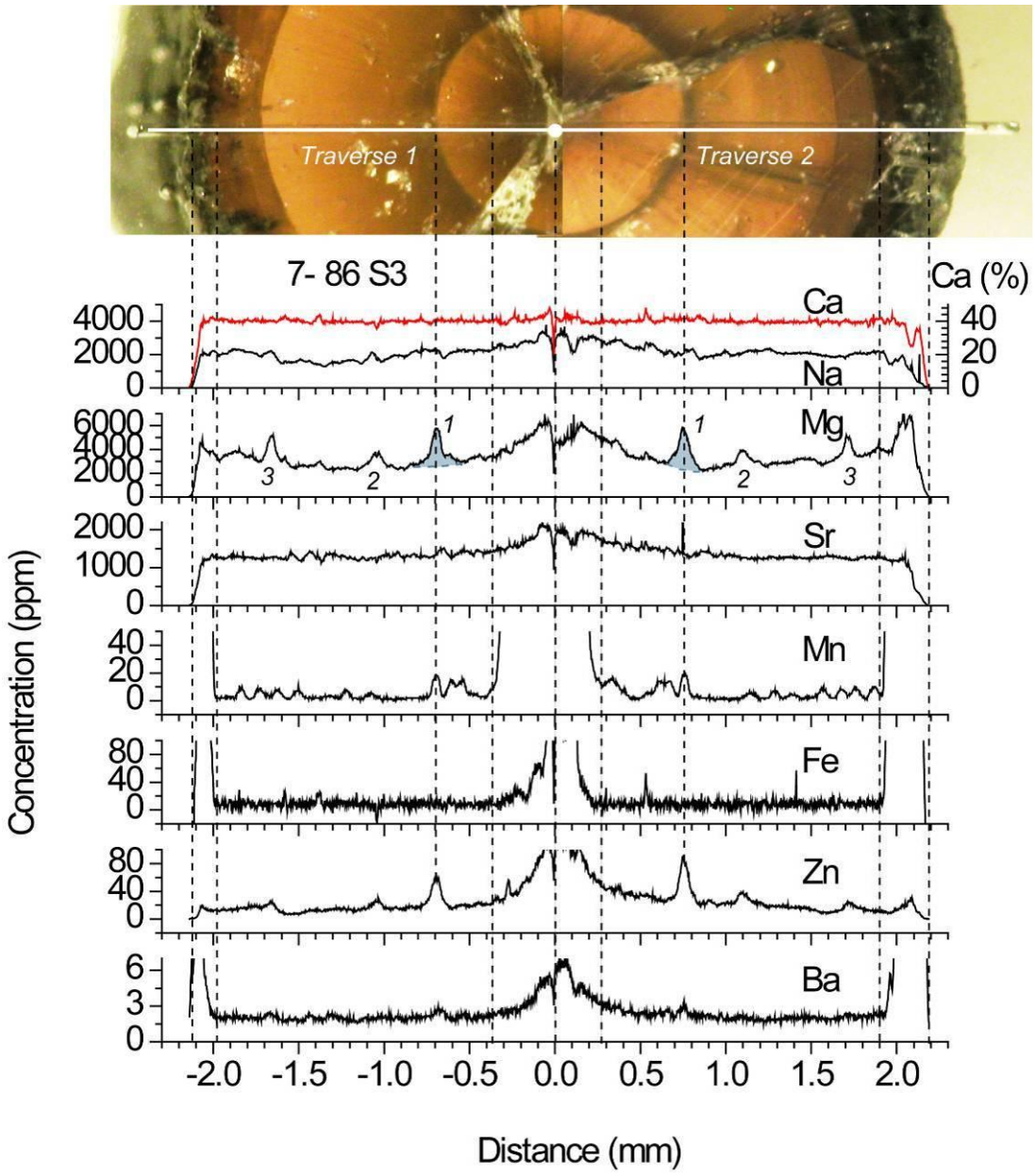

Fig. 4.29 Multi-elemental profiles (Ca, Na, Mg, Sr, Mn, Fe, Zn and Ba) of *H. stonebarroensis* specimen 7-86 S3 obtained by LA-ICP-MS. The three peaks are supposed to reflect primary geochemistry.

Moreover, in the Mg profile of specimen 7-70 S3, the major Mg peaks look very broad and overlap with adjacent small peaks. The outer two wide peaks on each traverse in Fig. 4.30 (named peak area 1 and 4) undoubtedly line up with the thick and blunt growth boundaries which also give high Mn values. In contrast, the two inner broad Mg peaks line up with the thin and sharp bands which show no Mn anomalies. In this case, Mg peaks 1 and 4 cannot be primary according to the above explanation.

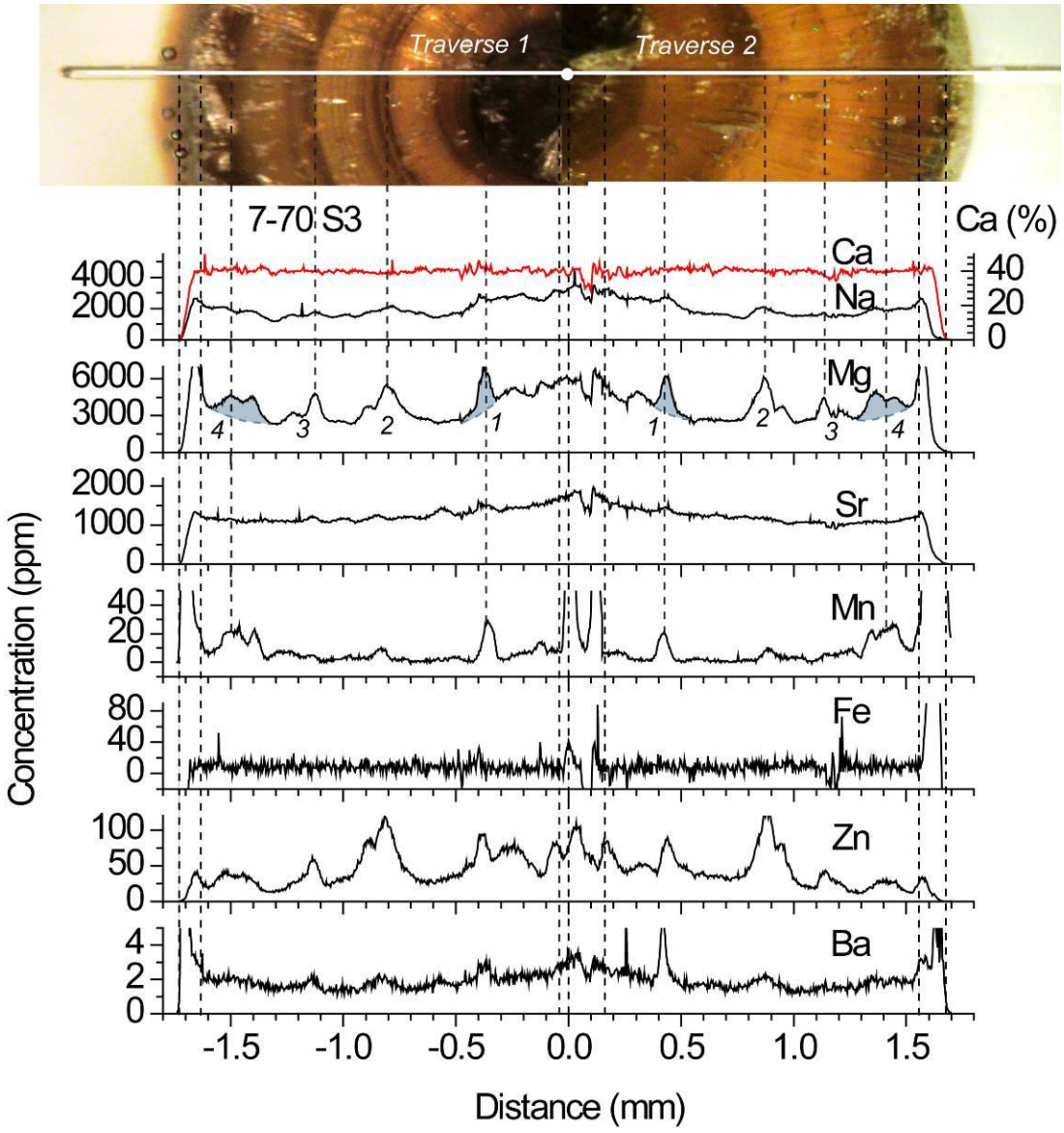

Fig. 4.30 Multi-elemental profiles (Ca, Na, Mg, Sr, Mn, Fe, Zn and Ba) of *H. stonebarroensis* specimen 7-70 S3 obtained by LA-ICP-MS. Numbers 1, 2, 3 and 4 mark the four Mg peaks from core to rim on both traverse. Because of their co-incidence with Mn and small Fe peaks, peak 1 and 4 (highlighted in grey) are thought to be alteration signatures whereas peaks 2 and 3 are supposed to be real geochemical signs.

The same examination of peaks can be applied to specimen 7-84 S3. The innermost Mg peaks that line up with peaks of Mn, Fe and Zn (peaks 1 in Fig. 4.31) is again suspected to have originated by alteration. The other two Mg peaks between 1.3 to 1.8 mm away from the centre (peak 2 & 3 in Fig. 4.31) are considered real.

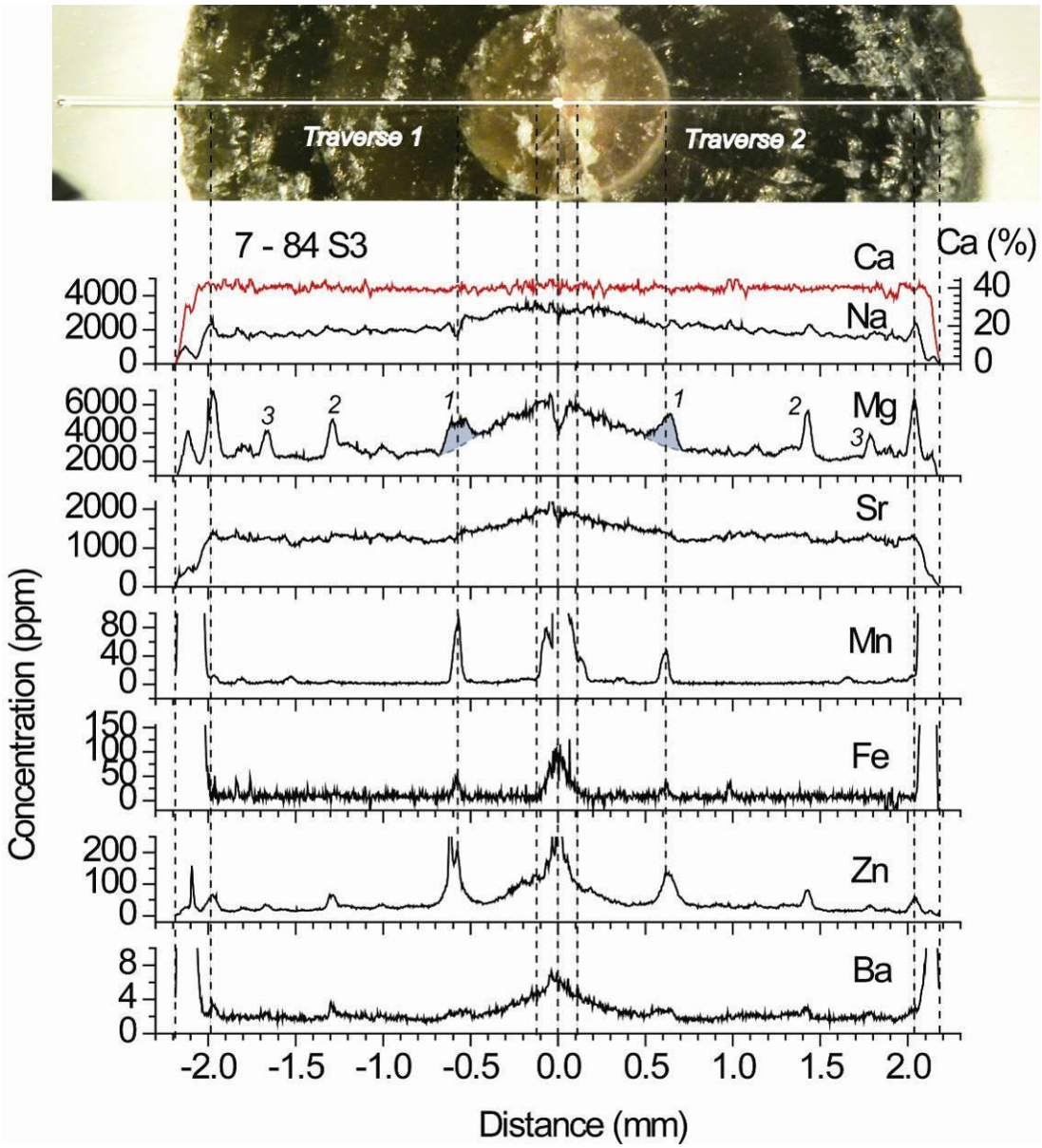

Fig. 4.31 Multi-elemental profiles (Ca, Na, Mg, Sr, Mn, Fe, Zn and Ba) of *H. spadixari* specimen 7-84 S3 obtained by LA-ICP-MS. The number 1, 2 and 3 stand for the Mg peaks. Peak 1 lines up with the innermost growth boundary and Mn peaks; hence is considered as alteration signature. Peaks 2 and 3 are considered real.

Once the alteration signals are removed, the adjusted Mg profiles give similar three peaks bowl-shape pattern. The primary Mg peaks commonly appear in the middle and outer part of the rostra, which suggests brief changes in growth pace, or metabolic activities that may result from migration, e.g. moving inshore for a couple of times and then offshore again during their overall adulthood. This behaviour may be associated with spawning as the modern analogue of belemnites, cuttlefish, are found to spawn in shelf seas. If so, these specimens may have a life span of three years and mated twice.

From an ontogenetic point of view, for the two species of *Hastites*, their closely related growth patterns and similarly slender and hastate rostra form suggest that they are likely to have lived in the same Pliensbachian seas of early Jurassic, and hence had experienced similar changes in living conditions at similar stage of their life. Possibly, they represent both genders of a belemnite family.

4.4.4.5 For P. elongata

The two sections were derived from the alveolus area due to the lack of available sub-sample fragments. The rounded alveolus filled with clay is shown in Fig. 4.32 & Fig. 4.33. The cross-sections only reflect the geochemistry of the middle and outer part of the rostra. Sample 7-27 S3 is visually less well-preserved than 7-29 S3. The high degree of alteration in the former is also indicated by common Mn peaks across the section (Fig. 4.32). The resemblance between Mg and Mn concentration profiles of this sample suggests that the high Mg is caused by diagenetic alteration.

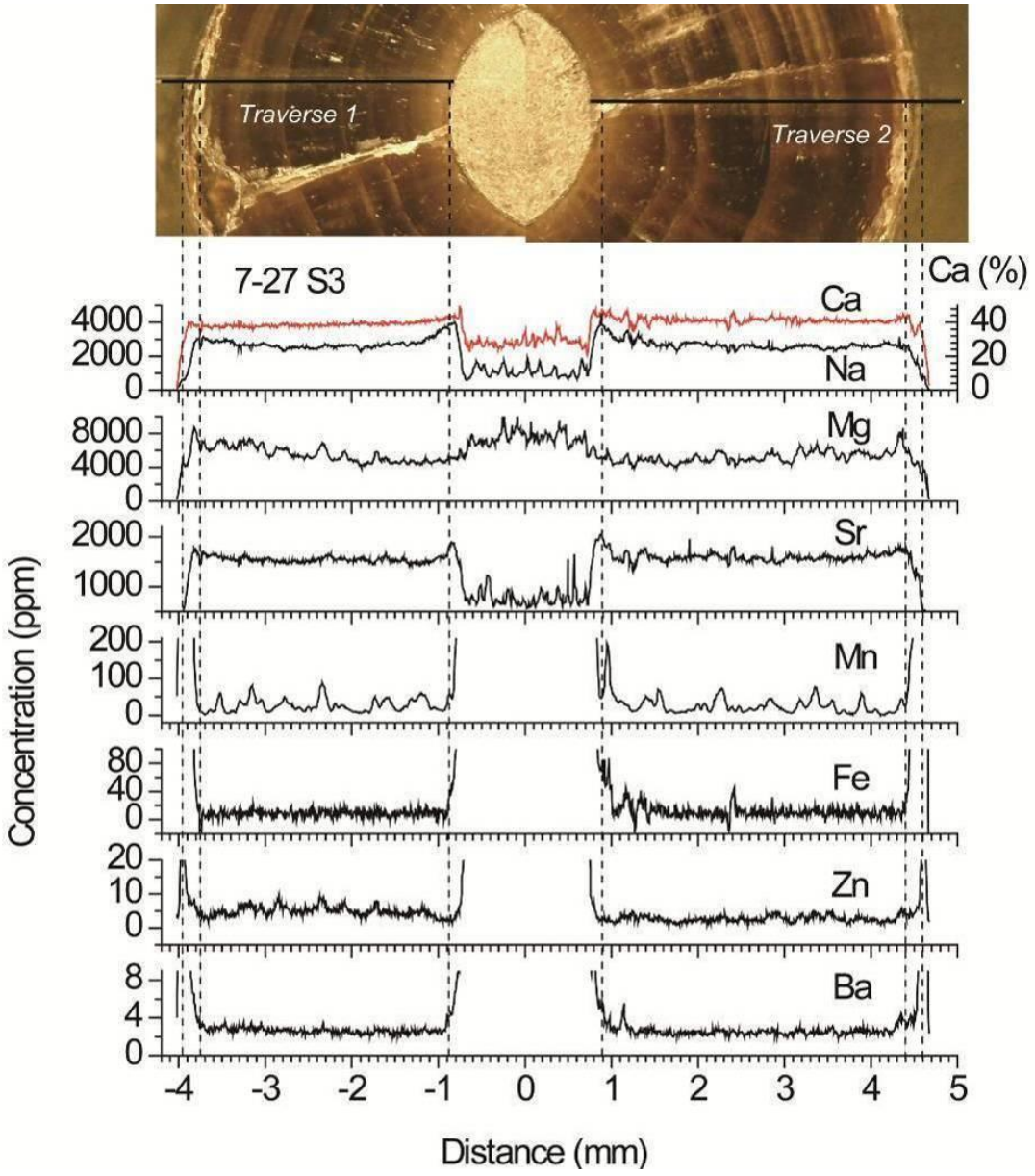

Fig. 4.32 Multi-elemental profiles (Ca, Na, Mg, Sr, Mn, Fe, Zn and Ba) of *P. elongata* specimen 7-27 S3 obtained by LA-ICP-MS. The section was cut above the base of alveolus due to lack of sample fragments, and the clay fillings in it are visible.

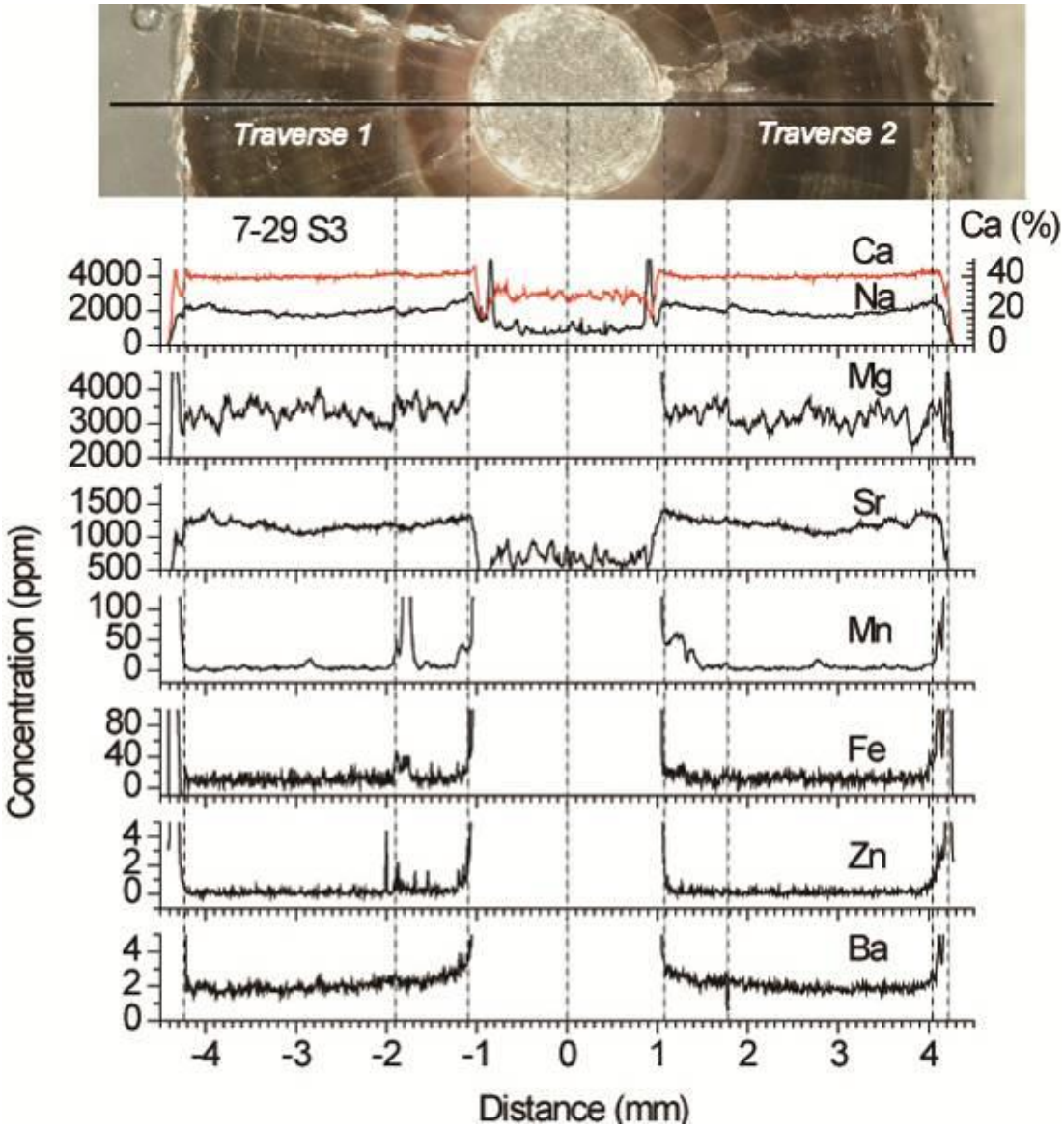

Fig. 4.33 Multi-elemental profiles (Ca, Na, Mg, Sr, Mn, Fe, Zn and Ba) of *P. elongata* specimen 7-29 S3 obtained by LA-ICP-MS.

4.4.5 Heavy metal (Zn) concentration

In belemnites, Zn is expected to behave similarly to Mg because the charge of Zn^{2+} and Mg^{2+} are the same and the ironic radius of them are very close (i.e. the radius of Zn^{2+} is 74 picometre and that of Mg^{2+} 72 picometre). Zn was then particularly considered among the heavy metals analysed in this study. It decreases from core to edge in all species except *P.elongata* (Fig. 4.32 - Fig. 4.33). Zn profiles interestingly lines up well with Mg in two species (*Hastites spadixari* and *Hastites stonebarroensis*, Fig. 4.27 - Fig. 4.31).

Zinc is known as one of the essential elements for metabolism in cuttlefish *Septa officinalis* (Miramand and Bentley, 1992), the modern analogue of belemnites. It has been reported to vary in the cuttlebone from 30 ppm in hatching to 150 ppm at reproductive stage (the parrallel of belemnite rostrum) during its life cycle (Bustamante *et al.*, 2002; Miramand *et al.*, 2006). However, the Zn profiles across belemnite sections of this study, in most cases, demonstrate a decreasing trend from early to late adulthood life. These opposite findings here to the above results in Bustamante *et al*. (2002) and Miramand *et al.* (2006) are likely due to factors like ontogenetic differences between belemnites and their analogue cuttlefish, and environmental differences between Pliensbachian and modern seas.

Zn profiles in both species of genus *Hastites* parallel with Mg (Fig. 4.27 & Fig. 4.29). When peaks of Zn line up with those of Mg and Mn (and or Fe), they indicate alteration (appearing as diagenetic sulphide ZnS_2, Mn and Fe sulphides). For high of Zn and Mg which lines up without the coexisting peaks of alteration indicators (e.g. Mn and/or Fe), they are supposed to be real signals and represent brief changes in growth rate and ontogeny.

4.4.6 Compositional differences in bulk chemistry

4.4.6.1 Isotopic Compositions within and between Species

Both *P.cuspidatus* and *N.acutus* specimens show broader ranges in isotopic compositions than other species. Despite that their $\delta^{18}O$ values overlap largely, *P.cuspidatus* specimens are consistantly 2‰ higher in $\delta^{13}C$ than specimens of *N.acutus*. If these well-preserved belemnites record the primary palaeo-envrimental settings of their living habitats, the large overlapping of $\delta^{18}O$ between the two species would probably suggest their sharing living conditions (eg. depth and temperature). The relatively big difference in $\delta^{13}C$ between them is therefore more likely to reflect species fractionation in carbon during calcification than differing living habitats. The differences in isotopic composition between specimens of each species should indicate, at least partially, the internal differences within a rostrum.

B. junceus specimens, in most cases, plot in the *N. acutus* compositional region, suggesting this species may relate more closely to *N.acutus* than *P. cuspidatus*. The

specimens of *P. elongata* seem to share the living niches with the *N. acutus, P. cuspidatus* and *B. junceus* species (Fig. 4.18). The 5 *H. spadixari* specimens that fall in the composition area of *P.cuspidatus* may show an artefact of limited samples numbers. More *H. spadixari* specimens are therefore needed to test whether this observation is true.

4.4.6.2 Elemental Compositions within and between Species: El/Ca

The elemental concentrations of bulk analysis do not differ much between species. Small inter-species difference is also seen in their oxgen isotopic compositions. This seems to further surpport the result that these Pliensbachian belemnites once lived in shared environmental niches.

On the other hand, the internal variations in Na, Mg and Sr within a rostrum are found to be larger than the differences between specimens of a species. For instance, between *P. cuspidatus* specimens, the bulk analysis shows a range of 600 ppm in Mg, but the intra-rostral variation of Mg is around 2000 ppm within the well-preserved regions of specimen 7-37 S3 (Fig. 4.10). This larger intra- than inter-rostral variations in elemental compositions is also seen in *N.acutus* specimens. Besides, two *B. junceus* specimens (7-38 S3 and 7-39 S3) were analyzed for both intra- and inter-rostral variations in composition for comparison. Their concentrations of Mg, Na and Sr in bulk analysis fall in the intra-rostral compositional ranges of the three elements (see Appendix C and Fig. 4.25 - Fig. 4.26). For example, the elemental profiles show ~1650-2000 ppm of Na, 2500-3400 ppm of Mg and ~1150-1330 ppm of Sr in specimen 7-38 S3, bracketing the concentrations of 1832, 2625, and 1211 ppm for Na, Mg and Sr in bulk analysis, respectively.

Although values of bulk analysis on elemental concentrations are comparable to intra-rostral data, it is likely to give homogenized values within a rostrum, so is unable to relect the larger internal compositional variations and the variation pattern of each specimen (such as the Mg peaks in the profiles of *H. spadixara* specimen 7-84 S3 in Fig. 4.31).

4.4.6.3 Palaotemperature Proxy: Correlation between El/Ca & $\delta^{18}O$?

The studied species here show no significant correlation between Mg/Ca and $\delta^{18}O$ ($r = -0.24$, $n = 44$, $P > 0.1$) in bulk analysis. Previous literature, nevertheless, reflects good correlations between $\delta^{18}O$ and Mg/Ca (and later Sr/Ca) in large populations of Plienbachian – Toraician belemnites from Yorkshire of the UK (McArthur *et al.*, 2000; Bailey *et al.*, 2003) and in northern Spain (Rosales *et al.*, 2004a,b) and perhaps in some Valanginian belemnites from SE Vergol (McArthur *et al.*, 2007a). These correlations have only been demonstrated in undifferentiated belemnites as a whole. No one has ever investigated the correlation within an individual species. For the species studies here, the correlation between $\delta^{18}O$ and Mg/Ca is not present in each individual species. This seems to imply that the correlation with $\delta^{18}O$ for Mg found previously may be only an overall trend reflected by large numbers of specimens. A question is therefore raised whether the correlation between Mg/Ca and $\delta^{18}O$ is just a statistical result of differently patched data but not present at species level. Were this the case, Mg/Ca couldn't be used as a palaeo-proxy in belemnites. To understand whether this is true in general, or whether the lack of correlation between Mg/Ca and $\delta^{18}O$ only occurs in some belemnite species, more belemnite samples from a number of Mesozic strata need testing. The study of the other three belemnite populations in the following chapters will shed light in the understanding of the correlation between Mg/Ca and $\delta^{18}O$ at species level.

4.5 Conclusion

1) The comparison between the EMP and LA results clearly indicate that each method has its own limits and preference for measuring intra-rostral variations in compositions. Both methods give reliable data of Ca, Mg and Na; but LA produces more reasonable Sr, Fe, and Mn while EMP is sensitive for S.

2) Mg profiles in specimens of *P.cuspidatus, N.acutus, B. junceus, H.stonebarroensis* (7-77 S3) and *H.spadixari* (7-68 S3*)* show a bowl/plate-shaped pattern, indicating a life style which includes a fast-growing adolescence, a follow-up slow growth in adulthood, and perhaps a quick fattening associated with physiological maturity in late ontogeny. Mg profiles

along the cross sections confirm that belemnites were mobile and migrated during their lifespan.

3) The profiles of Mg, Na and Sr show different variations in amplitudes and radial trends within a specimen. Mg possesses the highest amplitude variations while Sr gives the smoothest concentration profiles (*e.g.* Fig. 4.10). Sodium undulations seem to line up well with those of Mg, but its radial trend looks more similar to that of Sr. This may suggest that the three elements have different sensitivity to temperature changes, biological fractionation and/or alteration.

4) Concentration differences in LA profiles between specimens of a species are likely to reflect differing preservation degree, differing life stage the sections have preserved, or gender difference. Meanwhile, similarities in the radial trends of elemental concentration profiles are noticeable between specimens within a species and between species, although differences occur in their compositional ranges.

5) Mg/Ca and $\delta^{18}O$ ratios in bulk analysis show no significant correlation in all specimens of these Pliensbachian belemnites, or in each individual species. This finding questions the geochemical significance of the correlation between the two parameters, and the use of belemnites for palaeooceanographic studies should be done with caution.

Chapter 5 Toarcian Belemnites from Yorkshire

Chapter 5 compares the ranges of isotopic and chemical compositions from bulk analysis of the four species *A. subenuis, A. vulgaris, S. dorsalis* and *Y. simpsoni* that were found in the Early Toarcian seaway of northwestern Europe. Their compositions are interpreted in terms of the habitat and palaeo-environment of these belemnites. Both inter-species comparisons and intra-species variations in composition are included in this study. The compositional variations within an individual rostrum are not provided here due to the lack of enough well-preserved material for an isotopic/elemental probe profile along the radius of a cross-section.

5.1 Introduction

A recent study of Toarcian belemnites deposited in a geological instant revealed apparent differences in belemnite compositional ranges between two species, *A. subenuis* and *A. vulgaris*. The compositions of *A. vulgaris* specimens were shown to group tightly, whilst the compositions of *A. subtenuis* specimens were shown to range more widely. The differences were interpreted as reflecting differing habitats, or differing degrees of biofractionation, or both (McArthur *et al.*, 2007b). Here, the ranges of compositions of the same two belemnite species are reported, together with two other species (*S. dorsalis* and *Y. simpsoni*). All four species are accumulated in the Early Toarcian seaway of northwestern Europe over a period of around 400,000 years (estimated using the near-linear Sr isotope trend from McArthur *et al*., 2000). The sampling interval of this study brackets the stratigraphic level where belemnites in McArthur *et al*. (2007b) were sampled. A comparison of the compositional ranges of the four species from a relatively longer period of time with the data range and distribution found by McArthur *et al*. (2007b) for two contemporaneous belemnite species (*A. vulgaris* and *A. subtenuis*) collected from near the top of this study interval would potentially enable us to understand whether these four belemnites reflect variable conditions of their habits in Toarcian seas, or climate changes through time.

5.2 Geologic setting and sampling

Samples came from Lower Toarcian Whitby Mudstone Formation (Mulgrave Shale Member and the overlying Alum Shale Member) of the Cleveland Basin that are exposed in foreshore and cliff sections at Saltwick Bay, near the town of Whitby on the coast of Yorkshire, UK (Fig. 5.1). The lithostratigraphy and biostratigraphy of the section is well-recorded (Howarth, 1963, 1973; Powell, 1984) and shown in Table 5.1. Samples were derived from the base of Bed 43 to the top of Bed 51, and this sampling interval corresponds to the middle *falcifurum* Subzone of the *Harpoceras falciferum* Zone to the lower *commune* Subzone of the *bifrons* Zone of Howarth (1963, 1973). The *Harpoceras falciferum* Zone is now termed the *H. serpentinum* Zone, and the *commune* Subzone of the *Bifrons* Zone now the *H. laticosta* Subzone (Page, 2004), but the old names are retained here to provide a link to the previous literature. The duration of the sampling interval is around 400 kyrs as deduced from Sr-isotope stratigraphy (McArthur *et al*., 2000, Table 2).

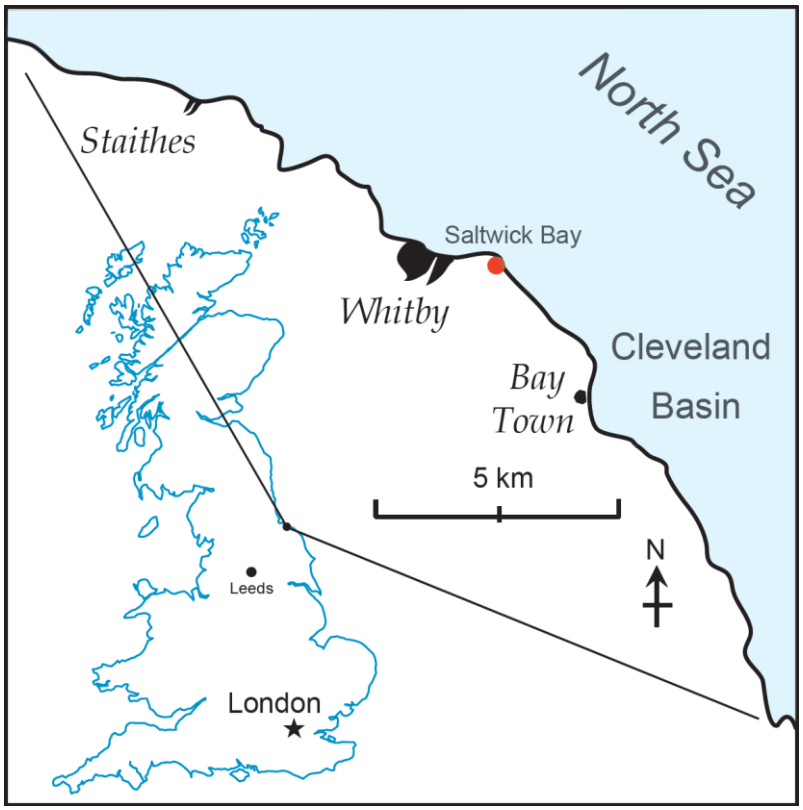

Fig. 5.1 Simplified sampling locality map. The study area is in Saltwick Bay, Yorkshire, UK, marked as a red filled circle. Diagram modified from McArthur *et al.* (2008).

The four analyzed species with specimen numbers (in parenthesis) are *A. subtenuis* (24), *S. dorsalis* (10), *Y. simpsoni* (9) and *A. vulgaris* (5), the descriptions and pictures of which are shown in Table 5.2 and Fig. 5.2. The stratigraphic levels of samples are given in meters above a zero datum placed at the Pliensbachian/Toarcian boundary.

Table 5.1 The biostratigraphy and lithostratigraphy of the *bifrons* and *falciferum* Biozones on the north Yorkshire coast, UK. Modified from Fig. 1 in Little (1996). D is the thickness of the beds. The sampling interval is highlighted in bold.

Stage	Zone	Subzone	Formation	Members	Bed No.	Lithology	D (m)
TOARCIAN (PART)	*Hildoceras bifrons* (part)	*fibulatum*	Whitby Mudstone (71.38m)	Alum Shale (part)	51-64	Main Alum Shales, grey, doggers, limestone nodules, siderite mudstone	15.48
		commune			**50**	Hard Shales, continuous bed of siderite mudstone	0.13
					49	Hard Shales, grey	6.20
	Hildoceras falciferum (top)	*falciferum*		Mulgrave Shale (part)	**48**	Ovatum Band, double row of large doggers containing siderite	0.25
					47	Shale, grey and bituminous	5.59
					46	Siderite mudstones	0.13
					45	Shale, grey, bituminous	3.35
					44	A row of scattered doggers	0.15
					43	Shale, grey, bituminous	7.67
					42	A row of oval scattered doggers	0.13
					41	Shale, grey bituminous	5.87

Table 5.2 The identification of Toarcian belemnites collected from Yorkshire. Pictures are provided in Fig. 5.2.

Species	No.	Description
Acrocoelites subtenius	24	Medium sized, conical to slightly cylindriconical rostrum with depressed elliptical cross-section, very acute apex, 3 apical grooves and clear lateral lines.
Simpsonibelus dorsalis	10	Small sized, subhastate rostrum with subquadrate to elliptical cross-section, acute to attenuate apex, weakly developed 3 apical grooves, but very clear alveolar groove.
Youngibelus simpsoni	9	Medium sized (6-9 cm), cylindrical rostrum with elliptical to pyriform cross-section; symmetrial outline, but less symmetrical profile with a slight ventral inflation, no definite apical grooves, but striated apex confined to the apical-most tip.
Acrocoelites vulgaris	5	Medium sized (~6 cm), robust and cylindriconical shape, symmetrical outline, but asymmetrical profile, elliptical tranverse section, 3 weak apical grooves and moderate apex.
Total	**48**	

Note: Specimens less than 5cm long are small sized, between 5 to 10 cm medium sized, and longer than 10 cm large sized.

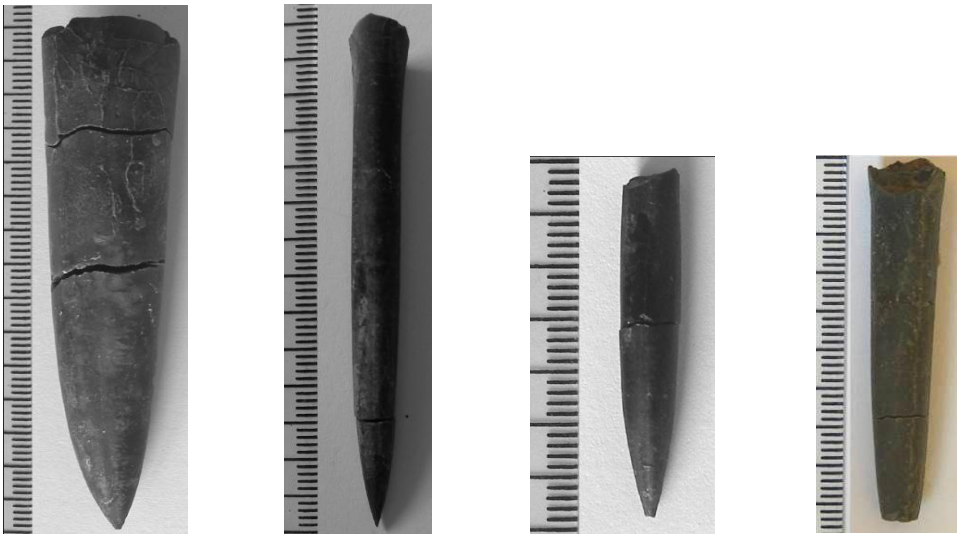

a) *A. vulgaris* 51/60 b) *A. subtenuis* 49/63 c) *S. dorsalis* 51/75 A d) *Y. simpsoni* 43/362

Fig. 5.2 Specimens of the four species studied from Toarcian of Yorkshire, UK. Scale is in mm and cm. Apex missing for *Y.simpsoni*.

5.3 Results

The isotopic and elemental data are given in Appendix D and Fig. 5.3. Concentrations of Fe and Mn were below detection (< 4 ppm Fe, <1 Mn; Appendix D) in most specimens. Concentrations of Mg, Na, and Sr are typically consistent with those in well-preserved belemnites from elsewhere (Podlaha *et al.*, 1998; McArthur *et al.*, 2000; Rosales *et al.*, 2001; 2004a,b).

For elemental compositions, specimens of *A. vulgaris* group tightly in compositions, with *S. dorsalis* also showing narrow compositional ranges except in Sr/Na. In contrast, specimens of *A. subtenuis* and *Y. simpsoni* show a wide spread of composition. Most specimens of *A. subtenuis* have lower Sr/Ca, higher Mg/Ca than those of *A. vulgaris* (Fig. 5.3e). Specimens of *S. dorsalis* are higher in Na/Ca but slightly lower in Mg/Ca than are specimens of *Y. simpsoni*, though overlaps between the two occur, but their Sr concentrations have a similar range (Fig. 5.3a, c). For all the four belemnite species, Mg/Ca data show no correlation with $\delta^{18}O$, but Sr/Ca values do (Fig. 5.3 d & f).

For isotopic compositions, all specimens in this study have $\delta^{13}C$ values from 1.3‰ to 5‰ PDB and and $\delta^{18}O$ from -3.31‰ to -1.05‰ PDB (Fig. 5.3 b). Specimens of

A.subtenuis largely overlap with *Y. simpsoni*, in isotopic compositions, but not with either *A. vulgaris* or *S. dorsalis*. All *A. vulgaris* and *S. dorsalis* specimens plot at the heavy end of the $\delta^{13}C$, while *A.subtenuis* and *Y. simpsoni* are mostly lighter in $\delta^{13}C$ values, despite apparent variations among specimens (Fig. 5.3b). *A. vulgaris* are more negative in $\delta^{18}O$ than the other three species.

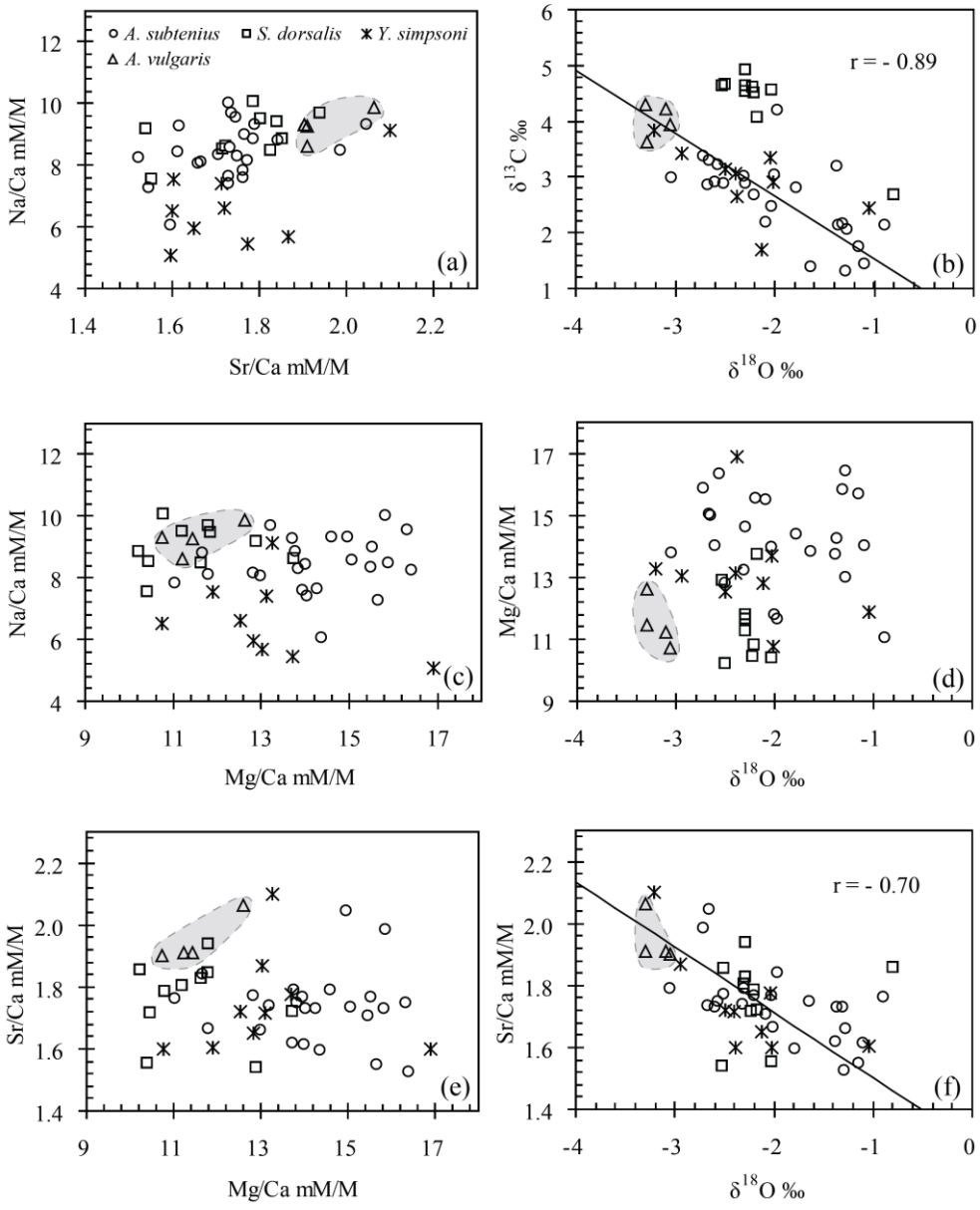

Fig. 5.3 Cross plots of elemental and isotopic data of belemnites, fitted by reduced major axis regression lines. Solid correlation line in b and f exclude specimens of *S. dorsalis*, which form a subpopulation enriched in ^{13}C and so are distinctive. Dotted correlation in b) defines possible correlation for *S. dorsalis*, but the correlation is wholly governed by one outlier. Shaded areas define the range of *A. vulgaris*, highlighted to illustrate its restricted composition.

The distribution of size (expressed as cross-sectional area here) and compisition of all species are unimodal (Fig. 5.4). The size bimodality for *A. subtenuis* reported by McArthur *et al*. (2007b) is not present in the large sample population here, so is clearly an artifact of a small sample population. The small number of *A. vulgaris* population (4 specimens) fails to resolve the issue of whether or not a putative negative correlation exists between $\delta^{18}O$ and size in this species (Fig. 5.4), as was tentatively suggested by McArthur *et al*. (2007b).

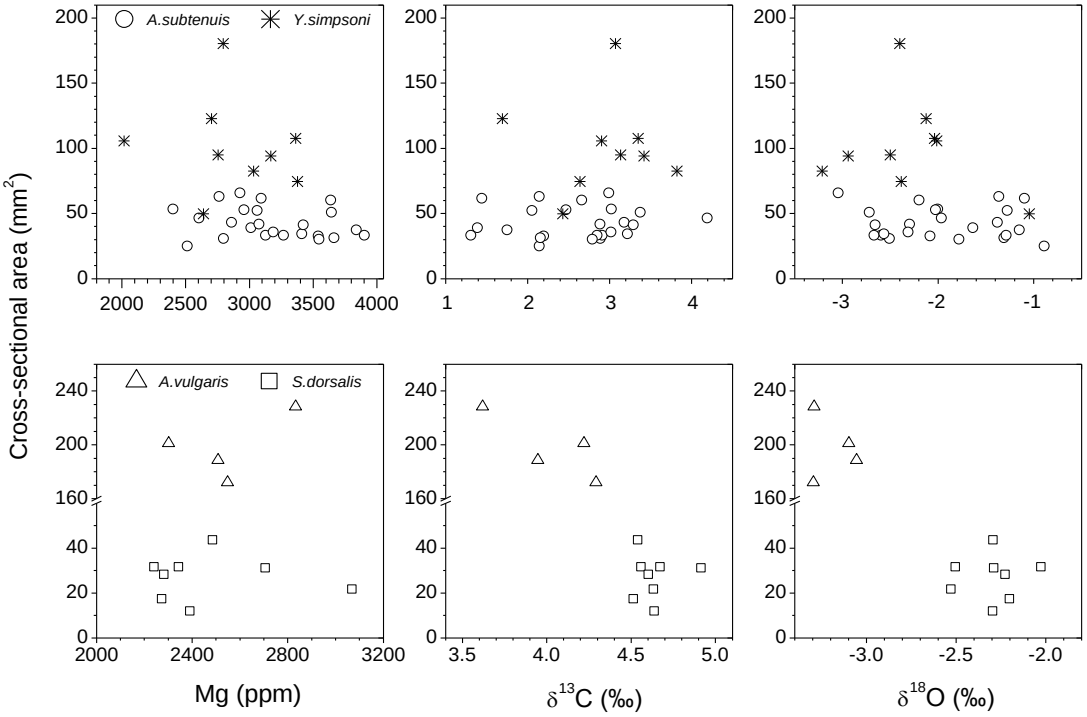

Fig. 5.4 Relation between composition and size as cross-sectional area. Note the difference of scales of each spieces. Areas calculated assuming circularity with a mean diameter calculated from the dosal-ventral and lateral diameters.

5.4 Discussion

5.4.1 Elemental composition (El/Ca) and correlation with $\delta^{18}O$

By analogy with modern cuttlefish, belemnite species were likely to have lived a mobile life, with different species inhabiting different environmental niches and so experiencing differing ranges of temperatures and salinities over their individual lifetime. In consequence, the El/Ca ratios and $\delta^{18}O$ values in well-preserved bulk

belemnites, if interpretable in terms of palaeotemperature, may reflect the thermal range of the Toarcian seas where belemnites once lived, and possibly migrated.

In this study, differences in elemental compositions and ranges are found among the four species. Specimens of *A. subtenuis* have a higher and broader range of Mg/Ca, but are lower in Sr/Ca ratios. Specimens of *A.vulgaris* and *S. dorsalis* contain lower Mg/Ca but higher Na/Ca values. *Y. simpsoni* specimens tend to have lower Na/Ca than other three species. The data clearly show that values of Mg/Ca do not correlate with $\delta^{18}O$ in any of the individual species, nor in all collected species (Fig. 5.3 d). This finding confirms that of McArthur *et al*. (2007b), that Mg/Ca in Early Toarcian belemnites is a poor recorder of palaeotemperature.

Conversely, in both of the presumed more cosmopolitan species *A. subtenuis* and *Y. simpsoni*, Sr/Ca correlates reasonably well with $\delta^{18}O$ ($r = -0.70$, $n = 36$ and $P < 0.001$). Specimens of *A. vulgaris* are too few in number to reveal whether the correlation holds for this species alone, but they fall on a line of correlation drawn for the two cosmopolitan species (The regression line in Fig. 5.3 f is hence based on all three). For *S. dorsalis* alone, Sr/Ca does not correlate with $\delta^{18}O$ although it, too, spreads around the regression line for *A. subtenuis*, *Y. simpsoni* and *A. vulgaris*. Assuming that Sr/Ca ratios in belemnite calcite mainly reflect temperature, and that values of $\delta^{18}O$ reflect temperature, salinity and the $\delta^{18}O$ of the ambient seawater, the good correlation between Sr/Ca and $\delta^{18}O$ for these species, excepting *S. dorsalis*, seems to imply that Sr/Ca is potentially a good palaeotemperature recorder. Sr/Ca was previously proposed by McArthur *et al*. (2007b) as a potential palaeotemperature indicator for Toarican belemnites. The data in this study further top up their proposal.

Although salinity in Toarcian shelf sea might vary and changes in salinity would entail variations in $\delta^{18}O$, its effects on Sr/Ca ratios are shown to be negligible in Fig. 5.5. The modeled Sr/Ca ratios in the Early Toarcian sea of the Cleveland basin hardly show any changes with a decrease in salinity from 35 to 30 psu (Fig. 5.5). A few studies on modern planktonic foraminifera (Lea *et al*., 1999) imply that Sr/Ca temperature sensitivity is approximately ten times lower than that of Mg/Ca. In modern mollusks, Sr/Ca appears to be influenced predominantly by physiological factors (Klein *et al*., 1996). For belemnites, Sr, compared with Mg, is assumed to be

less sensitive to temperature and species-related fractionation (Bailey *et al*., 2003; McArthur *et al*., 2007b and this PhD thesis). The dependence of Sr on temperature and species-specific biofractionation in biological calcite, however, still remains poorly quantified, and the use of Sr/Ca as a palaeotemperature proxy in general still needs better understanding and further testing of its temperature sensitivity.

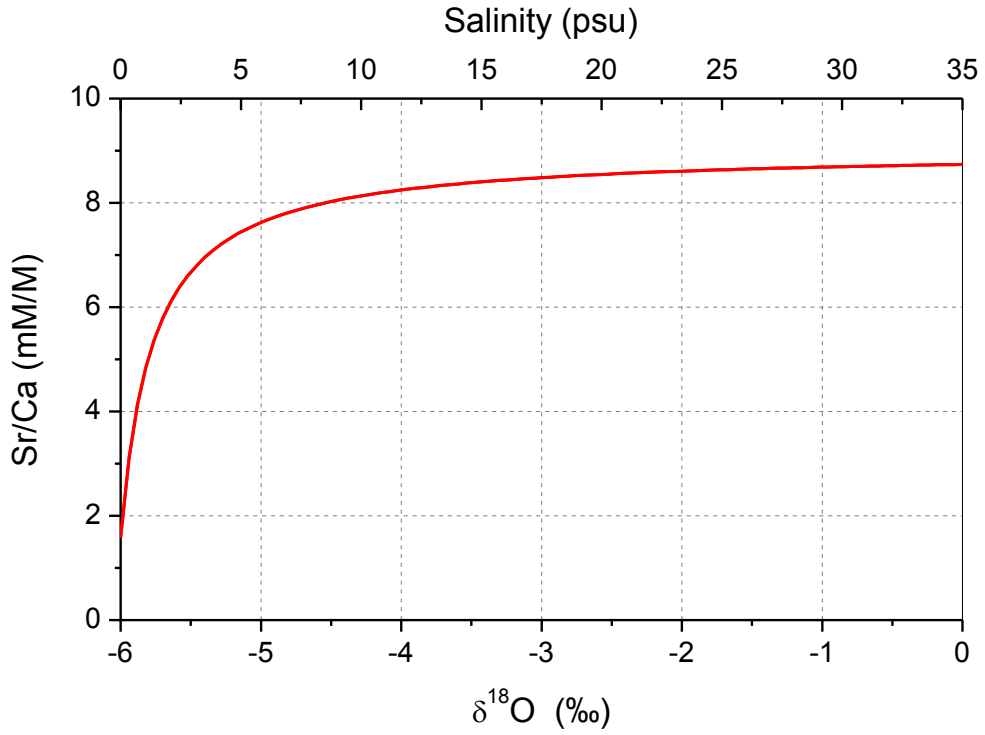

Fig. 5.5 Modelled Sr/Ca ratios in the Early Toarcian sea of the Cleveland basin as a function of salinity and δ18O of ambient seawater. End-member values for marine δ18O (0 ‰) at normal salinity of 35 psu and riverine δ18O (– 6‰) from Saelen et al., (1996). End-member values for Sr and Ca concentrations in average seawater and river water from Table 7-1 of Chapter 7 in Murray(2004)and Wikipedia.

5.4.2 Variations in isotopic composition: $\delta^{13}C$ & $\delta^{18}O$

A negative correlation is found between $\delta^{13}C$ and $\delta^{18}O$ for belemnite species *A. subtenuis*, *A. vulgaris* and *Y. simpsoni* of this study (Fig. 5.3 b). Saelen *et al*. (1996) found such a negative correlation in a large number of Toarcian belemnites of mixed species when plotted against bed numbers, rather than species. The species differences in isotopic compositions were therefore not reflected in their paper. A similar negative correlation between $\delta^{13}C$ and $\delta^{18}O$ exists for undifferentiated belemnites of Kimmeridgean-Tithonian age (Nunn and Price, 2010). The trend is here interpreted as reflecting belemnite habitats across a wide depth range of

Toarcian seas. In the oceans, surface seawater $\delta^{13}C$ is made positive by the export of substantial amounts of isotopically light organic matter. With increasing depth, $\delta^{13}C$ of dissolved inorganic carbon (DIC) would become less positive, and seawater colder, as a consequence of the remineralization of surface-derived organic matter. It then follows the trend of Fig. 5.3 b to isotopically heavier $\delta^{18}O$ (cooler temperature) as $\delta^{13}C$ decreases (becomes isotopically lighter). On this assumption, the $\delta^{13}C$ of *A. vulgaris* suggests that it would have inhabited a shallower environmental niche than would *A. subtenuis* or *Y. simpsoni*, and one in which warm surface water, with high surface productivity, was enriched in ^{13}C as a result of the strong export of organic matter. Such a scenario accords with the fact that the Toarcian sediments through the study interval contain > 2 % TOC (McArthur *et al.*, 2008). The more cosmopolitan *A. subtenuis* and *Y. simpsoni* specimens probably ranged in Toarcian shelf seas to certain depth where $\delta^{13}C$ was more negative and $\delta^{18}O$ was more positive (McArthur *et al.*, 2007b). For *S. dorsalis*, the anomalously positive $\delta^{13}C$ is postulated to represent species fractionation of around +2 ‰ in carbon during calcification.

5.4.3 Estimation of palaeotemperature range (ΔT) from $\delta^{18}O$

Specimens of *A. vulgaris* and *S. dorsalis* show a limited range of ≤ 0.5‰ in $\delta^{18}O$ (Fig. 5.3 & Table 5.3), which translates to a temperature range of < 3ºC, using the palaeotemperature equation of Anderson and Authur (1983). This is slightly lower than that of 3.5 ºC for *A. vulgaris* specimens alone reported in McArthur *et al.* (2007b). This calculation assumes that the $\delta^{18}O$ reflects temperature only. Were the range of $\delta^{18}O$ also affected by variations in salinity, the palaeotemperature change for these two species would be even smaller. It is hence confirmed that *A. vulgaris* and *S. dorsalis* once occupied restricted and specialized shallow living niches in Early Toarcian shelf seas. This finding is also implied in their narrow ranges of Mg/Ca, Sr/Ca, Na/Ca, $\delta^{18}O$ and $\delta^{13}C$.

For specimens of *A. subtenuis* and *Y. simpsoni*, the $\delta^{18}O$ range of 2.16‰ equates to a temperature range of 9.6 ºC (Table 5.3), assuming no salinity effect on $\delta^{18}O$. Whether or not this assumption is correct, the broader variations in isotopic and elemental compositions of *A. subtenuis* and *Y. simpsoni* is interpreted to attest to a

wider ranging, cosmopolitan lifestyle that experienced a greater range of temperature, probably moderated by changes in salinity, than was seen by *A. vulgaris*.

Attempts to separate the effects of temperature and salinity on the $\delta^{18}O$ of belemnite calcite (Saelen *et al.*, 1996; Bailey *et al.*, 2003; Price and Mutterlose, 2004) rest on assumptions about the magnitude of each. Attempts by these authors to circumvent the assumptions by modelling made them more explicit, and emphasized the difficulty of applying such interpretations in deep time. The range of salinity and temperature with depth to 400 m in the modern oceans varies geographically, but seems to be no more than 1.5 psu in salinity and no more than 10°C for present day subtropical regions at 30 to 40° N (Emery and Dewar, 1982), a latitude range that encompassed the palaeo-latitude of the Cleveland Basin in Early Toarcian time (Saelen *et al.*, 1996). In coastal environments, where riverine influences are stronger, a 3 psu lowering of salinity is not uncommon and the temperature-depth profile can be complex (e.g. Fig. 4 of Blanton *et al.*, 2003). A reduction in salinity by 1.5 psu would therefore entail a decrease in $\delta^{18}O$ of around 0.75 ‰, assuming a $\Delta\ \delta^{18}O/\Delta S$ ratio of 0.5 per 1 psu change for open oceans (Bailey *et al.*, 2003). The range in $\delta^{18}O$ of belemnites in this study is around 2.5‰, so less than 30% of that range might be related to salinity effects. It therefore seems reasonable to infer that, for the stratigraphic interval studied here, and specifically for the lifetime of the belemnites considered here, salinity influences in the Toarcian Seaway of Europe were probably subordinate to those of temperature. It is important to note that the studied interval does not include Beds 32 to 40, a time of extreme water-mass restriction (McArthur *et al.*, 2008) when salinity influences may have been greater (Saelen *et al.*, 1996 and refs therein; McArthur *et al.*, 2008).

Had the above belemnite species lived in a seaway similar to that of modern oceans at 30 – 40 °N, and ignoring the effects of changing salinity, a seawater temperature change of 3 ºC, deduced from the range of $\delta^{18}O$ for *A.vulgaris*, would reflect a depth range of around 50 meters, whilst the large temperature ranges of ~10 ºC, calculated from the ranges of $\delta^{18}O$ for *A. subtenuis* and *Y. simpsoni*, would indicate a depth of up to a few hundred meters from the sea surface (see Appendix A – B). This comparison, although approximate, demonstrates the inferred differences in living conditions and lifestyles between these species.

Table 5.3 Possible temperature changes associated with the range in $\delta^{18}O$ from the mid-*falciferum* zone to the *commune* zone. Range in temperature (ΔT) derived using the equation of Anderson and Author (1983) and a value of -1‰ for Toarcian surface seawater $\delta^{18}O$.

Belemnite species	No. of specimens measured	$\Delta\delta^{18}O$ (‰ PDB)	ΔT (°C)
A. subtenuis	24	2.16	9.5
Y. simpsoni	9	2.16	9.6
A. vulgaris	4	0.25	1.1
S. dorsalis	8	0.50	2.2

5.4.4 Comparison to the previous studies

The isotopic data of belemnites in this study were compared at species level with data of belemnites from Saelen *et al*. (1996) in Fig. 5.6. The one specimen of *A. subtenuis* and one of *Y.simpsoni* of Saelen *et al*. (1996) fall in the compositional ranges of the two species found in this study, but only about half of their *S. dorsalis* specimens cluster in the heavy-isotopic area defined by *S. dorsalis* specimens of this work, with the remaining half (triangles with a number in the middle) scattering along specimens of other species. The outliers of *S. dorsalis* of Saelen *et al*. (1996) may reflect diagenetic alteration (e.g. specimens 1 and 2) or transcription errors in identification during sample preparation (specimens 3 – 5). *S. dorsalis* is therefore thought to be a restricted species with limited range of compositions.

Saelen *et al.* (1996, 1998) explained the bed by bed differences in $\delta^{13}C$ and $\delta^{18}O$ in terms of fractionation of carbon through high primary productivity and varying salinity (ibid; Saelen *et al.*, 1998). These authors dismissed species differences as the cause, and emphasised changing palaeoceanographic conditions that were reflected in successive beds. Finding a very similar relationship of decreasing $\delta^{13}C$ with increasing $\delta^{18}O$ in the contemporaneous belemnites *A. subtenuis* and *A. vulgaris* from above Bed 48 of the sequence led McArthur *et al*. (2007b) to postulate that the relation reflected species and habitat differences; that is, differing depth ranges of habitats of different species in an ocean that was thermally stratified. These different interpretations are explored here in the light of the new data of belemnites from a range of strata (Bed 43 – 51) presented here.

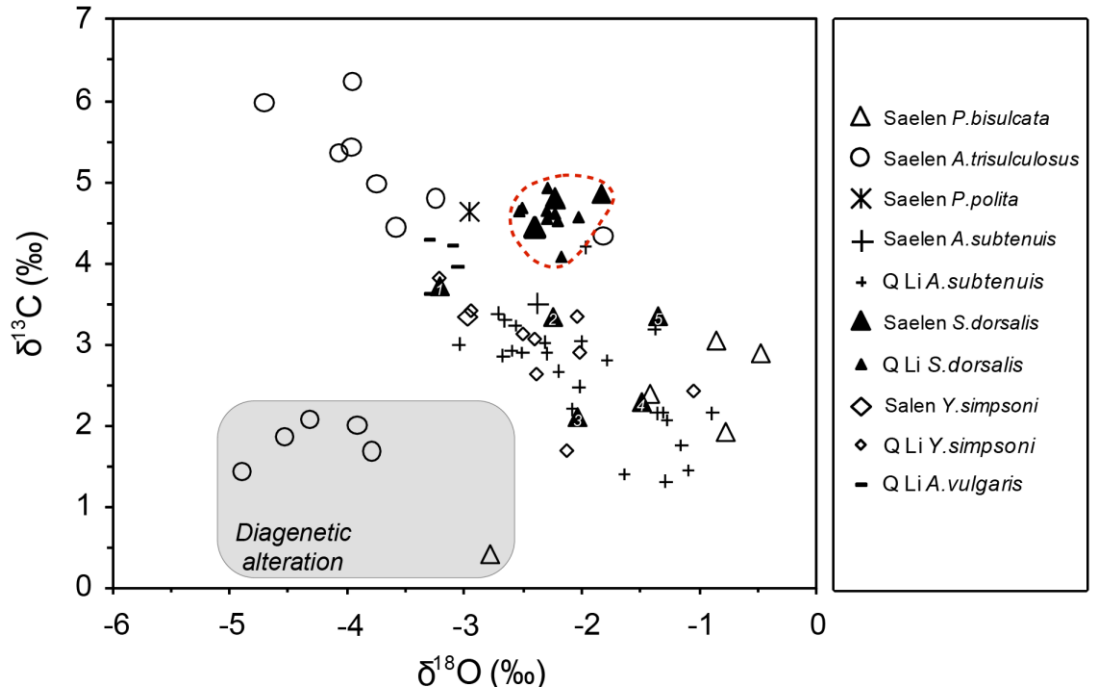

Fig. 5.6 $\delta^{18}O$ verse $\delta^{13}C$ of belemnites at species level from this study and Saelen *et al.* (1996). For specimens with multiple isotopic analyses in Saelen *et al.* (1996), the mean values are plotted here. The grey rounded rectangle area contains specimens that show diagenetically altered isotopic compositions. The dashed area is the compositional range of *S.dorsalis* specimens of this study. Four of the 9 *S.dorsalis* specimens of Saelen *et al.* (1996) fall in this area; the remaining specimens that are plotted out of this area are numbered as 1 to 5.

In Fig. 5.7, data for *A. vulgaris* and *A. subtenuis* here are compared with that of McArthur *et al*. (2007b). The new data for the two species separate them more clearly than do the data of McArthur *et al.* (2007b). The new data cluster more tightly, and show less overlap of the two species than do the previous data. This tighter clustering is believed as a result of using better-preserved belemnites and improved sub-sample selection process involving picking under the microscope from an alcohol bath. The new findings therefore confirm those of McArthur *et al*. (2007b) that *A. vulgaris* and *A. subtenuis* differ compositionally and strengthen the suggestion that the differences result from differing habitats and habitat ranges.

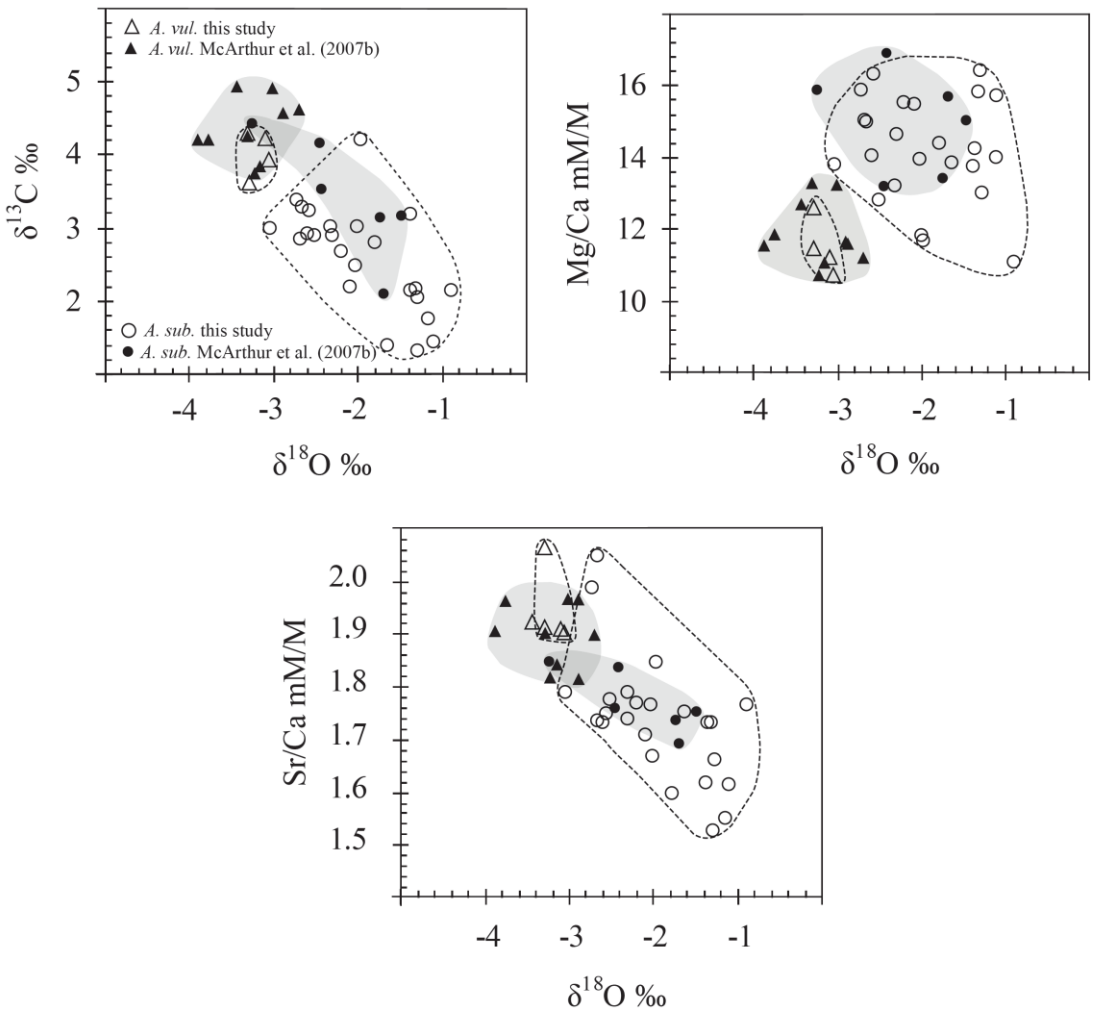

Fig. 5.7 Compositional ranges of *A. vulgaris* and *A. subtenuis* of this study (open symbols), compared with the ranges for these species found by McArthur *et al.* (2007b; closed symbols) Specimens in this study represent a time period of 400,000 years, those of McArthur *et al.* (2007b) represent an instant of geological time.

The inter-element trends seen in the new data (Fig. 5.3) also confirm those reported by McArthur *et al*. (2007b) that Sr/Ca ratios correlate well with $\delta^{18}O$, but Mg/Ca values do not. These findings differ from those reported by others for largely undifferentiated belemnites of Pliensbachian and Toarcian age. In such belemnites from both Yorkshire (McArthur *et al.*, 2000; Bailey *et al.*, 2003) and Spain (Rosales *et al.*, 2004a, b) good correlations were observed between $\delta^{18}O$ and both Mg/Ca, and Sr/Ca and interpreted in terms of variation in both temperature and salinity. Rosales *et al.* (2004) also observed that in the belemnites from Spain, $\delta^{18}O$ did not correlate with $\delta^{13}C$, but McArthur *et al*. (2007b) and this study both found that $\delta^{18}O$ does not correlate with Mg/Ca but does correlate with $\delta^{13}C$.

The differences seen between this study and the above workers may arise from having analyzed specimens identified to species level, and having analyzed only four species in this research, two of which have a very restricted data range. In contrast, the previous studies sampled a longer stratigraphic range, more specimens, and including (presumably) more species from a greater range of palaeo-environments than did in this study, so reflecting an overall regression of El/Ca with $\delta^{18}O$. Further work is required to test whether the correlations of $\delta^{18}O$ with Mg/Ca and/or Sr/Ca exist at species level and whether the interpretation of belemnite compositions in terms of palaeotemperature works for individual species.

The internal variations in composition within an individual rostrum, observed in McArthur *et al*,. (2007b), cannot be tested here because optical examination undoubtedly shows highly altered regions on the cross sections of the reminder of Toarcian specimens after chemical and isotope analyses; and that the remaining material is not sufficient enough for a probe profile (Fig. 5.8). However, this alteration was avoided in bulk chemical analysis by careful hand-picking of only pristine material.

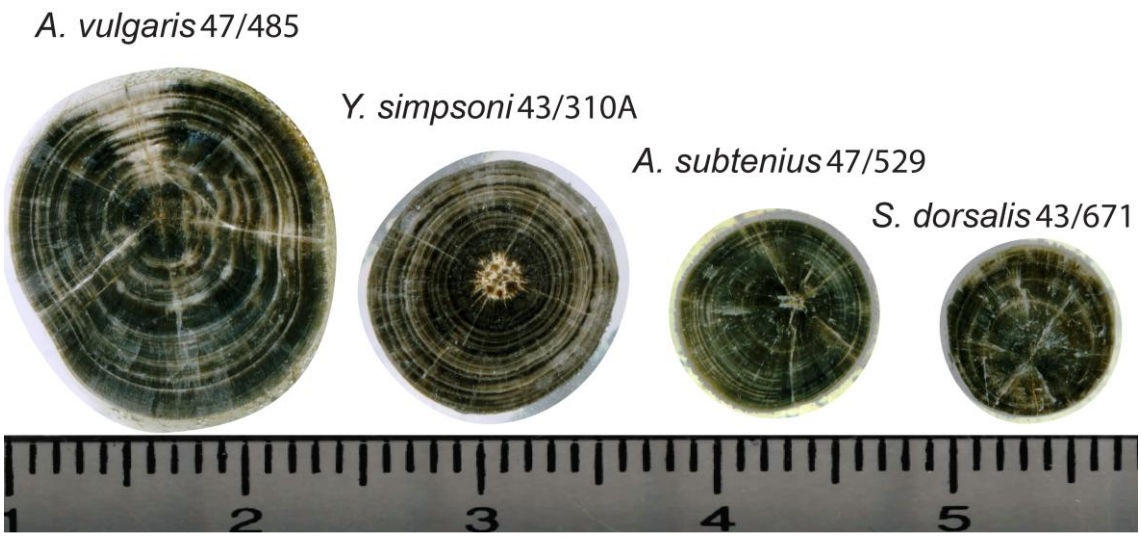

Fig. 5.8 Cross-sections of Toarcian specimens. Apical region of Y06-47/485 showing the lateral compression. Preservation of a small part of the central phragmocone in Y06D 43/310. All sections show cracking typical of Toarcian belemnites, and alteration rings picked out in lighter calcite.

5.4.5 The stratigraphic profile of $\delta^{13}C$

In Fig. 5.9, the stratigraphic profiles of $\delta^{13}C$ and $\delta^{18}O$ plot on the isotopic trends derived from McArthur *et al*. (2000, 2008). These trends were based largely on undifferentiated belemnites from the interval of *falciferum* to *bifrons* zone, which includes the Toarcian regional oceanic anoxic event (RAE) in *exaratum* Subzone. A positive marine carbon isotope excursion (CIE) of up to +6.5 ‰ in overlying Subzones was previously proposed to follow this RAE, as a consequence of the removal of large amounts of isotopically light organic matter into black shales (Jenkyns and Clayton, 1997). However, a few short-term returns to near-normal $\delta^{13}C_{belemnites}$ during the major positive CIE have been revealed in the carbon isotopic trend of Toarcian belemnites from Yorkshire (McArthur *et al*., 2000). The new data in Fig. 5.9 add details to the data already published for this interval of Yorkshire (Saelen *et al.*, 1996; Jenkyns and Clayton, 1997; McArthur *et al.*, 2000); and confirm the presesnce of a minimum in $\delta^{13}C$ within Bed 43 that was shown by the data of McArthur *et al.* (2000). The small differences between data of this study and that of McArthur *et al.* (2000) are likely attributed to factors like species differences and internal variations in belemnite composition. The lowest values of $\delta^{13}C$ here are mostly yielded by *A. subtenuis* and sometimes come from *Y. simpsoni*; Specimens of *S. dorsalis* (and *A. vulgaris*) appear to be responsible for all the high values of $\delta^{13}C$ above Bed 43. This raises the question of whether, and by how much, the apparent isotopic excursion through the sequence in $\delta^{13}C$ of belemnite calcite is defined in previous data by varying speciation with stratigraphic level *i.e.* reflects the species of belemnite analyzed, and how much reflects true environmental change. Further work at species level on belemnites from Beds 36 to 41 is needed to settle the issue.

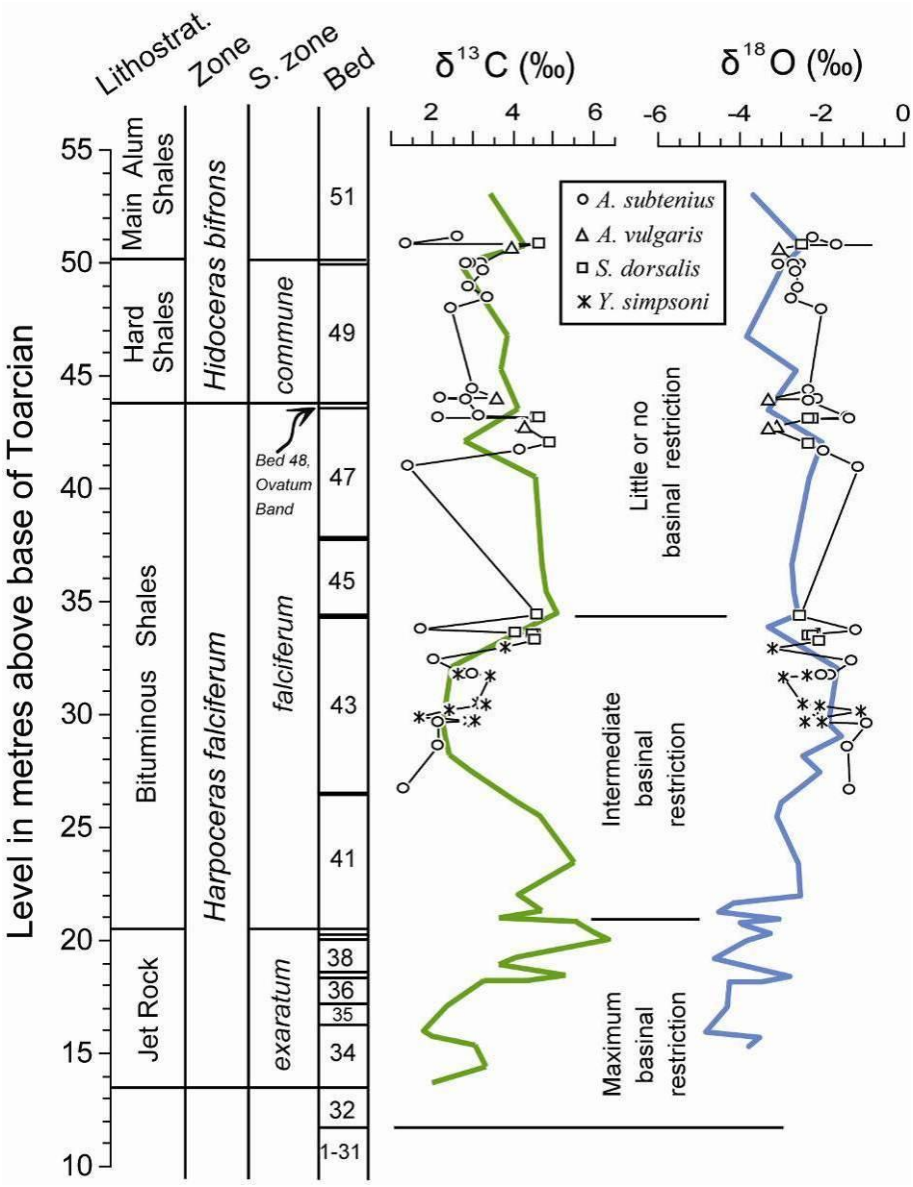

Fig. 5.9 Profile of $\delta^{18}O$ and $\delta^{13}C$ of belemnite calcite through the interval from the *semicelatum* to the *commune* Subzones. Blue and green lines represent data trends of McArthur *et al.* (2000). *D. tenui* is *Dactylioceras tenuicostatum* Zone, *semi is semicelatum* Subzone. Belemnites reported in McArthur *et al.* (2007) were from the top of Ovatum Band (Bed 48).

5.4.6 The palaeo-environment of the Early Toarcian seaway

The degree of pyritization (Raiswell and Berner, 1985; Wignall *et al.*, 2005; Pearce *et al.*, 2008) and Mo/TOC ratios of the Toarcian black shales of Yorkshire (McArthur *et al.*, 2008) reveal that the Toarcian seaway reached maximal euxinia between upper-*semicelatum* and *exaratum* Sz (Bed 32 to 40). A strong freshwater influence in the Toarcian seaway of NW Europe has been proposed to trigger the development of a strong pycnocline, then the isolation of deepwater, and high

biological productivity, which eventually lead to the deposit of organic rich sediments (with TOC >2%) through the interval and give rise to deepwater euxinia (Küspert, 1982; Saelen *et al.*, 1996; Saelen *et al.*, 1998; Saelen *et al.*, 2000; Rohl *et al.*, 2001; Schmid-Rohl *et al.*, 2002; Bailey *et al.*, 2003; Frimmel *et al.*, 2004; Schwark and Frimmel, 2004; van de Schootbrugge *et al.*, 2005). From the *falciferum* to lower *commune* Subzone (the sampling interval in this work), restriction was not very severe and euxinic conditions remained intermediate until Bed 50, after which restriction was absent (McArthur *et al.*, 2008). As a response to unfavorable conditions, faunal diversity and richness through the interval reduced to low levels through Beds 32 to 51 (Harries and Little, 1999).

During the long-term euxinia in the Cleveland Basin, some Early Toarcian faunas, such as belemnites, have been found at uncommon, discrete, horizons within the *exaratum* Subzone in Yorkshire sections (Howarth, 1963), and German equivalent level and above (Rohl *et al.*, 2001; Schmid-Rohl and Rohl, 2003). Those authors concluded that the euxinic conditions in the Early Toarican seas were occasionally interrupted by short episodes of oxic conditions that allowed benthos and planktonic life to briefly be re-established in the Early Toarcian seaway. So, belemnites (and other fossils) therefore captured the geochemical signals of these short-term events in their isotopic compositions (Little and Benton, 1995; McArthur *et al.*, 2008; Caswell *et al.*, 2009). However, many geochemical parameters, such as Mo/TOC of black shales, seem not to reveal these short-term intervals. It may be because the open-ocean oxic conditions were too short to affect the Mo or sampling intervals of black shales for Mo/TOC were too big to reflect these events. Therefore, the Cleveland Basin in the Early Toarcian (*exaratum* to lower *commune* Subzones) experienced a long-term, severe to moderate, euxinia well-represented by Mo/TOC of black shales, but were occasionally interrupted by brief oxic intervals recorded by belemnites. It is therefore no surprise that, for example, the $\delta^{13}C$ profile of belemnites doesn't reflect the negative carbon isotope excursion shown by Early Toarcian organic matter in the *exaratum* Sz. through the Toarcian RAE (Jenkyns, 1988). Belemnites and the organic matter are apparently not recording the same events during Early Toarcian time.

5.4.7 Belemnite living niches

Belemnites are not common in sediments except where concentrated by, for example, condensation of the sequence, the rare preservation of spawning grounds, or regurgitation from the stomachs of marine predators. Of these, the most common in Yorkshire is condensation, as inferred by the strong concentration of belemnites at the levels of carbonate concretions (*e.g.* Beds 33, 35, 37, 40) or thin units of carbonate-cemented sediments (Beds 39, 42, 44, 46, 48, 50).

Belemnites lived only for a few years (Guerra, 2006; Rexfort and Mutterlose, 2006). The question then arises as to whether the four species of belemnites studied here coexisted in the Toarcian seaway during the short oxygenation moments and so reflected a range of conditions of their habitats in those seas, or whether the appearance of different belemnites at different stratigraphic levels signaled a change in environmental conditions. This point is illustrated in Fig. 5.10, where two belemnite species found through a section might represent cyclic changes in environmental conditions. It is clear from McArthur *et al*. (2007b) that *A. vulgaris* and *A. subtenuis* inhabited the same sea at the same time, as specimens of both derived from the stomach contents of a marine predator and so must have been contemporaneous. The specimens of *A. vulgaris* and *A. subtenuis* in this study derive from 25 m of sediments that represent a time interval of around 400 kyrs (mid-*falciferum* to lower *commune* Szs.) yet show the same pattern of behaviour as do the specimens from the top of Bed 48. Had the main reason for compositional differences between *A. vulgaris* and *A. subtenuis* been changes in environmental conditions (shown in Fig. 5.10), the contemporaneous records of *A. vulgaris* and *A. subtenuis* from McArthur *et al*. (2007b) would have behaved differently from the long-term records of *A. vulgaris* and *A. subtenuis* here. However, the similarity of the presented data here to the data for that instant of geological time militates against the climate change scenario, but indicates that the brief return to oxygenation at the belemnite levels sampled re-established very similar conditions each time. Each belemnite species then re-occupied the same environmental niche on each occasion, and hence recorded short-term oxic geochemical signals during the long-term euxinia of the Early Toarcian Seas. So, intra- and inter-species compositional

variations in the four belemnites species studied here are not climate-related, but are likely to reflect factors like differing habitats and species effects.

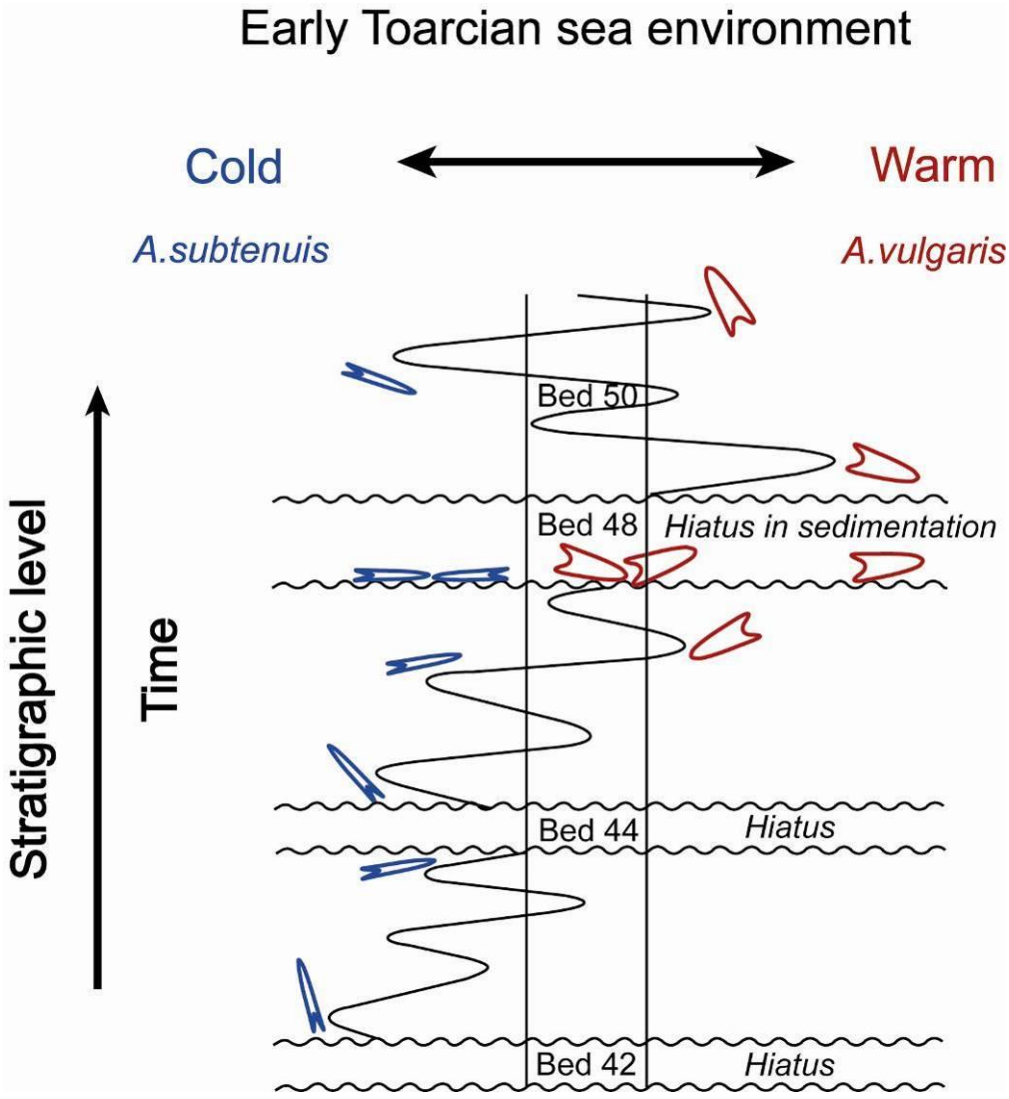

Fig. 5.10 Schematic of how two belemnite species, tolerant of different conditions, might appear in a sediment section. Such specimens could be interpreted either in terms of changing conditions or in terms of co-existing belemnite populations that inhabited differing environmental niches if it was not known that the recorded occurrences of each were mutually exclusive in time.

5.5 Conclusion

1) Of the four species studied here (*A. subtenuis*, *Y. simpsoni*, *A. vulgaris* and *S. dorsalis*), specimens of *A. vulgaris* are likely to possess highest Sr/Ca, *Y. simpsoni* the lowest Na/Ca and *A. subtenuis* the highest Mg/Ca. Specimens *of A. subtenuis* and *Y. simpsoni* have similar chemical compositional ranges, so

do *S. dorsalis* and *A. vulgaris*. *S. dorsalis* and *A. vulgaris* specimens are heavier in $\delta^{13}C$ and lighter in $\delta^{18}O$ values than *A. subtenuis* and *Y. simpsoni* specimens. The species *S. dorsalis*, appears to exhibit a strong species-specific fractionation of around +2 ‰ in carbon during calcification.

2) For *A. vulgaris* and *S. dorsalis* specimens, the tight compositional variation and the narrow temperature range indicate their restricted and shallow living environments. In contrast, *A. subtenuis* and *Y. simpsoni* specimens likely lived in broad habitats with differing thermal conditions in Early Toarican seas, shown in their wide isotopic and elemental contents.

3) The lack of correlation between Mg/Ca and $\delta^{18}O$ within and between species suggest that Mg/Ca cannot be used as a palaeotemperature proxy in Toarcian belemnites. Values of Sr/Ca correlate with $\delta^{18}O$ well and may be reflecting palaeotemperature of calcification.

4) The palaeo-information contained in well-preserved Early Toarcian belemnites is likely to reflect the primary open-oceanic conditions and effects of species differences and biological fractionation. Other independent palaeo-proxies should also be considered and compared with belemnite records, so as to understand the differences and limits of differing palaeo-indicators, and the primary background environmental conditions of the study interval.

5) These complexities found from belemnites may also exist in other palaeo-indicative fossils like foraminifera, so a better understanding of the complexities will lead to a better use of fossil palaeo-proxies.

Chapter 6 Callovian Belemnites from Cambridgeshire

In order to decipher the palaeo-ecology of belemnite species *Cylindroteuthis pusoziana* (*C. pusoziana*), and to assess the potential of the palaeo-proxies for this species, this chapter investigates the chemical variations within the species *C. pusoziana* of Callovian time, that were collected from the Oxford Clay Formation, Peterborough, Cambridgeshire. The investigation was done first through the study of the size of around 250 specimens of this species that reflect a complete range of ontogenetic phases *i.e.* the small juveniles, mid-juveniles and adults. In addition, compositional data, including intra-rostral composition and the bulk chemistry (isotopes and elements) of a few of the least altered specimens, have also been obtained.

6.1 Introduction

The Oxford Clay Formation is one of the classical units in British Jurassic stratigraphy. It has been well-studied for its superb fossils (Martill and Hudson, 1991). Excellent ammonite faunas in the sequence are significant in the international bio-stratigraphic correlation of the Callovian and Oxfordian Stages. Most of the early work published up to the 1970s was on stratigraphical palaeontology and palaeo-ecology of Oxford Clay biota (Callomon, 1968; Duff, 1975 and many more). The sedimentary, isotopic records and particularly the depositional environment of the Formation were then studied by many authors (Hudson, 1978; Williams, 1988; Hudson and Martill, 1991; Martill and Hudson, 1991; Hudson, 1994).

Carbon and oxygen isotopic compositions of calcareous fossils (*e.g.* aragonite ammonites and bivalves, calcite belemnites) from the Peterborough Member of Oxford Clay Formation have been used to interpret the palaeo-environmental conditions (temperatures and thermal stratification of the water column) of the Middle Callovian time (Williams, 1988; Anderson *et al.*, 1994). The isotopic investigations on fossil ammonites, belemnites and bivalves in Anderson *et al.* (1994) inply that the accumulation of the Peterborough Member underwent short-term seasonal palaeo-environmental fluctuations but exhibited long-term palaeoceanographic stability in the shallow-shelf setting. However, the sample

screening criteria (fossils containing <1000 ppm of Fe and <100 ppm of Mn being accepted as well-preserved) in Anderson *et al.* (1994) is too loose. According to the elemental criteria on well-preserved belemnites (Fe < 100 ppm and Mn < 30 ppm) made after analyses of hundreds of Mesozoic belemnites in this study, only 5 out of their 54 belemnites and 1 out of their 23 bivalves fall in my well-preserved sample field whereas the majority contains 100 – 10000 ppm of Fe and 50 – 500 ppm of Mn. The palaeo-environmental implications made from these samples with apparent alteration signals need further validation by comparison to better preserved samples. The well-preserved belemnite specimens obtained in this study will serve this purpose.

In addition, in the sample population studied here, more small juveniles are present than large adults of the same species. Traditionally, only big well-preserved belemnites are picked for analysis because the small ones are not easy to identify and provide limited useful bits for analysis after cleaning. This sampling bias has prevented us from knowing the palaeo-ecological and -biological effects that belemnite juveniles have. The collection of around 250 specimens of belemnite *C.pusoziana* representing the complete growing phases hence provides a good chance to study the autecology and ontogeny of this belemnite community.

6.2 Geologic background of the sampling interval

A collection of over 250 specimens of *C. pusoziana*, obtained from Prof. Peter Doyle, came from a single stratum, Bed 13, at the base of Peterborough Member (Mid-Callovian), Oxford Clay Formation of Kings Dyke (Hansen Quarry), Whittlesey, near Peterborough, UK (Fig. 6.1). The lithostratigraphy and biostratigraphy of the section were documented in Callomon (1968) and Duff (1978), refined by Hudson & Martill (1991, 1994), and summarized in Table 6.1. The sampled bed 13 (0.02m in thickness) is the upper most layer of the strongly condensed *jason* Subzone in the lower Peterborough member, and is a well-developed shell-bed with abundant ammonite fragments and belemnites in a clay matrix (Hudson and Martill, 1994). Bed numbers shown in Table 6.1 are from Hudson *et al.* (1994).

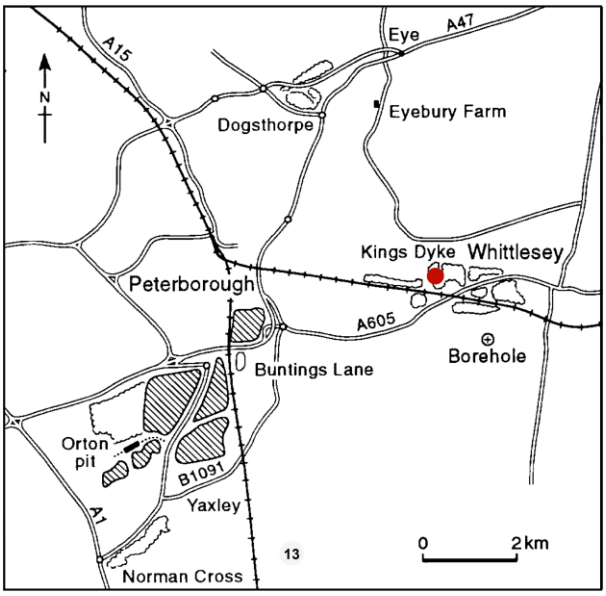

Fig. 6.1 The simplified map of the sampling area (marked with a red dot), King's Dyke of Whittlesey, the Peterborough district, UK. Diagram modified from Hudson & Martill, 1994.

During Callovian times, the Oxford Clay Sea was probably no more than a few tens of metres deep. Oxford Clay mudstones in the King's Dyke pit of central England were possibly deposited in a shallow, productive, epeiric sea, with long periods of non-deposition being interrupted by short periods of rapid sediment accumulation (Hudson and Martill, 1991; Kenig *et al.*, 1994; Macquaker, 1994).

The Peterborough Member biota, investigated in Duff (1975) and updated in Martill & Hudson (1991) were diverse. Marine vertebrates (e.g. fish and reptiles) were abundant; and invertebrates (such as ammonites, belemnites and bivalves) also occured as many species and in large numbers, with single species dominating some shell beds of the Peterborough Member. Particularly, belemnites of the species *Cylindroteuthis* occurred in high abundance and grew to a considerable length of 20 cm in *Jason* Zone. The shallow burial of Oxford Clay sediments allowed high degree of preservation of fossils.

A large number of specimens obtained in this study probably represent spawning accumulations. There are uncommon *Hibolites* specimens, but the vast majority was identified to belong to a single species *Cylindroteuthis pusoziana* (*C. pusoziana*), and reflect a range of ontogenetic stages (Table 6.2). All the specimens have been measured for size and selected well-preserved ones for composition.

Table 6.1 The biostratigraphy and lithostratigraphy of the *coronatum* to *jason* Zones of Peterborough Member at Whittlesey, UK. The sampling bed (bed 13) is highlighted in bold.

	Zone	Subzone	Formation	Members	Bed No.	Lithology	D(m)
CALLOVIAN (PART)	*coronatum*	*grossouvrei (part)*	Oxford Clay Formation (part)	Peterborough Member (part)	18	Dark bed, shale, not very fissile	1.17
		obductum			17	Nuculacean shell-bed, pyritic	0.10
					16	Shale	0.20
					15	Shale, fissile, white-weathering, 2cm nuculacean shell-bed at top	0.16
					14	Shale, not very fissile & soffiliferous.	3.80
	jason (part)	*jason*			**13**	**Shell-bed, rounded clasts of wood**	**0.02**
					12	Shale, organic-rich, fissils in lower part	0.46
					11	Shell-bed	0.04
					10	Shale, fissile, organic-rich, burrows in upper part; abundant ammonites, large calcareous septatian concretions.	0.17

Table 6.2 The descriptions of species *C. pusoziana* at different growth stages, pictures are provided in Fig. 6.2.

Species	Ontogenetic stage	Description	No.
C. pusoziana	Juvenile	Small sized (L<4 cm), subhastate in shape, subquadrate to compressed elliptical cross-section. Lateral depression and vertral line present, acute apex.	118
	Mid-juvenile	Medium sized (L= 4-8 cm), slender, cylindroconical rostrum with subquadrate to round cross-section, symmetrical outline and profile, deep ventral line, acute apex.	114
	Adult	Large sized (L>8 cm), cylindroconical to cylindrical rostrum, elliptical to round cross-section, no apical grooves, but well-developed ventral line, acute apex.	20

Note: L refers to the length from the base of alveolus (the protoconch) to the apex tip. Fig. 1.1 in Chapter 1 shows the structure of belemnite rostrum and indicates these positions.

a) Small juvenile *C.pusoziana* 1S 39

b) Mid-juvenile *C.pusoziana* 13/45

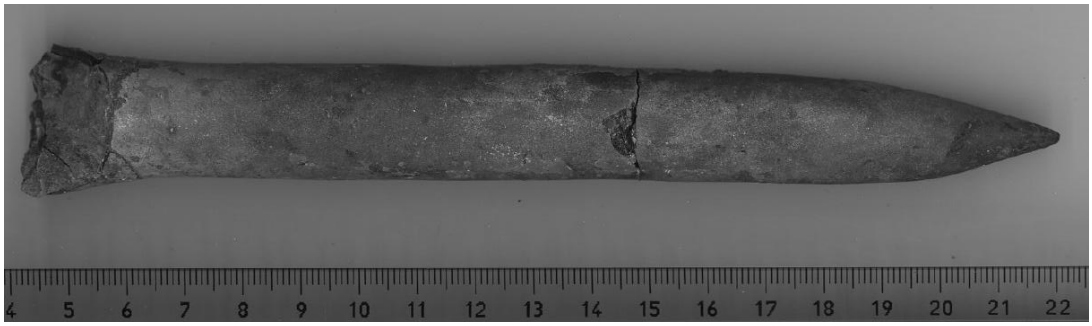

c) An adult specimen of *C.pusoziana*: 2S 116

Fig. 6.2 Specimens of species *C. pusoziana* from Callovian of Oxfordshire, UK, at three ontogenetic stages: a) small juvenile to b) mid-juvenile to c) mature form. Scale is in mm and cm.

6.3 Results

6.3.1 Size data of Belemnite *C. pusoziana*

The size data of 252 specimens of *C. pusoziana* are shown in Fig. 6.3 and Fig. 6.4. The length (L) of a specimen refers to the distance between the base of alveolus and the apex of the rostrum, and the diameter (D) is the average of the maximal and minimal diametral distances at the base of the alveolus. The population distribution histogram (Fig. 6.3 a) shows that the nearly 50% of the *C. pusoziana* specimens have a length from 3 to 5 cm and 78% fall in the length interval of 2-6 cm, followed by 10% of specimens with length ranging from 6 to 8 cm. Oversized (L>8 cm) and undersized (L<2 cm) specimens only account for 8% and 4% of *C. pusoziana* population, individually. Fig. 6.3 b shows that the D/L ratios of 70% of the specimens range between 0.10 and 0.13.

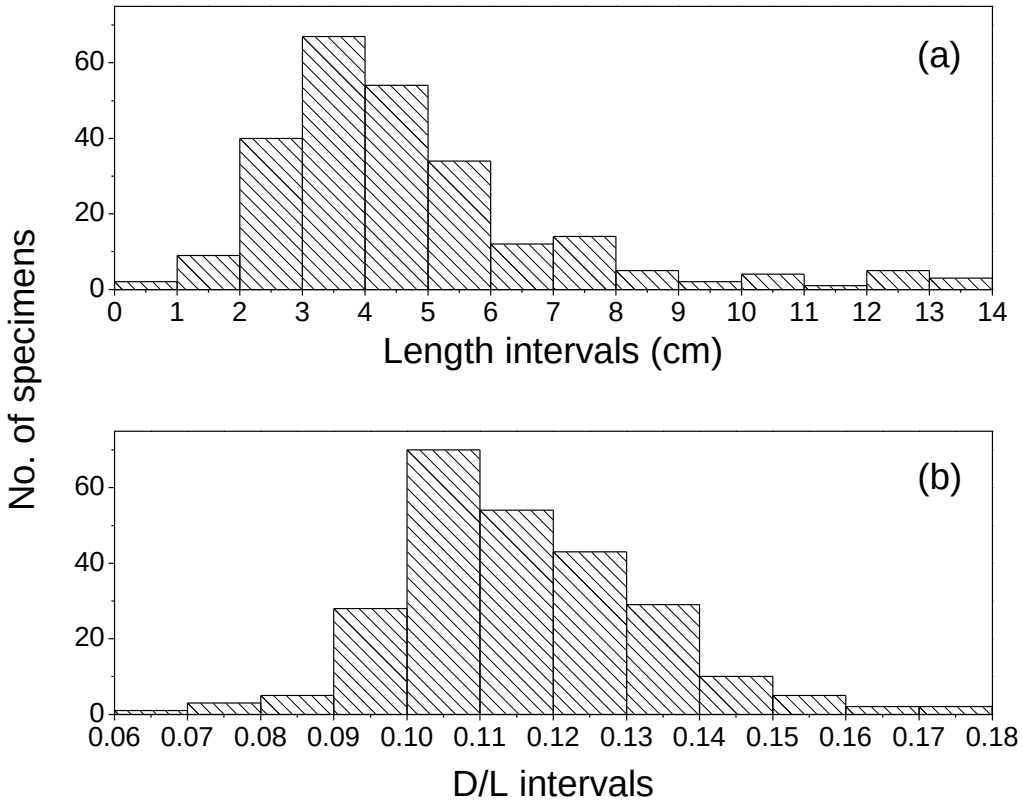

Fig. 6.3 The histograms of size data of specimens of belemnite *C.pusoziana*. D/L refers to the ratios of diameter to length.

Length and diameter of belemnite rostra correlate lineally, with the increase in long axis (L), the diametral distance (D) of a transverse increases (Fig. 6.4 a). The ratios of diameter to length (D/L) is plotted against length (L) in Fig. 6.4 b. Adult belemnites (L>8cm) appear to have higher D/L ratios but less wider D/L range than juveniles of the same species. At any constant D/L ratio between 0.09 and 0.14, there are plenty of specimens with length ranging from 2 to 8 cm (Fig. 6.3b & Fig. 6.4 b), and vice versa.

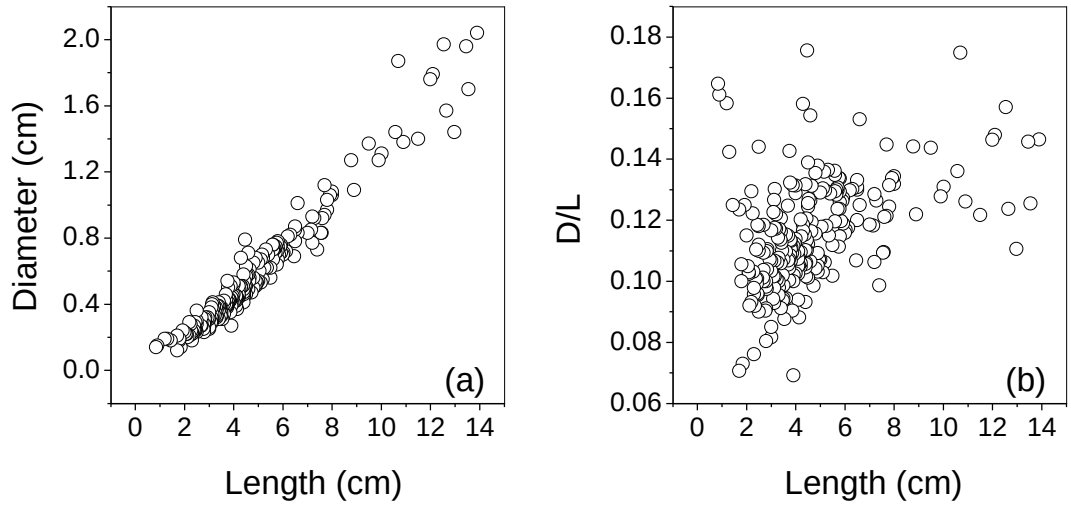

Fig. 6.4 The plots of length vs. diameter and D/L ratios of 252 specimens of belemnite *C.pusoziana*. D/L – the ratio of diameter to length.

6.3.2 Thick section observations

The polished thick cross-sections of the specimens are shown in Fig. 6.5. The concentric growth pattern is discernible. Large areas of clear light-brown calcite are preserved in each section, although cloudy and altered calcite is visible around the apical line, the exterior and along the fractures. Fractures and the apical line are also commonly stained by dark materials (e.g. iron oxide and/or pyrite). Growth boundaries are densely distributed in specimens of this species, and up to a few hundred of these boundary bands are visible in specimens, such as 13-49 a, 1S 57 and 2S 72 (Fig. 6.5). Sample sections show variable degrees of preservation. The inner growth boundaries are thick and dark whilst outer boundaries are thin and light in specimens 13-49 a, 1S 57, 2S 116, 13-46, 13-48, 1S 35, 13-109. The remaining 4 specimens (2S 72, 2S 30, 13-165, and 2S 16) show a uniform pattern of faded growth boundaries from apical line to the exterior of the sections.

13-49a

1S 57

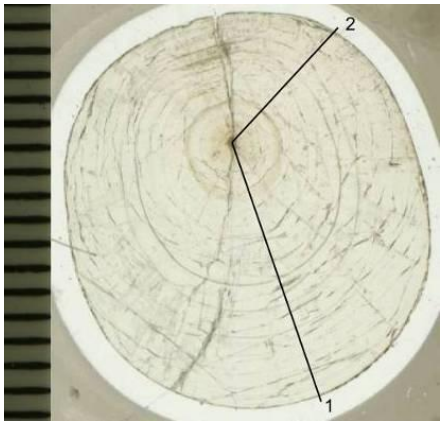

1S 35

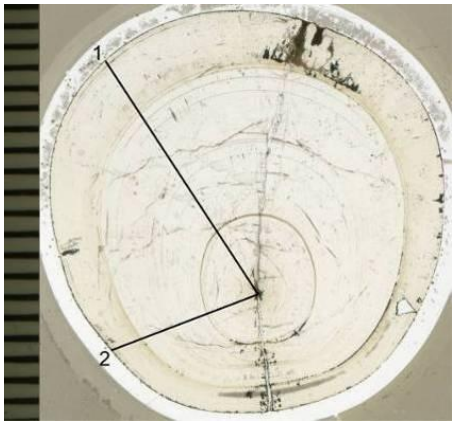

2S 116

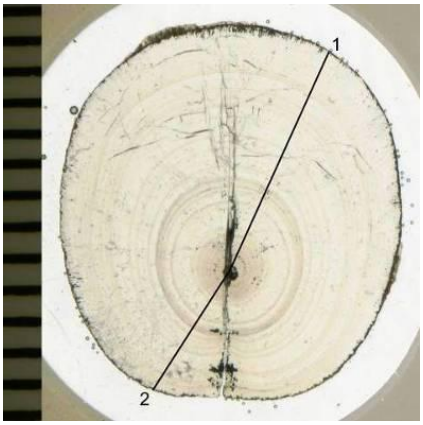

13-109

13-46

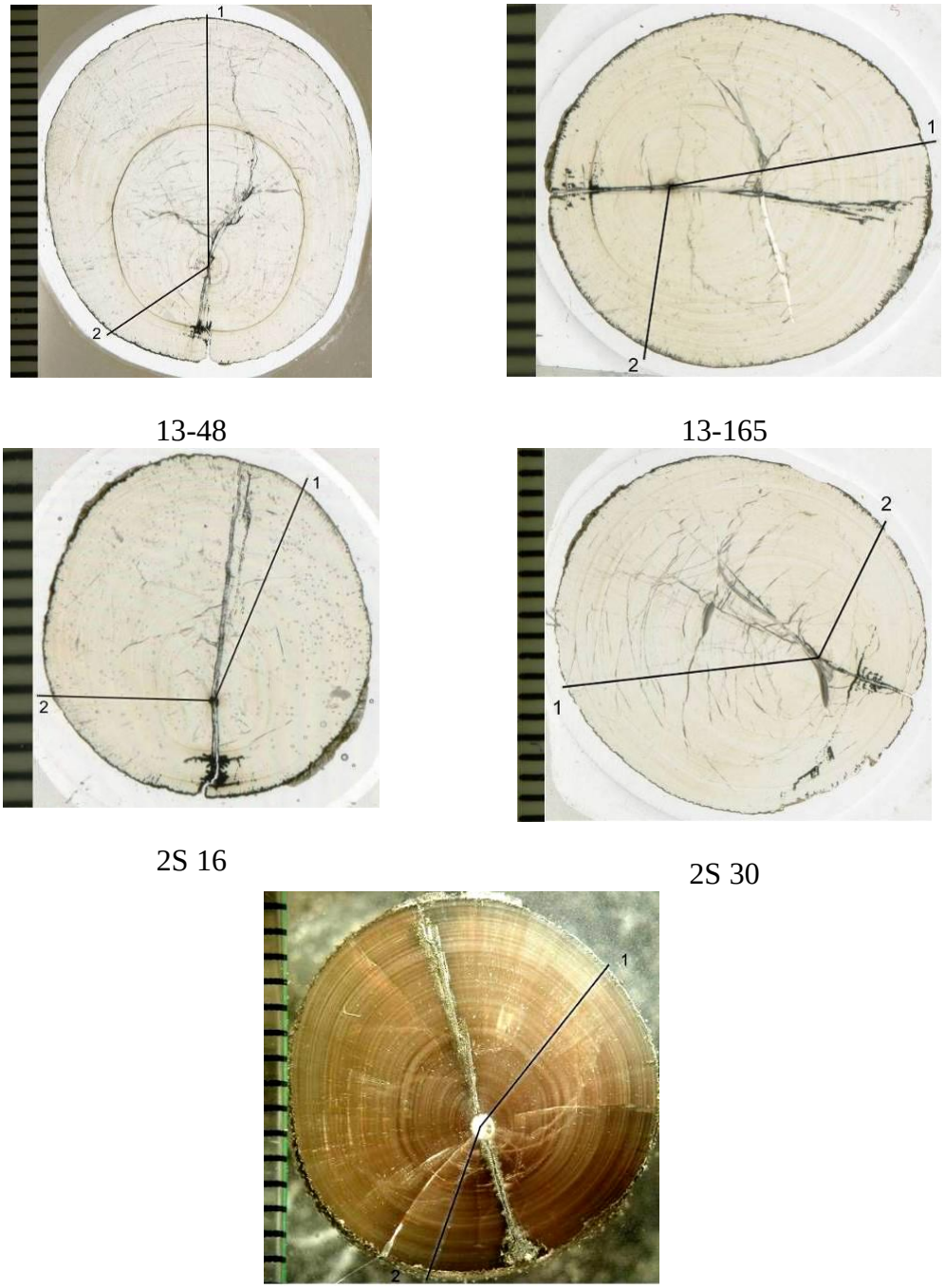

Fig. 6.5 Polished cross-sections of C.pusoziana specimens. The numbers 1 and 2 refer to the two traverses analyzed for concentration profiles by laser ablation ICP-MS and electron micro probe. The scale in each graph is 1mm.

6.3.3 Elemental profiles across sections of *C. pusoziana* specimens

Multi-elemental profiles of *C. pusoziana* specimens were obtained by both laser ablation-ICP-MS (LA) and electron microprobe (EMP). The analysed elements include Na, Mg, Ca, Mn, Fe, Zn, Sr, Ba and S. The LA profiles of 11 specimens,

with a resolution of 44 µm, are shown in Fig. 6.7 to Fig. 6.14; and electron microprobe profiles of two other specimens, with a spot size of 50 µm and 70 µm, are present in Fig. 6.15 and Fig. 6.16. Both methods have been compared and verified in section 4.4.1 of Chapter 4, and reveal the same overall radial trends of Ca, Mg and Na here. The majority of *C.pusoziana* samples were profiled using LA approach; so the LA profiles of multi-elements are the focus when interpreting intro-rostral compositional variations.

The profiles of Ca, Mg, Na and Sr show very similar radial variation magnitudes that have been seen previously in the profiles of Pliensbachian belemnites. From the well-preserved areas of the sections (excluding the apical line and edge), magnesium shows the broadest variation of 1000 – 6000 ppm within a rostrum, whereas strontium gives the smallest variation range of 600 – 1800 ppm; and sodium varies between 1000 and 2500 ppm.

The Mg, Na and Sr profiles of most specimens present a sharp decline in concentration from near the apical line to the inner quarter of the section, followed by a slow decrease towards the edge. Specimens with the distinct inner ring structure are characterized with major Mg peaks at where the inner rings are present (e.g. 1S 57 in Fig. 6.6). The regions between the centre (apical line) and the inner ring show a decrease and then an increase in Mg concentration (e.g. 13-49a in Fig. 6.7). The Mg profiles are characteristic of regular small-scaled (10-100 µm) peaks that mostly line up with the growth boundaries in the sections. Concentrations of Mn, Fe, Zn and Ba are typically low in the unaltered regions of the sections. Mn and Fe are generally below 20 ppm, but occasionally spikes up to ~200 ppm in areas of the inner part of a section, fractures and inner growth boundaries. The concentration of Zn is generally below 50 ppm, but can reach to around 100 ppm where it spikes. The undulations in the profiles of Zn are parallel to Mg profiles in all specimens; and the overall trend of Zn follows that of Mg, apart from one specimen 2S-72. The concentration of Ba is consistently around 2 ppm and few Ba spikes are visible.

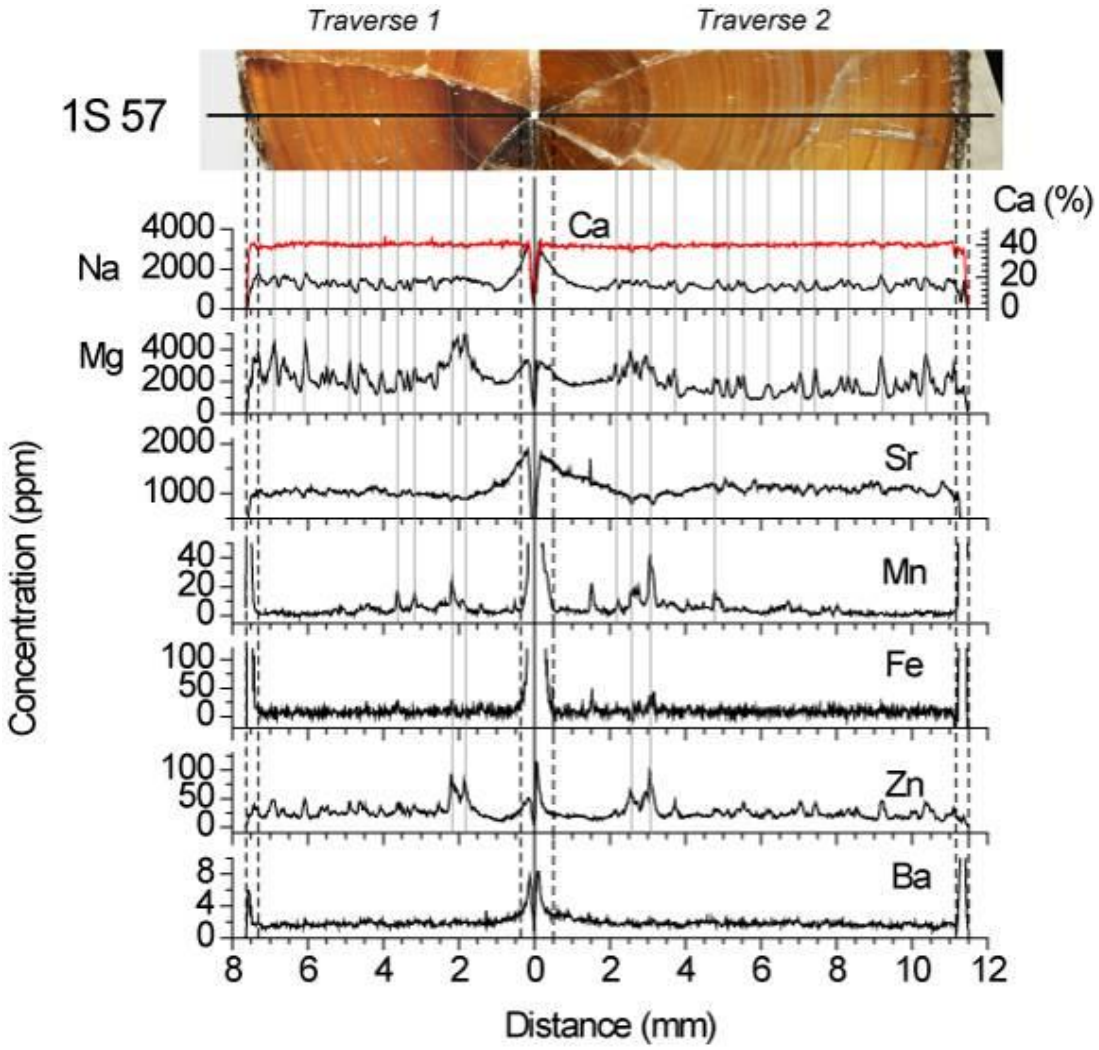

Fig. 6.6 Multi-elemental profiles (Ca, Na, Mg, Sr, Mn, Fe, Zn, and Ba) of *C. pusoziana* specimen 1S 57 obtained by LA-ICP-MS. The two laser ablation traverses are shown in the picture on the top. They are not on one line. The real positions of t/ hem on the sample section are shown in Fig. 6.5. Altered areas of the rim and apical line (central canal) of the belemnite section are enclosed within dotted lines and are not used in palaeotemperature reconstructions. The solid grey lines line up the Mg spikes with the white bands in the picture. X axis represents the distance to the centre of the apical line (which is marked as the 0 mm).

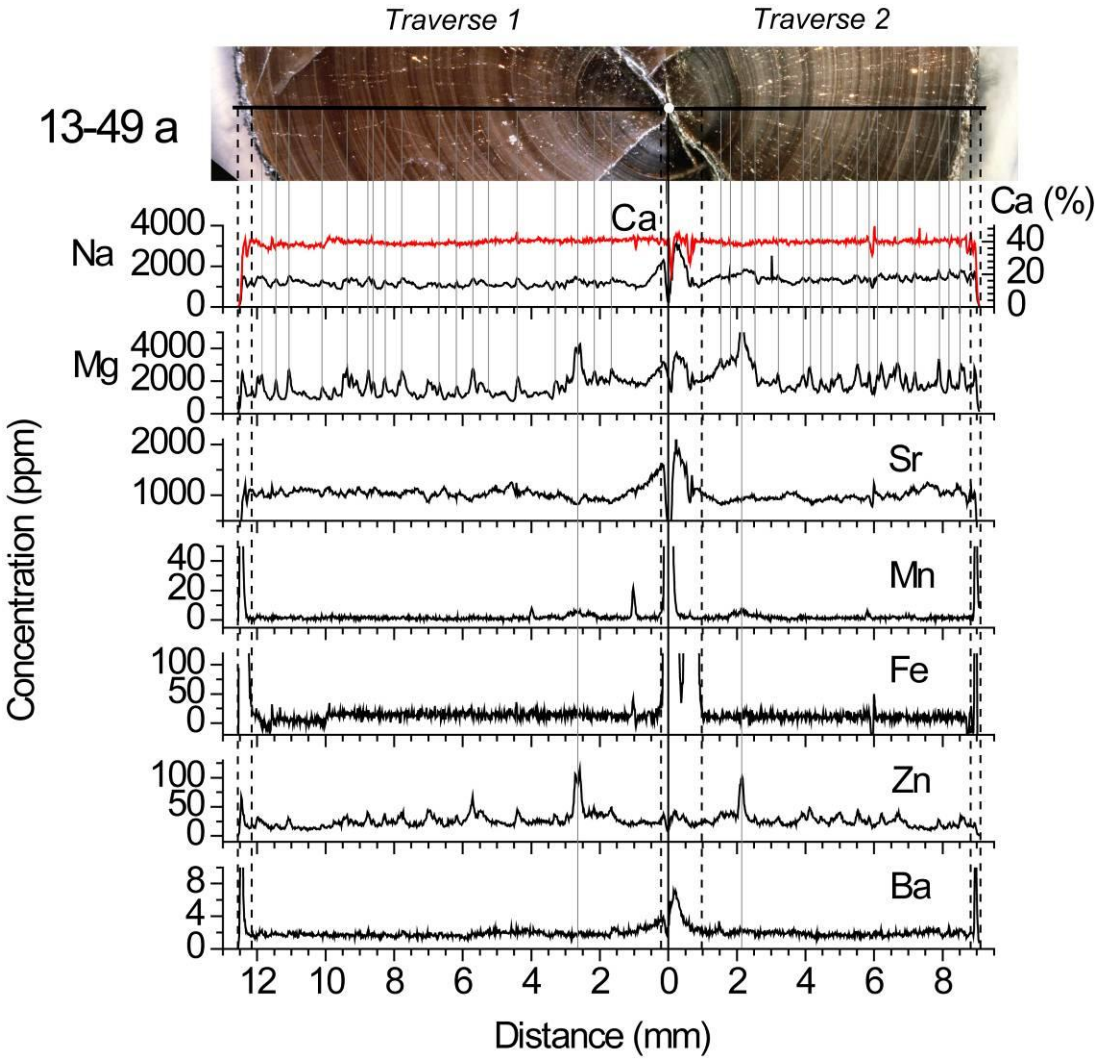

Fig. 6.7 Multi-elemental profiles (Ca, Na, Mg, Sr, Mn, Fe, Zn, and Ba) of *C. pusoziana* specimen 13-49a obtained by LA-ICP-MS.

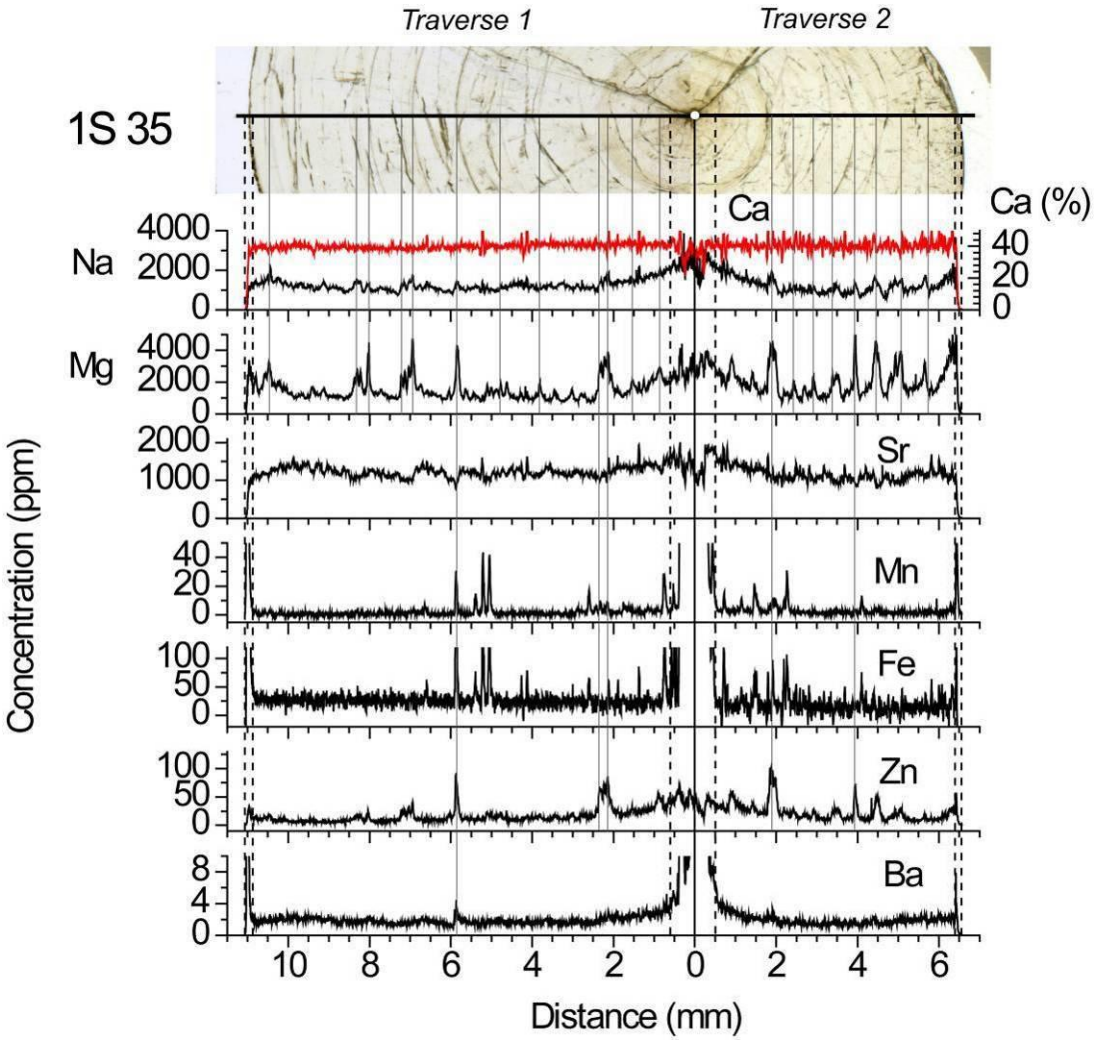

Fig. 6.8 Multi-elemental profiles (Ca, Na, Mg, Sr, Mn, Fe, Zn, and Ba) of *C. pusoziana* specimen 1S 35 obtained by LA-ICP-MS. Two radial fractures are seen on the section, but do not cut the two tranverses.

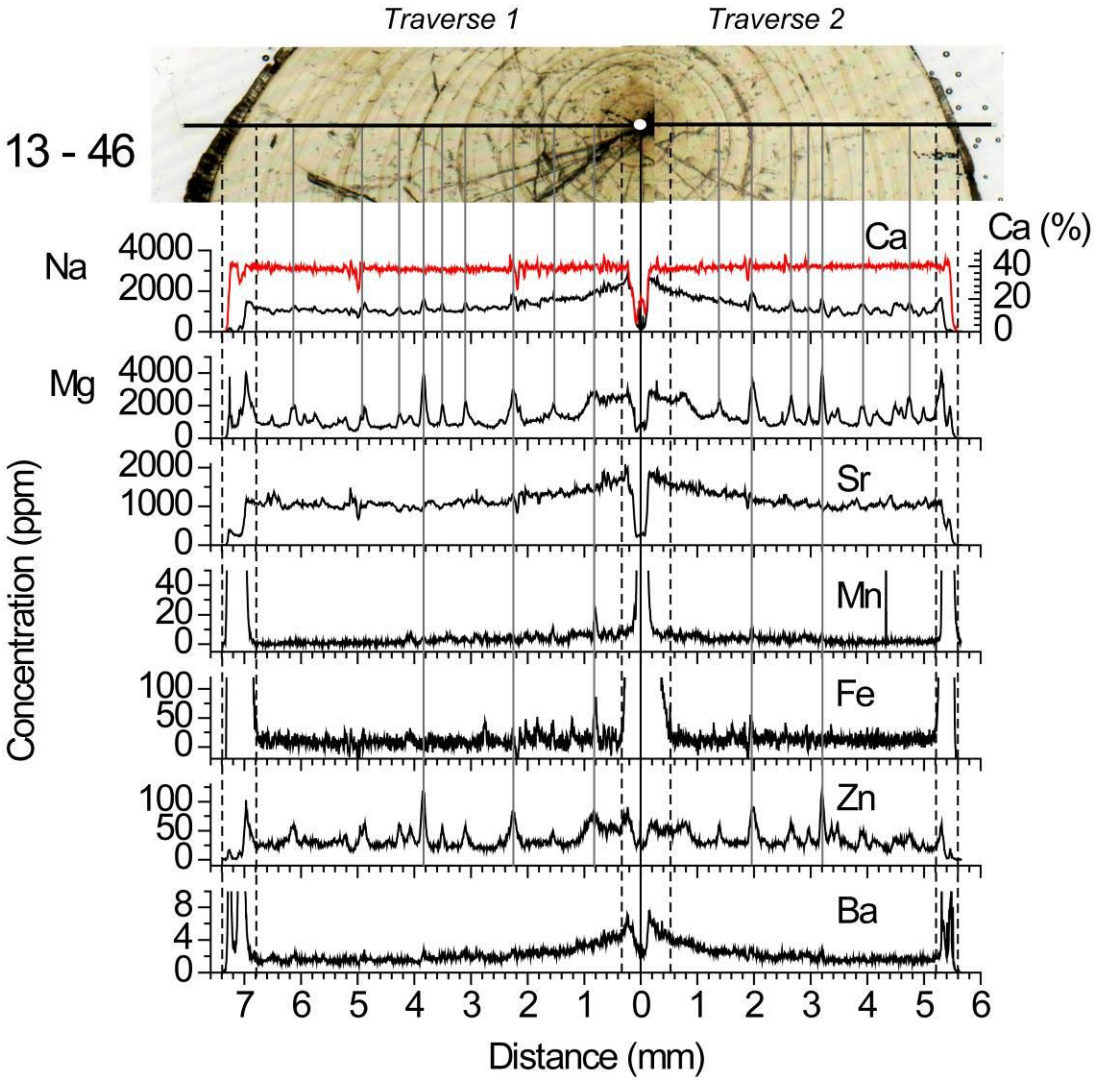

Fig. 6.9 Multi-elemental profiles (Ca, Na, Mg, Sr, Mn, Fe, Zn, and Ba) of *C. pusoziana* specimen 13-46 obtained by LA-ICP-MS.

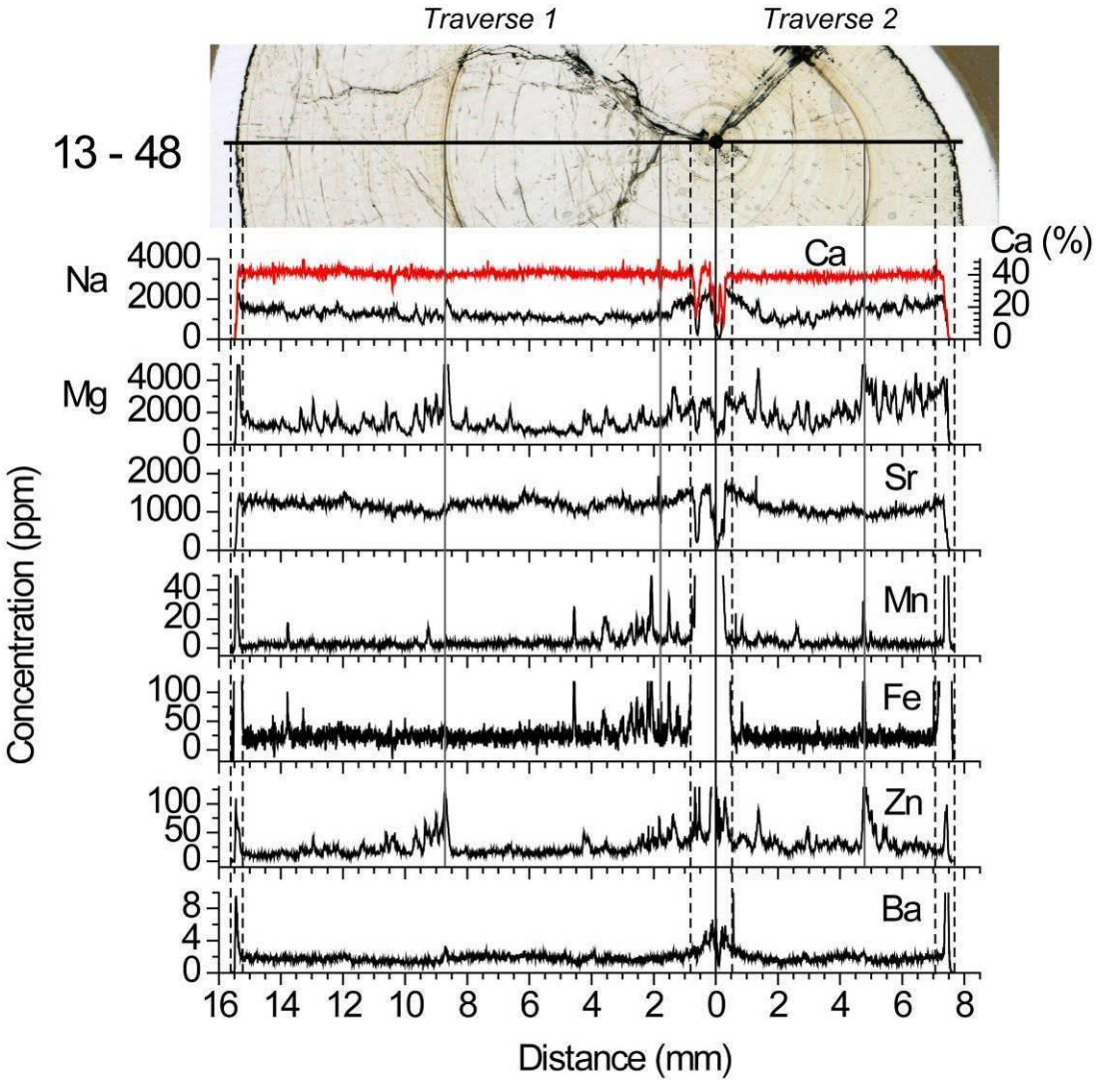

Fig. 6.10 Multi-elemental profiles (Ca, Na, Mg, Sr, Mn, Fe, Zn, and Ba) of *C. pusoziana* specimen 13-48 obtained by LA-ICP-MS.

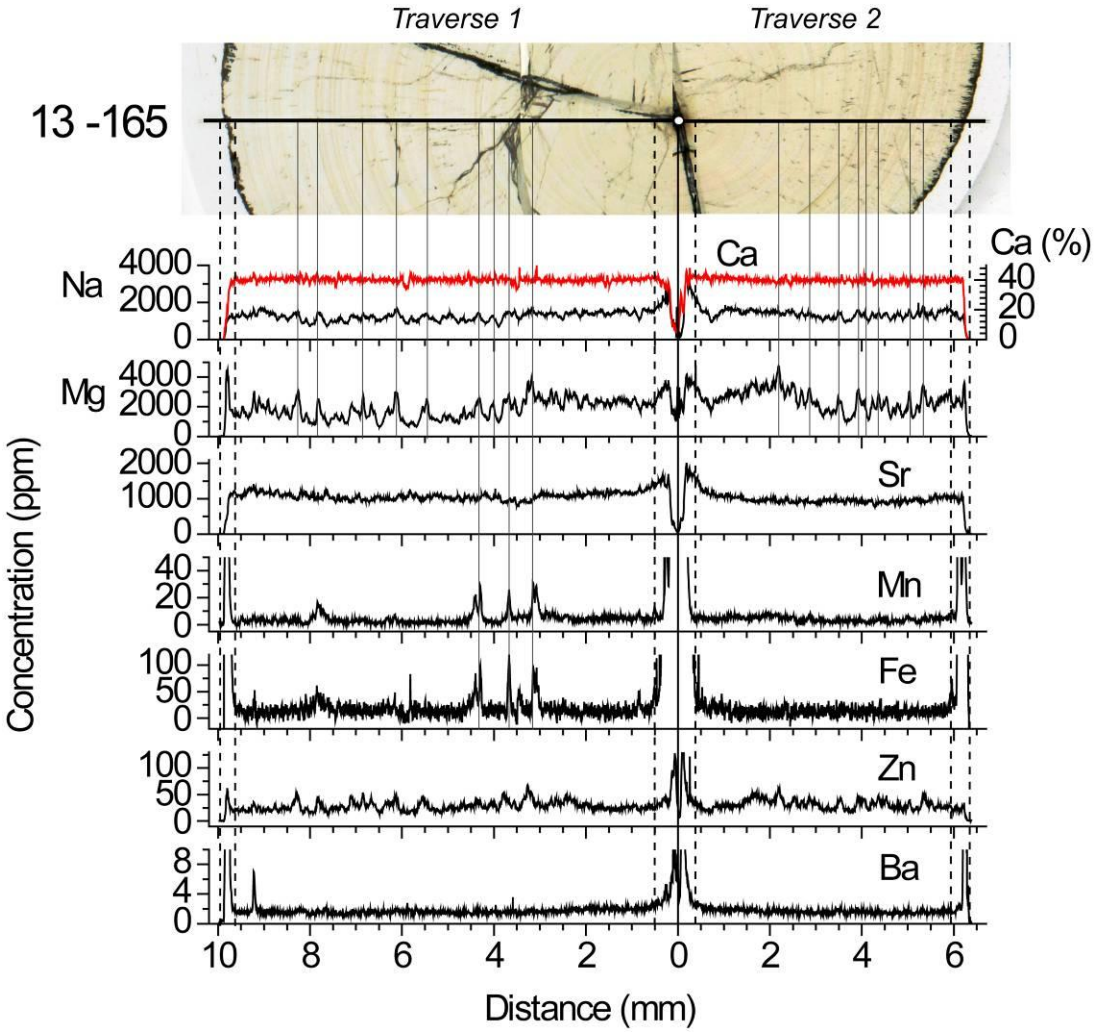

Fig. 6.11 Multi-elemental profiles (Ca, Na, Mg, Sr, Mn, Fe, Zn, and Ba) of *C. pusoziana* specimen 13-165 obtained by LA-ICP-MS.

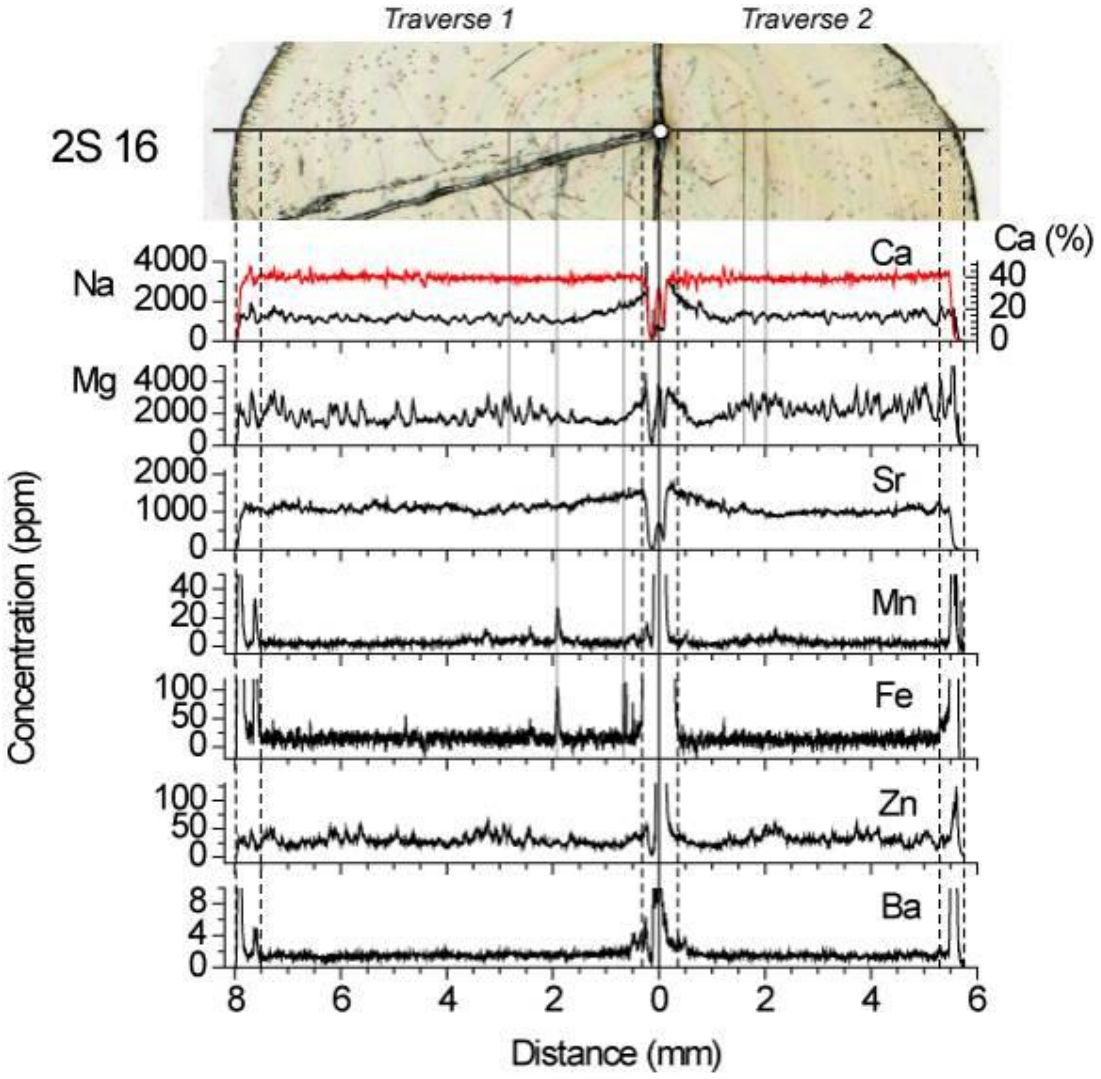

Fig. 6.12 Multi-elemental profiles (Ca, Na, Mg, Sr, Mn, Fe, Zn, and Ba) of *C. pusoziana* specimen 2S 16 obtained by LA-ICP-MS. The two dark lines in the top picture show two big fractures on the section, but the two tranverse analysed are not interrupted by them.

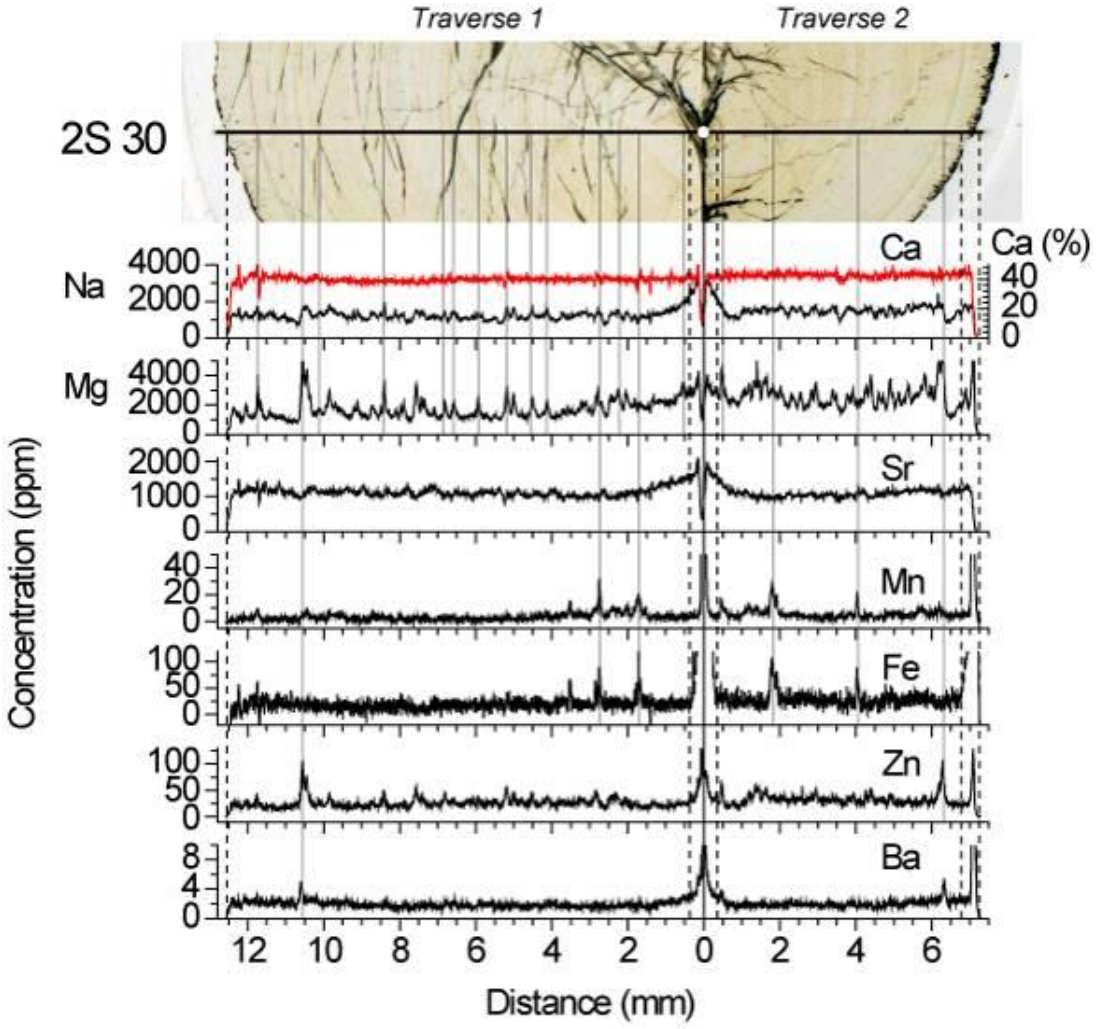

Fig. 6.13 Multi-elemental profiles (Ca, Na, Mg, Sr, Mn, Fe, Zn, and Ba) of *C. pusoziana* specimen 2S 30 obtained by LA-ICP-MS.

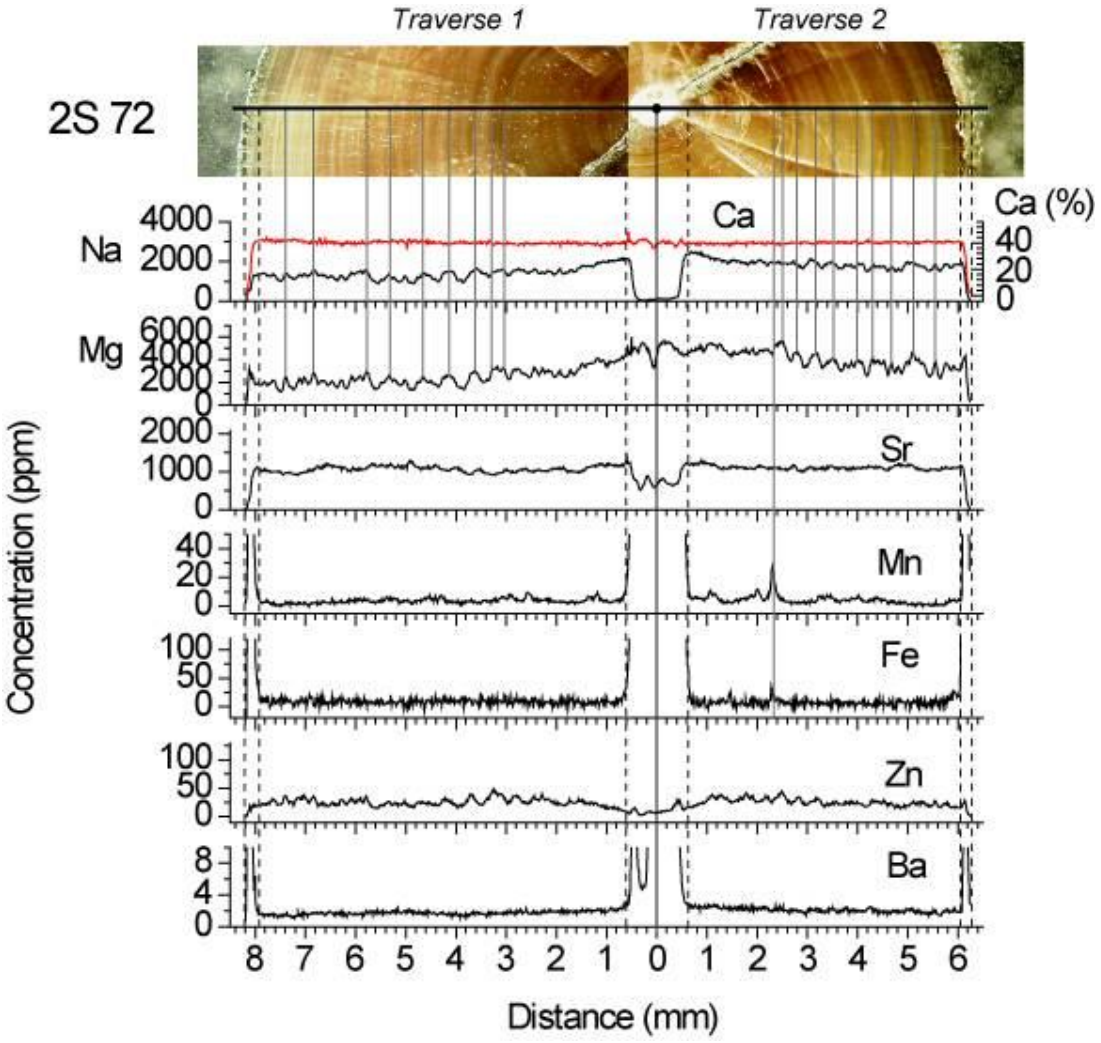

Fig. 6.14 Multi-elemental profiles (Ca, Na, Mg, Sr, Mn, Fe, Zn, and Ba) of *C. pusoziana* specimen 2S 72 obtained by LA-ICP-MS.

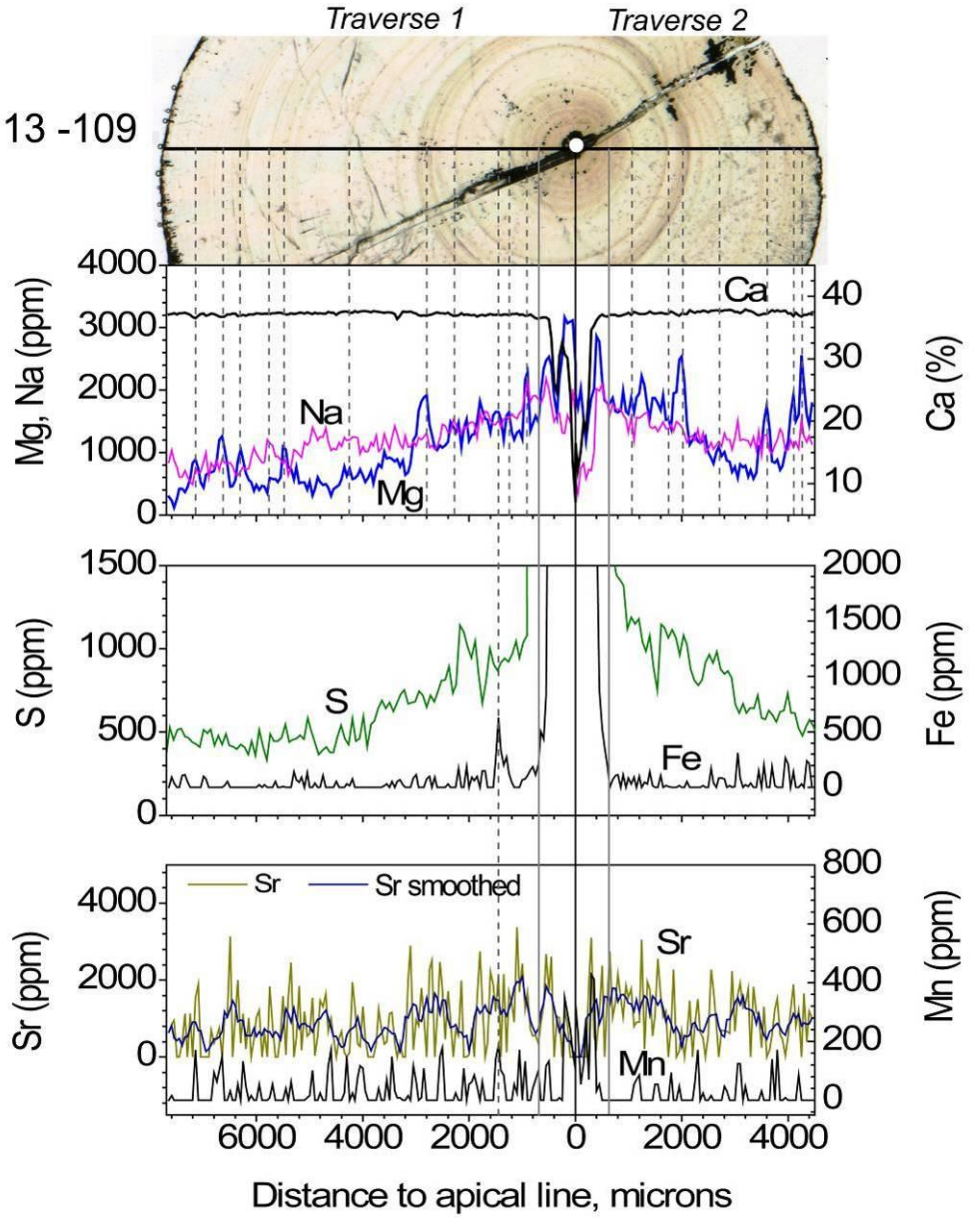

Fig. 6.15 Multi-elemental profiles (Ca, Na, Mg, S, Mn, Fe, and Sr) of *C. pusoziana* specimen 13-109 obtained by electron microprobe. The smoothed Sr curve is plotted using five-spot averages. The two laser ablation traverses are shown in the picture on the top. They are not exactly on one line, and the real positions of them on the sample section are shown in Fig. 6.5. Altered areas of the rim and apical line (central canal) of the belemnite section are enclosed within solid grey lines. The dotted grey lines line up the Mg spikes with the dark bands in the picture.

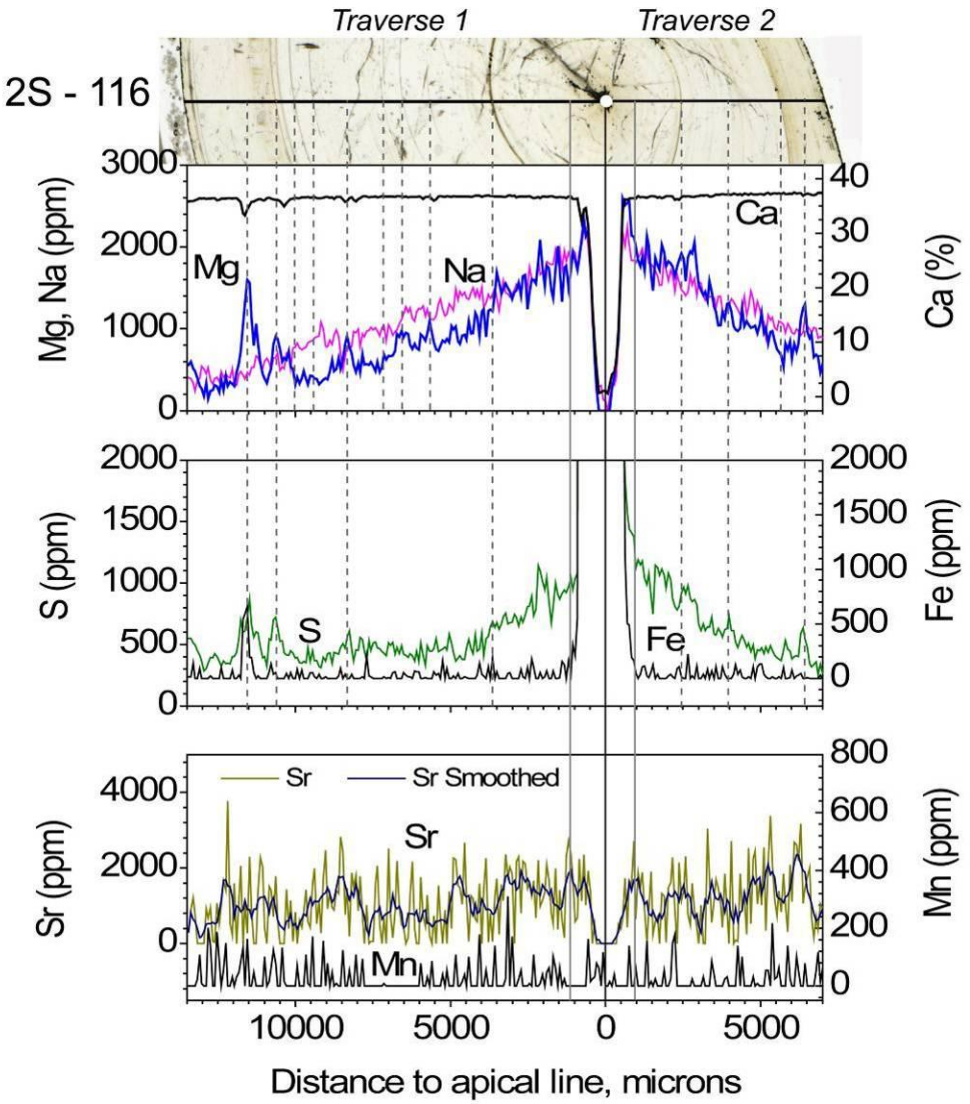

Fig. 6.16 Multi-elemental profiles (Ca, Na, Mg, S, Mn, Fe, and Sr) of *C. pusoziana* specimen 2S-116 obtained by electron microprobe.

6.3.4 Intra-rostral variations in isotopic composition

The profiles of $\delta^{13}C$ and $\delta^{18}O$ are shown across a longitudinal section of the *C.pusoziana* specimen 13-49 in Fig. 6.17. The section of this specimen is off-centered, so the patterns on each side of the alveolar centre are asymmetric. The long path on the right of the alveolar centre (see Fig. 6.17) is picked for discussion here because it is more expanded and so reveals more ontogenetic information than the short one on the left at a resolution of ~0.5mm.

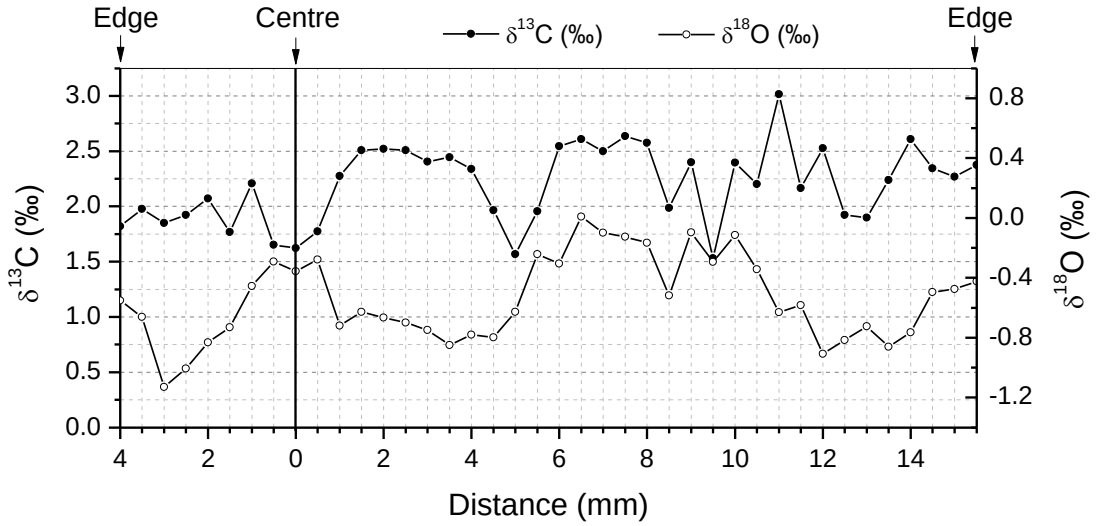

Fig. 6.17 The profiles of $\delta^{13}C$ and $\delta^{18}O$ along a longitudinal section of *C. pusoziana* specimen 13-49. The s axis shows the distance from the alveolar centre which is marked as 0 distance.

The ontogenetic isotopic composition ranges from -1.13 to +0.01‰ in $\delta^{18}O$ and from +1.53 to +3.01 ‰ in $\delta^{13}C$. Small undulations are observed in both $\delta^{13}C$ and $\delta^{18}O$ profiles. The $\delta^{18}O$ curve starts around -0.3 ‰ in the core, but decreases to -0.9 ‰ at 3.5 mm, from where it increases again and reaches the maximun of 0 ‰ at 6.5 mm. From this point, the $\delta^{18}O$ gradually declines to around -0.9 ‰ at 12 mm, followed by a slight increase to -0.4 ‰ at the rostral rim. Values of $\delta^{13}C$ are low (+1.6 ‰) in the core, but overall show a slight rise to +2.5 ‰ near the rim and a maximum of +3 ‰ at 11mm. The radial pattern of $\delta^{13}C$ seems to show a signal of cyclic changes within intervals of around 4 mm, which are only broadly comparable in the profile of $\delta^{18}O$.

6.3.5 Bulk chemistry

The compositional data of the least altered 26 specimens of *C. pusoziana* are shown in Fig. 6.18 to Fig. 6.20 and Appendix E. All the samples contain less than 20 ppm of Fe and <6 ppm of Mn. The concentration of S varies from 250 to 850 ppm, and Ba from 1 to 2.5 ppm. No correlation is present between Na and S, Fe and S and Ba and S.

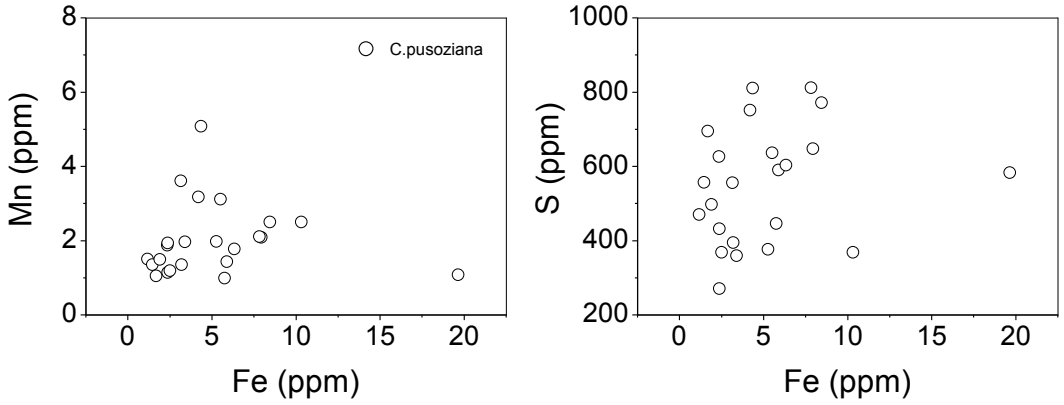

Fig. 6.18 Cross-plots of Fe against Mn, concentrations of Na, Fe, Ba againt S of *C. pusoziana* specimens from Bed 13. Fe and Mn are very low in all specimens, and no correlation is present between these elements.

In bulk analyses, the isotopic composition of specimens ranges between 0.89 – 2.71 ‰ in $\delta^{13}C$ ‰ and -1.31 – -0.17‰ in $\delta^{18}O$ (Fig. 6.19), respectively. The isotopic compositions of *C. pusoziana* specimens from Anderson *et al.* (1994) are also plotted in Fig. 6.19 for comparison. The $\delta^{18}O$ values of the two data sets overlap greatly, but $\delta^{13}C$ values from Anderson *et al.* (1994) show a larger range than values of this study. The well-preserved and altered (high Fe) specimens of the same species from Anderson *et al.* (1994) do not differ much isotopically.

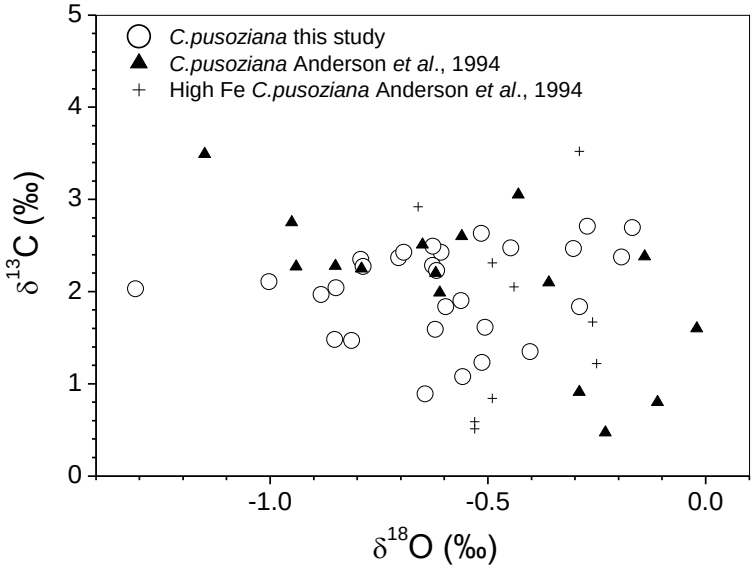

Fig. 6.19 Isotopic compositions of *C.pusoziana* specimens from Bed 13 of the Oxford Clay in this study and in Anderson *et al*. (1994).

For specimens of *C. pusoziana* in this study, Mg/Ca, Na/Ca and Sr/Ca ratios show narrow variation ranges of 3.03 – 6.8, 3.79 – 6.06, and 0.82 – 1.28, individually.

Mg/Ca ratios show poor correlation with $\delta^{18}O$. Sr/Ca and Na/Ca have no corrleation with $\delta^{18}O$, but correlate well with each other (r = 0.68, n = 0.26 and P <0.001, Fig. 6.20).

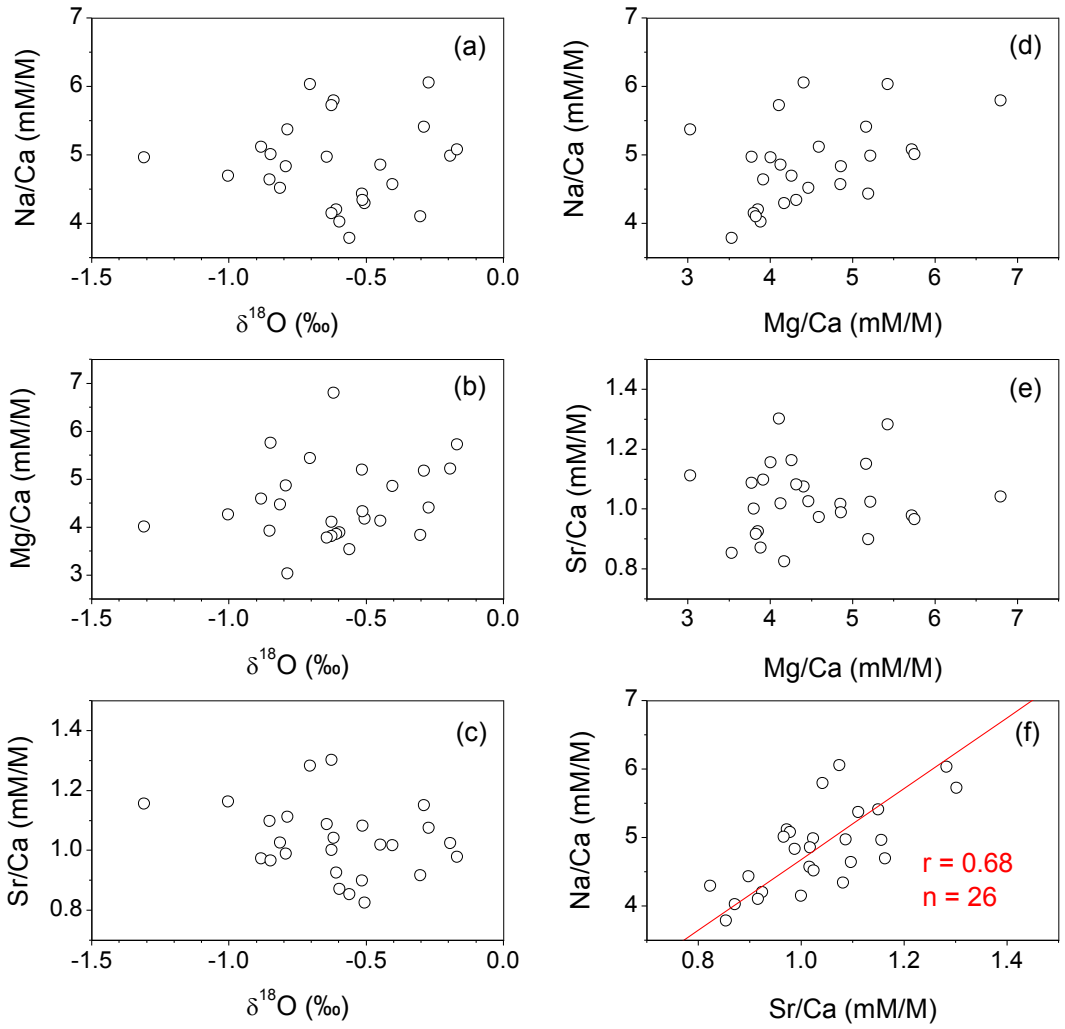

Fig. 6.20 Cross-plots of elemental and isotopic compositions of *C.pusoziana* specimens from Bed 13 of the Oxford Clay. The straight line shown in (f) is reduced major axis (RMA) regression obtained from all the 26 data points.

6.4 Discussion

6.4.1 Population distribution and growth pattern

The size data of *C. pusoziana* population show that over 92% of the specimens of this species are juveniles with length of <8 cm and diameter of <1.2 cm, while only 8% of the specimens are large adults with length of 8 – 14 cm and diameter of 1.2 – 2.0 cm. Small and middle juveniles are proved to indeed constitute a great portion of

a belemnite community. The D/L ratios, on the other hand, bring out more detail of belemnite growth patterns than either length or diameter alone. A D/L interval of 0.10 – 0.13 has been noticed to cover ~ 70% of the analyzed specimens (Fig. 6.3 b), leading to the conclusion that 0.10 – 0.13 is likely to be the interval of most common size ratio of the *C.pusoziana* population.

Large belemnites appear to have higher D/L ratios than normal interval, indicating a faster growth of width than length in adulthood. For small and middle juveniles, the D/L ratios vary from 0.07 to 0.16, suggesting a wide range of growth rates and body shapes. Specimens with the same D/L ratio but different length indicate an isometric growth of both length and width proportionally in early and adolescent time. This can happen when these belemnites lived in a stable shallow-water environment with sufficient food supply and hence grew at a constant pace. Specimens with the same length can also have different D/L ratios. This suggests that either they were born with difference in body size but grew at the same pace under the same environmental settings, or they were born with little difference in shape and weight but grew at the different paces as a result of changes in nutrition availability, or they had birth difference in size and grew at different rates. Considering the environment of the Oxford Clay seas possibly being productive, shallow and warm, the first assumption may be more possible than the other two. Belemnites *C.pusoziana* may have grown isometrically (with length and width growing at a certain pace) in their early life, but allometrically with dominant width-growth in late life.

6.4.2 LA compositional profiles: Mg, Na and Sr

All elemental profiles consist of variation patterns along two traverses, which together represent an edge-to-centre-to-edge area of a cross-section. The cross-sections of all *C.pusoziana* specimens analysed here are off-centred, resulting in the unequal-length of the two radial traverses. Here, the radial trend along the long traverse of each concentration profile is discussed simply because the long traverse provides more extended growth pattern than the short compact one.

6.4.2.1 Alteration signals

The specimens picked for concentration profile measurements are among the largest adults of *C.pusoziana* (diameters up to 2.5 cm) with closely distributed growth boundaries. The Mg profiles of them are characterised by dense and sharp peaks which line up well with the dense and thin growth boundaries on a scale of ~100 µm. Only a couple of these Mg peaks appear to match the Mn and/or Fe spikes in some specimens (e.g. 1S 57, 1S 35 and 13-165, see Fig. 6.6, Fig. 6.8 and Fig. 6.11). The Mg peaks that follow them should originate from diagenetic fluids with high Mg, Mn and Fe concentrations. However, other Mg peaks with no matching Fe and Mn spikes but lining-up growth boundaries may probably indicate high-Mg secondary calcite precipitated in the boundaries (McArthur *et al*., 2007b; Wierzbowski *et al*, 2009).

6.4.2.2 Sharp decline in Mg profiles during early ontogeny

For *C. pusoziana* specimens, Mg shows a sharp decline by 40 - 50% from the centre to the inner quarter of the sections of specimens 2S 72 (Fig. 6.14), 2S 16 (Fig. 6.12) and 2S 30 (Fig. 6.13). Fast decreases in early ontogeny are also seen in Sr and Na profiles of these specimens. They are likely to suggest a rapid slowdown in the incorporation of these substitution elements to Ca as a result of the decrease in growth rate (i.e. the pace of calcite precipitation rate), which is presumably associated with ontogenetic changes. Fast growth in early ontogeny has also been observed in Pliensbachian belemnites, and so is considered as a common feature during belemnite growth.

On the other hand, a few specimens with a distinct inner growth boundary, such as 1S 57 (Fig. 6.6), 13-49a (Fig. 6.7) and 1S 35 (Fig. 6.8), feature of a fast decrease by ~1500 ppm with a follow-up increase up to 5000 ppm in Mg concentration within the inner ring area. Growth boundaries are prone to alteration during the diagenetic burial as they are zones of weakness in the belemnite calcite structure. A broad Mg peak (Fig. 6.6 - Fig. 6.8) with the lining-up inner ring implies that the peak is likely to show some degree of alteration. However, Mn and Fe are not always seen to peak at the position of the inner ring for these samples to confirm complete alteration. Therefore, the inner ring might also imply some biological changes in the early life

of these beasts, which is yet hardly known to us. When taking the above explanation into account, the *C. pusoziana* specimens with an inner growth boundary show similar growth rate in the early life to the ones of the same species without it.

The interesting thing about these inner broad Mg peaks is that the magnitude of the peak on the long traverse (on the dorsal side) is less than that on the short traverse (on the ventral side). A possible explanation for this phenomenon is that the degree of diagenetic alteration on the dorsal part is lower than on the ventral part. Considering that the cross-sections of these specimens are off-centred, the ventral part should be more compact and have denser zones of weakness than the expanded dorsal part with looser zones of weakness. With the same amount of burial time and surrounding diagenetic fluids, the compact ventral part were apparently more vulnerable to the penetrating of diagenetic fluids, and therefore suffered relatively higher degree of alteration than the expanded dorsal part. The cross-sections of specimens in Fig. 6.5 clearly show the lower degree of preservation on the ventral part (shown as dark material stained spots along the growth boundaries and fractures) than the dorsal part in most cases.

6.4.2.3 The radial trend of Mg profiles

A decreasing to increasing radial trend in Mg profile of Pliensbachian belemnites was termed a bowl-shaped (or plate-shaped if the trend is less distinctive) variation pattern. Here, the term, with some modification, is adapted for *C. pusoziana* specimens.

Specimens 2S 72, 2S 16 and 2S 30 (Fig. 6.12 to Fig. 6.14) each display a broad single bowl-shaped Mg profile on a radial traverse. This fits well the hypothesis of the growth history proposed for Pliensbachian belemnites with the same feature in Mg profiles. That is a life including a fast growing early ontogeny, followed by a slow growth in adolescence-adulthood, and a quick fattening late ontogeny associated with physiological maturity.

Specimens of 1S 57, 13-49a and 1S 35 (Fig. 6.6 - Fig. 6.8) with a distinct inner growth boundary show a double bowl-shaped Mg variation pattern along a radial traverse. The small and higher inner Mg bowl in 13-49a, 1S 35 and 1S 57 represent

the inner quarter of the each of the sections (also the fast growth region), and the broader and lower outer Mg bowl reflect the Mg variations along the rest of each section, with the distinct inner growth band being the boundary between the two Mg bowls.

The growth boundary structure and Mg profiles seen in *C. pusoziana* specimens show some likeness to the two Pliensbachian species *H.spadixari* and *H.stonebarroensis* of Genus *Hastites*. These two species have been interpreted as representing both genders of Genus *Hastites* based on their similar rostral shape, closely related growth patterns and intra-rostral elemental profiles. For similar reasons, *C. pusoziana* specimens with and without inner growth boundary here presumably reflect the gender difference, overprinted and magnified by the later diagenetic alteration during burial in sediments.

6.4.3 Ontogenetic isotope records: $\delta^{13}C$ and $\delta^{18}O$ profiles

6.4.3.1 $\delta^{18}O$ profile

Ontogenetic isotopic records of fossil belemnites available for comparison are from Dutton *et al.* (2007) and Wierzbowski and Joachimski, (2009), in which an intro-rostral variation of ~2‰ in $\delta^{18}O$ has been observed. However, the specimens analyzed in both researches appear to be diagenetically altered. They clearly show well-developed growth boundaries that are filled with white secondary calcite (e.g. Figure 2 of both papers). Here, the oxygen isotopic composition of one well-preserved *C. pusoziana* specimen of Callovian age has a range of 1.1‰, less than the range found by the above authors. This shift in $\delta^{18}O$ transfers to a total temperature change of a few degrees (~4°C, Fig. 6.21) using the palaeotemperature equation of Hays and Grossman, (1991). If the beast migrated, it is likely that it experienced salinity changes, but the salinity range should be very small and the effect of salinity on $\delta^{18}O$ less than one third of the temperature influence (Li *et al.*, 2011). It is therefore not subtracted in the calculation of temperatures.

The calculated absolute temperature values in Fig. 6.21 mean little, as it can vary with using different assumptions of seawater isotopic compositions and palaeotemperature equations, but the temperature range and trend would largely

reduce the significance of these effects and therefore are better to reflect the environmental variations of belemnite habitats. The area within the 0.5 mm away from the centre is identified as altered apical line area by the high Fe and Mn peaks in its LA profile (Fig. 6.7), and hence is excluded in the interpretation of intra-rostral variations in isotopic composition.

Fig. 6.21 shows that *C. pusoziana* was hatched and stayed or horizontally migrated in warm shallow waters for perhaps a few months (season 1) before descending into a certain depth with low temperature in season 2 (with depth $\delta^{18}O$ increases, but temperature decreases). The temperature change of 3 - 4 °C between the two stages seem to inply a depth change of only a few tens of metres for this belemnite (using the temperature profiles of the modern North Sea as a reference, see Appendix A). The animal then returned to warm conditions similar to the hatching place probably for breeding in season 3. Such migrations have been noticed to be common in cuttlefishes (Rexfort and Mutterlose, 2006), and the similar lifestyle (reflected by the trend in $\delta^{18}O$ profiles) of cuttlefish and belemnites strengthens the biological connection between the two, and the idea of using cuttlefish as a modern analogue of belemnites. Price *et al.* (2009) compares squid *Spirula* with belemnites, and proposed that belemnites, like *Spirula*, were hatched in cold water, experienced warm water conditions (for food) as juveniles, and then sought to cold water for breeding after reaching sexual maturity. This is the opposite of what is seen here in the ontogenetic profiles of belemnites and cuttlefishes.

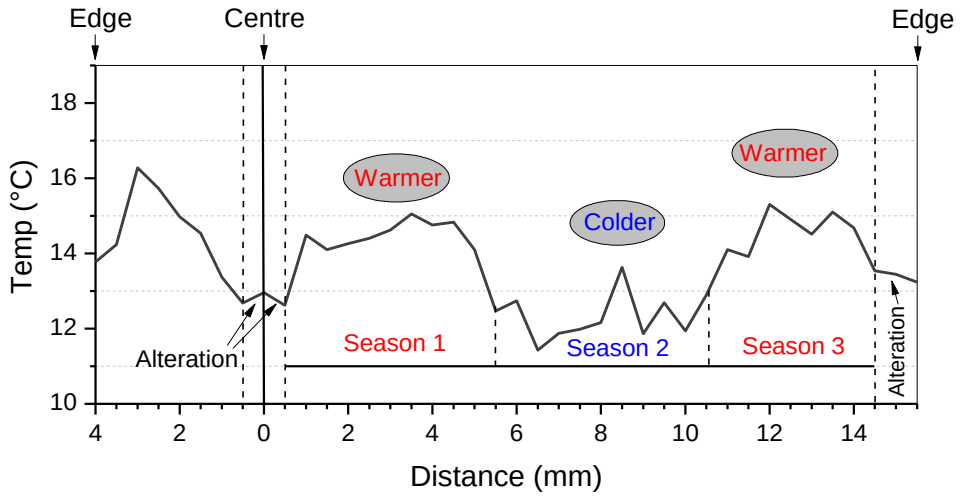

Fig. 6.21 The temperature profile calculated from the ontogenetic profile of $\delta^{18}O$ (Fig. 6.17) of specimen 13-49a, using the palaeotemperature equation from Hays and Grossman (1991).

The intra-rostral profile of $\delta^{18}O$ is also plotted against the Mg profile of the same specimen in Fig. 6.22. The two profiles were obtained from two separate tracks with different length, due to the difficulty in microsampling for isotope analyses at µm resolution. In the warmer season 1 of early ontogeny, with the decrease in $\delta^{18}O$ by 0.5 ‰ (so the increase in temperature by ~2.5 °C in Fig. 6.21), Mg concentration decreases by ~40%. Then the general colder season 2 witnesses a temperature fluctuation of 2°C, but a consistant low Mg concentration (probably showing a slow growth during adolescent-adulthood); and the warmer season 3 hardly sees any obvious increase in Mg concentration, although the Mg profile is shorter than that of $\delta^{18}O$. Given the Mg temperature dependance of 10% per 1°C in Bailey *et al*. (2003), a temperature change of ~3°C should not be too small to show in Mg profile. Magnesium, therefore, does not seem to correlate well with temperature for *C. pusoziana* belemnites. Meanwhile, the $\delta^{18}O$ profile doesn't reflect the details seen in LA profile of Mg, such as the inner Mg peak and the small undulations of Mg (Fig. 6.22). The main reason for this is that the resolution $\delta^{18}O$ profile is 5 times lower than that of LA profile of Mg, making it too broad to reveal any signals of these details.

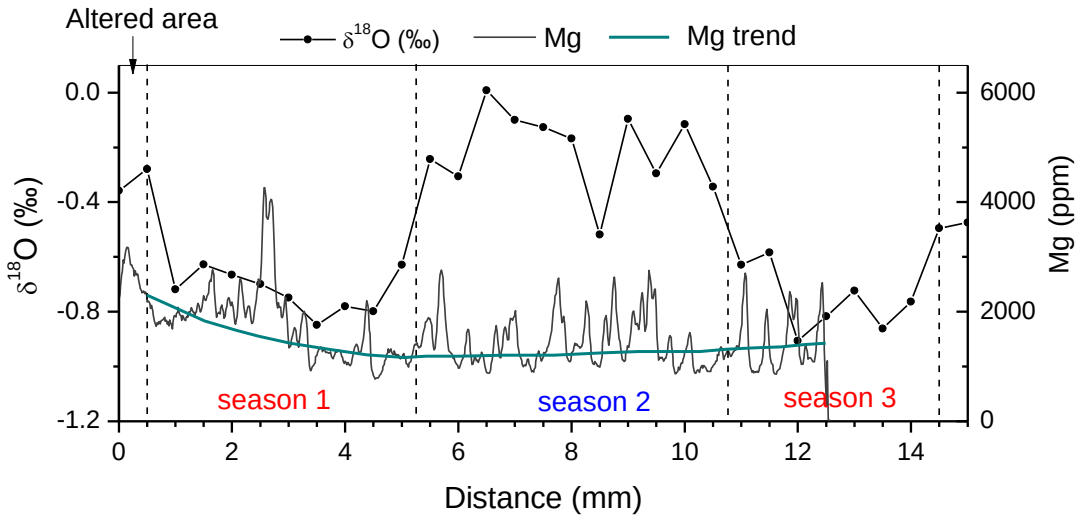

Fig. 6.22 The profiles of $\delta^{18}O$ and Mg along two separate tracks from the centre to the edge of the sections of *C. pusoziana* specimen 13-49. X axis shows the distance to the alveolar centre (marked as 0 distance). The dark green line is the eye-fitted trendline of Mg profile.

6.4.3.2 $\delta^{13}C$ profile

The $\delta^{13}C$ profile reflects sharper fluctuations than that of $\delta^{18}O$ (see the longer part on the right of the centre in Fig. 6.17). Carbon isotopes in marine biogenic carbonates are understood less well than oxygen isotopes. This is because firstly carbon can have multiple sources during carbon fixation. The main source of carbon for the marine calcareous skeletons is certainly the dissolved inorganic carbon (DIC), but metabolic carbon and food can also be carbon origins (McConnaughey *et al.*, 1997; McConnaughey and Gillikin, 2008). The second reason is that $\delta^{13}C$ disequilibrium or biological fractionation of carbon isotopes often occur in biogenic carbonates (McConnaughey, 1989a). Callovian belemnite species *C. pusoziana* have $\delta^{13}C$ ranging from +1.53 to +3.01 ‰, so if we assume the $\delta^{13}C_{DIC}$ of Oxford Clay sea was similar to average modern ocean waters (+2.0 to ~ 0% from surface to anoxic water region, Kroopnick, 1985), metabolic carbon and food can be then ruled out as carbon sources as they have much lighter $\delta^{13}C$ and could have resulted in decrease, rather than increase in belemnite $\delta^{13}C$. This leaves the biological fractionation of carbon isotopes a possible explanation for the fluctuations in $\delta^{13}C$ profile of belemnite *C. pusoziana*. Similar variations of $\delta^{13}C$ have been reported in the cuttlebone of a cuttlefish *Sepia* by Rexfort and Mutterlose, (2006), and interpreted as the metabolically controlled biofractionation of carbon isotopes.

Vertical migration of belemnites can also bring changes in their $\delta^{13}C$ values because seawater $\delta^{13}C$ decreases with depth as a result of increased mineralization of surface-derived organic carbon. The $\delta^{13}C$ values of *C. pusoziana* actually show no correlation with $\delta^{18}O$, so no signal of temperature changes as inferred by the $\delta^{18}O$ profile. The cyclic signal of $\delta^{13}C$ values in the specimen of *C. pusoziana* could be resulting from changes in fractionation rate caused by varying metabolic activity (Rexfort and Mutterlose, 2006; Wierzbowski and Joachimski, 2009).

6.4.4 Compositional variations in bulk analysis

The compositional ranges of both oxygen and carbon isotopes in this study are slightly smaller than the ranges in Anderson *et al*. (1994). This small discrepancy is most likely to be attributed to large sample numbers and diagenetic alteration in most samples of the previous work (which tend to bring both $\delta^{18}O$ and $\delta^{13}C$ values down).

For the studied species *C. pusoziana*, neither Mg/Ca nor Sr/Ca ratios show a correlation with $\delta^{18}O$ that is significant. This may result from the relatively narrow range of $\delta^{18}O$ ratios (~1.2 ‰) and El/Ca ratios measured from specimens of this species. The similar lack of correlation between $\delta^{18}O$ and Mg/Ca has been observed for the six Pliensbachian belemnite species from Dorset (Chapter 4) and four Toarcian species from Yorkshire (Chapter 5). Such similar results from three different belemnite populations with different ages are more likely to indicate that the correlation between $\delta^{18}O$ and Mg/Ca is not present at species level for the studied belemnite communities, and that Mg/Ca ratios are not a good palaeo-proxy in belemnites. Sr/Ca ratios, however, have been found to correlate well with $\delta^{18}O$ in individual species and specimens as a whole obtained from Toarcian strata of Yorkshire, but the correlation between the two doesn't show in Pliensbachian and Callovian belemnites. It is then concluded for now that some species may preserve the correlation, some may possibly not, largely due to biologically controlled species specific effects on these elements. Meanwhile, Na/Ca and Sr/Ca correlate well with each other, and the profiles of both show resembling trend. This also holds true for the six species of Pliensbachian belemnites. The correlation between the two is thought not to be species-specific.

6.5 Conclusion

1) The size data of 252 *C. pusoziana* specimens show that several generations of this belemnite population once lived together, with small and middle juveniles constituting over 90% of this belemnite community.

2) The diameter to length ratios (D/L) of *C. pusoziana* specimens, together with length, reveal that belemnites may have grown proportionally with certain D/L ratios in early-middle stages of ontogeny, but allometrically with dominant width-growth in its adulthood.

3) Sharp decrease in LA Mg profiles outwards in the inner part of the cross-sections may be more appropriately interpreted to a rapid slowdown of growth pace associated with changes of ontogeny. Fast growth in early ontogeny with a follow-up slow growth in adolescent-adulthood may be applicable to belemnites in general as it is observed in Pliensbachian and

Callovian belemnites of this study with variable species and stratigraphic ages.

4) Specimens with a distinct inner growth boundary and so an inner Mg peak may not just show alteration along the inner growth boundary, it might also reveal some physiological difference (gender difference) from the specimens of the same species without the inner growth ring structure.

5) The ontogenetic $\delta^{18}O$ profile of one *C. pusoziana* specimen suggests an overall 'warmer-colder-warmer' lifestyle. However, the temperature change of only ~4°C degrees during ontogeny reflects a narrow-ranging lifestyle of this species that fits in the overall shallow Oxford Clay Sea. The profiles of Mg and $\delta^{18}O$ across one *C. pusoziana* section show little comparability between the two, suggesting that Mg does not reflect temperature well.

6) For the species *C. pusoziana*, neither Mg/Ca nor Sr/Ca ratios correlate with $\delta^{18}O$ in bulk analysis, suggesting that Mg/Ca can not be a suitable palaeo-proxy in these belemnites.

Chapter 7 Valanginian Belemnites from Vergol, SE France

The Valanginian stage is reported to be a time of climate change and biotic crisis. A pronounced positive carbon isotope excursion of ~ +2‰ in mid-Valanginian is well documented around Western Europe (and possibly worldwide). More importantly, this time is one when the existence of polar ice caps in a greenhouse interval has been proposed (Price, 1999; McArthur *et al.*, 2007a). To test whether palaeo-proxies in belemnite calcite (Mg/Ca, Sr/Ca, Na/Ca, Sr/Ca, $\delta^{18}O$, and $\delta^{13}C$) provide evidence of the presence of polar ice and C-isotope anomalies in the Valanginian, the isotopic and elemental data of belemnites were obtained through a single Valanginian section at Vergol, SE France, via 5 genera *viz. Berriasibelus*, *Castellanibelus*, *Duvalia*, *Hibolithes*, and *Pseudobelus*. Belemnites of this study were also compared with those of same origin and age in McArthur *et al.* (2007a) for trends in $\delta^{13}C$ and $\delta^{18}O$ profiles during Valanginian. A mid-Valanginian C-excursion is found to be present in the $\delta^{13}C$ profile of belemnites from this study. Data of $\delta^{18}O_{belemnite}$ suggest a possible decrease in temperature by only 2 °C in Upper Valanginian which is too small to trigger the ice-formation in polar regions. Further evidence is required to confirm the assumption of the presence of polar ice in Upper Valanginian - Lower Hauterivian time.

7.1 Introduction

7.1.1 The existence of polar ice during Valanginian – Hauterivian time

The Cretaceous period was presumed by many to be a time of ice-free greenhouse conditions (e.g. Barron *et al.*, 1981; Barron, 1983; Lini *et al.*, 1992; Barron *et al.*, 1993; Barron *et al.*, 1995). More recent work questioned this scenario, and proposed a generally warm climate with some cold snaps that resulted in the formation of polar ice (Price, 1999; Grocke *et al.*, 2005; Miller *et al.*, 2005). For example, Valanginian-Aptian time (Early Cretaceous) has been recognized as an episode of cold or sub-freezing polar climate, based on reports of glacial sediments on palaeogeographic reconstructions, and a Valanginian ice cap approximately one third the size of the present day has been advocated (Price, 1999). The suggestion has

been supported by the discovery of a glacial diamictite of Berriasian to Valanginian age from the Cadna-owie Formation of South Australia (Alley and Frakes, 2003) as evidence of Early Cretaceous glaciation. The evidence of the formation of polar ice in Cretaceous was also given in McArthur *et al*. (2007a) by very positive values of $\delta^{18}O$ of seawater (peaking at 1.6 ‰ in *C. loryi* Subzone of lower Hauterivian) deduced from Mg/Ca ratios and the $\delta^{18}O$ of Valanginian - Hauterivian belemnites from SE France and Spain. In this study, data of Mg/Ca, Sr/Ca, Na/Ca, $\delta^{18}O$ and $\delta^{13}C$ are obtained in the rostra of 5 species of Valanginian belemnites to first examine whether Mg/Ca ratios in these belemnites can be used as a palaeo-thermometer, and then to test whether belemnite oxygen isotope profile suggests a strong cooling and the presence of polar ice in Valanginian.

7.1.2 The positive carbon isotope excursion in middle Valanginian

A positive carbon isotope excursion recorded in Valanginian strata shows some synchronicity in a global context. It has been reported in bulk marine carbonates (Lini *et al.*, 1992; Channell *et al.*, 1993; Weissert *et al.*, 1998; Erba *et al.*, 2004; Westermann *et al.*, 2010) and marine and terrestrial organic matter (Grocke *et al.*, 2005) from NW Tethys, and correlates with $\delta^{13}C$ excursions recorded in cores of ODP from the western North Atlantic, Gulf of Mexico and the Central Pacific (Lini *et al.*, 1992), and in Erba *et al*. (2004). This Valanginian $\delta^{13}C$ excursion has also been noted in belemnites from SE France and Spain (van de Schootbrugge *et al*., 2000; McArthur *et al*., 2007a) and Siberia (Price and Mutterlose, 2004).

The positive $\delta^{13}C$ excursion in the North Italy was dated by Lini *et al*. (1992), with its onset falling in magnetozone CM12, the peak at CM11 and return to pre-excursion values from CM10N upwards, using nannofossil stratigraphy and magnetostratigrphy of Channell *et al*. (1987) and Channell and Erba (1992). According to Channell *et al*. (1993), the C-excursion started through the upper part of CM12 which is now termed as CM11A. Hennig *et al.* (1999) provided a link among the ammonite stratigraphy, magnetostratigraphy and nannofossil zonation of South Europe, using the carbon-isotope stratigrapy of bulk marine carbonate from South Fance. The onset of the C-excursion was then correlated to the *biassalense* Subzone of *B. campylotoxus* Zone. Therefore, the *biassalense* Subzone is correlated

to magnetozone CM11A (Hennig *et al.*, 1999; McArthur *et al.*, 2007a). The positive $\delta^{13}C$ excursion actually started in the uppermost part of the Lower Valanginian, reached a maximum in the S.*verrucosum* Zone of the lower Upper Valanginian, and then reduced to less positive values in the late Valanginian.

Several hypotheses have been proposed to explain the cause of the Valanginian positive $\delta^{13}C$ excursion (Lini *et al.*, 1992; van de Schootbrugge *et al.*, 2000; Erba *et al.*, 2004; Price and Mutterlose, 2004; Westermann *et al.*, 2010). The assumption of enhanced burial of isotopically-light organic-rich sediments during Valanginian oceanic anoxic event (Erba *et al.*, 2004) has been questioned because of the lack of widespread organic-rich black shale deposits of Valanginian age (Reboulet *et al.*, 2003; Grocke *et al.*, 2005; McArthur *et al.*, 2007a). The C-isotope excursion in mid-Valanginian does not seem to have been triggered by sea level rise and the consequential increase in burial of organic matter. This is because the positive excursion in $\delta^{13}C$ has been found to coincide either very loosely with the putative sea-level rise (McArthur *et al.*, 2007a); or with a projected sea-level fall (Price and Mutterlose, 2004). Besides, the mid-Valanginian C-isotope excursion of belemnites from SE France and Spain is shown to predate the Parana-Etendeka continental volcanism, making the increase in the atmospheric CO_2 and the enhanced weathering irrelevant to this positive excursion (McArthur *et al.*, 2007a). Furthermore, a C-excursion of ~2 ‰ from terrestrial plants was noted in Crimean strata of Valanginian age (Gröcke *et al.*, 2005); however, their correlations make the onset of the terrestrial CIE one ammonite Zone younger than the CIE in the profile of carbonate $\delta^{13}C$. This terrestrial excursion is from condensed strata, so brings difficulties in C-isotope correlation with European sequences. Thereafter, Westermann *et al.* (2010) proposed that the enhanced production and storage of organic matter (OM) on continent, in association with drowning of shallow-water carbonate platform, as the mechanisms for the positive CIE in $\delta^{13}C_{carbonate}$.

The mid-Valanginian positive C-isotope excursion in belemnites could be influenced by species/generic – specific effects (e.g. differing living habitats and biofractionation) since an oscillation of 2 ‰ has been observed through the excursion between belemnite species (McArthur *et al.*, 2007a). The second object in

this study is therefore to test whether the species-specific biofractionation is the main cause of the positive excursion in belemnite calcite.

7.2 Geological settings and samples

From Dr. S. Reboulet, of Lyon University, a collection of 62 belemnites was obtained. They were derived from Valanginian sedimentary rocks of Vergol section, in the Vocontian Basin, SE Fance (Fig. 7.1). The stratigraphy and lithology of the section have been described in French literature and summarized in McArthur *et al*. (2007a). The sequence is composed of interbedded dark-colored marls and light-coloured limestones. The sampling interval is from the middle *Tirnovella pertransiens* Zone to the lower *Neocomites peregrinus* Zone of the Valanginian (Table 7.1). The ammonite zonation in Valanginian used here is from the IUGS subcommission on Cretaceous stratigraphy (Hoedemaeker and Herngreen, 2003; Reboulet *et al*., 2006). The duration of the samping interval is estimated to be ~2.5 Ma according to the geologic time scale of Gradstein *et al*. (2004).

The identification of 62 specimens measurable for their compositions is provided in Table 7.2. They are (with specimen numbers in parenthesis): *Hibolithes* (26), *Duvalia* (13), *Berriasibelus* (8), *Castellanibelus* (8) and *Pseudobelus* (2). The stratigraphic levels of samples are given in metres above a zero datum placed at the base of Valanginian stage. Around 80% of samples from the section have a positional uncertainty of less than ± 1 m, with the remaining showing ± 2 m uncertainty in position.

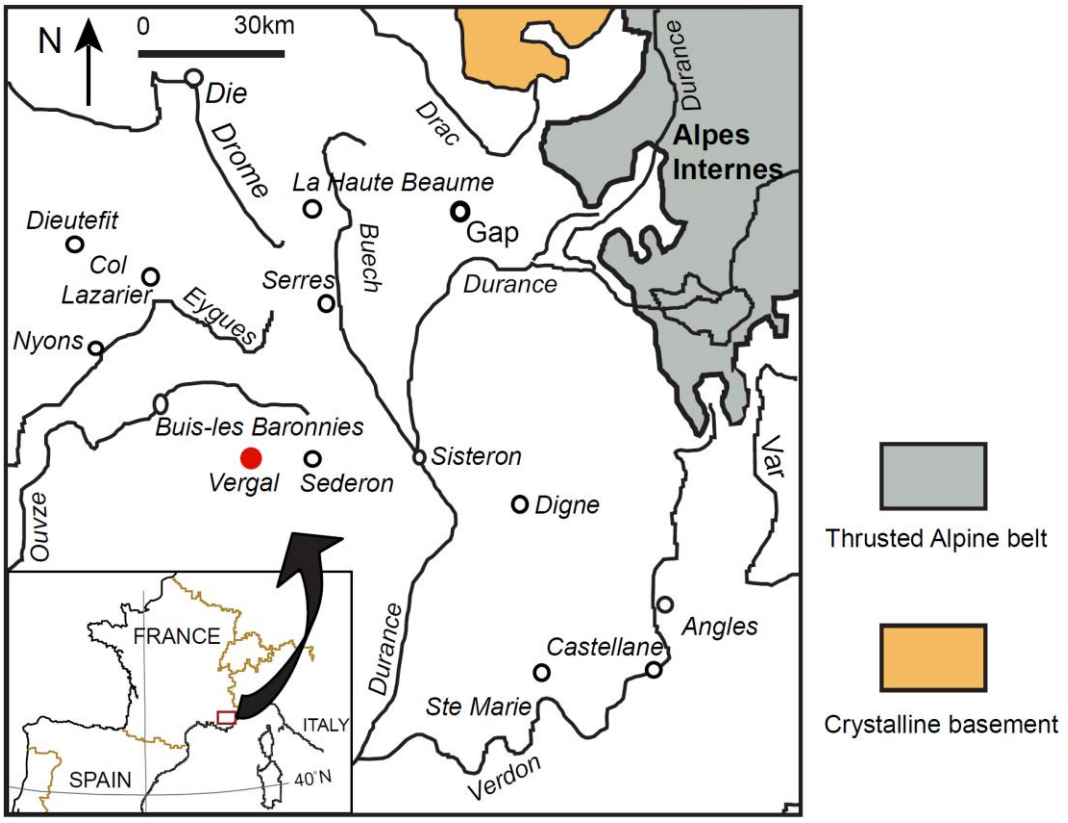

Fig. 7.1 The map of sampling area (marked as a red dot) and the surrounding geology in SE France, modified from McArthur *et al.* (2007a).

Table 7.1 The ammonite zonation applied here, modified from Hoedemaeker *et al.* (2003), Reboulet *et al.* (2006). The blue box highlights the sampling interval.

STAGES		ZONES	SUBZONES	HORIZONS
VALANGINIAN		*Criosarasinella furcillata*	*Teschenites callidiscus*	
			C.furcillata	
	Upper	*Neocomites peregrinus*	*Olcostephanus (O). nicklesi*	
			N.peregrinus	
		Saynoceras verrucosum	*Karakaschiceras pronecostatum*	
			S.verrucosum	Sampling interval
	Lower	*Busnardoites campylotoxus*	*Karakaschiceras biassalense*	*Neocomites platycostatus*
				Saynoceras fuhri
			B.campylotoxus	
		Tirnovella pertransiens		

Table 7.2 The identification of Valanginian belemnites from Vergal, SE France. Pictures of the analyzed species are provided in Fig. 7.2.

Genera	Species	No.	Brief descriptions
Berriasibelus	*B. exstinctorius*	4	Medium sized, robust and cylindriconical shape, nearly round tranverse section, one deep long alveolar groove vanishes before reaching the apex.
	B. gr. conicus	4	Smaller than *B. exstinctorius*, compressed elliptical cross-section.
Castellanibelus	*C. orbignyanus*	7	Small sized, cylindricall to subhastate shape with depressed elliptical cross-section, one deep long alveolar groove similar to *Berriasibelus*.
Duvalia	*D. binervia*	6	Small sized, distinct fish-shaped rostrum with strongly compressed cross-section; the dorso-ventral diameter is 3-4 times more than the lateral diameter; no grooves, but two lateral lines sometimes are visible; very acute apical tip.
	D. gr. binervia (aff. gervaisiana)	3	Similar to *D. binervia*, but larger in size and the rostrum is curved.
	D. cf. emericii	2	Larger than *D. gr. binervi*, rostrum not curved.
	D. gr. lata	1	Much fatter and larger than other *Duvalia* species, the cross-section is less compressed.
Hibolithes	*Hibolithes sp.*	15	Small sized; conical, slight subhastate or cylindriconical rostrum with nearly round cross-section, no apical grooves and acute apex.
	Hibolithes sp. (cf. jaculoides)	7	Similar to normal *Hibolithes* specimens, but medium sized.
	H. cf. laryi	5	Slightly subhastate shape, small to medium sized rostrum with short alveolar groove, round cross-section.
Pseudobelus	*P. jantikensis*	3	Small sized, slender, slightly subhastate shape, pyriform cross-section, a pair of long lateral grooves, but no alveolar groove.
	Pseudobelus sp. indet.	2	Small sized, cylindriconical rostrum with pyriform cross-section, a pair of deep long lateral grooves.
	P. cf. sultanovkaensis	2	Medium sized, cylindriconical rostrum with dented pyriform cross-section, a pair of well-developed long lateral grooves extending to apex, and one short deep alveolar groove on the venter.
	P. gr. bipartitus	1	Similar to *P. cf. sultanovkaensis*, a pair of long lateral grooves and a short alveolar groove.
Total		**62**	

a) *Berriasbelus sp.* 34-1

b) *Castellanibelus sp.*107-17

c) *Hibolithes sp.* 89c-7

d) *Pseudobelus sp.* 123-4

e) *Duvalia sp.* 107-7

Fig. 7.2 Specimens of the studied species from the Valanginian of Vergol, SE France. Scale is in mm and cm.

7.3 Results

7.3.1 Preservation assessment

The bulk chemistry results from Vergol belemnite samples are presented in Fig. 7.3 to Fig. 7.9 and Appendix F. Concentrations of Fe and Mn, in all specimens, are <100 ppm and <20 ppm (Fig. 7.3), respectively. As the threshold level of Fe and Mn for pristine belemnites in this PhD study is set as <100 ppm and <30 ppm (first defined in chapter one and thereafter applied in each chapter), the specimens here should be little altered. The S content varies from 300 to 5500 ppm and no correlation with S is observed for Fe (Fig. 7.3).

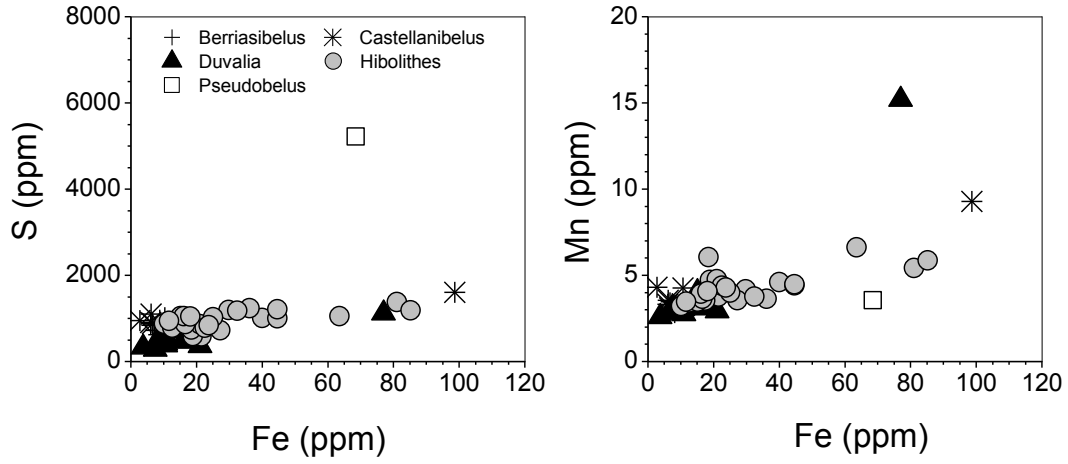

Fig. 7.3 The cros-plots of concentrations of Fe, Mn and S in Valanginian belemnites from Vergol, SE France.

7.3.2 Isotopic composition between species: $\delta^{13}C$ and $\delta^{18}O$

The isotopic compositions of the specimens vary between -2.2 and +2.55 ‰ for $\delta^{13}C$ and between -1.0 and +0.36 ‰ for $\delta^{18}O$ (Fig. 7.4), respectively. The isotopic compositions differ a lot between genera, and variations in $\delta^{13}C$ are much larger than in $\delta^{18}O$. Most specimens of *Duvalia* have higher $\delta^{13}C$ and $\delta^{18}O$ and so plot at the upper, heavy end (Fig. 7.4), whereas *Berriasibelus and Castellanibelus* specimens are isotopically lighter in $\delta^{13}C$, and to a small extent, in $\delta^{18}O$. Specimens of *Hibolithes*, on the other hand, show the largest spread of isotopic composition among all species (Fig. 7.4). The number of *Pseudobelus* specimens is too small to show any trend in their isotopic compositions. Within each genus, only *Hibolithes* specimens present a positive correlation between $\delta^{13}C$ and $\delta^{18}O$ ($r = 0.44$, $n = 24$, $P < 0.5$) when taking the two outliers out (see the legend in Fig. 7.4), but all the 5 genera together (without the two *Hibolithes* and one *Pseudobelus* outliers) show a better correlation ($r = 0.57$, $n = 55$, $P < 0.001$) in Fig. 7.4.

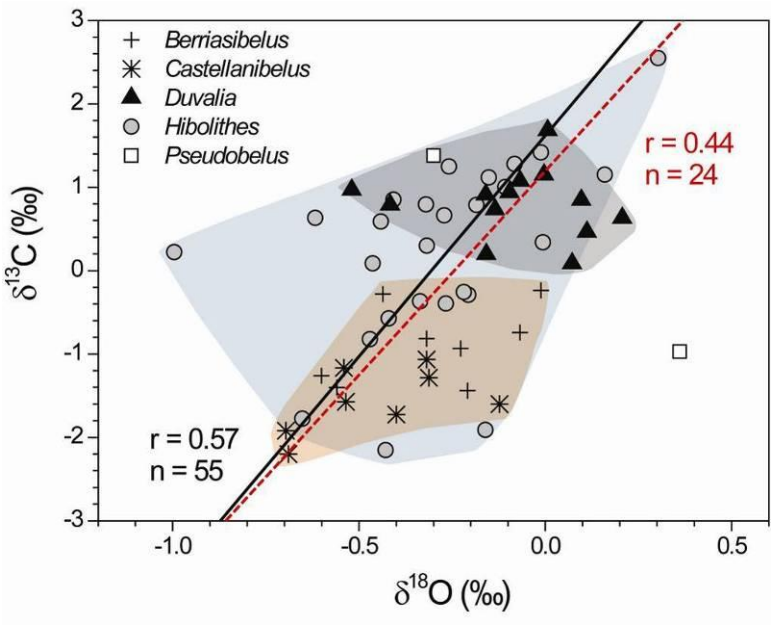

Fig. 7.4 Isotopic compositions of the Valanginian belemnites from this study. The light blue shaded area highlights the compositional range of genus *Hibolithes*, the grey area is occupied by *Duvalia*; and the orange region is for *Berriasilelus and Castellanibelus*. The two lines (dashed read and solid black) are from reduced major axis regressions. The dashed red line was obtained for *Hibolithes* only, but with two outliers (the one with the most negative $\delta^{18}O$ and the one with the highest $\delta^{13}C$) excluded, while the solid black line are calculated from data of all the 5 genera (excluding the two *Hibolithes* outliers and one *Pseudobelus* with the heaviest $\delta^{18}O$).

7.3.3 Elemental compositions between species: Mg/Ca and Sr/Ca

Concentrations of Mg, Na, and Sr are typical of well-preserved belemnites described by others (Podlaha *et al.*, 1998; McArthur *et al.*, 2000; Rosales *et al.*, 2001; 2004a; Rosales *et al.*, 2004b). *Hibolithes* specimens have the highest Mg/Ca ratios (9.5-16 mM/M), whereas *Duvalia* specimens are the lowest in Mg/Ca with most specimens falling in a range of 7.4 -10.6 mM/M (Fig. 8.3). The Mg/Ca ratios of the other three genera vary in between. The Sr/Ca ratios of both *Hibolithes* and *Duvalia* range similarly between 1.3 and 1.7mM/M, and appear to vary more widely than the other three genera. The genus *Castellanibelus* seem to retain lower values and smaller ranges of Sr/Ca (1.3 – 1.5 mM/M) than others.

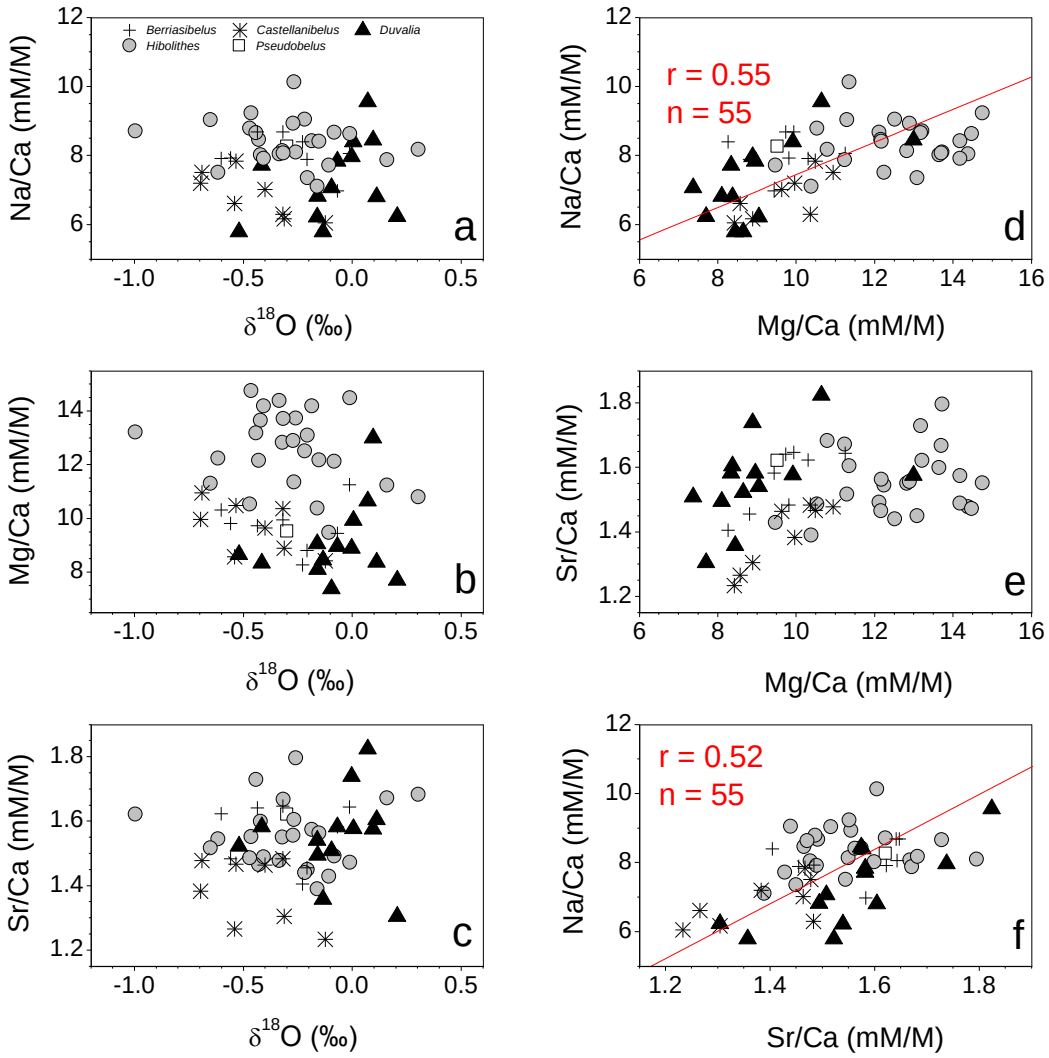

Fig. 7.5 Elemental and isotopic data of Valanginian belemnites from Vergol, SE France. Correlation lines were obtained by reduced major axis regression. Regressions in d and f are for the data of all specimens.

In none of the five genera, does Mg/Ca or Sr/Ca correlate with $\delta^{18}O$ significantly (Fig. 7.5). Only the small number of *Castellanibelus* specimens appears to show a weak negative correlation between Mg/Ca and $\delta^{18}O$ ($r = -0.51$, $n = 8$ and $P < 0.1$, Fig. 7.6), but the correlation degrades when plotted with 5 other *Castellanibelus* specimens from the same location from McArthur *et al.* (2007a). Na/Ca ratios of all samples display a good correlation with either Mg/Ca or Sr/Ca, but no correlation between Sr/Ca and Mg/Ca is observed (Fig. 7.5).

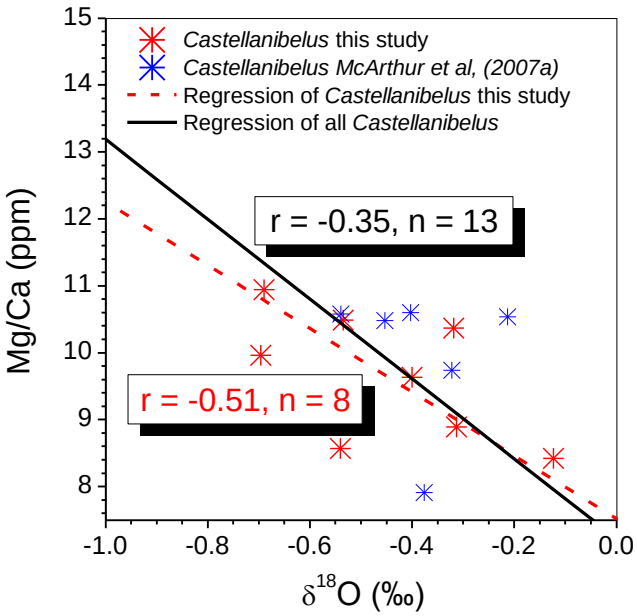

Fig. 7.6 Covariation between $\delta^{18}O$ and Mg/Ca in species *Castellanibelus*. The solid and dashed lines are the reduced major axis regressions obtained from different numbers of *Castellanibelus* specimens.

7.3.4 Stratigraphic profiles of $\delta^{13}C$ and $\delta^{18}O$

Data of $\delta^{13}C$ and $\delta^{18}O$ against stratigraphic level (in metres) are plotted and compared with those from McArthur *et al.* (2007a) in Fig. 7.7. Values of $\delta^{13}C$ in *T. pertransiens* and *B. campylotoxus* Zone of Lower Valanginian are negative and undulate from -3 to 0 ‰ between four genera (*Hibolithes, Pseudobelus, Berriasibelus* and *Castellanibelus*). From the top of *biassalense* Subzone, $\delta^{13}C$ ratios shift steeply to positive values and reach up to +2.55‰ in the *S. verrucosum* Zone (Fig. 7.7). Values of $\delta^{13}C$ then gradually decrease to around 0.5 ‰ in the *N. peregrinus* Zone of the Upper Valanginian. Overall, values of $\delta^{13}C$ show a negative excursion in the Lower Valanginian and a broad positive excursion of up to 2.55‰ in the Mid-Valanginian, but this positive excursion contains occasional short-term returns to around -2‰ in the *S. verrucosum* Zone. The $\delta^{13}C$ data of this study follows the general trend of $\delta^{13}C$ defined by McArthur *et al.* (2007a), but add a good deal of details in the gaps between their data (particularly in the mid-Valanginian).

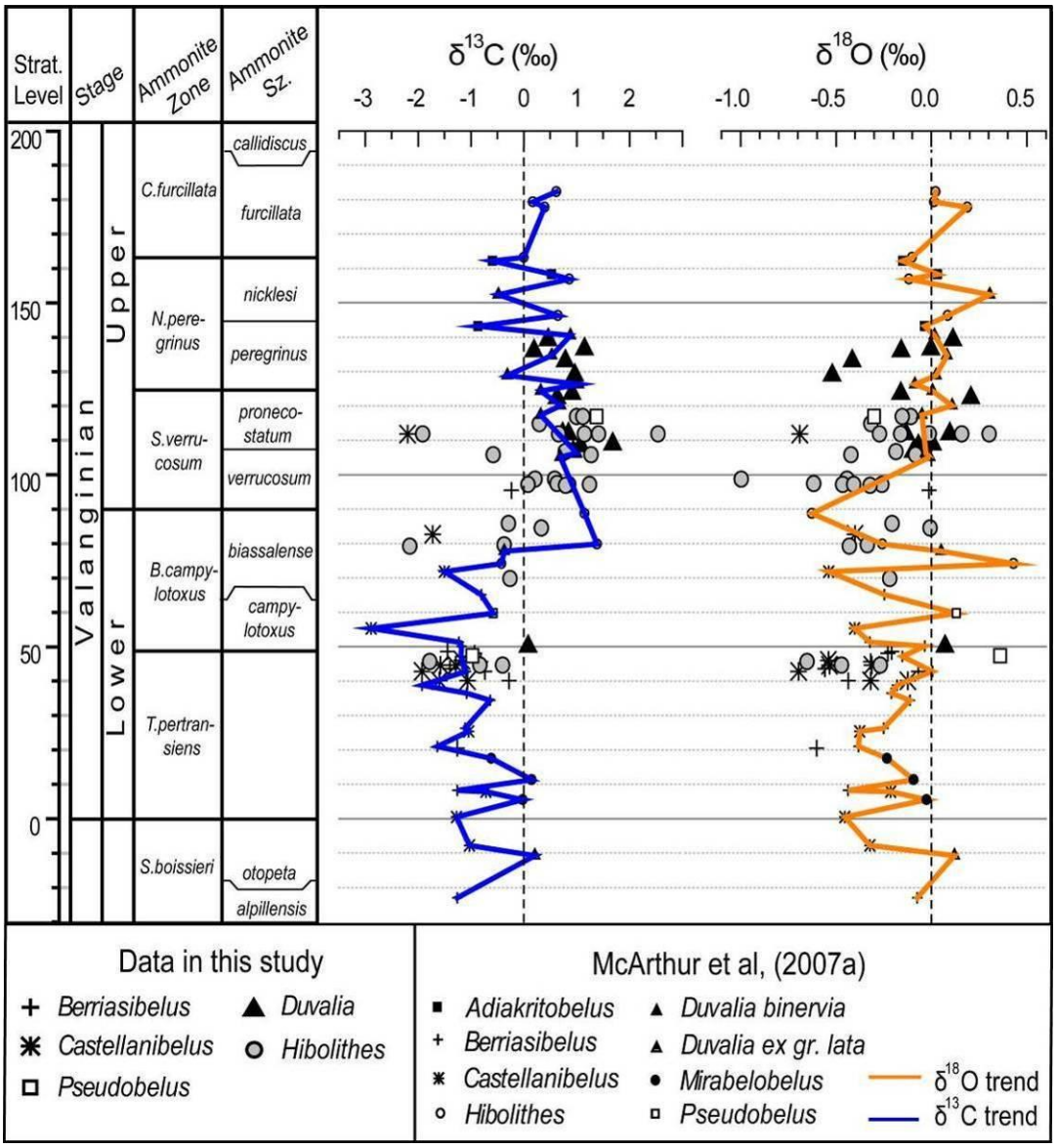

Fig. 7.7 Profile of $\delta^{18}O$ and $\delta^{13}C$ of belemnite calcite through the study interval from the *T. pertransiens* to the *C. furcillate* Zone. Blue and orange lines represent data trend of McArthur *et al.* (2007a). The new data presented here confirm the presence of the negative C-excursion in Lower Valanginian and the broad positive C-excursion in lower Upper Valanginian that were shown by the data of McArthur *et al.* 2007a (reproduced here) Belemnites reported in McArthur *et al.* (2007a) were also from Vergol of SE France.

Values of $\delta^{18}O$ are generally negative through the Lower Valanginian and the bottom of Upper Valanginian, with a minimum of -1‰ (given by a *Hibolithes* specimen) occurring at the *verrucosum* Subzone of *S. verrucosum* Zone. Thereafter, data of $\delta^{18}O$ demonstrate a gradual increasing trend upsection to the top of the study interval – the *N. peregrinus* Zone of Upper Valanginian. Data of $\delta^{18}O$ here are consistent with those in McArthur *et al*. (2007a).

The smoothed profiles of $\delta^{13}C$ and $\delta^{18}O$ are obtained from the 3-point means of combined isotopic data of this study (Appendix F) and McArthur *et al*. (2007a), and plot against stratigraphic heights in Fig. 7.8. Negative $\delta^{13}C$ ratios in the Lower Valanginian are followed by a rise in $\delta^{13}C$ to positive values in the *biassalense* Sz. and then a broad C-isotope peak in the above *S. verrucosum* Zone before $\delta^{13}C$ decreases slightly through the above *N. peregrinus* and *C. furcillata* Zones. Meanwhile, the smoothed $\delta^{18}O$ profile simply reflects a Lower Valanginian with negative $\delta^{18}O$ ranging from -0.5 to 0.0 ‰, but an Upper Valanginian with an increase in $\delta^{18}O$ of ~0.4 ‰ (Fig. 7.8). The smoothed profiles of $\delta^{13}C$ and $\delta^{18}O$ also show that the negative C-excursion in Lower Valanginian coexists with the negative $\delta^{18}O$ interval, whereas the broad C-isotope peak in the Upper Valanginian correlates to an overall increase in $\delta^{18}O$ with two small negative excursions in $\delta^{18}O$.

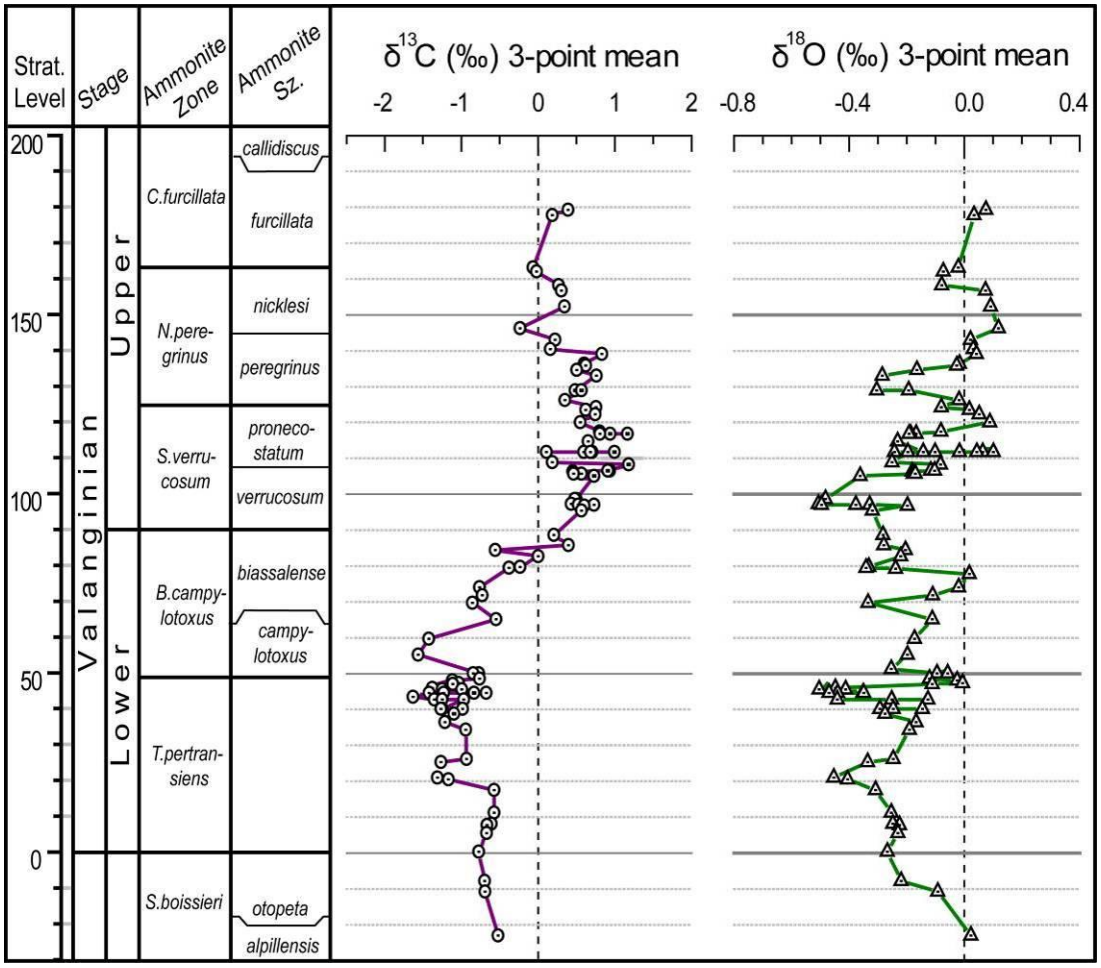

Fig. 7.8 The detailed trend in $\delta^{13}C$ and $\delta^{18}O$ of Valanginian belemnites with stratigraphic levels through the Vergol section studied. The zero level is set at the base of Valanginian stage. Values plotted are 3-point means of isotopic data from Appendix F and McArthur *et al*. (2007a).

7.4 Discussion

7.4.1 Isotopic compositions within and between genera

Different species are found to have different isotopic ratios and ranges. This may reflect differences in environmental conditions that were favorable for different species, or reflect dissimilar biological fractionation, or both. The specimens of *Hibolithes* have the broadest isotopic composition among the five species, with a range of 4.7 ‰ in $\delta^{13}C$ and 1.3 ‰ in $\delta^{18}O$ (Fig. 7.4). Therefore, they are thought to have had a cosmopolitan lifestyle and so lived and migrated in a wide range of habitats with variable isotopic compositions. The species *Duvalia, Berriasibelus* and *Casterllanibelus* are all interpreted to have occupied more restricted habitats as their compositional ranges are all smaller than that of *Hibolithes*. These habitats, were, nevertheless, shared by some *Hibolithes* specimens. The distributions of their carbon isotopes are different. The *Duvalia* specimens appear to be heavier in $\delta^{13}C$ by 2‰ than the average C-isotope ratios of the specimens of *Berriasibelus and Casterllanibelus*, both of which show an intra-rostral variation of ~1.2‰ in $\delta^{13}C$ (Fig. 7.4). The offset in $\delta^{13}C$ between species is more likely to show the species specific fractionation on carbon isotopes than differing living habitats, since metabolic/non-equilibrium fractionation of carbon isotopes has been reported in biogenic calcite (McConnaughey *et al.*, 1997; Rexfort and Mutterlose, 2006).

The spread in isotopic composition within a genus is between 1 and 2‰ for all genera in this chapter except for the range of $\delta^{13}C$ (4.7 ‰) of *Hibolithes*. Similar compositional variations have been observed in the high-resolution isotopic profiles across belemnite sections (Dutton *et al.*, 2007; Wierzbowski and Joachimski, 2009 and data in this PhD thesis). The compositional differences within a species/genus should then indicate, if not all, intra-rostral variations. The range in C-isotopic ratios of *Hibolithes* is too large to be only caused by internal compositional variations; changes in environmental conditions during life (and vital effects) should be more appropriate to explain it.

Hibolithes has the largest population (25 specimens), and is the only genus among all the studied genera that shows a positive correlation between $\delta^{13}C$ and $\delta^{18}O$, but the 5 genera together indicate a better correlation (Fig. 7.4). The isotopic data of *Duvalia*,

Berriasibelus and Casterllanibelus specimens show some species-distinct compositions, with *Duvalia* plotting at the upper isotopically heavy end, while *Berriasibelus and Casterllanibelus* specimens retaining the lower isotopically light area. This species difference, together with the good correlation seen in *Hibolithes* specimens, should account for the observed overall regression between C and O isotopic ratios, and therefore this regression between all genera has no environmental indication.

7.4.2 Elemental compositions and $\delta^{18}O$ within and between genera

These Valanginian belemnites apparently show differences in the elemental compositions (Mg/Ca, Na/Ca and Sr/Ca) between genera. As inferred from their distinct isotopic compositions, *Hibolithes* were cosmopolitan whilst *Duvalia* specimens were restricted, so they must have different preference and tolerance for living conditions. *Hibolithes* specimens tend to be higher in Mg/Ca and Na/Ca, whereas the specimens of *Duvalia* appear to have lower values of both ratios. The difference in their Mg/Ca (and Na/Ca) can then be explained to reflect differing environments and species/genus-related biofractionation. The little difference in Sr/Ca between the two seems to inply that Sr is not as sensitive as Mg to changes in environmental conditions or biofractionation.

Mg/Ca and Sr/Ca of all belemnites do not show any correlation with $\delta^{18}O$ values. When it comes to species/genus level, only a weak correlation ($r = -0.51$, $n = 8$, and $P > 0.1$) between Mg/Ca and $\delta^{18}O$ is found in the specimens of *Castellanibelus*. Interestingly, large numbers of belemnite of genera *Hibolithes* and *Duvalia* of Berriasian – Hauterivian age from broader stratigraphic levels and localities were found by McArthur *et al*. (2007a) to show some covariance between Mg/Ca and $\delta^{18}O$. Their 37 specimens of *Hibolithes* give a weak correlation only if outliers were ignored (Fig. 10 of McArthur *et al*., 2007a), and the 9 Vergol *Hibolithes* specimens of theirs do not show a correlation between Mg/Ca and $\delta^{18}O$. These 9 specimens were then added into the 26 Vergol *Hibolithes* of this study, but the new and slightly larger *Hibolithes* population (with 35 specimens) is still lack of correlation between Mg/Ca and $\delta^{18}O$ ($r = -0.01$, $n = 35$, $P > 0.1$, Fig. 7.9). Although *Duvalia* specimens from a number of Berriasian – Hauterivian sections of North Europe in McArthur *et*

al. (2007a) possess a strong correlation between Mg/Ca and $\delta^{18}O$ (r = 0.71, n = 35, P < 0.001) if outliers are excluded, the 12 Vergol specimens of this genus do not show a correlation that is significant (r = 0.10, n = 12, P > 0.1). The combined Vergol *Duvalia* samples of McArthur *et al.* (2007a) and this study again give no correlation (r = 0.20, n = 25, P > 0.1) between the two (Fig. 7.9). For genus *Castellanibelus*, the weak correlation between Mg/Ca and $\delta^{18}O$ present in 8 specimens (Fig. 7.6) degrades when adding in the 6 specimens of the same genus from McArthur *et al*. (2007a). This seems to indicate that the weak correlation is just an artefact of small sample numbers, so is probably not real.

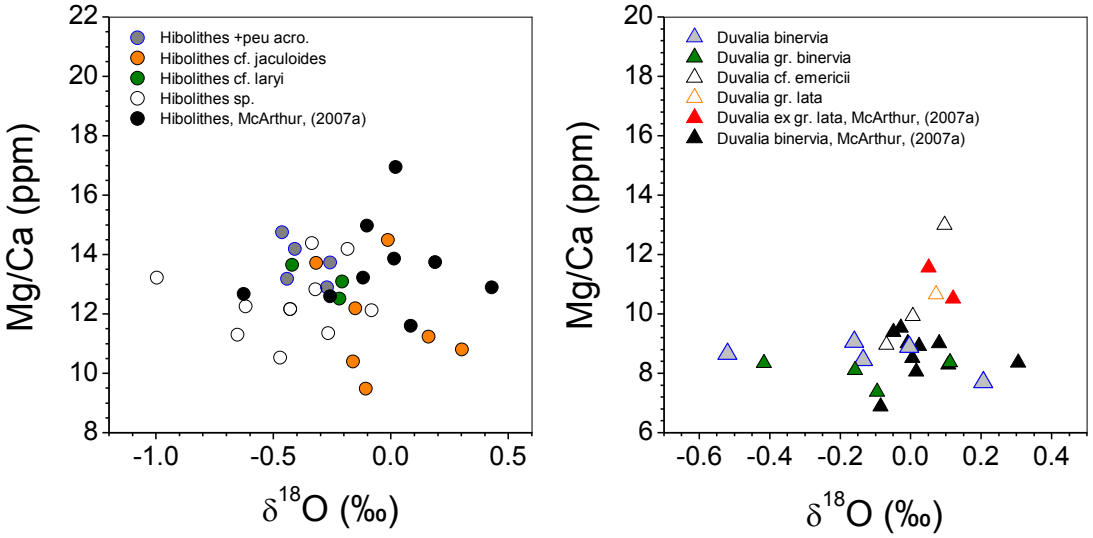

Fig. 7.9 Values of $\delta^{18}O$ versus Mg/Ca of *Hibolithes* and *Duvalia* from Vergol, SE France. Specimens plotted in the above two graphs are from this study and McArthur *et al.* (2007a).

It is then concluded that none of the five Vergol belemnite genera of this study preserve an observable correlation between Mg/Ca and $\delta^{18}O$. If Mg/Ca ratios of belemnite calcite, like modern biogenic calcite, reflect calcification temperature only (Chave, 1954), and values of $\delta^{18}O$ in belemnites reflect temperature, salinity and $\delta^{18}O$ of the ambient seawater, the two parameters should correlate well and potentially indicate the palaeotemperature. However, there are other factors such as species/genus – specific frationation, changes in salinity and the seawater $\delta^{18}O$ that can affect either or both of them. Changes in salinity and $\delta^{18}O_{seawater}$ may have influenced both El/Ca ratios and $\delta^{18}O$, but their effects may not be as strong as species/genus – specific effects for these belemnites. Biological fractionation (controlled by growth rate, metabolic activities, etc.) may have little effect on

belemnite $\delta^{18}O$ because cuttlefish *Sepia*, the modern analogue of belemnites, shows no biofractionation on oxygen isotopes (Rexfort and Mutterlose, 2006). Belemnites may have probably achieved oxygen isotope fractionation equilibrium with the surrounding seawater. This effect, on the other hand, has been shown to be strong in El/Ca ratios (Fig. 7.5), with different genera having differing elemental compositions and each genus preserving a range of compositions. Species/genus – specific fractionation therefore becomes a big influence on belemnite elemental concentrations (expressed as El/Ca, such as Mg/Ca).

Although *Duvalia* specimens of McArthur *et al*. (2007a) preserve a good correlation between Mg/Ca and $\delta^{18}O$, it is an overall regression of specimens of 5 different *Duvalia* species (*Duvalia.gr.lata, Duvalia lata, Duvalia gr.binervia, Duvalialata constricta and Duvalia gr.dilltata*). The correlation, however, is not present in the separate species. This probably means the correlation is not real in each species. *Duvalia* specimens in this study are also plotted in species in Fig. 7.9, together with those of McArthur *et al*. (2007a). Difference between species of genus *Duvalia* is observable, for example, *Duvalia binervia* and *Duvalia gr.binervia* specimens appear to be lower in Mg/Ca and have wider range of $\delta^{18}O$ than *Duvalia cf. emericii*. Neither a single *Duvalia* species nor all *Duvalia* specimens display a correlation between Mg/Ca and $\delta^{18}O$.

Therefore, Mg/Ca (and Sr/Ca) can not be used as a palaeotemperature indicator for Valanginian belemnites. The correlation observed between El/Ca ratios and $\delta^{18}O$ previously is probably just a statistic result of large numbers of specimens of variable species/genera with differing compositional ranges. It hence may only have statistic meaning, but no geochemical significance. The application of belemnite El/Ca ratios as palaeotemperature indicators without specifying species/genus difference in composition is questionable. The significance of this finding in the use of belemnites for palaeoceanographic study is then further explained in the summary Chapter 8 of belemnite palaeo-proxies evaluation.

7.4.3 Excursions in stratigraphic profiles of $\delta^{13}C$ & $\delta^{18}O$

7.4.3.1 Mid-Valanginian C-isotope excursion

Data of belemnite $\delta^{13}C$ in this study confirms the presence of the mid-Valanginian positive excursion which has been previously found by many authors (e.g. Lini *et al.*, 1992; Hennig *et al.*, 1999; van de Schootbrugge *et al.*, 2000; McArthur *et al.*, 2007a). The timing of this C-isotope excursion is consistent with the results in Hennig *et al.* (1999) and McArthur *et al.* (2007a), with its onset in the *biassalense* Sz. of *B. campylotoxus* Zone of the Lower Valanginian, and the broad peak in the S. *verrucosum* Zone of the lower Upper Valanginian. The $\delta^{13}C$ data of belemnites from Vergol in this study follow the overall trend of $\delta^{13}C$ defined by belemnites from the same interval and locality in McArthur *et al.* (2007a). However, differences between the two data sets do exist: The mid-Valanginian C-isotope excursion here is up to 2.55‰, given by a *Hibolithes* specimen in the *pronecostatum* Subzone of the *S. verrucosum* Zone. This value is about 1.2‰ larger and occurs 30 m higher in stratigraphic level (Fig. 7.7) than the maximal $\delta^{13}C$ of contemporaneous belemnites in McArthur *et al.* (2007a). Sampling in the interval that brackets the excursion is much denser in this study than theirs, so the data here bring more details in the trend of their belemnite $\delta^{13}C$ values. The smaller excursion at lower level in McArthur *et al.* (2007a) is then probably a result of lower sampling density.

Meanwhile, the positive excursion contains short-term returns to around -2‰ in the *S. verrucosum* Zone (Fig. 7.7) which are not present in the data of McArthur *et al.* 2007(a). The more negative $\delta^{13}C$ values are produced by one *Casterllanibelus* and a couple of *Hibolithes* specimens. *Casterllanibelus* specimens have been noticed to be isotopically lighter in $\delta^{13}C$ than other species of this study (Fig. 7.4). Its specimens occur mostly in the *T. pertransiens* Zone which is stratigraphically lower than the excursion, and very sparsely in the overlying *B. campylotoxus* and *S. verrucosum* Zone; therefore these specimens of this genus do not represent the excursion. The only two *Pseudobelus* specimens in this study are too limited to show a positive excursion. For *Hibolithes*, all specimens in the underlying *B. campylotoxus* Zone are negative in $\delta^{13}C$, but the $\delta^{13}C$ then shifts to positive values in most specimens in the overlying S. *verrucosum* Zone where it reaches +2.55 ‰. Although negative values of $\delta^{13}C$ are present in only a couple of specimens in the excursion interval, an overall

positive excursion is apparently present. These brief returns during the excursion are caused by two *Hibolithes* specimens with large compositional difference (Fig. 7.7), so may probably result from the cosmopolitan life and hence the large compositional ranges of this genus. Due to large sample number, stratigraphic continuity before and during the C-excursion, and steep shift from negative to positive $\delta^{13}C$ values in one subzone presented by *Hibolithes* specimens, this excursion should not be caused by species/genus – specific effects, but real changes of carbon isotopic composition of the ambient seawater.

The $\delta^{13}C$ profile of 3-point averages of combined data of this work and McArhur *et al*. (2007a) shows fewer details of species/genus differences in $\delta^{13}C$ and $\delta^{18}O$, but brings out a much smoother and clearer trend in $\delta^{13}C$. A quick rise in $\delta^{13}C$ from negative to positive values through the *biassalense* Sz. and a follow-up broad C-isotope peak in the above *S.verrucosum* Zone are much better-demonstrated in Fig. 7.8 than in Fig. 7.7. The returns of $\delta^{13}C$ to less positive values are also smoothed and become less distinctive. The smoothed $\delta^{13}C$ profile (Fig. 7.8) reflect well the general trend but less species/genus complexity, whilst the $\delta^{13}C$ profile plotted in terms of species/genus (Fig. 7.7) shows details of which species/genus preserve the Mid-Valanginian excursion and which don't. The combination of the two $\delta^{13}C$ profiles with combined data from two separate work not only confirms the existence of the positive C-excursion in middle Valanginian, but also defines the species/genus that actually preserve it and answers why according to the features of their geochemistry.

7.4.3.2 The formation of polar ice?

The combined data of $\delta^{18}O$ in Fig. 7.8 indicate a Lower Valanginian with more negative $\delta^{18}O$ and an increase in $\delta^{18}O$ in Upper Valanginian. If changes in belemnite $\delta^{18}O$ represent temperature mainly, the seawater of Lower Valanginian appears to be warmer than large parts of Upper Valanginian as $\delta^{18}O$ ratios are more negative from the Lower Valanginian to the base of the Upper Valanginian (Fig. 7.8). The increasing trend in $\delta^{18}O$ in the Upper Valanginian should therefore be approximately interpreted as cooling. Using the palaeotemperature equation of Hays and Grossman (1991), the temperature change from *S.verrucosum* Zone to *C. furcillata* Zone is estimated to be around 2°C from shift of ~0.4 ‰ in $\delta^{18}O$. This temperature calculation assumes salinity has negligible influence on belemnite $\delta^{18}O$. Were the

range of $\delta^{18}O$ increased also by variation in salinity, the range in temperature would be smaller. Even if the total transfer of shift in $\delta^{18}O$ to temperature change was acceptable, the 2°C decrease in seawater temperature is very unlikely to be strong enough to trigger ice-formation in polar regions. Unfortunately, Mg/Ca ratios of Valanginian belemnites from Vergol do not correlate with $\delta^{18}O$, so both parameters cannot be used together to deduce the palaeotemperature and $\delta^{18}O$ of the seawater, which therefore is not suitable to indicate the existence of polar ice.

Meanwhile, there are some fossil records that reflect a cold climate in late Valanginian. For example, the study area - the Vocontian Basin in the SE France which was at the north-western extremity of the warm Tethyan Ocean at a paleolatitude of 20 – 30 °N during Valanginian time. The migration of Boreal fauna of Northern Europe into this Tethyan Realm was probably a consequence of a cold Late Valanginian climate (Mutterlose, 1992; Hennig *et al.*, 1999). Meanwhile, a sea level lowstand is seen in the Upper Valanginian - Lower Hauterivian period in Arabian Shield (Haq and Al-Qahtani, 2005). Other indirect evidence for a sea level decrease in Late Valanginian is a recorded Upper Valanginian hiatus and lack of Upper Valanginian sediments across parts of Europe (Reboulet *et al.*, 2003; McArthur *et al.*, 2007a). Sea level decrease and faunal evidence may allow the formation of polar ice in Late Valanginian, but without further evidence on glacial deposits and indicators, this assumption of the formation of polar ice in Late Valanginian – Early Hauterivian is not convincing.

7.5 Conclusion

1) Of the genera studied here, *Hibolithes* specimens have the broadest isotopic composition, whereas *Duvalia*, *Berriasibelus* and *Casterllanibelus* have narrower isotopic composition ranges than *Hibolithes*. Specimens of *hibolithes* are thought to be cosmopolitan, whilst *Duvalia*, *Berriasibelus* and *Casterllanibelus* seem to occupy less broad living habitats.

2) *Duvalia* specimens are heavier in $\delta^{13}C$ by 2‰ than *Berriasibelus* and *Casterllanibelus*, but their $\delta^{18}O$ overlaps. The difference in C-isotope ratios between them is more likely to reflect differing biological fractionation, and the similar ranges in $\delta^{18}O$ may indicate their sharing living habitats.

3) *Hibolithes* specimens are higher in Mg/Ca and Na/Ca, whereas the specimens of *Duvalia* are lower in both ratios. The other three genera have these ratios in between. Sr/Ca ratios, however, do not change much between genera. The difference in Mg/Ca (and Na/Ca) between genera is interpreted as reflecting differing environments and species/genus – related biofractionation, and the small difference in Sr/Ca may inply that Sr is less sensitive to environmental changes and vital effects.

4) The lack of correlation between $\delta^{18}O$ and Mg/Ca or Sr/Ca in all the Valanginian belemnite species/genera from Vergol suggests that species/genus – specific effects (or biofractionation) may possibly be one of the major controls besides temperature on El/Ca ratios. The correlation between Mg/Ca and $\delta^{18}O$ previously observed in Valanginian belemnites may only be a statistical result on large populations of variable belemnite species/genera, the correlation actually doesn't seem to be present in each individual species/genus; and thus Mg/Ca cannot be used as a palaeotemperature proxy in Valanginian belemnites.

5) A positive C-excursion of up to 2.55 ‰ in belemnites is present in the *S.verrucosum* Zone of the lower Upper Valanginian. This excursion is real and not caused by species/genus specific effect because it is present by the genus with large sample numbers and stratigraphic continuity during the excursion interval.

6) Data of $\delta^{18}O$ of belemnites are consistent with a possible decrease in temperature by 2 °C in Upper Valanginian. The hypothesis of the formation of polar ice in Valanginian – Hauterivian is questionable without further glacial evidence.

Chapter 8 Belemnite Palaeo-proxies Evaluation

8.1 Belemnite palaeo-proxies: valid or not?

Studies on numerous belemnites from a number of Mesozoic strata of North Europe in this PhD have found that the correlation between Mg/Ca and $\delta^{18}O$ doesn't exist at species level. Pliensbachian belemnites from Dorset (chapter 4) show no significant correlation between Mg/Ca and $\delta^{18}O$ among the 6 species studied and within each individual species. The similar lack of correlation between $\delta^{18}O$ and El/Ca has also been observed in the large single-species population of Callovian belemnites from Cambridgeshire (see chapter 6). Furthermore, the belemnites from Vergol (chapter 7) show no observable correlation of Mg/Ca with $\delta^{18}O$ within a single species/genus or among all the genera. The repeating result from different belemnite populations with widely differing ages and from a number of stratigraphic levels hence confirms that the finding of no correlation cannot be random, but may hold true for belemnites in general. The findings in this PhD, for the first time, reveal the problem in the current notion of belemnite elemental proxies; emphasize that specifying species difference in belemnite composition is the first step in the attempt of studying belemnite geochemistry; and hence have a great impact on the use of belemnites for palaeooceanographic study.

(1) No correlation between Mg/Ca and $\delta^{18}O$ at species level questions the assumption used in belemnite palaeo-environment interpretation that Mg/Ca reflects calcification temperature only.

Factors other than temperature that are suspected to affect both Mg/Ca and $\delta^{18}O$ can be environmental (e.g. changes in salinity and the seawater $\delta^{18}O$) and biological (species-specific fractionation). The effects of changes in salinity are very difficult to estimate in deep time and are considered to be subordinate to temperature (Li *et al.*, 2011); and biological fractionation on oxygen isotopes is found to be little (Rexfort and Mutterlose, 2006). This leaves biological control a considerable influence on Mg/Ca ratios.

Within each belemnite population of this PhD study, a range of species show in bulk analysis the overlap in $\delta^{18}O$, but distinct distributions of elemental concentrations between them. This implies little species-specific fractionation on oxygen isotopes and possibly sharing of living habitats between species, but strong species differentiation in the concentration of trace elements. Meanwhile, in the detailed studies of elemental profiles (mainly Mg, Na and Sr) across belemnite sections (McArthur *et al.*, 2007b; Wierzbowski and Joachimski, 2009 and this PhD thesis), different variation patterns for different elements in a specimen provides a good support for the effects of biological fractionation on trace elements within the belemnite rostrum. On the other hand, variations in elemental profiles between species (see the El profiles in Chapter 4 and 6) are a sign of species-specific difference in the incorporation of elements.

Therefore, the influence of species-related fractionation in these elements may be stronger than previously assumed. The explanation here doesn't exclude the control of temperature on elemental concentrations, but points out that the species effects may be as important as temperature. Because belemnites are extinct, the response of their Mg/Ca ratios to seawater temperature and the controls of their biological activities then cannot be tested experimentally. It's hence concluded that the reliability of Mg/Ca in belemnite calcite as a recorder of oceanic temperature is questionable.

(2) The lack of covariance between $\delta^{18}O$ and Mg/Ca within a species challenges the validity of using combined Mg/Ca and $\delta^{18}O$ as palaeotemperature indicator.

The observed correlation between El/Ca and $\delta^{18}O$ in McArthur *et al*. (2000), Bailey *et al*. (2003) and Rosales *et al*. (2004a,b) are for belemnites from the same geological interval (Pliensbachian – Toarcian of early Jurassic), but three different localities: Yorkshire of the UK, southern Germany and northern Spain. What's of interest in their data is that Yorkshire belemnites present a better correlation of Sr/Ca with $\delta^{18}O$; Data from Germany and northern Spain both demonstrate that $\delta^{18}O$ is better coupled with Mg/Ca (Fig. 8.1).

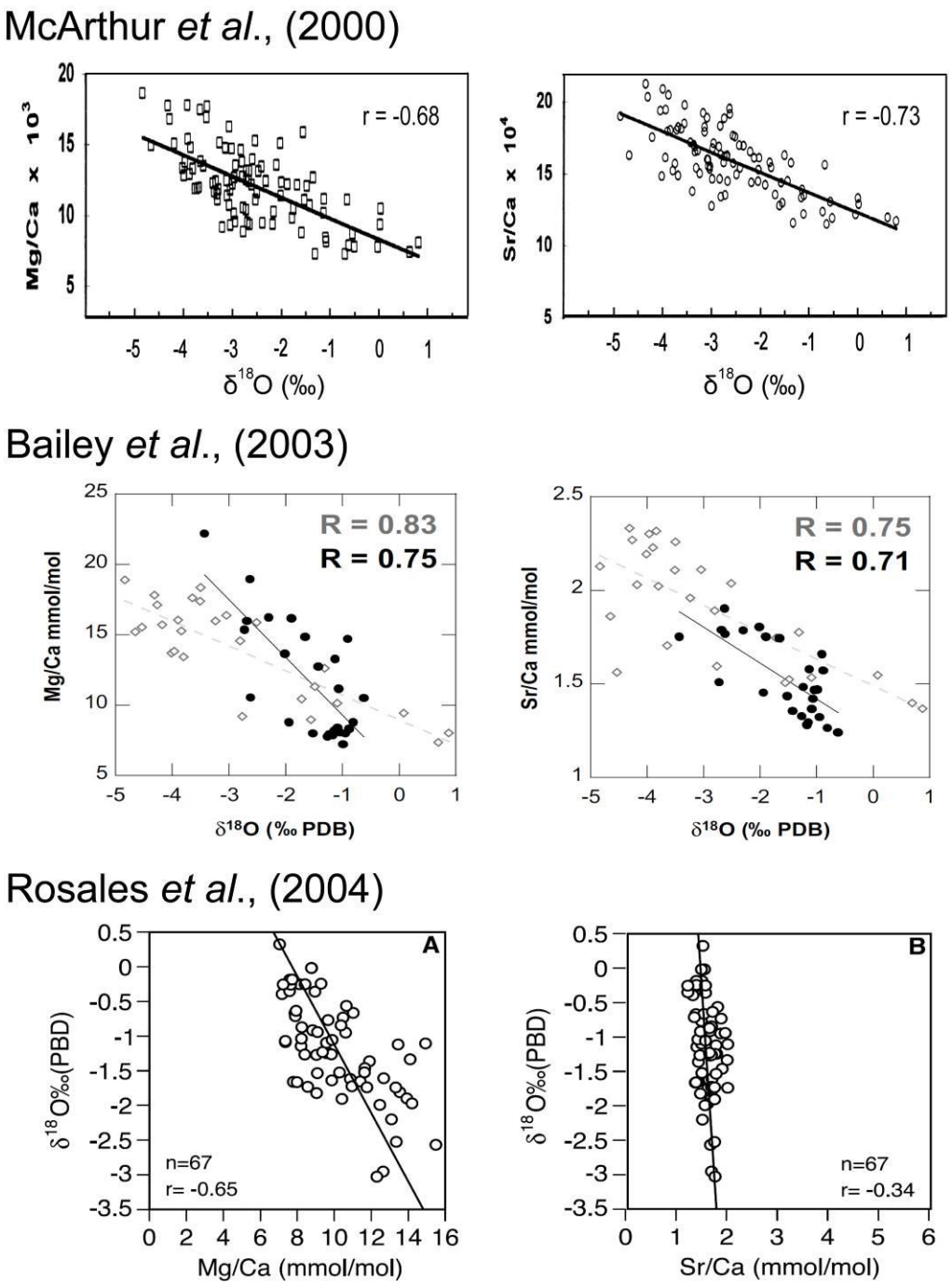

Fig. 8.1 Correlation between El/Ca and $\delta^{18}O$ for Pliensbachian – Toarcian belemnites from Yorkshire of the UK in McArthur *et al*. (2000), southern Germany in Bailey *et al*. (2003) and northern Spain in Rosales *et al*. (2004). Note that the grey and black data points and R numbers in Bailey *et al*. (2003) refer to data from Yorkshire and Germany, respectively.

Had all belemnites from the three localities uniformly showed a good correlation between Mg/Ca and $\delta^{18}O$, temperature would then be better confirmed as a dominant control and Mg/Ca ratios as a palaeotemperature recorder. The same arguement can be applied to Sr/Ca ratios. However, this is not the case of the belemnites studied above. The contradiction in their results seems to indicate that temperature is not the

sole influence for El/Ca and $\delta^{18}O$. Also, Mg/Ca and Sr/Ca are unlikely to have equal temperature sensitivity, and so equal covariance with $\delta^{18}O$, based on thermodynamic expectations and studies on modern biogenic calcite. The difference in the three localities may lie in regional environmental conditions (basically temperature), and possibly species assemblages. It is likely that species-specific discrimination in different elements plays a role in determining the El/Ca - $\delta^{18}O$ covariance.

In Bailey *et al.* (2003), Mg/Ca ratios of belemnites were used independently to estimate the ocean temperature because the temperature change calculated from the shift in the $\delta^{18}O$ ratios of their belemnites is so unacceptably large that a change in salinity (besides temperature) might have occurred as well. Meanwhile, because the assumption of the seawater $\delta^{18}O$ (usually -1‰ SMOW for ice-free oceans) used in palaeotemperature equation is not reasonable for their studied interval, McArthur *et al.* (2007a) used Mg/Ca ratios and $\delta^{18}O$ of Valanginian - Hauterivian belemnites to derive the seawater oxygen isotopic composition which was then used to indicate the formation of polar ice. The above palaeotemperature/or isotopic composition calculations are unfortunately unreasonable as some variations in belemnite Mg/Ca ratios do not result from temperature change, but species-specific fractionation.

The reason why data in this study show no correlation while unidentified specimens in previous work do, may be the species difference in composition. If different belemnite species show compositional data plotted in species-distinct fields, for example, some species have high El/Ca but low $\delta^{18}O$ whereas some are low in El/Ca but high in $\delta^{18}O$ (Fig. 8.2), there will be a high chance to get a good negative correlation between El/Ca and $\delta^{18}O$ (e.g. $r = -0.70$ for 54 samples at a significance level of 99% for the correlation between Mg/Ca and $\delta^{18}O$ in Fig. 8.2), although the correlation itself is not real within one species. If this is the case for previously observed covariance of El/Ca with $\delta^{18}O$, the correlation itself would have no validity and Mg/Ca ratios could not be used for palaeotemperature interpretation. Unfortunately, the belemnites in previous studies haven't been identified to species level, so the species differences in composition of those belemnites cannot be seen.

The absence of the correlation of El/Ca with $\delta^{18}O$ is also found by Wierzbowski and Rogov (2010) in each of the three belemnite genera of Callovian-Oxfordian age from Russian Platform. Their *Hibolithes* have lower and smaller range of $\delta^{18}O$, but higher

Mg/Ca (and Sr/Ca), whilst the other two genera (*Cylindroteuthis* and *Lagonibelus*) show the opposing compositional features. The whole compositional data of the three species hence show a clear species difference (Fig. 10 to 11 in Wierzbowski and Rogov, 2010, replotted in Fig. 8.2), and suggest false correlations of Mg/Ca (and Sr/Ca) with $\delta^{18}O$, which are not present within either genus. The data of their study confirms the finding in this PhD research that species difference in composition may be the reason for the observed correlation between El/Ca with $\delta^{18}O$ in undifferentiated belemnites, and that El/Ca ratios in belemnites are influenced by the bio-fractionation effects besides temperature and show no correlation with $\delta^{18}O$ at species level.

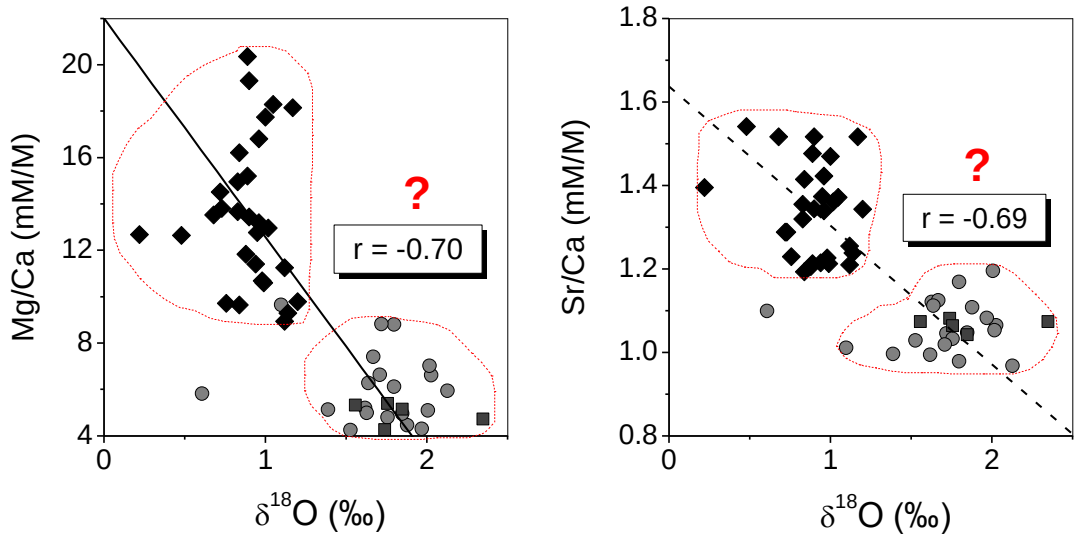

Fig. 8.2 False correlations obtained between $\delta^{18}O$ and Mg/Ca (and Sr/Ca) ratios for the three belemnite species (shown by different symbols) with distinct compositional ranges. The correlations are not present in each species. Samples are of Callovian – Oxfordian age of the Dubki sectionnear Saratov in the Russian Platform. Data are from Wierzbowski and Rogov, (2010).

8.2 Toarcian belemnites: Is Sr/Ca an alternative for Mg/Ca?

Among the belemnites of this PhD study, Toarcian species from Yorkshire differ from the other three belemnite populations in that, although Mg/Ca ratios do not correlate with $\delta^{18}O$, Sr/Ca correlates reasonably well with $\delta^{18}O$ for two Toarcian species *A. subtenuis* and *Y. simpsoni* (Fig. 5.3 d & f in chapter 5). These findings confirm that the overall correlation between Sr/Ca and $\delta^{18}O$ found by McArthur *et al.* (2007b) in large populations of Toarcian belemnites also exists in two individual

species (e.g. *A. subtenuis* and *Y. simpsoni*); and that Sr may be a good temperature recorder for Toarcian belemnites. On the other hand, compared with Mg, Sr is assumed to be less sensitive to temperature and biofractionation (Bailey *et al*., 2003, Lea *et al*., 1999 and different variation magnitudes of Mg and Sr profiles of belemnites in chapter 4 and 6). The dependence of Sr on temperature and species-specific biofractionation of this element still remains unknown, so whether Sr in belemnites can be used as a palaeotemperature proxy in general needs further testing and better quantification.

8.3 Conclusion

The uncertainties in using belemnite $\delta^{18}O$ ratios as palaeotemperature indicator lie in the poor knowledge of the past oceanic oxygen isotopic composition and unknown changes other than temperature (e.g. salinity) that can cause $\delta^{18}O$ variations (e.g. Spaeth *et al.*, 1971; Stevens and Clayton, 1971; Podlaha *et al.*, 1998; Rosales *et al.*, 2004a; 2004b). Also, belemnite isotope temperatures are found to be at least a few degrees cooler than those derived from other marine biogenic calcite or palaeo-proxy (e.g. TEX86, Mutterlose *et al*., 2010); hence the palaeotemperatures reconstructed from belemnite $\delta^{18}O$ have been questioned not to reflect sea surface temperature due to its nektonic life style (e.g. Wierzbowski, 2002; Mutterlose *et al.*, 2010). Accordingly, for palaeotempreature reconstructions, data of belemnite $\delta^{18}O$ should be compared with and corroborated by other palaeo-thermometers. On the other hand, the challenge in applying belemnite elemental concentrations (e.g. Mg/Ca) as a separate palaeo-proxy for palaeotemperature reconstructions is the poorly quantified temperature dependence and species-specific fractionation of these elements during belemnite calcification. The use of belemnites as palaeotemperature indicators is then greatly hampered for the reasons mentioned above. Unless the effects of temperature and species-specific fractionation on belemnite El/Ca ratios can be separately quantified, El/Ca ratios of belemnites are of restricted use as palaeotemperature indicator.

Part II:

Dating Mesozoic Carbonates

Chapter 9 U-Pb Dating of Mesozoic Carbonates

The aim of this chapter is to directly date Mesozoic carbonate fossils (e.g. belemnites) by the U-Pb method. This is because considerable parts of the Mesozoic timescale are relatively poorly calibrated by inadequate frequency of radiometric dates. At the same time, Mesozoic biogenic carbonate fossils are widely distributed and excellently preserved. Advances in U-Pb dating suggest that it might be fruitful to directly date Mesozoic carbonate by the U-Pb method using not only the biogenic components (e.g. fossil belemnites), but also early diagenetic calcite cements, which are found in abundance in Mesozoic fossils such as ammonites. This method might also be applied to determine whether the U-Pb ages of the cements might closely follow the depositional ages of the primary fossils.

Development of U/Pb attempts to date Mesozoic carbonate were undertaken in three phases. Firstly, a large number of belemnites and a range of biogenic carbonate and diagenetic calcite cements were screened for their U and Pb concentrations in order to assess their potential for dating. Then, selected carbonates were measured for U-Pb concentrations and isotopic ratios with a high-spatial resolution U-Pb protocol to assess their suitability for dating. Finally, those samples with high U/Pb ratios (>4) and/or showing undisturbed system for U-Pb were reanalyzed using isotope dilution method. The two U-Pb measurement protocols are explained later in the method section. The two approaches were thereafter combined to derive the best ages of the three datable samples. This innovative approach offers a real advantage in dating such samples over each method alone; and provides a useful strategy for improving the accuracy and precision of the U-Pb dating of carbonates.

9.1 Introduction

9.1.1 Mesozoic timescale

Our understanding of the Earth's history depends on precise knowledge of dates and rates of its evolution processes. A highly-calibrated timescale is crucial for a better understanding of how the Earth as a complete system has evolved. Uranium-lead dating of zircons in volcanic ash has become the mainstream mehod of calibrating the age of events in the Earth's history. However, in the Mesozoic, the lack of volcanic ash in sediments of many key biostratigraphic intervals means that calibrations can be poor. For example, the interval of the Aalenian-Albian stage (over 70 Ma) is numerically calibrated by only three primary radiometric dates; none come from Global Boundary Stratotype Section & Points (GSSPs) and European sequences (Table 17.2 in Gradstein *et al.,* 2004 and Fig. 9.1). One of these three ages – Kimmeridgian, has an uncertainty at 2 s.d. of ± 6.8 Ma. These radiometric ages are not precise enough themselves, and cannot be correlated reliably to European sections with required confidence.

On the other hand, fossils (e.g. belemnites and ammonites) are common in European Mesozoic sequences, which are well-defined and -calibrated by ammonite biostratigraphy. However, due to faunal endemism and diachroneity, regional/local biostratigraphic calibrations cannot be extrapolated to global stratigraphic records. Geologic time boundaries in the Mesozoic, currently based on fossil records and calibrated numerically by scattered volcanic ash ages, could potentially be further constrained by direct dating of fossil carbonates with the U-Pb system, if they could remain a closed system for U-Pb. Therefore, in this study, directly dating Mesozoic carbonates, particularly primary belemnites, using the U-Pb methodology, was investigated for feasibility.

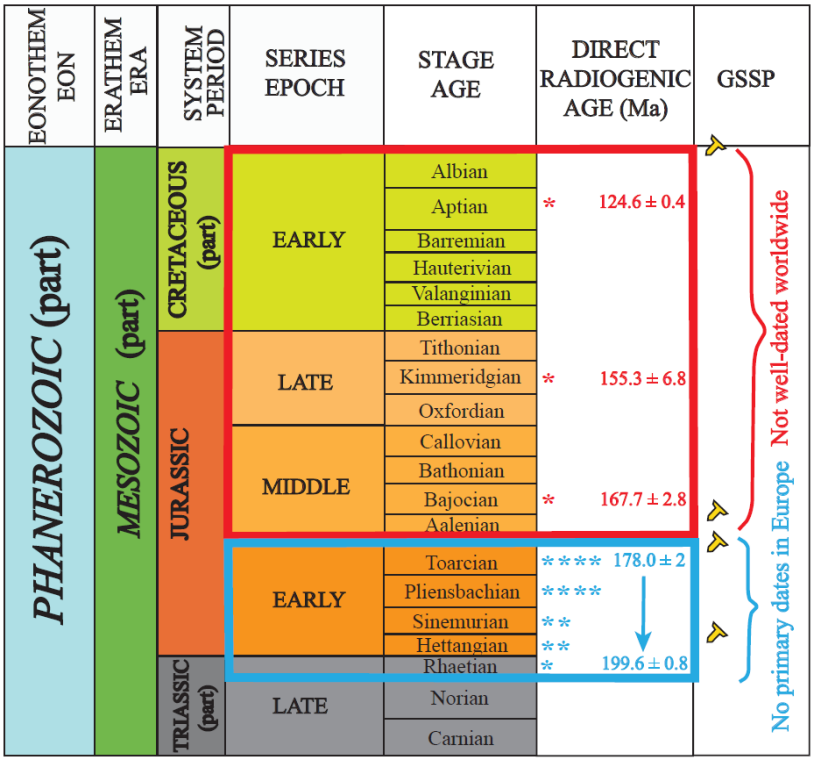

Fig. 9.1 Primary radiometric tie pints for the proposed interval of study, shown by red and blue boxes. In the upper red box, only three primary calibrating points exist, and the validity of some is disputed. In the lower blue box, more numerical ages exist, but are for strata in N and S. America, far from the European standard sections.

9.1.2 Previous studies on U-Pb dating for marine carbonates

Direct dating of biogenic carbonates using the U-Pb method has proven challenging (Rasbury and Cole, 2009). For marine biogenic carbonate, although it should contain little Pb due to its low abundance in seawater, it is not clear that it should form with a homogeneous initial Pb isotopic composition. Diagenetic alteration during burial in sediments and precipitation of secondary calcite can involve interactions with clastic sediment and so affect such early lead reservoirs. All these factors may cause heterogeneity in the initial Pb isotopic composition and abundance and could also facilitate gain or loss of U (and/or Pb), and hence result in difficulties with dating the carbonate depositional age. However, U-Pb dating of carbonate is possible in favorable circumstances. A few previously published studies have shown some success in getting sufficient range of U/Pb ratios in marine carbonates and obtaining reliable ages (Smith and Farquhar, 1989; Jones *et al.*, 1995; Israelson *et al.*, 1996;

Wang *et al.*, 1998; Getty *et al.*, 2001; Rasbury *et al.*, 2004; Denniston *et al.*, 2008), some of which are listed in Table 9.1.

Table 9.1 Reliable U/Pb data of fossils and marine cements, modified from Rasbury *et al*. (2009).

Period/Stage	U/Pb Age (Ma)	±2σ	MSWD	U (ppm)	Material	Minerology	Reference
Pleistocene	1.02	0.07	4.3	2.5	Coral	Aragonite	*Getty et al. 2001*
	1.288	0.03	0.3	1.8	Coral	Aragonite	*Getty et al. 2001*
Miocene	5.52	0.15	2.4	1.6	Coral	Aragonite	*Denniston et al. 2008*
Late Permian	246.1	7.9	324	3.5	Marine cement	Aragonite-replacing calcite	*Jones et al. 1995*
Carboniferous	300.1	3.8	0.88	4.7	Marine cement	Aragonite-replacing calcite	*Rasbury et al. 2004*
Devonian	376	10	4.6	0.3	Coral	Secondary calcite	*Smith & Farquhar,1989*

Marine fossils appeared on the U-Pb dating list very early due to their good preservation and great abundance. The U-Pb dating method has been proven to work for well-preserved corals from the Devonian to the Quaternary. Smith and Farquhar (1989) first dated the Devonian *Heliophyllum* corals from Ontario producing a ^{238}U-^{206}Pb age of 376 ± 10 Ma (MSWD = 4.6), a result that is consistent with the Middle Devonian stratigraphic age (375-385 Ma). Diagenetic calcite in porous corals was studied in their subsequent work (Smith *et al.*, 1991), but didn't produce reliable ages. Hence, it was concluded that only primary depositional carbonates gave a reliable age. Thereafter, Pleistocene aragonite corals from Costa Rica were precisely dated with ages of 1.02 ± 0.07 Ma (MSWD = 4.3) and 1.288 ± 0.034 Ma (MSWD = 0.33) in Getty *et al*. (2001). A late Cenozoic coral from Dominican Republic yielded a ^{238}U-^{206}Pb concordia age of 5.52 ± 0.15 Ma (MSWD = 2.4), which was used to constrain the marine coral species origination rates related to the closure history of the Central American Seaway (Denniston *et al.*, 2008).

Aragonite, however, is not as stable as calcite. Mesozoic fossils (if they were originally aragonite) have largely inverted from high-U aragonite to low-U calcite during diagenesis. There are currently no U/Pb dates of Mesozoic carbonates available, and well-preserved fossil (biogenic) calcite, such as that from belemnite, has not been dated by U-Pb system due to its close-to-detection-limit U content. Owing to recent advances in analytical instrumentation, U at ppb level is now precisely detectable and hence there is a need to develop U/Pb method to date calcite in deep time.

Marine calcite cement is another target for U-Pb dating. These cements are usually secondary calcite replacing original aragonite; so they may preserve fabrics of their aragonite precursor and contain higher U content (1-5 ppm) than biogenic calcite (Rasbury and Cole, 2009), rendering them potentially dateable. Because the initial Pb isotopic composition in such samples may not be homogeneous and because the resulting Pb isotopes in carbonates may be only moderately radiogenic, the $^{206}Pb^{*}_{radiogenic}/^{238}U$ ages are inevitably less precise than in accessory minerals like zircon. At the same time, the achievable precision can still be biostratigraphically useful. Few attempts to date aragonite-converted marine calcite cement have been made, and this material has yielded U-Pb ages consistent with depositional ages. For example, botryoidal calcite cement, recrystallized from aragonite, from the Late Permian Reef Complex of the New Mexico, gives a $^{206}Pb^{*}_{radiogenic}/^{238}U$ age of 250.2 ± 3.2 Ma (Jones *et al*., 1995), which overlaps with the Permian-Triassic boundary age of 251.4 ± 0.3 Ma (Bowring *et al.*, 1998). In addition, Rasbury *et al*. (2004) dated the aragonite-converted botryoidal calcite cements from algal mounds of Late Carboniferous Laborcita Formation. The yielded U/Pb age of 300.1 ± 3.8Ma (MSWD = 0.88) is in good agreement with the Carboniferous – Permian boundary age of 299.0 ± 1.0 Ma from zircons (Ramezani *et al.*, 2003). This published work proves that marine calcite cements can be dated by the U/Pb method, if the age relationship with the primary carbonate deposit can be constrained and reasonably precise measurements and corrections (e.g. common Pb) made for the U/Pb ages. Careful sampling is crucial for obtaining a spread of U/Pb ratios in order to improve age precision.

9.1.3 Mesozoic carbonates for U-Pb dating

Secondary calcite cements in-filled in Mezosoic fossils with less open space to surroundings, such as the body chambers of uncrushed ammonites, was explored because they may form early in the diagenetic processes and remain a closed system for U-Pb. Curtis *et al.* (2000) demonstrated two stages of cement formation in Lower Jurassic ammonites in concretions from Dorset. They are the early fringing, turbid calcite and later sparry, clear calcite infills. These authors qualified a two-stage cement formation model in well-preserved ammonites, but did not quantify the timing of each cement formation stage. Marine carbonate cements certainly formed after the biogenic carbonate and therefore postdate the depositional age. The key point of dating them is to understand the age relationship between the diagenetic cements and the primary carbonate. When dating carbonates with the U-Pb method, the highest achievable precision of an age appears to be ~ 1-2 % given current published data, but this could be improved significantly in favourable circumstances. If the early cement formed within a couple of million years in ≥100 Ma old ammonites, the ages obtained would provide a reasonable biostratigraphic age constraint within the uncertainty of the analysis.

Consequently, in this study, belemnites of the middle Mesozoic age were initially investigated for feasibility of U-Pb dating; and then a range of biogenic calcite (e.g. inoceramid, bivalve) and ammonite aragonite was examined further. Meanwhile, thin early cements were sampled for U-Pb dating from three uncrushed Jurassic ammonites (Fig. 9.3) from Somerset, UK, in order to test the theory of Curtis *et al.* (2000) that the fringing cements formed at the early stage after fossil burial. Finally, the U-Pb ages of the early cements and the biostratigraphic ages of the ammonites were compared to find out whether the early cements represent the depositional age of the fossils within the error of analysis.

9.1.4 U in seawater and incorporation into biogenic calcite

Uranium in modern oxic oceans predominantly exists as U^{6+} and strongly complexes with CO_3^{2-} to form the soluble phases $UO_2CO_3^0$, $UO_2(CO_3)_2^{2-}$ and $UO_2(CO_3)_3^{4-}$, which prevent U from being adsorbed onto surfaces of solids (Djogic *et al.*, 1986;

Barnes and Cochran, 1990; Yu *et al.*, 2008). Consequently, the U concentration in seawater is conservative and shows little variation along the water column. In seawater, uranium is thought to have a residence time of 200-600 kyr, which is much longer than the ocean overturning time of around 2000 years (Ku *et al.*, 1977; Barnes and Cochran, 1990). The reported U concentration in modern seawater is 3.3 ng/ml or 13.9 nmol/kg (Spence, 1968; Dunk *et al.*, 2002; Misra *et al.*, 2006; Shen *et al.*, 2006; Kumar *et al.*, 2008). However, the U concentration and U/Ca in oceans in deep time remain largely unknown. Seawater uranium concentrations over the past 30 kyrs have been estimated using analyses of uranium in corals, which have a small range of 2.5-3.5 ppm (Bard *et al.*, 1990). However, corals are not ideal for recording U in seawater in deep time due to diagenetic changes in their U content and short living time scale (10^5-10^6 years). Foraminiferal calcite has also been studied for U concentration and the U/Ca ratios have been used as an indicator of changes in seawater U content. The U/Ca ratios in foraminifera over the last ~50 kyrs show a range of 5 – 29 nmol/mol, and the U concentration varies from <1 ppb to 23 ppb in a clay-free foraminiferal sample (Delaney and Boyle, 1983; Russell *et al.*, 1996; Yu *et al.*, 2005; Harding *et al.*, 2006). U/Ca ratios in cultured foraminifera were found to be in proportion to seawater U concentration (Russell *et al.*, 1994). If an analogue or proxy could be applied to well-preserved Mesozoic belemnites, their U content and U/Ca ratios may indicate the U concentrations in Jurassic and Cretaceous seas, and hence provide a comparison to seawater U content derived from foraminifera in the past 50 kyrs.

The mechanism of uranium incorporation into biogenic calcite is still poorly known. Studies on planktonic U concentrations suggest a possible incorporation mechanism of uranyl carbonate complexes substitution for carbonate ions (Russell *et al.*, 1994; Yu *et al.*, 2008); and show that the distribution coefficient (D) for uranium incorporation into organic calcite (e.g. foraminiferal calcite) was at least five times lower than for inorganic calcite (Russell *et al.*, 1994); therefore, living organisms may discriminate against U. The incorporation of uranium in biogenic calcite is probably governed biologically. However, U and Pb can be bound with organic material as an U-organic complex into the calcite structure (McCall *et al.*, 2001), or exist as a surface-adsorbed species during diagenetic burial. Well-preserved biogenic

calcite, such as in belemnites, should prevent incorporation of U from surface-adsorption and may have a reasonable level of structural U incorporated into its organic matrix; therefore, they were screened for U concentrations in the early dating procedures.

9.2 Samples

Biogenic carbonates screened for U-Pb dating are: 1) forty-six well-preserved belemnites (belonging to over 20 species) obtained from the Pliensbachian (Lower Jurassic) to the Maastrichian (Late Cretaceous) in the UK, France, Antarctica, and Germany; 2) Coniacian to mid-Campanian calcite inoceramids and bivalve from Antarctica and 3) Upper Campanian to Maastrichtian aragonite ammonites from US Western Interior. Details of sample identities are shown in in Appendix G and Table 9.2.

In addition to the biogenic components, marine diagenetic calcite samples for dating include: 1) cements in Pliensbachian marine concretions from Yorkshire (well-constrained biostratigraphically in Howarth (1955); 2) alveolar cements in Pliensbachian belemnites from Dorset (Fig. 9.2); 3) infills in body chambers of the three Jurassic ammonites obtained from Somerset, UK (Fig. 9.3 & Table 9.2). Ammonite specimen SS2 is of excellent quality, but its biostratigraphic age was not precisely known; it is only known to be ~170 Ma in age. Because of its exceptional development and preservation of cements, it was used to test the analytical feasibility of U-Pb dating of cement. The detailed biostratigraphic ages of sample IS1 and IS2 of *Hildoceras* sp. can be directly compared to the U/Pb ages.

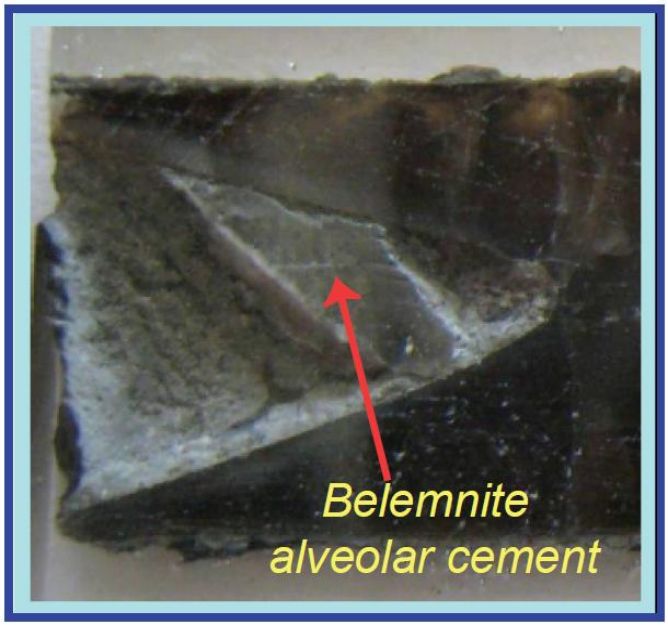

Fig. 9.2 The diagenetic calcite cement infilled in the alveolus of P.cuspidatus specimen D08 7-19 S3 from Dorset, UK.

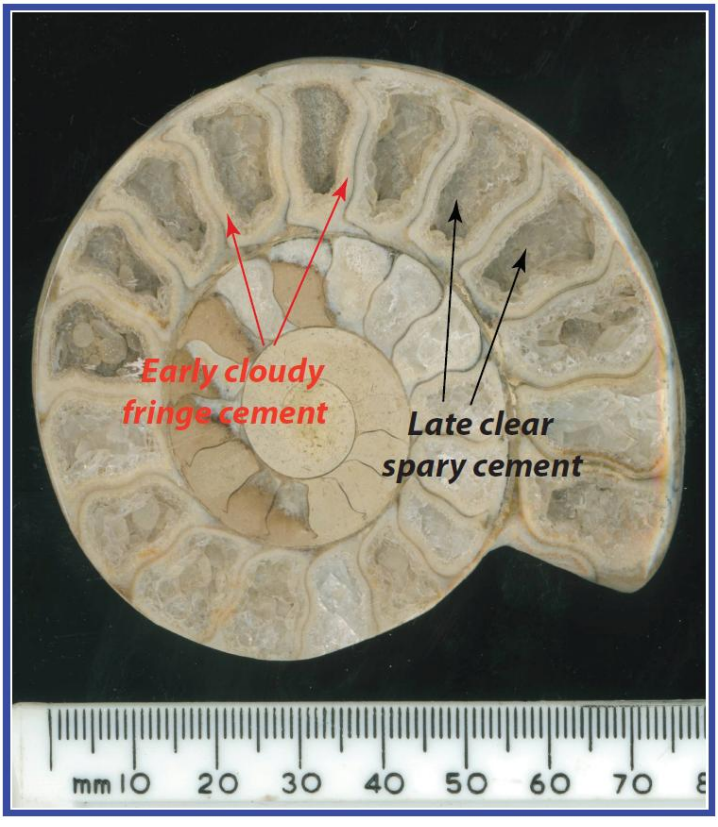

Fig. 9.3 A cross-section of ammonite 1S1 from Somerset, *Bifrons* Zone, *Hildoceras* spp. Early thin, cloudy and fringe diagenic calcite and late thick, clear and sparry cements are easily distinguished. This picture is provided by John McArthur.

Table 9.2 Descriptions of the three ammonites with calcite cements from Somerset, UK.

Sample No.	Species	Mineralogy	Location	Biostrat. Age	Age (Ma)
IS1	*Hildoceras* sp.	Calcite	Hurcott Lane Cutting, Ilminster, Somerset	*Hildoceras bifrons* Zone	~180
IS2	*Hildoceras* sp.	Calcite	Hurcott Lane Cutting, Ilminster, Somerset	*Hildoceras bifrons* Zone	~180
SS2	Ammonite	Calcite	Somerset, UK	*Stephan humphriesianum* Zone (estimated)	~170

Note: The estimated biochronologic age of SS2, derived from its approximate age using the time scale of Gradstein *et al*. (2004) is shown here.

9.3 Sample preparation and U-Pb Methodology

9.3.1 Sample preparation

Samples were initially screened for dating feasibility by measuring their U and Pb concentrations with a laser ablation protocol. Fossil specimens were broken into small pieces to select clear calcite fragments which were then mounted in resin for laser ablation analysis. Belemnite alveolar cement was removed using a scalpel blade, hand-picked, sonicated, and washed with pure water and acetone before mounting into resin. Polished cross-sections of ammonites and thick sections of carbonate concretion samples were also prepared. Resin blocks were ground, polished and cleaned prior to analysis.

Following the initial sample screening, a high-precision isotope dilution (ID) dating protocol was applied to selected samples. Subsamples of the chosen belemnites, inoceramids, ammonite aragonite and alveolar cement specimens, were hand-picked under the microscope. Early fringing cements from ammonites were carefully sampled by a New Wave Research microdrill to avoid contamination by later cements. The microdrill-sampling procedures are as follows: in a chosen chamber (the inset in Fig. 9.3), the dark material from septa (shown as black lines in Fig. 9.3) was drilled out using a microdrill in a clean-air environment. The resulting powder was transferred to centrifuge tubes for later use using a piece of weighing paper and scalpels. The boundary between early cloudy calcite and late clear calcite was easily

distinguished under the microscope, and a trench was therefore drilled to mark it. After that, the late sparry calcite was completely cleaned out using a hand drill; the remaining thin early calcite wall was finally broken into pieces with a scalpel. More than 5 subsamples of the thin early calcite wall were prepared in the attempt to produce a useful spread of U/Pb ratios.

As to U and Pb purification and separation for ID-U-Pb dating, the ultrasonically-cleaned carbonate sample pieces were completely dissolved in ultrapure 4N HNO_3 before spiked with a mixed ^{205}Pb-^{233}U-^{235}U tracer. Following sample – to – spike equilibration, organic matter in samples was destroyed by addition and evaporation of 0.5 ml of concentrated HNO_3 and 0.5ml H_2O_2. The precipitate was then re-dissolved in 1ml 1N HBr for anion exchange chemistry. Eichrom® anion exchange resin (equivalent to BioRad AG1 X8) was used to separate and purify Pb. U was purified using Eichrom UTEVA resin in nitric acid. The purified U and Pb were taken up in 1.2 ml 2% HNO_3 for isotope dilution MC-ICP-MS analysis. The U blank was less than 10 pg, and Pb blank was <60 pg for MC-ICP -MS and <20 pg for TIMS.

9.3.2 U-Pb decay schemes

There are two U to Pb decay schemes. The ultimate parent-daughter pairs are listed in Table 9.3 below:

Table 9.3 Ultimate parent-daughter pairs of the two uranium decay schemes, modified from Dickin, (2005), and the decay constants are from Steiger & Jäger (1977).

Parent isotope	Abundance (%)	Daughter isotope	Half life ($t_{1/2}$, yr)	Decay constant (λ, yr^{-1})
^{238}U	99.2743	^{206}Pb	4.4683×10^{9}	1.55125×10^{-10}
^{235}U	0.7200	^{207}Pb	7.0381×10^{8}	9.8485×10^{-10}

The radiogenic Pb concentration equations for the above two U-Pb decay schemes can be written as:

$$^{206}Pb_m = {}^{206}Pb_i + {}^{238}U(e^{\lambda_{238}t} - 1) \quad (9\text{-}1)$$

$$^{207}Pb_m = {}^{207}Pb_i + {}^{235}U(e^{\lambda_{235}t} - 1) \quad or \quad {}^{207}Pb_m = {}^{207}Pb_i + \frac{^{238}U}{137.88}(e^{\lambda_{235}t} - 1) \quad (9\text{-}2)$$

The subscript ***m*** and ***i*** refer to measured and initial values of the isotope. $\boldsymbol{\lambda}$ is the decay constant of the appropriate scheme and ***t*** is the time elapsed from the initial formations to the present (Dickin, 2005). The number 137.88 is the natural abundance ratio of ^{238}U to ^{235}U as recommended by Steiger & Jäger (1977). The previous equations can be re-written with ^{204}Pb as denominator of each parameter.

$$\left(\frac{^{206}Pb}{^{204}Pb}\right)_m = \left(\frac{^{206}Pb}{^{204}Pb}\right)_i + \frac{^{238}U}{^{204}Pb}(e^{\lambda_{238}t} - 1) \quad (9\text{-}3)$$

$$\left(\frac{^{207}Pb}{^{204}Pb}\right)_m = \left(\frac{^{207}Pb}{^{204}Pb}\right)_i + \frac{^{235}U}{^{204}Pb}(e^{\lambda_{235}t} - 1) \quad (9\text{-}4)$$

^{204}Pb is commonly used as a reference isotope because it is the only non-radiogenic Pb isotope. In Th-free systems, approximated by biogenic calcite, no radiogenic ^{208}Pb should be produced by the decay of ^{232}Th; and therefore ^{208}Pb can be used as a denominator in such equations instead of ^{204}Pb. The decay equations can be used with measurements documenting a spread in the U/Pb ratios to construct U-Pb isochrons and ages, which are subject to assumptions of a) initially homogeneous Pb isotope composition and b) closed U-Pb system behavior (Rasbury and Cole, 2009). The slope of an isochron (e.g. $e^{\lambda t} - 1$) in equation (9-3) and (9-4) then can be used to derive the age and the y-intercept gives the initial Pb isotope ratio.

Besides U-Pb isochrons, the Tera-Wasserburg concordia diagram is also widely used. It is based on equations (9-1), (9-2), and the following two:

$$\frac{^{238}U}{^{206}Pb^{*}} = \frac{1}{e^{\lambda_{238}t} - 1} \tag{9-5}$$

$$\left(\frac{^{207}Pb}{^{206}Pb}\right)^{*} = \frac{1}{137.88}\left(\frac{e^{\lambda_{235}t} - 1}{e^{\lambda_{238}t} - 1}\right) \tag{9-6}$$

where the * refers to the radiogenic isotope. Tera-Wasserburg concordia plots $^{238}U/^{206}Pb$ against $^{207}Pb/^{206}Pb$ (see Fig. 9.4). The concordia curve represents the locus of all closed system compositions incorporating radioactive decay in the absence of initial Pb. Because initial common Pb is always present to some extent, a variable mixture of initial and radiogenic ingrowth of Pb for different aliquots will define a linear array between the closed system radiogenic and common Pb end members (the dashed line in Fig. 9.4). This discordia line intersects the concordia curve at two points. It is the lower intersect with the concordia that gives the ratio of ^{238}U to radiogenic ^{206}Pb, from which the age can be derived using equation (9-5). In this case, the age is 195 Ma for the sample shown in Fig. 9.4. The $^{207}Pb/^{206}Pb$ of the common Pb component is given by the y-intercept (Fig. 9.4). If the system is not closed, and has been disturbed in terms of U-Pb, the linearity of the array will be lost and scattered data should result. Clearly, Tera-Wasserburg concordia diagram does not depend on the measurement of ^{204}Pb or ^{208}Pb and requires no assumption of initial Pb isotopic composition (Faure and Mensing, 2005). For the carbonates analyzed in this study, all the data are plotted on Tera-Wasserburg concordia diagrams.

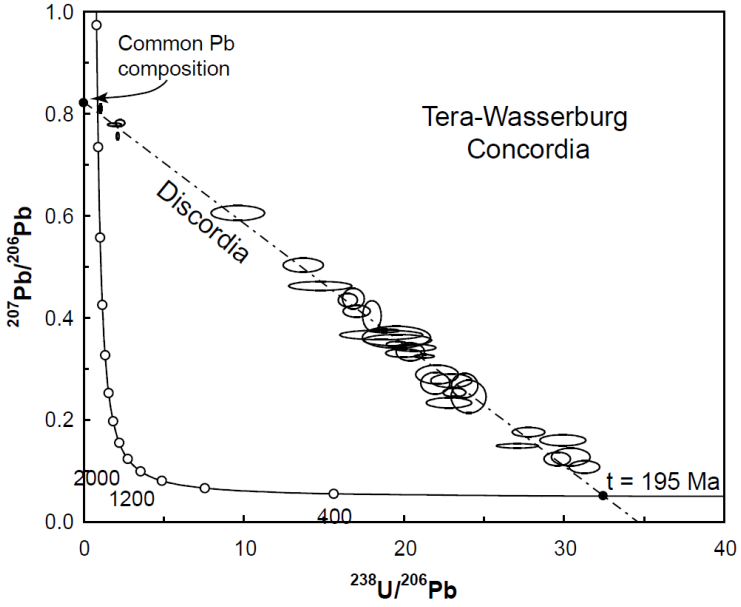

Fig. 9.4 Tera-Wasserburg Concordia diagram of an Early Jurassic ammonite from Somerset, UK. Data are given by laser ablation multiple collector inductively coupled mass spectrometer (LA-MC-ICP-MS), and plotted using Isoplot version 3.00 (Ludwig 2003).

9.3.3 Laser ablation measurement protocol

In the initial part of the dating procedures, fossil carbonates and cements from belemnite alveolus and marine concretions were analyzed by laser ablation inductively coupled plasma multiple collector mass spectrometer (LA-ICP-MC-MS) to rapidly assess U and Pb concentrations only. The sample screening analysis was made using the Nu HR ICP-MC-MS (Laser ablation MC-ICP-MS) at NIGL, British Geological Survey in Keyworth, UK. The HR Nu was coupled to a New Wave Research UP193FX (193 nm) excimer laser ablation system. The laser sampling protocol employed ablation with a spot size of 100 μm, a dwell time of 15 seconds, and a fluence at 10Hz at ~6.7J/cm^2. NIST 614 glass and Zircon 91500 were used as ablation standard monitors for approximate quantification, and a two second pre-ablation on each spot was applied in order to remove the surface layer that would undoubtedly contain surface Pb contamination. U and Pb concentrations were calculated using the ratios of expected concentrations to measured intensities of NIST 614. The detection limit of the Nu HR instrument for ^{206}Pb was ~ 1ppb.

Isotopic ratios (^{238}U/^{206}Pb and ^{207}Pb/^{206}Pb) were measured by LA-ICP-MC-MS only for the three ammonite cement samples. Cement samples IS2 and SS2 were analyzed

in the same run with a Tl-^{235}U solution and standard glass NIST 614, whereas cement IS1 was measured at a separate time using zircon 91500 as a standard monitor. The ^{207}Pb/^{206}Pb ratios of the cements were corrected using known ^{203}Tl/^{205}Tl ratio and further normalized using NIST 614 or zircon 91500. The ^{238}U/^{206}Pb ratios were first mass-bias corrected and then adjusted by U-Pb inter-element fractionation factor. Sample screening was also done with a RESO M-50 ICP-QMS (Laser Ablation-Inductively Coupled Plasma-Quadrupole Mass Spectrometer) at Royal Holloway, Egham. The operating conditions of RESO M-50 ICP-QMS were as follows: an ArF excimer (193nm) laser-ablation system (RESOlution M-50, Resonetics LLC, USA) was coupled to a two-volume laser-ablation cell (Laurin Technic, Australia), and this LA unit was connected to an Agilent 7500ce/cs quadruple ICP-MS at a RF power of 1250 W. NIST 612 was used as a reference glass to bracket sample analysis. Pre-ablation was done to clean the mount surface before scanning across the sample. Data were then normalized to NIST 612. Analyses done with this instrument did not attempt to measure ^{207}Pb/^{206}Pb values.

9.3.4 Isotope dilution measurement protocol

High-precision U-Pb dating of picked and drilled material was made using both a Nu HR ICP-MC-MS and a Triton TIMS instrument at the NERC Isotope Geocience Laboratories, Keyworth. The MC-ICP-MS analysis employed a mixed multiple collector array using both Faraday cups and ion counting secondary electron multipliers with off-line gain calibration. For TIMS analysis, the dried U and Pb separates were loaded separately with silica gel and H_3PO_4 onto single outgassed rhenium filaments and analysed using a Thermo Scientific Triton mass spectrometer (fitted with an axial MasCom secondary electron multiplier [SEM]). Data were obtained in dynamic single-collector mode on the SEM with Pb and U typically run to exhaustion. Pb and U standards SRM 981 and U500 were analysed to monitor mass spectrometer performance, ensuring that the SEM linearity, accuracy and reproducibility was better than ± 0.1%. Not all analyses performed by ID-TIMS were successful on account of variable emission of U and/or Pb from the Re filament. A combined ID-TIMS – ID ICP-MC-MS approach was used as necessary.

Data reduction, error propagation and plotting were carried out using customized data reduction spreadsheets based on the EARTHTIME data reduction spreadsheet following standard parametric statistical methods (Schmitz and Schoene, 2007) and Isoplot version 3.00 (Ludwig, 2003). The decay constants used were those proposed by Jaffey *et al.* (1971), as recommended by Steiger & Jäger (1977) and listed in Table 9.3.

9.4 Results

9.4.1 U and Pb concentrations

9.4.1.1 Preliminary sample screening for U and Pb

The ranges of intensity-derived ^{238}U and ^{206}Pb concentrations of Mesozoic sample categories are shown in Table 9.4. Because these were rapid screening analyses, there was no attempt to quantify the uncertainty of these analyses; and because no calcite standard was available at the time, these estimates of concentration may have inherent modest inaccuracy. The detection limit of ^{238}U and ^{206}Pb, was <5 ppb. Fossil ammonite nacre (aragonite) has U contents from 1 to 8 ppm, but the concentration of Pb varies broadly from < 0.5 ppm in a well-preserved sample to 19 ppm in an altered specimen. Biogenic calcite, however, contains much less U and Pb. Pristine belemnite calcite possesses < 10 ppb of U and < 40 ppb of Pb, with many below detection limit, but U in altered belemnites can be up to 160 ppb (Fig. 9.5). The cements from belemnite alveolus and marine concretions (39-1 CN and 62-1 CN) are subject to contamination and have more elevated Pb (up to 10 ppm) than U (<0.7 ppm), suggesting a disturbance to the U-Pb system. The rarely well-preserved alveolar cement VGL-34 contains no higher than 1 ppm of U and <0.3 ppm of Pb (Table 3), making it promising for dating.

Table 9.4 Summary of U and Pb concentrations in different categories of Mesozoic carbonate samples obtained by LA-MC-ICP-MS. Concentrational ranges are provided when large variations are present between samples in the same category. Standards zircon 91500 and NIST 614 glass were used as monitors for approximate quantification. Normalizations of samples to the two different standards do not bring significant differences in concentrations.

Carbonate sample category	^{238}U ppm	^{206}Pb ppm
Biogenic aragonite	1 - 8	0.5 -19
Belemnite alveolar cement (contaminated)	0.1 - 0.6	0.5 – 5.5
Belemnite alveolar cement (clean)	0.6	0.3
Marine concretion cement	0.1	2 - 10
Biogenic calcite (non-belemnite)	0.02 – 2.8	0.4
Pristine belemnite calcite	<0.01	<0.04
Altered belemnite calcite	~0.1	~0.02

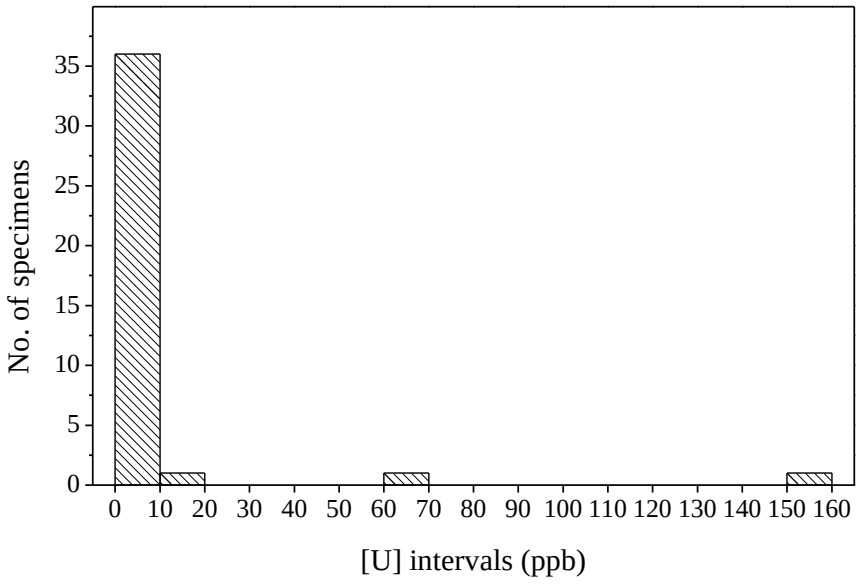

Fig. 9.5 The histogram showing the distribution of U concentration in 39 Mesozoic belemnites collected from Europe. Only two belemnites exhibit up to 160 ppb of U but are worse-preserved than the rest.

9.4.1.2 Fossil Aragonite and Belemnite Alveolar Cement

The follow-up isotope dilution (ID) U-Pb concentration data of ~1 – 50 mg aliquots of aragonite and the alveolar cement are given in Table 9.5. The ID U-Pb data show

smaller U and Pb concentrations and ranges than laser ablation (LA) estimates likely due to homogenization in larger aliquots of samples. Differences in concentrations between the two approaches are likely attributed to LA - normalization inaccuracies since no calcite standard was available.

Table 9.5 Summary of U and Pb contents and U/Pb ratios of macrofossils and cements from the UK by ID-MC-ICP-MS.

Samples	^{238}U (ppm)	Total Pb (ppm)	^{207}Pb/^{206}Pb	1σ %	^{238}U/^{206}Pb	1σ%	^{206}Pb/^{208}Pb	1σ%	^{238}U/^{208}Pb	1σ%
Ammonite aragonite										
USWI-17*	0.279	0.266	0.799	0.54	1.819	4.15	0.504	0.31	0.918	4.14
USWI-17	0.357	0.370	0.843	1.15	1.791	7.37	0.471	0.57	0.844	7.35
USWI-10	0.345	0.155	0.829	0.72	3.989	2.58	0.488	0.38	1.946	2.55
Belemnite alveolar cement										
VGL-34 a	0.064	0.048	0.764	0.04	4.260	2.54	0.525	0.02	2.238	2.54
VGL-34 b	0.088	0.063	0.762	0.03	4.534	1.05	0.526	0.01	2.385	1.05

9.4.1.3 Early Calcite Infill in Ammonites

The LA U-Pb data (Appendix H – I, normalized to zircon 91500 for sample IS1 but to NIST 614 for samples SS2 and IS2) of the early calcite cements in the three ammonites show that they have up to 15 ppm of U and <4 ppm of Pb. In these materials, U-Pb concentrations vary by a factor of 10 and in part indicate that some samples have relatively radiogenic lead. The ID-MC-ICP-MS and -TIMS data of the early ammonite cements are comparable and listed in Table 9.6 to 9.7. The U and Pb concentrations vary from 0.47 to 5.31 ppm and 0.06 to 2.1 ppm, respectively, with these ranges being about half of and ranges of their LA measurements, for the reason mentioned in the previous paragraph.

9.4.2 U-Pb Isotopic ratios and ages

9.4.2.1 Fossil Aragonite and Belemnite Alveolar Cements

A limited spread of U/Pb ratios was measured by ID-ICP-MC-MS in aragonite specimens and inorganic belemnite alveolar cement. Reasonably high U/Pb ratios (>4) suggests dating potential (Table 9.5). High common Pb in the biogenic aragonite, with limitted variation in U/Pb ratios may be caused by addition of common Pb in biofilms separating aragonite plates. While strategies could be explored to mitigate this, such experiments have not been explored further.

9.4.2.2 Early Calcite Infill in Ammonites

a) LA $^{207}Pb/^{206}Pb$ and $^{238}U/^{206}Pb$ data and T-W arrays

Laser ablation (LA) U-Pb data show that early calcite cements in the three ammonites of Early – Middle Jurassic age from Somerset, have $^{238}U/^{206}Pb$ ratios as high as 24, and $^{207}Pb/^{206}Pb$ ratios from 0.11 to 0.83 (Fig. 9.6, Appendix H – I), demonstrating a high proportion of radiogenic Pb in some zones. These samples were therefore chosen for detailed analysis using isotope dilution method with the objective of producing high precision ages.

Three samples of early cements from ammonites produced a considerable co-variation and linear arrays in both $^{207}Pb/^{206}Pb$ and $^{238}U/^{206}Pb$ ratios of LA analysis on the Tera – Wasserburg (T – W) plot. The measured, non-normalized arrays of samples SS2, IS2 and IS1 (Fig. 9.6) produced ages of 257.7 ± 3.1 Ma (MSWD = 14), 258.0 ± 4.9 Ma (MSWD = 2.7) and 171.2 ± 2.3 ma (MSWD = 0.77), with uncertainties of 1 – 2 %. These ages of cements are inaccurate due to the lack of U/Pb inter-element fractionation correction. However, these data clearly demonstrate a single array that implies closed system behavior with a uniform common Pb composition ($^{207}Pb/^{206}Pb$) of around 0.83 ± 0.1 (Fig. 9.6).What is also apparent from these data is that cement regions in each sample contain very different proportions of common to radiogenic lead, at the scale of ~100 μm. Sample SS2, for example, contains regions that vary from < 2% to > 90% radiogenic Pb, a remarkable variation within a sub-mm region.

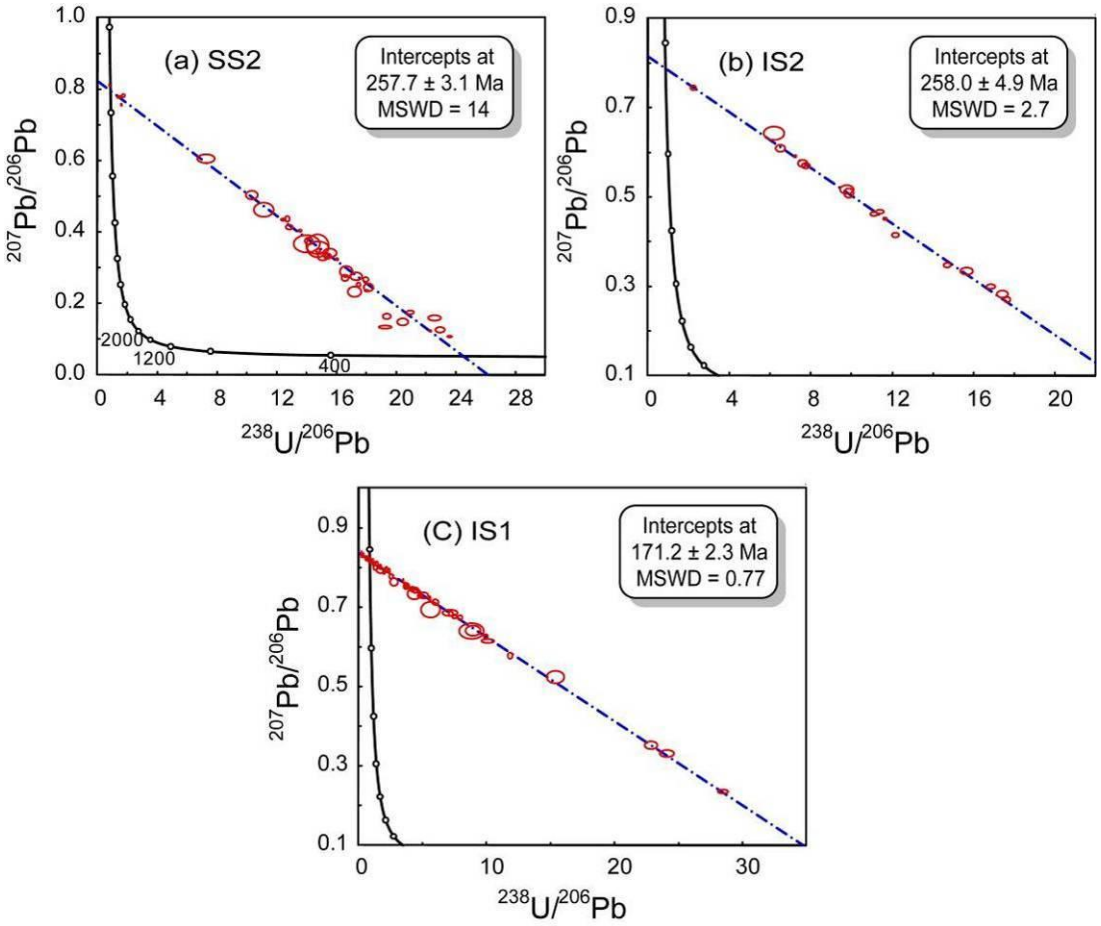

Fig. 9.6 Total U-Pb concordia diagrams for 3 ammonite specimens: (a) SS2; (b) IS2 and (c) IS1. Data are obtained from LA ICP-MS, and errors are shown at 2σ. The Pb isotope ratios are normalized to reference glass NIST 614, but not common Pb corrected. The U/Pb ratios are mass-bias corrected only. The actual ages have little meaning due to the lack of U-Pb inter-element fractionation correction.

b) ID U-Pb ratios and ages

The use of a mixed ^{205}Pb-^{233}U-^{235}U spike and isotope dilution (ID-) methodology is inherently much more accurate and precise than other methods, and does not rely implicitly on a mineral standard. The ID-MC-ICP-MS and ID-TIMS data of ammonite infillings show good comparability, and MC-ICP-MS data are used to construct the Tera-Wasserburg concordia diagrams. Their U/Pb ratios ($^{238}U/^{206}Pb$) fall in a range of 3-19 (Fig. 9.7), and the $^{207}Pb/^{206}Pb$ ratios vary from 0.46 to 0.78. ID- MC-ICP-MS data alone give U/Pb ages of 156.2 ± 4.8 Ma (MSWD = 0.68), 170 ± 11 Ma (MSWD = 10.8), and 171 ± 16 Ma (MSWD = 0.53) for cement samples from SS2, IS2 and IS1, respectively (Fig. 9.7). Cement samples SS2 and IS2 show ages younger than the LA results (lack of calibration on $^{238}U/^{206}Pb$ ratios), and are

~10 Ma younger than the corresponding biostratigraphic ages of the fossils. The ID - age uncertainties of sample IS2 and IS1 are poorly constrained due to the small spread in the measured ratios.

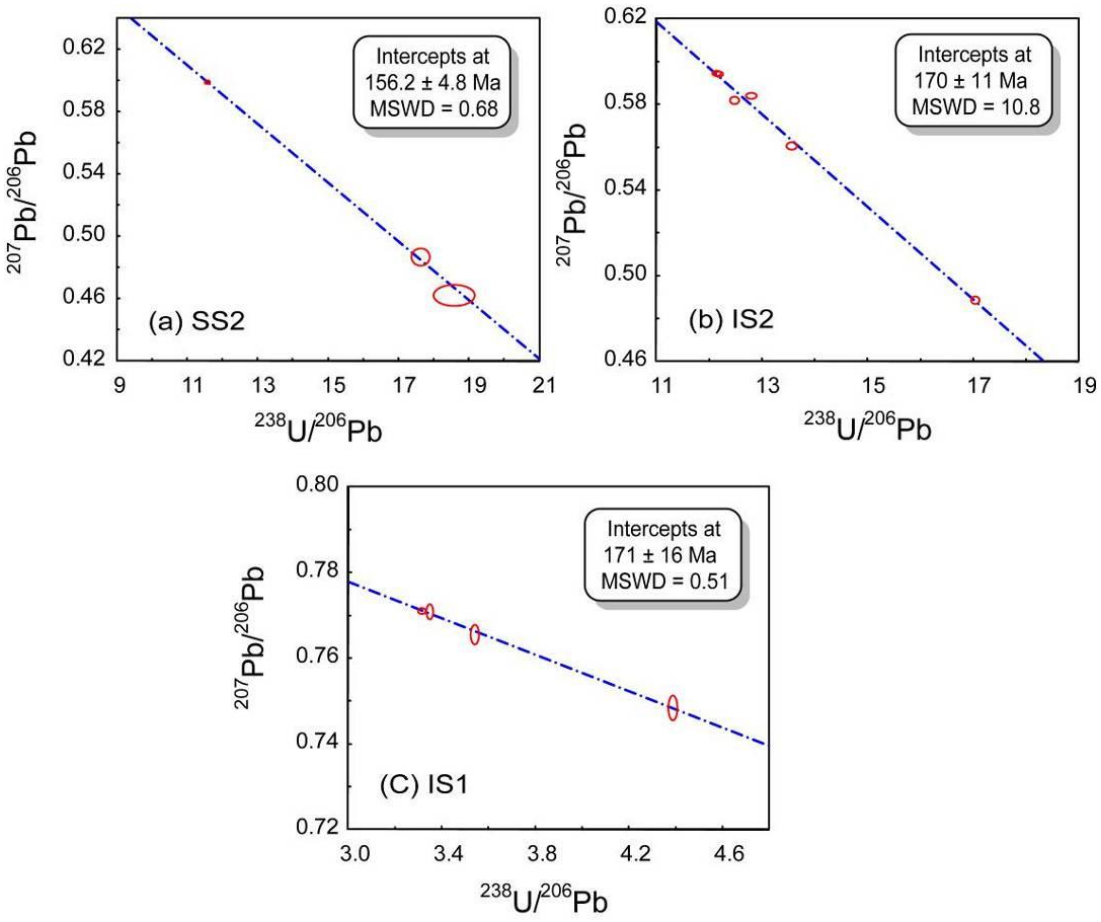

Fig. 9.7 Tera-Wasserburg concordia diagrams of U/Pb data obtained by ICP-MC-MS isotope dilution on three separate ammonites (a) SS2; (b) IS2 and (c) IS1. Errors are shown at 2σ. Both axes do not start from 0 in order to give a better view of the data ellipse in the diagrams. Concordia lines are not shown in these diagrams because they are plotted in the intervals outside of the ranges of axes.

Table 9.6 ID-MC-ICP-MS data of U-Pb concentrations and isotopic ratios for the early cements from three ammonite samples IS1, IS2 and SS2.

Sample	Wt. mg	U ppm	Pb ppm	Pb (pg)	238U/206Pb	% err	207Pb/206Pb	% err	204Pb/206Pb	% err	corr. coef. 8/6-7/6	corr. coef. 8/6-4/6	corr. coef. 7/6-4/6
IS2 A-d2-1	7.7	3.30	0.689	5275	12.48	0.57	0.5820	0.24	0.03616	0.24	-0.29	-0.22	0.24
IS2 A-d2-2	6.9	2.68	0.549	3771	12.79	0.6	0.5840	0.19	0.03629	0.18	-0.64	-0.52	0.81
IS2 A-d2-3	6.9	2.65	0.577	3964	12.18	0.5	0.5941	0.18	0.03696	0.16	-0.73	-0.62	0.81
IS2 A-d4	5.0	3.35	0.630	3124	13.57	0.6	0.5605	0.25	0.03473	0.24	-0.80	-0.68	0.84
IS2 A-d2-3 Re	6.9	2.65	0.579	3979	12.14	0.5	0.5944	0.17	0.03694	0.16	-0.74	-0.61	0.80
IS2 A-d2	8.0	5.31	0.720	5760	17.04	0.4	0.4887	0.30	0.02975	0.24	-0.36	-0.39	0.38
IS1 AO-e2	5.8	1.96	1.901	10985	3.32	0.4	0.7710	0.08	0.04898	0.09	-0.12	0.01	-0.11
IS1 AO-e3	9.4	1.94	1.861	17565	3.35	0.4	0.7708	0.19	0.04887	3.96	-0.11	0.01	-0.02
IS1 AO-f2	6.4	2.08	1.490	9578	4.39	0.4	0.7484	0.32	0.04733	0.23	-0.10	0.13	-0.17
IS1 AO-f3	3.7	2.32	2.095	7711	3.54	0.4	0.7655	0.25	0.04847	0.30	-0.14	0.09	-0.17
SS2 A-c6	1.6	0.99	0.120	190	18.58	2.6	0.4623	1.21	0.02814	1.32	-0.53	-0.52	0.98
SS2 A-c1	5.4	0.83	0.190	1027	11.57	0.5	0.5990	0.16	0.03750	0.21	-0.57	-0.26	0.17
SS2 A-c1 Re	5.4	0.83	0.190	1027	11.58	0.5	0.5992	0.16	0.03743	0.21	-0.57	-0.26	0.18
SS2 A-c2	3.7	0.47	0.062	232	17.63	1.2	0.4868	0.91	0.02987	0.99	-0.98	-0.95	0.96

Table 9.7 ID-TIMS data of U-Pb concentrations and isotopic ratios for the early cements from three separate ammonites IS1, IS2 and SS2.

Sample	Wt. mg	U ppm	Pb ppm	Pbc (pg)	238U/206Pb	% err	207Pb/206Pb	% err	204Pb/206Pb	% err	corr. coef. 8/6-7/6	corr. coef. 8/6-4/6	corr. coef. 7/6-4/6
IS2 A-d2-1	7.7	3.30	0.689	4687.0	12.48	0.57	0.5820	0.24	0.03615	0.26	-0.29	-0.28	0.31
IS2 A-d2-2	6.9	2.68	0.549	3353.5	12.79	0.6	0.5840	0.19	0.03627	0.23	-0.64	-0.56	0.88
IS2 A-d2-3	6.9	2.65	0.577	3547.0	12.18	0.5	0.5941	0.18	0.03694	0.21	-0.73	-0.66	0.88
IS2 A-d4	5.0	3.35	0.630	2738.3	13.57	0.6	0.5605	0.25	0.03471	0.30	-0.80	-0.72	0.90
IS2 A-d2-3 Re	6.9	2.65	0.579	3556.2	12.14	0.5	0.5944	0.17	0.03692	0.21	-0.74	-0.66	0.88
IS2 A-d2	8.0	5.31	0.720	4755.2	17.04	0.4	0.4887	0.30	0.02974	0.27	-0.36	-0.43	0.43
IS1 AO-e2	5.8	1.96	1.901	10729.5	3.32	0.4	0.7710	0.08	0.04897	0.09	-0.12	-0.08	-0.06
IS1 AO-e3	9.4	1.94	1.861	17122.9	3.35	0.4	0.7708	0.19	0.04887	3.96	-0.12	0.01	-0.02
IS1 AO-f2	6.4	2.08	1.490	9248.2	4.39	0.4	0.7484	0.32	0.04732	0.23	-0.10	0.09	-0.16
IS1 AO-f3	3.7	2.32	2.095	7494.2	3.54	0.4	0.7655	0.25	0.04846	0.31	-0.14	0.04	-0.16
SS2 A-c6	1.6	0.99	0.120	154.9	18.58	2.6	0.4623	1.21	0.02814	1.32	-0.53	-0.52	0.98
SS2 A-c1	5.4	0.83	0.190	927.0	11.57	0.5	0.5990	0.16	0.03750	0.21	-0.57	-0.26	0.17
SS2 A-c1 Re	5.4	0.83	0.190	924.1	11.58	0.5	0.5992	0.16	0.03743	0.21	-0.57	-0.26	0.18
SS2 A-c2	3.7	0.47	0.062	193.7	17.63	1.2	0.4868	0.91	0.02987	0.99	-0.98	-0.95	0.96

9.4.3 Combined LA and ID approach for best U-Pb ages

The LA – results show coherent U-Pb arrays, limited scatter, and good precision on the initial $^{207}Pb/^{206}Pb$; the ID data are accurate, but not so precise due to the limited U-Pb spread. A combination of these two datasets to derive the accurate, high precision ages of the cements is then developed. The approach includes a self-normalization of two cements (SS2 and IS1) and an independent normalization of cement IS2 to SS2, explained below:

Cement SS2 and IS2 were analyzed together with the same standard (NIST 614 glass) and under the same laser condition. Cement SS2 was chosen for self-normalization to derive the inter-element fractionation factor because its ID T-W regression is better than that of IS2 (e.g. smaller errors and less scatter). Its well-defined y-intercept (the initial $^{207}Pb/^{206}Pb$) and its uncertainty of LA T-W regression (Table 9.8) were used to anchor the ID data precisely. This anchored ID-data regression (Fig. 9.8 a) produces a better-constrained x-intercept that is accurate, unlike that of initial LA T-W data alone. Comparison of the slope and x-intercept (42.9 ± 0.9) of this array with the x-intercept (26.15 ± 0.33) of the non-normalised initial LA-data yields an inter-element fractionation factor of 1.64 (Table 9.8). Next, the non-normalized $^{238}U/^{206}Pb$ ratios of the LA data were corrected by this factor of 1.64. The corrected LA data then produce a LA T-W concordia age of 159.7 ± 2.7 (MSWD = 10.6) shown in Fig. 9.9 which overlaps with and has smaller uncertainty than the ID and anchored ID T-W ages (Table 9.9). The fractionation factor of 1.64 derived from SS2 was then applied to sample IS2 to normalize its inaccurate LA $^{238}U/^{206}Pb$ values. This then produces a corrected LA-based age of 158.7 ± 3.1 (MSWD = 2.1) for IS2 (Fig. 9.9), a significant improvement on ID- or LA-anchored ID datasets alone (Table 9.9).

Cement IS1 was run with reference zircon 91500 at different laser and standard conditions from the other two samples, but the self-normalization procedure is the same as that of SS2, and a LA U/Pb inter-element fractionation factor of 1.07 (Table 9.8) was derived, and the final age of cement from sample IS1 is 159.7 ± 2.3 (MSWD = 0.76). The difference in the calculated fractionation factors when using glass v. zircon is not surprising given the different standard material, gas flow and

running conditions inherent to each sample session. All of these final ages are interpreted as dating formation age of early cements.

Table 9.8 The regression parameters in T-W diagrams of LA, ID-MC-ICP-MS and LA corrected ID-MC-ICP-MS data of ammonite cements IS1 and SS2.

	LA				LA anchored ID				Inter element fractionation factor
	Y-int	2σ	X-int	2σ	Y-int	2σ	X-int	2σ	
SS2	0.8231	0.0092	26.15	0.33	0.8204	0.0067	42.86	0.83	1.64
IS1	0.8390	0.0016	39.49	0.54	0.83652	0.0018	42.30	1.10	1.07

Note: Data are all reported in 2σ (absolute values). X-int and Y-int refer to x and y intercepts. Sample IS2 is normalized to SS2, so the inter element fractionation factor used to correcte its LA $^{238}U/^{206}Pb$ ratios is the one derived from sample SS2. The reason for this calculation is explained in the text.

Table 9.9 The T-W age regression results for LA and ID data of cements SS2, IS2 and IS1.

	LA			**ID**			**LA anchored ID**			**Corrected LA**		
	Age	2σ	MSWD	Age	2σ	MSWD	Age	2σ	MSWD	Age	2σ	MSWD
SS2	257.7	3.1	14	156.2	4.8	0.68	157.8	3.3	0.53	**159.7**	**2.7**	**10.6**
IS2	258.0	4.9	2.7	170	11	10.8	166.3	9.7	15	**158.7**	**3.1**	**2.1**
IS1	171.2	2.3	0.77	171	16	0.51	160.1	4.1	0.69	**159.7**	**2.3**	**0.76**

Note: All ages are reported in Ma at 2σ. Ages in bold are taken as the formation time of the cements.

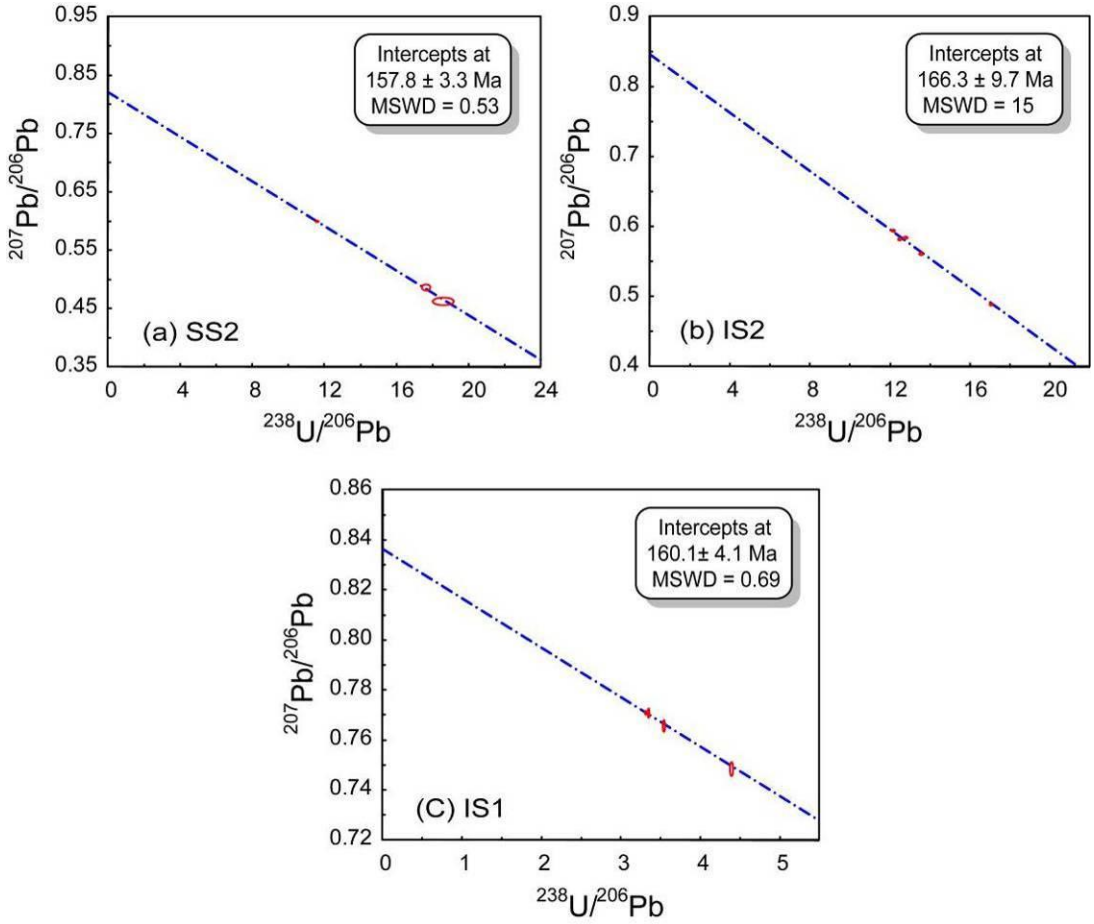

Fig. 9.8 Tera-Wasserburg concordia diagrams for sample (a) SS2; (b) IS2 and (c) IS1 obtained from LA anchored ID data. Errors are shown at 2σ.

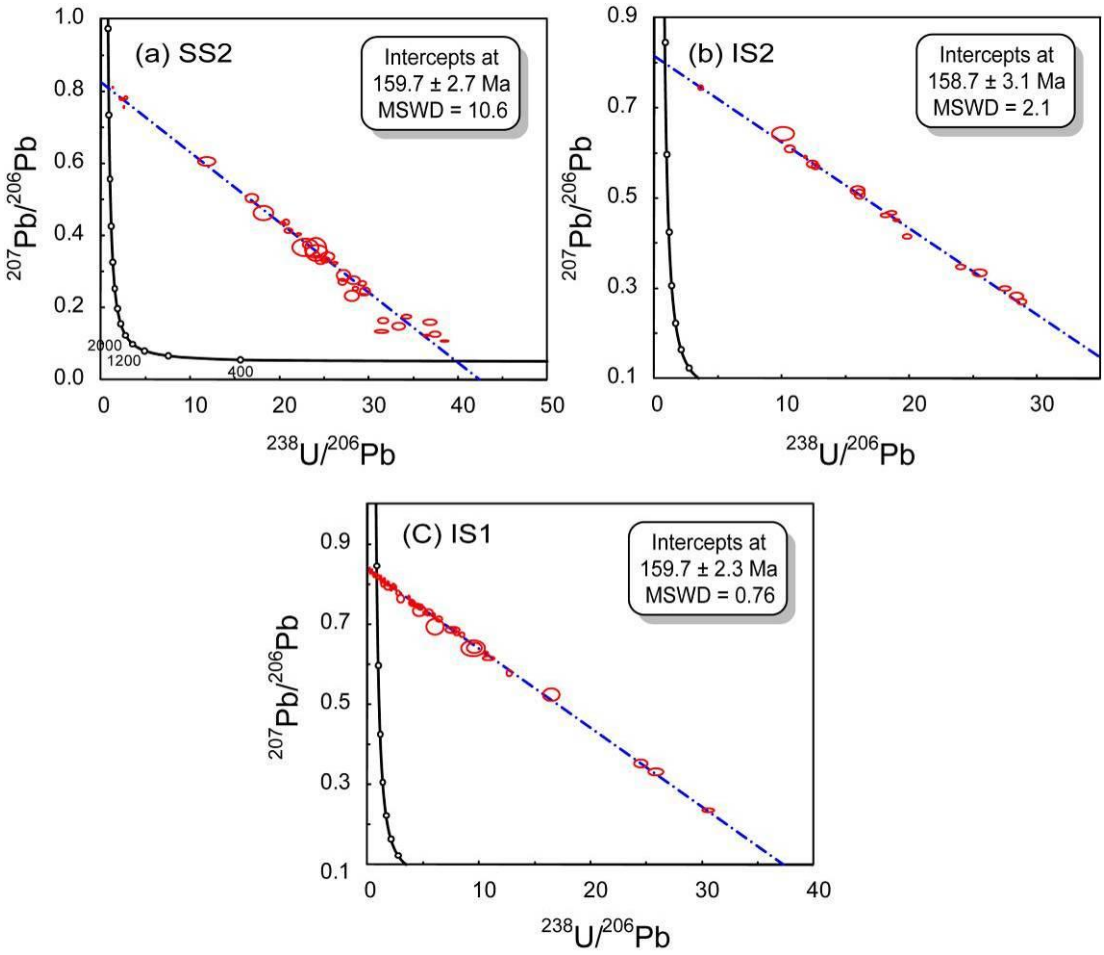

Fig. 9.9 Tera-Wasserburg concordia diagrams of U-Pb inter-element fractionation factor corrected LA-ICP-MC-MS data for sample (a) SS2; (b) IS2 and (c) IS1. Errors are shown at 2σ.

9.5 Discussion

9.5.1 U/Pb dating on Mesozoic fossils and diagenetic cements

This study indicates that most biogenic calcite, in particular, the stable low-Mg belemnite calcite, exhibit a U concentration of <10 ppb and < 60 ppb of Pb. Samples with U content of around 100 ppb reflect alteration and U and Pb addition at some time fillowing death of the animal. Consequently, for pristine biogenic calcite, the lack of U and Pb makes this material unsuitable for dating by the current U-Pb methodology. The well-preserved Mesozoic belemnites are estimated to have U/Ca ratios of 4 nmol/mol, assuming its calcite content is 40% and U content 10 ppb. If the U concentration of belemnites can be used to record the seawater U at that time, as do foraminifera (Russell *et al.*, 1994; 1996), the lower U content and U/Ca ratios

in them than foraminifera may indicate that U concentrations in Jurassic and Cretaceous seas were lower than in the past 50 kyrs.

The laser ablation and isotope dilution U-Pb data show that biogenic aragonite available to this study contains 1 - 8 ppm of U, has < 0.5 ppm of common Pb where well-preserved, and has relatively large U/Pb ratios; thus it should have the potential to allow dating by the U/Pb method. However, with data of this study, common Pb contamination in biogenic aragonite is problematic. Well-preserved aragonite samples are rare, and the removal of potentially secondary common Pb, on the other hand, is very challenging and might only be achieved with leaching, microscopic sub-sampling, and perhaps micro-milling; such work was therefore considered beyond the scope of this PhD project.

Inorganic belemnite alveolar calcite is found to be subject to small sample size and diagenetic contamination; and therefore is not easily datable. The early-diagenetic calcite in uncrushed ammonite chambers, however, is abundant, remains a closed system for U and Pb and can produces usable ages.

9.5.2 Using a combined methodological U-Pb dating approach

When comparing LA U-Pb measurements with the follow-up ID U-Pb data, the latter show smaller values and ranges of U-Pb concentrations and isotopic ratios than do the former. Sample heterogeneity and different sample aliquots in each method are plausible reasons for the discrepancy.

Provided that a mass bias corrected LA-ICP-MC-MS Pb isotope data is made (as was done in this study using Tl and Pb isotope standards), LA- data can provide an accurate determination of common Pb (initial $^{207}Pb/^{206}Pb$). In addition, LA-data produces coherent arrays of much larger variation in U-Pb than ID methods that depend on larger, homogenized aliquots. Isotope Dilution analysis on at least moderately radiogenic portions of such samples provides accuracy for anchoring the U-Pb measurements, and the determination of accurate inter-element fractionation factors. A combined approach using the strengths of each method together is capable of more precise and accurate data than either method alone, and with a higher efficiency of effort.

In this study, three samples of ammonite early cement all produced coherent, evidently undisturbed arrays on a Tera-Wasserburg plot using LA-data, and this is particularly useful because it justifies a general assertion of lack of disturbance when there is limited scatter in the arrays. A combined LA- and ID- approach results in accurate ages of these early diagenetic cement formation from ammonites with 2σ uncertainties as little as 1%, the highest achievable precision for this material so far. Such small uncertainties are potentially useable in time-scale calibration in the absence of high precision Ar-Ar or U-Pb ages of volcanic materials from ash beds.

This combined approach offer a real advantage over the use of either method alone. It appears to be a robust and efficient method to produce precise ages of these early diagenetic cements from ammonites. This method has been used because of the current absence of a well-calibrated calcite laser ablation age standard, and as such is not dependent upon the use of either glass or calcite mineral standards, however desirable. It also allows us to evaluate the variations in inter-element fractionation factors and their possible relationship to both laser conditions but also the material characteristics of the calcite. This approach could be even more efficient if a well-characterized calcite standard(s) was available for LA-normalization; if this were the case, a limited number of ID-analyses could be measured to verify and validate the more easily-obtained LA-data. This is the way forward in the future for this type of carbonate U-Pb dating.

9.5.3 Depositional ages verses diagenetic ages

1) The Numerical Ages of Three Mid-Toarcian Ammonites

The early calcite cements in three ammonites from Somerset, England, uniformly produce isotopic dates over 10 Ma younger than their biostratigraphic ages. To confirm whether the early cements postdate the fossils significantly, it is only needed to know how well the biostratigraphic and numerical ages of the fossils are constrained to absolute time. Samples IS1 and IS2 both belong to *Hildoceras* species, and thus must come from the interval of late *falciferum* Subzone of *Serpentinum* Zone to *Variabilis* Zone where *Hildoceras* species only occurred in British Toarcian strata. Although their biostratigraphic ages are defined, there is no radiometric date in Middle Toarcian available from European strata acting as a reference point for

precise numerical calibration. Instead, the absolute age of the interval is estimated using the near-linear Sr isotope trend from McArthur *et al.* (2000) and equal-subzone scale of upper Toarcian, and this age is estimated to be ~181.5 – 180.5 Ma (Gradstein *et al.*, 2004). Meanwhile, in the middle Toarcian, a U-Pb zircon age of 181.4 ± 1.2 (2σ) is available from an ash layer near the base of *Crassicosta* Zone of Yakoun River, Queen Charlotte Islands of British Columbia (Palfy *et al.*, 1997). That age was obtained from the type section of Middle Toarcian North American standard ammonite zone, and the base of *Crassicosta* Zone falls within an interval of very late *bifrons* to the base of *variabilis* Zone of the standard northwest European sequences, with an uncertainty of ± 1 standard subzone (Palfy *et al*., 1997). This radiometric age apparently came from the top of the above ~1 Ma sample interval and overlaps with it; hence it is used as a reference date for the ammonites in this study. Specimens IS1 and IS2 accordingly probably have depositional ages ranging from 180.2 – 183.6 Ma.

The third specimen SS2 has an approximate age of 170 Ma (not precisely biostratigraphically constrained), which probably falls in the *Stephan humphriesianum* Zone of Bajocian. There are, however, no primary radiometric dates in this stage to act as reference points; the numerical calibration is then based on the biostratigraphic correlation using an Ar-Ar bentonite age of 166.3 ± 0.8 (2σ) from the Carmel Formation, Utah, USA (Gradstein *et al.*, 2004). Recent U-Pb dating suggests that Ar-Ar ages are ~0.5 – 1.0% too low (Kuiper *et al.*, 2008), and an age of ~167-168 Ma is probably more appropriate. Although there are uncertainties associated with the age of this particular fossil and with the numerical calibration in Bajocian, the large age difference (4.6 - 11 Ma, 2σ) between the cement (159 Ma) and the fossil (~168 Ma) is unlikely to be explained by age calibration/correlation errors.

2) Diagenetic Formation of the Ammonite Cement

Curtis *et al*. (2000) invoked a rapid precipitation of early calcite cements in ammonite chambers shortly after the burial of the organism as the mechanism of cement formation. It is clear that the formation of this secondary calcite was quick and brief because the process is known to be driven and mediated by microbes during the decay of the organism; however, the cements are likely only start being precipitated when ammonite beasts are buried in anoxic sediments. Samples IS1 and

IS2 were from the mid-Toarcian Beacon Limestone Formation exposed at Hurcott Lane Cutting of Somerset, which is highly condensed with no more than 2m sequences representing 4 ammonite zones and about a few million years of time (Simms *et al.*, 2004), suggesting a slow sedimentation rate at that time. These ammonites may have lain for long periods on the sea-floor before being buried, which may explain how they could have avoided being crushed while preserving potential void space. The upper sections at Hurcott Lane cutting have all been weathered out, but the overlying Late Toarcian stratum was possibly Yeovil Sands, shown to surround this plateau area on the Geological Survey of Great Britain (England & Wales) Sheet 312 (published in 1958), and later assumed to be Bridport Sand Formation in Simms, (2004). The Yeovil Sands formation of Late Toarcian (38 to 64 m thick) might not be able to provide the favorable anoxic cement-formation environment, due to its porous nature. Above the Yeovil Sands/ Bridpot Sand Formation is the Inferior Oolite Formation of Aalenian – Bajocian stages which outcrops at nearby Chiselorough, North Coker, and expands southwards to reach Wessex Basin. The Inferior Oolite Formation varies from 2 to 39 m thick and is a highly condensed limestone of great stratigraphical complexity (Wilson *et al.*, 1958; Hesselbo and Jenkyns, 1995). Again, this high degree of condensation of the strata suggests slow burial of ammonites. Clays that could provide favorable cement formation conditions started depositing on top of the Oolite Formation only until Bathonian time; and reached a thickness of 50 to 100 meters by late Callovian. Perhaps, the early cements in the two Toarcian ammonites of Somerset were not formed until late Callovian when the porewater conditions in sediments finally reached anoxic conditions and so facilitated the formation of cement.

Interestingly, by late Callovian, there could be up to 100 – 200 meters of sediments being deposited above late Toarcian beds (without taking into account of penecontemporaneous erosion); the reasons why the early diagenesis happened 10 - 20 Ma later when the fossils had been buried by a couple of hundred meters of sediments may be explained as the slow burial of ammonites and the unfavorable cement formation conditions, coupled with the uncertainties in the calibrated ages of ammonites. Had the strata not been condensed and the anoxic conditions for calcite precipitation been reached in marine pore water early in diagenesis, the quick burial of fossil ammonites could have easily led to earlier generation of cements and thus

older diagenetic ages. The stratigraphical context is likely to have been an important factor to explain this multi-million-year duration. Whether the diagenetic ages can approximately represent the depositional ages of the fossils depends on the sedimentary rate, the nature of the original sediments, and stratigraphical development of the fossil origins.

Furthermore, a sequence of zones with differing characteristics has been identified from early calcite infills in these ammonites (Curtis *et al*., 2000). Cathodoluminescence and electron microprobe analyses of the early cements show a ferroan dull-luminescent Zone 1, a slightly later Zone 2 with low Fe and brighter luminescence, and the youngest Zone 2* that is similar to Zone 2, but with pyrite inclusions (See Fig. 1 in Curtis *et al*., 2000). Accordingly, following burial in sediments, the ammonites were surrounded in anoxic conditions, the early cements started precipitating progressively from calcite-saturated marine pore water, then were modified by the activities of respirative bacteria, Mn and Fe-reducing bacteria and, finally, microbial sulphate reduction (Curtis *et al*., 2000). So these zones must represent different formation times. Further work may be needed to sample those zones separately and date them sequentially to determine these potential age variations. The cement from the innermost zone should give an older age than the average age of the substance from mixed zones. Sampling those materials in zones at sub-mm thickness for U-Pb dating, however, would be a great challenge for further work unless done by laser ablation methods alone with an appropriately characterized calcite standard.

The U-Pb dating results herein demonstrate the feasibility of precisely dating marine calcite cements. Our data clearly defines a cement age ~10 Ma after fossil deposition upon the death of the organisms, in contrast to some other studies showing a closer concordance (Rasbury and Cole, 2009). The extent to which generalization of this cement-formation chronology can be deduced will depend upon further detailed studies.

9.6 Conclusion

(1) According to the U-Pb data in this study, most pristine biogenic calcite contains <10 ppb of U, making it unfeasible for U-Pb dating without

substantial method improvements to sensitivity. Well-preserved biogenic aragonite has a potential to be dated by the U/Pb method if the overprint of contaminant common Pb in the thin biofilms between aragonite laminas could be removed or minimized.

(2) The early-diagenetic calcite cements preserved in fossils with enclosed chambers, such as uncrushed ammonites, can remain a closed system for U and Pb and produce precise U-Pb ages with uncertainties potentially of 1-2% (2σ).

(3) Combined LA-ICP-MC-MS and ID U-Pb data of carbonate can result in more accurate and precise U-Pb ages than either method on its own, and together they appear to form a useful strategy for improving the accuracy and precision of the U-Pb dating of carbonate.

(4) Tera-Wasserburg regression of mainly Jurassic ammonite early diagenetic cements yield ages of 159.7 ± 2.3 (MSWD = 0.76), 158.7 ± 3.1 (MSWD = 2.1), 159.7 ± 2.7 (MSWD = 10.6) for sample IS1, IS2 and SS2, all of which postdate the biostratigraphically correlated numerical ages of the deposition by at least 10 Ma, and suggest that ammonite chamber cement formation can postdate the fossil deposit significantly.

Appendix

Appendix A The temperature (Temp) and salinity (S) profiles of 12 sites from North Sea in variable years. Sites information provided in Appendix B.

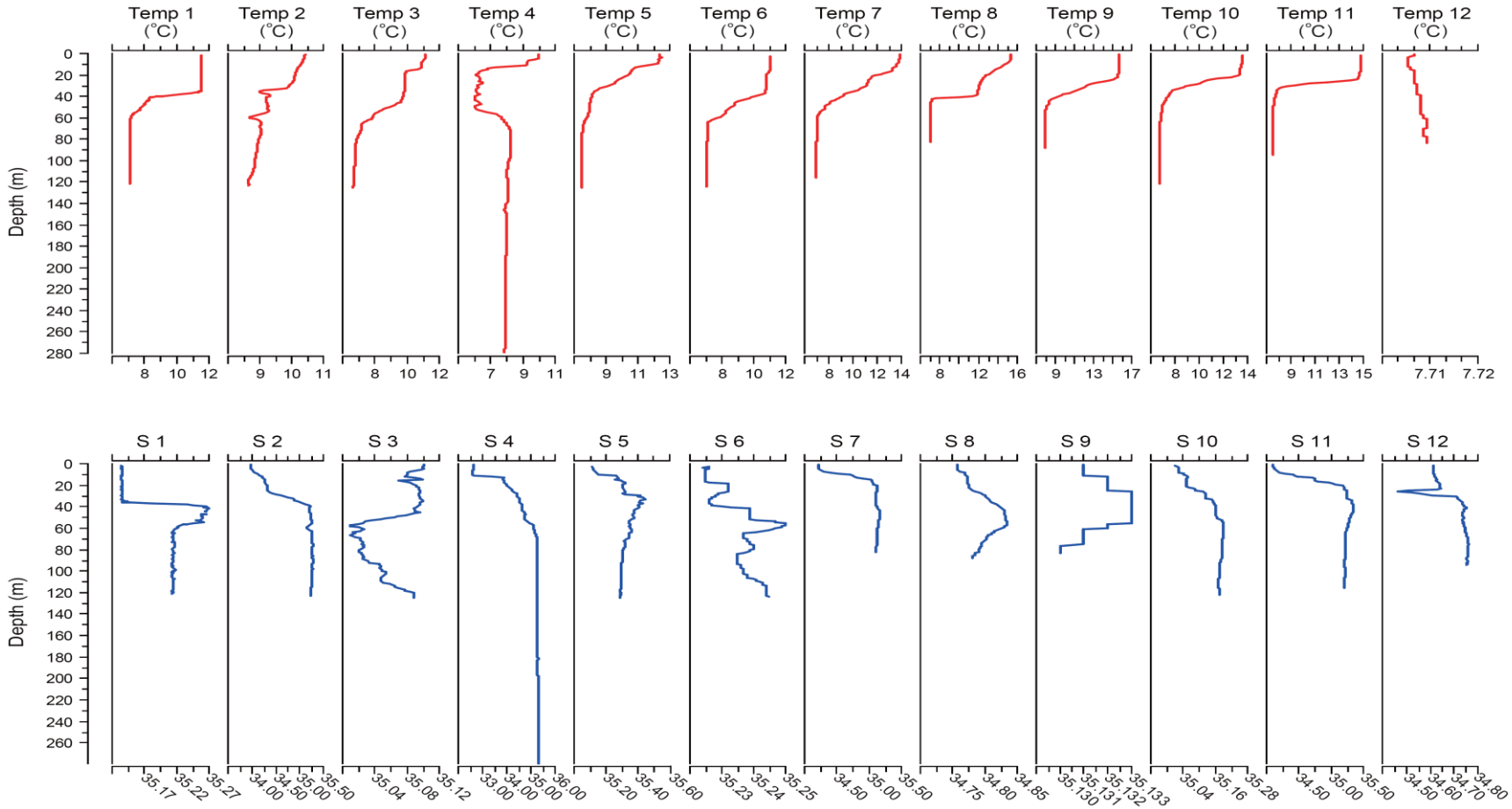

Appendix B Temperature and salinity profiles in 12 sites in the North Sea.

Sites	Series Reference	Latitude (Deg Min)	Longitude (Deg Min)	Start Date (yyyy-mm-dd)	Sea Floor Depth (m)	Min. Sensor Depth (m)	Max. Sensor Depth (m)
1	176553	059°45.0'N	000° 0.0'E	1988-09-30	130	1.58	121.51
2	466666	059°44.5'N	003°30.5'E	1996-06-24	270	1.00	155.00
3	467018	059°45.1'N	000°29.9'E	1996-06-29	137	1.00	125.00
4	481780	059°60.0'N	003°35.0'E	1997-06-06	287	0.99	279.15
5	482377	059°55.0'N	000°12.2'E	1997-07-14	127	0.99	124.77
6	560057	059°53.6'N	000° 3.6'E	2000-07-14	129	2.97	123.79
7	560659	057°40.9'N	002° 6.0'E	2000-08-17	87	1.98	82.22
8	561116	055°55.3'N	000°18.8'W	2000-08-27	93	0.99	88.17
9	571473	057°42.8'N	002° 5.8'E	2001-01-24	87	0.99	83.21
10	573443	059°42.1'N	000°20.4'E	2001-08-02	126	1.98	121.81
11	560499	059°41.7'N	000°20.0'E	2000-08-14	124	0.99	115.87
12	573989	055°54.8'N	000°19.1'W	2001-08-14	96	1.98	94.11

Appendix C Mean isotopic and elemental data of Pliensbachian belemnites from Dorset, UK. The bed numbers are taken from Lang *et al.* (1928) and Hesselbo and Jenkyns (1995). VPI stands for vidual perservation index, which ranks from 1 (essentially unaltered) to 5 (completely altered).

Sample	Zone	Subzone	Bed No.	VPI	$\delta^{18}O$ ‰	$\delta^{13}C$ ‰	Ca %	Mg ppm	Na ppm	Sr ppm	Fe ppm	Mn ppm	Ba ppm	S ppm	Mg/Ca mM/M	Na/Ca mM/M	Sr/Ca mM/M
Passaloteuthis cupidatus																	
D08 120/2	*Prodactylioceras ibex*	*valdani*	120	1	-0.60	3.36	39.5	1995	2402	1428	14	7	1	384	8.33	10.6	1.65
D08 120/3	*Prodactylioceras ibex*	*valdani*	120	2	-1.30	1.70	39.5	2130	2233	1305	239	47	2	479	8.90	9.86	1.51
D08 120/4	*Prodactylioceras ibex*	*valdani*	120	2	-0.98	1.11	39.5	2239	2172	1306	18	12	2	578	9.35	9.59	1.51
D08 120/5	*Prodactylioceras ibex*	*valdani*	120	2	-0.62	0.47	39.5	1985	2238	1224	59	51	2	246	8.28	9.87	1.42
D08 120/7	*Prodactylioceras ibex*	*valdani*	120	1	-0.48	1.32	39.5	2256	2313	1339	6	6	2	352	9.42	10.2	1.55
D08 7/1 S3	*Prodactylioceras davoei*	*maculatum*	7	1	-1.18	2.25	39.5	2200	2147	1232	3	11	3	363	9.18	9.47	1.43
D08 7/14 S3	*Prodactylioceras davoei*	*maculatum*	7	2	-1.64	0.99	39.5	2386	2182	1204	4	14	3	695	9.96	9.63	1.39
D08 7/22 S3	*Prodactylioceras davoei*	*maculatum*	7	2	-0.78	0.85	39.6	2138	2020	1157	6	13	3	393	8.91	8.91	1.34

Sample	Zone	Subzone	Bed No.	VPI	$\delta^{18}O$ ‰	$\delta^{13}C$ ‰	Ca %	Mg ppm	Na ppm	Sr ppm	Fe ppm	Mn ppm	Ba ppm	S ppm	Mg/Ca mM/M	Na/Ca mM/M	Sr/Ca mM/M
D08 7/3 S3	*Prodactylioceras davoei*	*maculatum*	7	2	-1.19	0.98	39.5	2428	2334	1241	2	11	3	752	10.1	10.3	1.44
D08 7/3 S3 diff. prep.	*Prodactylioceras davoei*	*maculatum*	7	2	-1.19	0.98	39.5	2592	2333	1242	2	11	3	672	10.8	10.3	1.44
D08 7/7 S3	*Prodactylioceras davoei*	*maculatum*	7	1	-0.86	1.21	39.5	2310	1998	1250	5	6	3	338	9.64	8.81	1.45
Nannobelus acotus																	
D08 118/10	*Prodactylioceras ibex*	*valdani*	118	1	-0.84	0.31	39.6	2017	1978	1327	4	2	2	215	8.41	8.72	1.53
D08 118/12	*Prodactylioceras ibex*	*valdani*	118	3	-1.10	-0.65	39.5	2465	2169	1410	14	4	2	263	10.3	9.58	1.63
D08 118/5	*Prodactylioceras ibex*	*valdani*	118	2	-0.93	-0.05	39.4	2723	2223	1427	10	4	2	308	11.4	9.83	1.65
D08 118/6	*Prodactylioceras ibex*	*valdani*	118	1	-0.88	-0.73	39.5	2584	1736	1099	9	2	2	568	10.8	7.65	1.27
D08 7/1 S2	*Prodactylioceras davoei*	*maculatum*	7	3	-1.14	1.41	39.5	2013	2230	1231	60	44	2	350	8.40	9.84	1.42
D08 7/2 S1	*Prodactylioceras davoei*	*maculatum*	7	2	-0.89	1.67	39.5	2030	2120	1221	17	16	2	483	8.47	9.35	1.41

Sample	Zone	Subzone	Bed No.	VPI	$\delta^{18}O$ ‰	$\delta^{13}C$ ‰	Ca %	Mg ppm	Na ppm	Sr ppm	Fe ppm	Mn ppm	Ba ppm	S ppm	Mg/Ca mM/M	Na/Ca mM/M	Sr/Ca mM/M
D08 7/3 S1	*Prodactylioceras davoei*	*maculatum*	7	2	-0.76	0.31	39.5	2110	2159	1290	7	17	2	253	8.80	9.52	1.49
D08 7/4 S3	*Prodactylioceras davoei*	*maculatum*	7	2	-0.84	0.52	39.5	2399	1918	1139	4	10	2	393	10.0	8.46	1.32
D08 7/42 S3	*Prodactylioceras davoei*	*maculatum*	7	2	-1.61	0.39	39.5	2360	2070	1230	6	12	2	577	9.85	9.13	1.42
D08 7/6 S1	*Prodactylioceras davoei*	*maculatum*	7	2	-0.85	0.87	39.5	2015	2163	1274	6	4	2	450	8.41	9.54	1.47
D08 7/6 S3	*Prodactylioceras davoei*	*maculatum*	7	3	-1.74	1.46	39.5	2504	2123	1302	18	13	3	374	10.5	9.37	1.51
D08 7/7 S2	*Prodactylioceras davoei*	*maculatum*	7	1	-0.97	0.09	39.6	2009	2002	1198	11	15	2	703	8.38	8.82	1.39
D08 7/8 S1	*Prodactylioceras davoei*	*maculatum*	7	1	-1.51	1.07	39.5	1860	2167	1309	10	10	2	338	7.76	9.55	1.51
Bairstowius junceus																	
D08 7/23 S3	*Prodactylioceras davoei*	*maculatum*	7	2	-1.43	0.48	39.6	2246	1506	954	5	13	2	318	9.35	6.63	1.10
D08 7/26 S3	*Prodactylioceras davoei*	*maculatum*	7	1	-0.85	-0.05	39.6	2092	2102	997	6	6	2	332	8.72	9.27	1.15

Sample	Zone	Subzone	Bed No.	VPI	$\delta^{18}O$ ‰	$\delta^{13}C$ ‰	Ca %	Mg ppm	Na ppm	Sr ppm	Fe ppm	Mn ppm	Ba ppm	S ppm	Mg/Ca mM/M	Na/Ca mM/M	Sr/Ca mM/M
D08 7/38 S3	*Prodactylioceras davoei*	*maculatum*	7	2	-2.00	0.77	39.5	2625	1832	1211	16	9	3	404	11.0	8.08	1.40
D08 7/39 S3	*Prodactylioceras davoei*	*maculatum*	7	1	-0.92	0.80	39.5	2191	2532	1164	3	6	3	388	9.15	11.2	1.35
D08 7/39 S3 diff. prep	*Prodactylioceras davoei*	*maculatum*	7	1	-0.92	0.80	39.5	2241	2569	1243	4	6	3	414	9.36	11.4	1.44
D08 7/43 S3	*Prodactylioceras davoei*	*maculatum*	7	1	-1.08	-0.10	39.4	2904	2240	1194	5	9	4	398	12.1	9.90	1.39
D08 7/46S3	*Prodactylioceras davoei*	*maculatum*	7	2	-1.03	1.74	39.4	3096	2187	1195	7	10	2	398	13.0	9.67	1.39
D08 7/49 S3	*Prodactylioceras davoei*	*maculatum*	7	1	-1.53	0.64	39.6	2292	1450	942	3	6	2	314	9.54	6.38	1.09
D08 7/5 S1	*Prodactylioceras davoei*	*maculatum*	7	3	-1.09	1.21	39.6	1976	1640	1140	24	8	2	380	8.23	7.22	1.32
D08 7/51 S3	*Prodactylioceras davoei*	*maculatum*	7	2	-1.22	0.43	39.4	2988	2091	1300	5	10	2	433	12.5	9.24	1.51
D08 7/9 S1	*Prodactylioceras davoei*	*maculatum*	7	3	-1.11	0.84	39.6	1963	1691	1142	33	16	2	381	8.18	7.45	1.32

Passaloteuthis elongata

Sample	Zone	Subzone	Bed No.	VPI	$\delta^{18}O$ ‰	$\delta^{13}C$ ‰	Ca %	Mg ppm	Na ppm	Sr ppm	Fe ppm	Mn ppm	Ba ppm	S ppm	Mg/Ca mM/M	Na/Ca mM/M	Sr/Ca mM/M
D08 7/25 S3	*Prodactylioceras davoei*	*maculatum*	7		-0.57	1.74	39.5	2116	2692	1447	15	9	3	541	8.85	11.9	1.68
D08 7/27 S3	*Prodactylioceras davoei*	*maculatum*	7	3	-0.94	0.71	39.3	3624	2377	1438	15	30	4	968	15.2	10.5	1.67
D08 7/29 S3	*Prodactylioceras davoei*	*maculatum*	7	2	-1.54	0.47	39.5	2402	1935	1091	5	7	3	378	10.0	8.53	1.26
D08 7/29 S3 diff. prep.	*Prodactylioceras davoei*	*maculatum*	7	2	-1.54	0.47	39.6	2372	1713	1105	4	7	3	240	9.89	7.55	1.28
D08 7/3 S2	*Prodactylioceras davoei*	*maculatum*	7	1	-0.95	0.22	39.7	1538	1473	1049	3	1	1	141	6.39	6.47	1.21
D08 7/5 S2	*Prodactylioceras davoei*	*maculatum*	7	1	-0.97	0.56	39.6	1846	1762	1276	16	5	2	248	7.69	7.76	1.47
D08 7/6 S2	*Prodactylioceras davoei*	*maculatum*	7	1	-1.09	0.02											
Hastites spadixari																	
D08 7/58 S3	*Prodactylioceras davoei*	*maculatum*	7	3	-1.01	1.86	39.6	2208	1934	1038	19	13	2	493	9.20	8.52	1.20
D08 7/68 S3	*Prodactylioceras davoei*	*maculatum*	7	3	-1.26	1.24	39.6	2102	1886	1092	23	13	3	551	8.76	8.31	1.26

Sample	Zone	Subzone	Bed No.	VPI	$\delta^{18}O$ ‰	$\delta^{13}C$ ‰	Ca %	Mg ppm	Na ppm	Sr ppm	Fe ppm	Mn ppm	Ba ppm	S ppm	Mg/Ca mM/M	Na/Ca mM/M	Sr/Ca mM/M
D08 7/78 S3	*Prodactylioceras davoei*	*maculatum*	7	2	-0.63	1.75	39.5	2398	2536	1195	13	12	2	1432	10.0	11.2	1.38
D08 7/82 S3	*Prodactylioceras davoei*	*maculatum*	7	3	-1.15	0.75	39.5	3152	1879	1166	15	15	2	611	13.2	8.30	1.35
D08 7/84 S3	*Prodactylioceras davoei*	*maculatum*	7	2	-1.30	0.63	39.6	2249	1684	1049	5	5	3	620	9.37	7.42	1.21

Appendix D Isotopic and chemical data for belemnites from the *falciferum* to *commune* Subzone in Toarcian, Yorkshire coast, UK.

Sample No.	Ammonite biozone	Species	Strat. Level (m)	VPI	$\delta^{13}C$	$\delta^{18}O$	Ca	Na	Mg	Sr	Ba	Fe	Mn	SO_4
					‰VPDB	‰ VPDB	ppm	ppm	ppm	ppm	ppm	ppm	ppm	ppm
Y06 51/110	*commune*	*A. subtenuis (L)*	51.2	4	2.66	-2.20	38.6	1996	3637	1491	1	< 1	< 1	2061
Y06 51/78	*commune*	*A.subtenuis (L)*	50.9	2	1.39	-1.64	35.8	1710	3013	1373	< 1	< 1	< 1	1126
Y06A 51/75	*commune*	*S. dorsalis*	50.9	1	2.73	-0.80	38.1	2066	2744	1540	< 1	< 1	< 1	934
Y06B 51/75	*commune*	*S. dorsalis*	50.9	2	4.67	-2.50	37.7	1921	2344	1531	< 1	< 1	< 1	684
Y06 51/60	*commune*	*A. vulgaris*	50.7	3	3.95	-3.05	38.5	2057	2509	1602	< 1	< 1	< 1	1267
Y06 51 base	*commune*	*A. subtenuis (L)*	50.0	2	2.99	-3.04	35.0	1782	2927	1370	< 1	< 1	< 1	1853
Y06* 51 base	*commune*	*A. subtenuis (L)*	50.0	2	2.85	-2.67	35.7	1764	3268	1356	< 1	< 1	< 1	2917
Y06A 49/620	*commune*	*A. subtenuis (s)*	50.0	2	2.89	-2.51	35.9	1677	2796	1394	< 1	< 1	< 1	2070
Y06B 49/620	*commune*	*A. subtricissus*	50.0	3	2.80	-3.26	35.2	1583	2911	1447	< 1	< 1	< 1	936
Y06C 49/620	*commune*	*A. subtenuis (L)*	50.0	3	3.22	-2.56	34.4	1888	3411	1315	< 1	< 1	1	4010
Y06 49/592	*commune*	*A. subtenuis (s)*	49.7	2	3.29	-2.65	37.6	2018	3423	1685	< 1	< 1	< 1	3390
Y06 49/519	*commune*	*A. subtenuis (L)*	49.0	2	2.92	-2.60	36.7	1563	3127	1390	< 1	< 1	< 1	1969
Y06 49/475	*commune*	*A. subtenuis (L)*	48.5	3	3.38	-2.72	37.8	1837	3643	1642	< 1	< 1	< 1	1837
Y06 49/420	*commune*	*A. subtenuis (L)*	48.0	2	2.47	-2.02	34.9	1518	2958	1349	< 1	< 1	< 1	1822

Sample No.	Ammonite biozone	Species	Strat. Level (m)	VPI	$\delta^{13}C$ ‰VPDB	$\delta^{18}O$ ‰ VPDB	Ca ppm	Na ppm	Mg ppm	Sr ppm	Ba ppm	Fe ppm	Mn ppm	SO_4 ppm
Y06 49/63	*commune*	*A. subtenuis (L)*	44.4	1	3.02	-2.31	39.7	2214	3186	1511	< 1	< 1	< 1	2932
Y06 49/30	*commune*	*A. vulgaris*	44.1	3	3.62	-3.29	37.0	2103	2833	1671	< 1	< 1	< 1	1214
Y06 49/25	*commune*	*A. subtenuis (L)*	44.0	3	2.20	-2.08	37.6	1803	3540	1407	< 1	< 1	< 1	1429
Y06 49/22	*commune*	*A. subtenuis (L)*	44.0	3	2.88	-2.30	34.6	1857	3075	1356	< 1	< 1	< 1	3553
Y06 47/529	*falciferum*	*A. subtenuis (L)*	43.2	2	3.18	-1.38	34.3	1824	2860	1215	< 1	< 1	< 1	2126
Y06 47/526	*falciferum*	*S. dorsalis*	43.2	2	4.60	-2.23	35.9	1763	2283	1350	< 1	< 1	< 1	821
Y06A 47/520	*falciferum*	*S. dorsalis*	43.1	2	4.64	-2.30	35.1	1920	2391	1387	< 1	< 1	< 1	782
Y06B 47/520	*falciferum*	*A. subtenuis (L)*	43.1	3	2.16	-1.31	38.1	2195	3663	1443	< 1	< 1	< 1	3365
Y06 47/492	*falciferum*	*A. vulgaris*	42.86	2	4.22	-3.10	33.8	1670	2302	1412	< 1	< 1	< 1	824
Y06 47/485	*falciferum*	*A. vulgaris*	42.79	2	4.29	-3.30	36.7	1958	2549	1535	< 1	< 1	< 1	278
Y06 47/416	*falciferum*	*S. dorsalis*	42.10	2	4.92	-2.29	37.8	2106	2706	1604	< 1	< 1	< 1	2283
Y06 47/379	*falciferum*	*A. subtenuis (L)*	41.73	3	4.19	-1.96	36.8	1862	2606	1485	< 1	< 1	< 1	1940
Y06 47/307	*falciferum*	*A. subtenuis (L)*	41.01	3	1.44	-1.09	36.3	1759	3093	1284	< 1	< 1	< 1	1483
Y06 45/0	*falciferum*	*S. dorsalis*	34.46	3	4.63	-2.53	39.2	2063	3069	1321	< 1	< 1	9	2294
Y06 43/718	*falciferum*	*A. subtenuis (L)*	33.82	2	1.75	-1.15	40.3	1689	3838	1367	< 1	< 1	< 1	618

Sample No.	Ammonite biozone	Species	Strat. Level (m)	VPI	$\delta^{13}C$ ‰VPDB	$\delta^{18}O$ ‰ VPDB	Ca ppm	Na ppm	Mg ppm	Sr ppm	Ba ppm	Fe ppm	Mn ppm	SO_4 ppm
Y06 43/698	*falciferum*	*S. dorsalis*	33.62	3	4.08	-2.17	40.2	1995	3359	1518	< 1	< 1	< 1	1795
Y06A 43/691	*falciferum*	*S. dorsalis*	33.55	2	4.54	-2.29	35.2	1715	2486	1409	< 1	< 1	< 1	665
Y06B 43/691	*falciferum*	*S. dorsalis*	33.55	2	4.51	-2.20	34.7	2007	2273	1356	< 1	< 1	< 1	625
Y06 43/671	*falciferum*	*S. dorsalis*	33.35	2	4.56	-2.03	35.5	1534	2242	1206	< 1	< 1	< 1	567
Y06 43/641	*falciferum*	*Y. simpsoni*	33.05	4	3.83	-3.21	37.6	1977	3033	1730	< 1	< 1	< 1	688
Y06B 43/580	*falciferum*	*A. subtenuis (L)*	32.44	3	2.06	-1.27	38.8	1793	3060	1409	< 1	< 1	< 1	1710
Y06B 43/516	*falciferum*	*Y. simpsoni*	31.80	4	2.64	-2.38	32.9	962	3376	1150	< 1	< 1	< 1	224
Y06C 43/516	*falciferum*	*A. subtenuis (s)*	31.80	4	2.79	-1.78	40.6	1412	3545	1419	100	< 1	< 1	1519
Y06 43/515	*falciferum*	*A. subtenuis (s)*	31.79	1	3.03	-2.00	33.5	1559	2401	1223	< 1	< 1	< 1	1090
Y06A 43/510	*falciferum*	*Y. tubularis*	31.74	4	3.17	-2.53	39.4	1577	3643	1348	< 1	< 1	< 1	1502
Y06B 43/510	*falciferum*	*Y. simpsoni*	31.74	3	3.42	-2.94	40.0	1302	3168	1637	< 1	4	< 1	506
Y06 43/392	*falciferum*	*Y. simpsoni*	30.56	3	3.13	-2.50	36.2	1378	2756	1364	< 1	< 1	< 1	418
Y06 43/387	*falciferum*	*Y. simpsoni*	30.51	4	3.35	-2.04	40.4	1268	3363	1569	< 1	13	< 1	472
Y06 43/362	*falciferum*	*Y. simpsoni*	30.26	3	2.43	-1.05	36.5	1588	2639	1284	< 1	< 1	< 1	801
Y06 43/326	*falciferum*	*Y. simpsoni*	29.90	3	1.69	-2.13	34.7	1188	2703	1253	1	< 1	3	400

Sample No.	Ammonite biozone	Species	Strat. Level (m)	VPI	$\delta^{13}C$ ‰VPDB	$\delta^{18}O$ ‰ VPDB	Ca ppm	Na ppm	Mg ppm	Sr ppm	Ba ppm	Fe ppm	Mn ppm	SO_4 ppm
Y06A 43/310	*falciferum*	*Y. simpsoni*	29.74	3	2.91	-2.02	30.9	1157	2017	1083	4	< 1	< 1	467
Y06B 43/310	*falciferum*	*Y. tubularis*	29.74	3	3.29	-2.41	41.6	1470	3270	1547	< 1	9	< 1	1098
Y06D 43/310	*falciferum*	*Y. simpsoni*	29.74	3	3.07	-2.40	35.1	1493	2794	1317	< 1	< 1	< 1	411
Y06A 43/307	*falciferum*	*A. subtenuis (s)*	29.71	3	2.15	-0.89	37.4	1684	2513	1445	< 1	< 1	< 1	294
Y06 43/200	*falciferum*	*A. subtenuis (L)*	28.64	4	2.15	-1.36	31.9	1403	2762	1207	< 1	< 1	< 1	634
Y06 43/7	*falciferum*	*A. subtenuis (s)*	26.71	3	1.31	-1.29	39.1	1855	3902	1307	< 1	< 1	18	2017

Note: The Pliensbachain/Toarcian boundary is set at the 0m level in this study. The 3rd column (level) is the vertical distance (in meter) above the base of the each Bed. Bed numbers are from Howarth (1962). VPI – visual preservation index. 1 stands for the best preserved belemnite calcite, the degree of alteration rises with the increase of number, and 5 indicates the completely altered. L – large, S – small, Y06 stands for site - Yorkshire and sampling date – 2006. Samples collected at the same levels are distinguished by labeling a capital letter behind Y06. Bed number of each sample / the level (cm) above the base of that bed is shown behind the code Y06.

Appendix E Isotopic and chemical data of *C. pusoziana* belemnites of Callovian time from Bed 13 of the *Jason* Zone of Oxford Clay Formation at Kings Dyke (Hansen Quarry), Peterborough.

Sample No.	Zone	Sz.	Bed No.	Species	VPI	$\delta^{13}C$ ‰ VPDB	$\delta^{18}O$ ‰ VPDB	Ba ppm	Fe ppm	Mg ppm	Mn ppm	Na ppm	S ppm	Sr ppm	Mg/Ca mM/M	Na/Ca mM/M	Sr/Ca mM/M
13-106	*Jason*	*Jason*	13	*C. pusoziana*	1	-0.60	1.83	1.25	2	938	2	919	627	758	3.89	4.02	0.87
13-107	*Jason*	*Jason*	13	*C. pusoziana*	1	-0.40	1.35	1.27	1	1171	1	1042	470	883	4.86	4.57	1.02
13-109	*Jason*	*Jason*	13	*C. pusoziana*	2	-0.88	1.97										
13-111	*Jason*	*Jason*	13	*C. pusoziana*	2	-0.61	2.42	1.20	6	1107	1	1168	590	845	4.59	5.12	0.97
13-112	*Jason*	*Jason*	13	*C. pusoziana*	3	-0.62	1.59	1.96	56	1042	9	989	356	940	4.32	4.34	1.08
13-113	*Jason*	*Jason*	13	*C. pusoziana*	2	-0.27	2.71										
13-165	*Jason*	*Jason*	13	*C. pusoziana*	2	-0.51	1.61	1.34	5	931	2	958	376	805	3.86	4.20	0.92
13-182	*Jason*	*Jason*	13	*C. pusoziana*	2	-1.31	2.03	1.31	6	1062	1	1381	446	934	4.41	6.06	1.07
13-183	*Jason*	*Jason*	13	*C. pusoziana*	1	-0.19	2.37	1.39	1	1006	1	979	557	717	4.17	4.29	0.82
13-184	*Jason*	*Jason*	13	*C. pusoziana*	1	-0.79	2.35	1.45	2	966	2	1132	271	1005	4.00	4.96	1.16
13-185	*Jason*	*Jason*	13	*C. pusoziana*	1	-0.45	2.47	1.35	2	1257	1	1137	695	890	5.22	4.98	1.02
13-44	*Jason*	*Jason*	13	*C. pusoziana*	2	-0.81	1.47	2.02	6	1172	2	1102	603	859	4.86	4.83	0.99
13-45	*Jason*	*Jason*	13	*C. pusoziana*	2	-0.79	2.27										
13-46	*Jason*	*Jason*	13	*C. pusoziana*	2	-0.63	2.28	1.80	8	995	2	1108	771	885	4.12	4.85	1.02

Sample No.	Zone	Sz.	Bed No.	Species	VPI	$\delta^{13}C$ ‰ VPDB	$\delta^{18}O$ ‰ VPDB	Ba ppm	Fe ppm	Mg ppm	Mn ppm	Na ppm	S ppm	Sr ppm	Mg/Ca mM/M	Na/Ca mM/M	Sr/Ca mM/M
13-47	*Jason*	*Jason*	13	*C. pusoziana*	2	-1.00	2.10	1.54	8	1077	2	1030	647	891	4.46	4.51	1.02
13-48	*Jason*	*Jason*	13	*C. pusoziana*	1	-0.30	2.47	1.51	2	732	1	1226	431	967	3.03	5.37	1.11
13-49	*Jason*	*Jason*	13	*C. pusoziana*	3	-0.69	2.43	1.77	89	990	2	1305	646	1131	4.11	5.73	1.30
1S 12	*Jason*	*Jason*	13	*C. pusoziana*	2	-0.62	2.23	1.57	10	918	3	947	369	871	3.80	4.15	1.00
1S 40	*Jason*	*Jason*	13	*C. pusoziana*	3	-0.56	1.08	1.89	75	1386	12	1141	746	839	5.75	5.00	0.97
1S 57	*Jason*	*Jason*	13	*C. pusoziana*	2	-0.29	1.84	1.53	6	1028	3	1070	636	1011	4.26	4.69	1.16
1S 59	*Jason*	*Jason*	13	*C. pusoziana*	1	-0.17	2.69	1.56	2	924	1	936	497	797	3.83	4.10	0.92
1S 61	*Jason*	*Jason*	13	*C. pusoziana*	2	-0.70	2.37	1.90	4	1636	3	1319	751	904	6.80	5.79	1.04
2S 116	*Jason*	*Jason*	13	*C. pusoziana*	1	-0.51	2.63	1.44	3	1245	1	1232	395	999	5.17	5.40	1.15
2S 13	*Jason*	*Jason*	13	*C. pusoziana*	2	-0.85	1.48	1.39	4	1379	5	1157	810	850	5.72	5.07	0.98
2S 21	*Jason*	*Jason*	13	*C. pusoziana*	2	-0.56	1.90	2.25	8	1307	2	1374	812	1113	5.43	6.03	1.28
2S 3	*Jason*	*Jason*	13	*C. pusoziana*	2	-0.64	0.89	1.45	3	1251	4	1010	556	781	5.19	4.43	0.90
2S 30	*Jason*	*Jason*	13	*C. pusoziana*	1	-0.63	2.49	1.50	3	944	2	1058	359	954	3.91	4.64	1.10
2S 70	*Jason*	*Jason*	13	*C. pusoziana*	2	-0.85	2.04	1.45	20	853	1	865	583	743	3.53	3.79	0.85
2S 72	*Jason*	*Jason*	13	*C. pusoziana*	1	-0.51	1.23	1.18	3	911	1	1133	368	945	3.78	4.97	1.09

Appendix F Istotopic and elemental compositions of belemnites of Valanginian age from Vergal, SE France.

Sample No.	Zone	Subzone	VPI	Bed No.	Strat. level	Species	$\delta^{18}O$ ‰ PDB	$\delta^{13}C$ ‰ PDB	Na ppm	Ca %	Mg ppm	Sr ppm	Fe ppm	Mn ppm	S ppm	Ba ppm
VGL 124b-1	*N. peregrinus*	*N. peregrinus*	2	124b-125a	138.1	*Duvalia gr. binervia - aff. gervaisiana*	0.11	0.46	1549	39.7	2016	1393	4	3	332	1
VGL 123-2	*S. verrucosum*	*k. pronecostatum*	1	123-124a	135.4	*Duvalia binervia*	0.00	1.15	1782	39.0	2103	1482	21	3	361	2
VGL 123-1	*S. verrucosum*	*k. pronecostatum*	2	123-124a	134.9	*Duvalia gr. binervia (aff. gervaisiana)*	0.16	0.20	1567	40.1	1970	1308	16	3	462	3
VGL 121-1	*S. verrucosum*	*k. pronecostatum*	2	121-122	132.0	*Duvalia gr. binervia (aff. gervaisiana)*	0.42	0.79	1706	38.5	1949	1333	8	3	486	2
VGL 118-4	*S. verrucosum*	*k. pronecostatum*	1	118-119	127.9	*Duvalia binervia*	0.52	0.97	1301	39.2	2058	1304	7	3	280	2
VGL 114c-1	*S. verrucosum*	*k. pronecostatum*	2	114c-115a	122.5	*Duvalia binervia*	0.16	0.91	1378	38.6	2122	1301	11	3	525	2
VGL 113b-1	*S. verrucosum*	*k. pronecostatum*	2	113b-114a	121.3	*Duvalia binervia*	0.21	0.63	1395	39.1	1824	1114	17	3	726	5
VGL 110-2	*S. verrucosum*	*S. verrucosum*	3	110-111a	115.8	*Pseudobelus cf. "sultanovkaensis*	-0.30	1.38	1843	38.9	2245	1378	69	4	5219	58
VGL 110-1	*S. verrucosum*	*S. verrucosum*	3	110-111a	115.8	*Hibolithes sp. (cf. jaculoides) imm.*	-0.15	1.12	1836	38.1	2812	1300	32	4	1175	5
VGL 110-3	*S. verrucosum*	*S. verrucosum*	2	110-111a	115.8	*Hibolithes sp. (cf. jaculoides) imm.*	-0.11	1.00	1692	38.2	2196	1193	16	4	1047	2
VGL 109a-1	*S. verrucosum*	*S. verrucosum*	3	109a	113.8	*Hibolithes sp. (cf. jaculoides) imm.*	-0.32	0.30	1817	39.3	3263	1431	25	4	1025	1
VGL 107-6	*S. verrucosum*	*S. verrucosum*	3	107-108	110.8	*Hibolithes sp. (+ acro.)*	-0.27	0.66	1976	38.6	3017	1312	85	6	1189	3

Sample No.	Zone	Subzone	VPI	Bed No.	Strat. level	Species	$\delta^{18}O$ ‰ PDB	$\delta^{13}C$ ‰ PDB	Na ppm	Ca %	Mg ppm	Sr ppm	Fe ppm	Mn ppm	S ppm	Ba ppm
VGL 107-2	*S. verrucosum*	*S. verrucosum*	3	107-108	110.8	*Hibolithes sp. (cf. jaculoides)*	0.16	1.15	1779	39.4	2685	1440	12	3	944	2
VGL 107-5	*S. verrucosum*	*S. verrucosum*	3	107-108	110.8	*Hibolithes sp. (cf. jaculoides)*	0.30	2.55	1846	39.4	2577	1448	18	4	1041	3
VGL 107-1	*S. verrucosum*	*S. verrucosum*	2	107-108	110.8	*Hibolithes sp. (cf. jaculoides)*	-0.16	1.91	1584	38.9	2448	1180	24	4	837	3
VGL 107-3	*S. verrucosum*	*S. verrucosum*	3	107-108	110.8	*Hibolithes sp. (cf. jaculoides)*	-0.01	1.42	1903	38.4	3375	1236	64	7	1051	6
VGL 107-7	*S. verrucosum*	*S. verrucosum*	2	107-108	110.8	*Duvalia binervia*	-0.13	0.73	1343	40	2075	1202	11	3	416	2
VGL 107-8	*S. verrucosum*	*S. verrucosum*	3	107-108	110.8	*Duvalia cf. emericii*	0.10	0.85	1935	39.9	3146	1374	77	15	1118	3
VGL 107-17	*S. verrucosum*	*S. verrucosum*	3	107-108	110.8	*Castellanibelus orbignyanus*	-0.69	-2.20	1654	38.4	2549	1240	6	3	906	3
VGL 106-6	*S. verrucosum*	*S. verrucosum*	2	106-107	107.9	*Duvalia cf. emericii*	0.01	1.68	1858	38.6	2321	1330	10	3	553	5
VGL 106-5	*S. verrucosum*	*S. verrucosum*	3	106	107.3	*Duvalia cf. emericii (imm.) juvenile*	-0.07	1.07	1735	38.6	2096	1334	15	3	695	2
VGL 105-5	*S. verrucosum*	*S. verrucosum*	3	105-106	105.6	*Hibolithes sp.*	-0.18	0.79	1872	38.8	3335	1335	45	4	1003	2
VGL 105-11	*S. verrucosum*	*S. verrucosum*	1	105-106	105.6	*Duvalia gr. binervia*	-0.10	0.94	1575	38.9	1738	1281	11	3	375	3
VGL 105-1	*S. verrucosum*	*S. verrucosum*	3	105-106	104.7	*Hibolithes laryi (+ acro.)*	-0.42	-0.57	1732	37.6	3115	1316	22	4	577	2
VGL 105-2	*S. verrucosum*	*S. verrucosum*	3	105-106	104.7	*Hibolithes sp.*	-0.08	1.28	1942	39.1	2872	1274	30	4	1196	2

Sample No.	Zone	Subzone	VPI	Bed No.	Strat. level	Species	$\delta^{18}O$ ‰ PDB	$\delta^{13}C$ ‰ PDB	Na ppm	Ca %	Mg ppm	Sr ppm	Fe ppm	Mn ppm	S ppm	Ba ppm
VGL 102-3	*S. verrucosum*	*S. verrucosum*	3	102-103	97.7	*Hibolithes sp.*	-1.00	0.22	1939	38.8	3112	1376	10	3	873	3
VGL 102-2	*S. verrucosum*	*S. verrucosum*	3	102-103	97.7	*Hibolithes sp. (+ peu acro.)*	-0.44	0.59	1994	40.2	3211	1519	15	3	1053	3
VGL 100-6	*S. verrucosum*	*S. verrucosum*	3	100-101	96.3	*Hibolithes sp.*	-0.62	0.63	1683	39.1	2902	1320	13	3	778	2
VGL 100-8	*S. verrucosum-B. campylotoxus*	*S. verrucosum-K. biassalense*	3	100-101	96.1	*Hibolithes sp. (+ peu acro.)*	-0.46	0.09	2029	38.4	3429	1300	17	4	869	2
VGL 100-9	*S. verrucosum-B. campylotoxus*	*S. verrucosum-K. biassalense*	3	100-101	96.1	*Hibolithes sp. (+ peu acro.)*	-0.41	0.85	1790	39.5	3394	1285	22	4	779	3
VGL 100-10	*S. verrucosum-B. campylotoxus*	*S. verrucosum-K. biassalense*	2	100-101	96.1	*Hibolithes sp. (+ peu acro.)*	-0.26	1.25	1864	40.2	3344	1576	27	4	719	2
VGL 100-4	*B. campylotoxus*	*K. biassalense*	3	100-101	95.8	*Hibolithes sp.*	-0.32	0.79	1783	38.2	2972	1295	17	4	827	2
VGL 99-3	*B. campylotoxus*	*K. biassalense*	3	99-100	94.4	*Berriasibelus gr. conicus*	0.01	0.24	1838	39.8	2715	1429	11	3	800	2
VGL 95-2	*B. campylotoxus*	*K. biassalense*	3	95-96a	84.8	*Hibolithes cf. laryi*	0.21	0.29	1725	40.9	3245	1296	19	5	585	3
VGL 93-3	*B. campylotoxus*	*K. biassalense*	2	93-94	83.4	*Hibolithes sp. (cf. laryi)*	0.01	0.34	/	/	/	/	/	/	/	/
VGL 92-1	*B. campylotoxus*	*K. biassalense*	3	92-93	81.7	*Castellanibelus (aff.) orbignyanus*	0.40	1.73	1575	39.1	2286	1252	7	3	880	3
VGL 89c-7	*B. campylotoxus*	*K. biassalense*	3	89b-89c	78.5	*Hibolithes sp.*	0.34	0.37	1807	39.2	3416	1265	18	6	741	35
VGL 89a-3	*B. campylotoxus*	*K. biassalense*	3	89a	78.2	*Hibolithes sp. juv.*	0.43	2.15	1881	38.8	2860	1243	21	5	869	24

Sample No.	Zone	Subzone	VPI	Bed No.	Strat. level	Species	$\delta^{18}O$ ‰ PDB	$\delta^{13}C$ ‰ PDB	Na ppm	Ca %	Mg ppm	Sr ppm	Fe ppm	Mn ppm	S ppm	Ba ppm
VGL 78-1	*B. campylotoxus*	*K. biassalense*	3	78-79	68.8	*Hibolithes cf. laryi*	0.22	0.26	2022	39.0	2959	1226	40	5	1006	7
VGL 58-2	*T. pertransiens*	/	3	58	49.0	*Duvalia gr. lata*	0.07	0.08	2158	39.3	2541	1569	15	4	896	3
VGL 56-1	*T. pertransiens*	/	2	56-57	47.6	*Berriasibelus sp. (exstinctorius)*	0.21	1.44	1745	38.6	2060	1227	9	3	985	3
VGL 55-2	*T. pertransiens*	/	2	55-56	47.1	*Berriasibelus gr. conicus*	0.23	0.93	1944	40.4	2022	1239	7	3	721	2
VGL 54-1	*T. pertransiens*	/	2	54-55	46.3	*Pseudobelus gr. Bipartitus*	0.36	0.97	/	/	/	/	/	/	/	/
VGL 53-4	*T. pertransiens*	/	2	53-54	45.0	*Castellanibelus aff. orbignyanus*	0.54	1.17	1513	39.9	2075	1105	3	4	950	5
VGL 52-1	*T. pertransiens*	/	3	52-53	44.6	*Hibolithes sp.*	0.65	1.78	2030	39.2	2683	1298	36	4	1233	37
VGL 52-2	*T. pertransiens*	/	3	52-53	44.6	*Berriasibelus cf. exstinctorius*	0.32	0.81	1958	39.3	2370	1416	10	3	1041	2
VGL 51-3	*T. pertransiens*	/	3	51a-52	43.6	*Hibolithes sp.*	0.27	0.40	2269	39.0	2687	1369	81	5	1382	28
VGL 51-2	*T. pertransiens*	/	2	51a-52	43.6	*Hibolithes sp. = aff. "pistilliformis" auct.*	0.47	0.82	1995	39.6	2528	1286	45	4	1207	43
VGL 51-1	*T. pertransiens*	/	3	51a-52	43.6	*Castellanibelus aff. orbignyanus*	0.31	1.28	1411	39.9	2153	1139	10	3	615	1
VGL 51-7	*T. pertransiens*	/	2	51a-52	43.6	*Castellanibelus sp. (aff. Orbignyanus)*	0.53	1.57	1763	39.2	2495	1258	99	9	1606	7
VGL 50-1	*T. pertransiens*	/	2	50-51a	42.5	*Berriasibelus*	0.56	1.40	1812	39.9	2373	1293	7	3	846	2

Sample No.	Zone	Subzone	VPI	Bed No.	Strat. level	Species	$\delta^{18}O$ ‰ PDB	$\delta^{13}C$ ‰ PDB	Na ppm	Ca %	Mg ppm	Sr ppm	Fe ppm	Mn ppm	S ppm	Ba ppm
						exstinctorius										
VGL 49-8	*T. pertransiens*	/	2	49-50	41.8	*Castellanibelus aff. orbignyanus*	0.70	1.92	1648	39.9	2410	1207	11	4	715	2
VGL 49-3	*T. pertransiens*	/	3	49-50	41.8	*Berriasibelus sp. (gr. Conicus)*	0.07	0.74	1580	39.5	2260	1366	6	3	836	1
VGL 46-4	*T. pertransiens*	/	3	46b-47	39.1	*Castell. sp.*	0.32	1.06	1438	39.8	2503	1291	15	3	878	1
VGL 46-5	*T. pertransiens*	/	2	46-47	39.1	*Castellanibelus aff. orbignyanus*	0.12	1.60	1416	40.8	2083	1101	6	4	1104	2
VGL 46-1	*T. pertransiens*	/	2	46b-47	39.1	*Berriasibelus gr. conicus*	0.44	0.28	1998	40.1	2368	1440	11	3	918	1
VGL 34-1	*T. pertransiens*	/	3	34-35a	20.5	*Berriasibelus exstinctorius*	0.60	1.26	1795	39.5	2471	1402	8	3	622	1

Appendix G List of Mesozoic samples for U and Pb measurements.

Sample No.	Taxa	Location	Biostrat Age	Age (Ma)
Biogenic aragonite				
USWI 10	*Baculites eliasi*	US Western Interior	Base *Maastrichtian*	73
USWI 17	Ammonite	US Western Interior	*Baculites cuneatus* Zone; Upper *Campanian*	72.6
DJ 1503.76	Oyster/Bivalve	Antarctica	mid-*Campanian*	80.3
Biogenic calcite				
USWI 73	*Ostrea glabra*	US Western Interior	Base *Maastrichian*	73
DJ 1455.50A	Inoceramid*	Antarctica	mid-*Campanian*	79.3
DJ 1459 7-10A	Inoceramid	Antarctica	*Coniacian*	87.1
H-Be-1	Belemnite	Hemmoor, Germany	Upper Cretaceous	~70
La-Be-1	Belemnite	Lagerdorf, Gemany	Upper Cretaceous	83.92
La-Be-2	Belemnite	Lagerdorf, Gemany	Upper Cretaceous	81.78
La-Be-3	Belemnite	Lagerdorf, Gemany	Upper Cretaceous	79.75
La-Be-4	Belemnite	Lagerdorf, Gemany	Upper Cretaceous	76.40
La-Be-5	Belemnite	Lagerdorf, Gemany	Upper Cretaceous	74.18
La-Be-6	*Gonioteuthis quadrata*	Lagerdorf, Gemany	Upper Cretaceous	80.3-82.2

Sample No.	Taxa	Location	Biostrat Age	Age (Ma)
La-Be-7	*Gonioteuthis westfalica*	Lagerdorf, Gemany	Upper Cretaceous	80.3-82.2
La-Be-8	*Gonioteuthis quadrata*	Lagerdorf, Gemany	Upper Cretaceous	80.3-82.2
Kr-Be-1	Belemnite	Kromsmoor, Germany	Upper Cretaceous	71.82
Kr-Be-2	Belemnite	Kromsmoor, Germany	Upper Cretaceous	71.01
Kr-Be-3	Belemnite	Kromsmoor, Germany	Upper Cretaceous	69.88
G3(S)	Belemnite	Dorest,UK	Upper Campanian	\
DJ 1042.22b	Belemnite	Antarctica	mid-*Maastrichtian*	68.4
DJ 1502.16	Belemnite	Antarctica	*Cenomanian*?	~ 94
DJ 1502.18	Belemnite	Antarctica	*Cenomanian*?	~ 94
DJ 1502.61	Belemnite	Antarctica	*Cenomanian*?	~ 94
A1/B1	*Neohibolithes*	Folkstone, UK	*Spathi of dentatus zone, Cenomanian*	108.8
A1/B2	*Neohibolithes*	Folkstone, UK	*Intermedius of loricatus zone, Cenomanian*	108.2
A1/B4	*Neohibolithes*	Folkstone, UK	*Cristatum of inflaturm zone, Cenomanian*	103.0
A1/B6	*Neohibolithes*	Folkstone, UK	*Orbignyi of inflaturm zone, Cenomanian*	102.4
A1/B7	*Neohibolithes*	Folkstone, UK	*Varicosum of inflaturm zone, Cenomanian*	101.7
J 1189	*Castillanibelus*	France	*Pertransiens,Valanginian*	140.2

Sample No.	Taxa	Location	Biostrat Age	Age (Ma)
J 1591	*Adiakritobelus*	France	*Verrucosum,Valanginian*	138.9
J 5146	*Hibolithes*	France	*Verrucosum,Valanginian*	138.9
J 5229	*Hibolithes*	France	*Verrucosum,Valanginian*	138.9
J 5351	*Duvalia emericii*	France	*Campylotoxus ,Valanginian*	139.8
J 5357	*Pseudobelus*	France	*Campylotoxus ,Valanginian*	139.8
J 5368	*Castillanibelus*	France	*Campylotoxus,Valanginian*	139.8
J 6919	*Berriasibelus*	France	*Boissieri, Berriasian*	141.2
J 7100	*Duvalia binerva*	France	*Peregrinus,Valanginian*	140.2
J 7182	*Adiakritobelus*	France	*Peregrinus,Valanginian*	140.2
Sp 1157	Belemnite	Yorkshire, UK	*P. elegans* Zone, mid-*Barremian*	128.3
Sp 1341	Belemnite	Yorkshire, UK	base *E. amblygonium* Zone, base *Hauterivian*	133.9
Sp 1372	Belemnite	Yorkshire, UK	top *P. elegans* Zone; mid-*Barremian*	127.1
Callomon 1	Belemnite	Germany	*Callovian/Bathonian* boundary	164.7
Callomon 3	Belemnite	Germany	*Callovian/Bathonian* boundary	164.7
13/111 a	*C.pusoziana*	Oxfordshire, UK	Top of *jason* Zone, *Callovian*	163.2
1S57	*C.pusoziana*	Oxfordshire, UK	Top of *jason* Zone, *Callovian*	163.2

Sample No.	Taxa	Location	Biostrat Age	Age (Ma)
80/20	Belemnite	Skye,UK	*Aalenian/Toarcian* boundary	175.6
75/5	Belemnite	Skye,UK	*Aalenian/Toarcian* boundary	175.6
BLQ 08/2-1	*Hastitus clavatus*	Blockley Quarry,UK	*Jason* Zone, *Callovian*	163.2
BLQ 08/5-5	*Nannobelus acutus*	Blockley Quarry,UK	*Jason* Zone, *Callovian*	163.2
BLQ 08/5-1	*Passolotusthis cf. elongata*	Blockley Quarry,UK	*Jason* Zone, *Callovian*	163.2
D08 118/3	*A. uriel*	Dorest,UK	*Valdani, ibex Zone, Pliensbachian*	188.5
D08 7/3 S2	*P. elongata*	Dorest,UK	*Maculatum, davoei Zone, Pliensbachian*	187.7
Diagenetic calcite				
39-1 CN	Carbonate concretion	Port Mulgrave, Staithes, UK	*Gibbosus, margaritatus* Zone, *Pliensbachian*	187.0
62-1 CN	Red ironstone	Port Mulgrave, Staithes, UK	*tenuicostatum, Toarcian*	183.0
7/1 AC S1	Belemnite alveolar cement	Dorset, UK	*maculatum, davoei Zone Pliensbachian*	. 187.7
7 AC1 S2	Belemnite alveolar cement	Dorset, UK	*maculatum, Pliensbachian*	187.7
7 AC2 S2	Belemnite alveolar cement	Dorset, UK	*maculatum, Pliensbachian*	187.7
7/19 AC S3	Belemnite alveolar cement	Dorset, UK	*maculatum, Pliensbachian*	187.7
120/8 AC	Belemnite alveolar cement	Dorset, UK	*maculatum, Pliensbachian*	187.7
120/9 AC	Belemnite alveolar cement	Dorset, UK	*maculatum, Pliensbachian*	187.7

Appendix H The LA-ICP-MC-MS data of U-Pb concentrations, U/Pb ratios and analytical uncertainties of the early cement SS2 and IS2. The U and Pb concentrations and $^{207}Pb/^{206}Pb$ ratios are normalized to NIST 614. The $^{238}U/^{206}Pb$ (measured) ratios are non standard-normalized, measured values with analytical uncertainties (1 standard error, or 1se) only. The $^{238}U/^{206}Pb$ (corrected) ratios of both samples are normalized to SS2 (i.e. using the fractionation factor of 1.64 derived from SS2), and their uncertainties are propagated using LA regressions.

Samples	^{206}Pb mV	^{207}Pb mV	^{238}U mV	Pb ppm	U* ppm	$^{238}U/^{206}Pb$ (measured)	1se %	$^{238}U/^{206}Pb$ (corrected)	1se %	$^{207}Pb/^{206}Pb$	1se %
SS2 outer s1	1.0	0.20	16.6	0.5	2.5	18.01	0.5	29.6	0.8	0.2365	0.7
SS2 outer s2	0.8	0.22	12.9	0.4	2.0	16.64	1.7	27.3	1.8	0.2886	3.5
SS2 outer s3	0.3	0.10	4.7	0.2	0.7	14.73	3.2	24.2	3.3	0.3618	5.9
SS2 outer s4	0.5	0.12	8.9	0.3	1.4	17.94	0.7	29.5	0.9	0.2671	1.4
SS2 outer s6	0.5	0.12	8.3	0.2	1.3	17.32	1.5	28.4	1.6	0.2765	2.7
SS2 outer s7	1.2	0.36	16.5	0.6	2.5	15.55	1.9	25.5	2.0	0.3411	2.4
SS2 outer s8	0.4	0.09	6.9	0.2	1.1	17.21	1.7	28.2	1.8	0.2332	4.2
SS2 outer s9	0.5	0.11	8.0	0.2	1.2	17.46	0.5	28.7	0.8	0.2535	1.4
SS2 outer s10	0.9	0.26	13.7	0.5	2.1	15.38	1.0	25.3	1.2	0.3331	1.6
SS2 outer s11	0.8	0.27	9.9	0.4	1.5	13.58	0.5	22.3	0.8	0.4038	0.7
SS2 outer s12	1.3	0.39	18.8	0.7	2.9	14.77	0.7	24.2	0.9	0.3478	1.0
SS2 outer s13	1.7	0.63	20.3	0.8	3.1	12.44	0.7	20.4	1.0	0.4346	0.6

Samples	^{206}Pb mV	^{207}Pb mV	^{238}U mV	Pb ppm	U* ppm	$^{238}U/^{206}Pb$ (measured)	1se %	$^{238}U/^{206}Pb$ (corrected)	1se %	$^{207}Pb/^{206}Pb$	1se %
SS2 outer s14	0.4	0.13	6.5	0.2	1.0	15.07	1.5	24.7	1.6	0.3307	2.2
SS2 outer s15 a	1.1	0.34	16.4	0.6	2.5	14.78	3.3	24.3	3.3	0.3561	3.4
SS2 outer s15 b	1.2	0.32	18.4	0.6	2.8	16.04	0.3	26.3	0.7	0.3245	0.7
SS2 outer s16 a	0.7	0.28	9.1	0.4	1.4	12.70	0.9	20.9	1.1	0.4372	1.2
SS2 outer s16 b	4.5	3.05	6.4	2.3	1.0	1.45	6.7	2.4	6.7	0.7786	0.3
SS2 outer s17	1.1	0.38	13.0	0.5	2.0	12.86	1.3	21.1	1.4	0.4129	1.1
SS2 outer s18	0.6	0.06	12.3	0.3	1.9	22.31	0.2	36.6	0.7	0.1231	0.7
SS2 outer s19	0.9	0.41	9.6	0.5	1.5	10.34	2.7	17.0	2.8	0.5032	1.6
SS2 outer s20	0.5	0.05	10.7	0.2	1.6	23.59	0.4	38.7	0.8	0.1073	1.2
SS2 outer s21	0.5	0.06	10.8	0.3	1.6	22.94	0.9	37.7	1.1	0.1268	3.7
SS2 outer s22	0.6	0.13	9.0	0.3	1.4	16.56	1.0	27.2	1.1	0.2716	1.9
SS2 outer s23	0.3	0.05	7.5	0.2	1.1	22.57	1.2	37.0	1.4	0.1597	3.5
SS2 outer s24	0.6	0.09	11.8	0.3	1.8	19.37	1.0	31.8	1.2	0.1639	2.8
SS2 outer s25	1.0	0.12	19.1	0.5	2.9	20.43	1.2	33.5	1.4	0.1487	4.6
SS2 outer s26	1.7	0.88	12.9	0.9	2.0	7.26	5.3	11.9	5.3	0.6052	1.4

Samples	^{206}Pb mV	^{207}Pb mV	^{238}U mV	Pb ppm	U* ppm	$^{238}U/^{206}Pb$ (measured)	1se %	$^{238}U/^{206}Pb$ (corrected)	1se %	$^{207}Pb/^{206}Pb$	1se %
SS2 outer s27	0.4	0.06	8.5	0.2	1.3	20.96	0.8	34.4	1.0	0.1757	2.0
SS2 outer s28	8.7	5.72	14.1	4.4	2.2	1.60	0.9	2.6	1.1	0.7560	0.2
SS2 outer s29	1.0	0.33	14.6	0.5	2.2	14.16	1.2	23.2	1.4	0.3745	1.6
SS2 outer s30	0.7	0.08	13.4	0.4	2.0	19.27	1.5	31.6	1.6	0.1338	2.1
SS2 outer s31	0.6	0.13	11.2	0.3	1.7	18.13	1.1	29.8	1.3	0.2451	3.0
SS2 outer s32	1.0	0.66	1.7	0.5	0.3	1.71	3.9	2.8	4.0	0.7819	0.4
SS2 outer s32 RE	1.1	0.79	0.9	0.6	0.1	0.79	2.2	1.3	2.3	0.8102	0.2
SS2 outer s33	0.7	0.20	8.9	0.3	1.4	14.02	4.2	23.0	4.3	0.3662	4.4
SS2 outer s34	0.4	0.15	4.3	0.2	0.7	11.14	4.0	18.3	4.1	0.4623	2.8
IS2 outter s1	5.4	1.35	60.0	2.8	15.2	17.40	1.0	28.6	1.2	0.2830	1.8
IS2 outter s2	4.1	0.97	46.7	2.2	11.8	17.65	0.6	29.0	0.8	0.2708	1.5
IS2 outter s3	2.8	1.25	18.1	1.5	4.6	9.86	1.6	16.2	1.7	0.5090	1.3
IS2 outter s4	4.1	1.66	29.0	2.1	7.3	11.10	1.1	18.2	1.3	0.4618	0.7
IS2 outter s5	4.3	2.76	6.3	2.2	1.6	2.23	3.6	3.7	3.6	0.7443	0.5
IS2 outter s6	1.6	0.69	9.8	0.8	2.5	9.77	2.2	16.0	2.3	0.5172	1.2

Samples	^{206}Pb mV	^{207}Pb mV	^{238}U mV	Pb ppm	U* ppm	$^{238}U/^{206}Pb$ (measured)	1se %	$^{238}U/^{206}Pb$ (corrected)	1se %	$^{207}Pb/^{206}Pb$	1se %
IS2 outter s7	3.5	1.00	33.5	1.8	8.5	15.64	1.3	25.7	1.4	0.3335	1.6
IS2 outter s8	3.7	0.98	38.9	1.9	9.8	16.83	0.8	27.6	1.0	0.3000	1.1
IS2 outter s9	1.2	0.61	5.3	0.6	1.3	7.26	0.4	11.9	0.7	0.5916	0.3
IS2 outter s10	2.2	0.66	19.8	1.1	5.0	14.71	0.8	24.1	1.0	0.3478	0.9
IS2 outter s11	3.0	1.18	22.4	1.6	5.7	11.64	0.5	19.1	0.8	0.4508	0.4
IS2 outter s12	2.0	0.79	14.2	1.0	3.6	11.40	1.1	18.7	1.3	0.4673	0.7
IS2 outter s13	2.2	1.16	9.2	1.2	2.3	6.50	2.4	10.7	2.5	0.6086	0.9
IS2 outter s14	3.3	1.19	26.0	1.7	6.6	12.15	0.9	19.9	1.1	0.4149	0.8
IS2 outter s15	3.0	1.49	15.0	1.6	3.8	7.75	1.6	12.7	1.7	0.5702	0.7
IS2 outter s16	1.8	0.91	8.8	0.9	2.2	7.60	2.1	12.5	2.2	0.5756	0.8
IS2 outter s17	7.3	4.08	29.1	3.8	7.4	6.19	5.6	10.2	5.6	0.6424	1.5

Appendix I The U-Pb analytical data (concentrations, isotopic ratios and errors) of the ammonite cement IS1 obtained by LA-ICP-MC-MS. The U and Pb concentrations and 207Pb/206Pb ratios are normalized to zircon 91500. The 238U/206Pb (corrected) ratios of IS1 are normalized to itself (i.e. using the fractionation factor of 1.07 derived from SS2).

Samples	^{206}Pb mV	^{207}Pb mV	^{238}U mV	Pb ppm	U* ppm	^{238}U/^{206}Pb (measured)	1se %	^{238}U/^{206}Pb (corrected)	1se %	^{207}Pb/^{206}Pb	1se %
IS1 early cement 1	1.1	0.22	30.3	0.9	19.8	28.48	0.9	30.6	1.1	0.2367	1.4
IS1 early cement 2	1.8	0.55	40.2	1.5	26.2	22.82	1.4	24.5	1.6	0.3523	1.8
IS1early cement 3	1.7	1.05	10.6	1.4	6.9	5.63	8.4	6.0	8.5	0.6944	1.9
IS1 early cement 3b	1.3	0.67	12.7	1.0	8.3	10.11	3.1	10.9	3.2	0.6141	0.5
IS1 early cement 4	1.2	0.68	10.3	1.0	6.7	8.84	7.2	9.5	7.3	0.6391	2.0
IS1 early cement 4b	1.0	0.48	11.1	0.8	7.3	11.86	1.1	12.7	1.3	0.5776	0.9
IS1 early cement 5	1.3	0.86	5.1	1.1	3.3	3.80	2.2	4.1	2.3	0.7546	0.5
IS1 early cement 6	0.5	0.23	7.6	0.4	5.0	15.38	2.9	16.5	3.0	0.5239	2.1
IS1 early cement 7	0.2	0.05	4.0	0.1	2.6	24.09	1.5	25.9	1.6	0.3320	1.8
IS1 early cement 8	1.3	0.75	13.6	1.1	8.9	9.94	0.9	10.7	1.1	0.6253	0.6
IS1 early cement 9	3.9	2.81	1.6	3.2	1.0	0.38	5.3	0.4	5.3	0.8310	0.5
IS1early cement 10	2.3	1.33	16.3	1.9	10.6	7.24	1.4	7.8	1.6	0.6838	0.5
IS1 early cement 11	1.2	0.80	4.6	1.0	3.0	3.72	2.2	4.0	2.3	0.7559	0.5

Samples	^{206}Pb mV	^{207}Pb mV	^{238}U mV	Pb ppm	U* ppm	$^{238}U/^{206}Pb$ (measured)	1se %	$^{238}U/^{206}Pb$ (corrected)	1se %	$^{207}Pb/^{206}Pb$	1se %
IS1 early cement 12	2.5	1.76	4.5	2.1	2.9	1.73	2.8	1.9	2.8	0.8011	0.5
IS1 early cement 13	4.3	3.03	4.1	3.5	2.7	0.93	6.9	1.0	6.9	0.8177	0.5
IS1 early cement 14	1.7	1.06	7.7	1.4	5.0	4.34	7.8	4.7	7.8	0.7334	1.2
Is1 early cement 14b	1.2	0.70	8.5	1.0	5.6	7.14	5.5	7.7	5.5	0.6859	0.7
IS1 outer septum 1	0.7	0.41	6.8	0.6	4.4	8.94	4.4	9.6	4.4	0.6406	1.3
IS1 outer septum 2	4.0	2.60	17.0	3.3	11.1	4.20	3.3	4.5	3.3	0.7452	0.6
IS1 outer septum 3	5.1	3.43	14.6	4.3	9.5	2.79	7.3	3.0	7.3	0.7639	0.8
IS1 outer septum 3b	3.2	2.04	15.7	2.7	10.2	4.85	2.5	5.2	2.6	0.7285	0.5
IS1 outer septum 4	4.4	2.95	11.4	3.6	7.4	2.57	4.1	2.8	4.2	0.7772	0.5
IS1 outer septum 5	7.3	5.08	9.7	6.1	6.3	1.28	7.7	1.4	7.7	0.7989	0.5
IS1 outer septum 5b	5.3	3.62	10.2	4.4	6.7	1.98	2.6	2.1	2.7	0.7884	0.5
IS1 inner septum 1	1.3	0.77	9.7	1.1	6.3	7.47	1.6	8.0	1.8	0.6765	0.6
IS1 inner septum 2	3.2	2.07	14.1	2.7	9.2	4.44	3.4	4.8	3.4	0.7427	0.6
IS1 inner septum 2b	2.6	1.62	14.5	2.1	9.4	5.57	0.7	6.0	1.0	0.7219	0.5
IS1 inner septum 3	1.2	0.72	9.8	1.0	6.4	7.91	1.5	8.5	1.7	0.6734	0.6

Samples	^{206}Pb mV	^{207}Pb mV	^{238}U mV	Pb ppm	U* ppm	^{238}U/^{206}Pb (measured)	1se %	^{238}U/^{206}Pb (corrected)	1se %	^{207}Pb/^{206}Pb	1se %
IS1 inner septum 4	1.1	0.69	5.7	0.9	3.7	5.09	4.7	5.5	4.7	0.7302	0.7
IS1 inner septum 4b	0.9	0.58	5.6	0.8	3.6	5.98	2.8	6.4	2.9	0.7132	0.6
IS1 inner septum 5	3.5	2.26	13.0	2.9	8.5	3.74	4.1	4.0	4.2	0.7527	0.6
IS1 inner septum 5b	3.0	1.95	13.5	2.5	8.8	4.43	2.0	4.8	2.1	0.7404	0.5
IS1 inner early cement 1	2.6	1.90	0.6	2.2	0.4	0.21	3.6	0.2	3.6	0.8353	0.5
IS1 inner early cement 1b	2.3	1.69	0.5	1.9	0.4	0.23	2.5	0.2	2.6	0.8323	0.5
IS1 inner early cement S1a	3.7	2.62	4.5	3.1	2.9	1.18	4.0	1.3	4.1	0.8094	0.5
IS1 inner early cement S2b	7.3	5.22	5.6	6.1	3.6	0.75	8.2	0.8	8.3	0.8219	0.5
IS1 inner early cement S3a	7.3	5.04	13.5	6.0	8.8	1.75	13.3	1.9	13.3	0.7928	0.6
IS1 inner early cement S3b	4.5	2.96	15.6	3.7	10.2	3.48	0.9	3.7	1.1	0.7661	0.4
IS1 inner early cement S4	1.6	1.12	1.8	1.3	1.2	1.15	1.3	1.2	1.4	0.8155	0.5
IS1 inner early cement S5	0.7	0.49	1.0	0.6	0.7	1.43	3.9	1.5	3.9	0.8087	0.5
IS1 inner early cement S6a	1.5	1.02	3.2	1.2	2.1	2.17	3.3	2.3	3.3	0.7954	0.5
IS1 inner early cement S6b	1.5	1.05	3.6	1.3	2.4	2.36	2.1	2.5	2.2	0.7912	0.5
IS1 inner early cement S7	2.8	1.96	1.6	2.3	1.1	0.58	7.0	0.6	7.0	0.8239	0.5

Reference

Alley, N.F., and Frakes, L.A., 2003, First Known Cretaceous glaciation: Livingston Tillite Member of the Cadna-owie Formation, South Australia: Australian Journal of Earth Sciences, v. 50, p. 139-144.

Anderson, T.F., Popp, B.N., Williams, A.C., Ho, L.Z., and Hudson, J.D., 1994, The Stable Isotopic Records of Fossils from the Peterborough Member, Oxford Clay Formation (Jurassic), Uk - Paleoenvironmental Implications: Journal of the Geological Society, v. 151, p. 125-138.

Andreson, T.F., and Arthur, M.A., 1983, Stable isotope of oxygen and carbon and their application to sedimentologic and paleoenvironmental problems. In: Arthur, M.A., Anderson, T.F., Kaplan, I.R., Veizer, J., Land, L.S. (Eds.), Stable Isotopes in Sedimentary Geology: Society of Economic Paleontologists and Mineralogists, Short Course Notes, v. 10, p. pp.1-151.

Bailey, T.R., Rosenthal, Y., McArthur, J.M., van de Schootbrugge, B., and Thirlwall, M.F., 2003, Paleoceanographic changes of the Late Pliensbachian-Early Toarcian interval: a possible link to the genesis of an Oceanic Anoxic Event: Earth and Planetary Science Letters, v. 212, p. 307-320.

Bard, E., Hamelin, B., Fairbanks, R.G., and Zindler, A., 1990, Calibration of the C-14 timescale over the past 30,000 years using mass-spectrometric U-Th ages from Barbados corals: Nature, v. 345, p. 405-410, doi: 10.1038/345405a0.

Barnes, C.E., and Cochran, J.K., 1990, Uranium Removal in Oceanic Sediments and the Oceanic-U Balance: Earth and Planetary Science Letters, v. 97, p. 94-101.

Barron, E.J., 1983, A WARM, EQUABLE CRETACEOUS - THE NATURE OF THE PROBLEM: Earth-Science Reviews, v. 19, p. 305-338, doi: 10.1016/0012-8252(83)90001-6.

Barron, E.J., Fawcett, P.J., Peterson, W.H., Pollard, D., and Thompson, S.L., 1995, A SIMULATION OF MIDCRETACEOUS CLIMATE: Paleoceanography, v. 10, p. 953-962, doi: 10.1029/95pa01624.

Barron, E.J., Fawcett, P.J., Pollard, D., and Thompson, S., 1993, MODEL SIMULATIONS OF CRETACEOUS CLIMATES - THE ROLE OF GEOGRAPHY AND CARBON-DIOXIDE: Philosophical Transactions of the Royal Society of London Series B-Biological Sciences, v. 341, p. 307-315, doi: 10.1098/rstb.1993.0116.

Barron, E.J., Thompson, S.L., and Schneider, S.H., 1981, An Ice-Free Cretaceous? Results from Climate Model Simulations: Science, v. 212, p. 501-508.

Be, A.W.H., Anderson, O.R., Faber, W.W., and Caron, D.A., 1983, Sequence of morphological and cytoplasmic changes during gametogenesis in the planktonic

foraminifer *Globigerinoides sacculifer* (Brady): Micropaleontology, v. 29, p. 310-325, doi: 10.2307/1485737.

Berlin, T.S., Naidin, D.P., Saks, V.N., Teis, R.V., and Khabokov, A.V., 1967, Jurassic and Cretaceous climate in northern USSR from palaeotemperature determinations: International Geological Review, v. 9, p. 1080-1092.

Blanton, B.O., Aretxabaleta, A., Werner, F.E., and Seim, H.E., 2003, Monthly climatology of the continental shelf waters of the South Atlantic Bight: Journal of Geophysical Research-Oceans, v. 108, doi: Artn 3264 Doi 10.1029/2002jc001609.

Bowring, S.A., Erwin, D.H., Jin, Y.G., Martin, M.W., Davidek, K., and Wang, W., 1998, U/Pb zircon geochronology and tempo of the end-Permian mass extinction: Science, v. 280, p. 1039-1045.

Bustamante, P., Teyssie, J.L., Fowler, S.W., Cotret, O., Danis, B., Miramand, P., and Warnau, M., 2002, Biokinetics of zinc and cadmium accumulation and depuration at different stages in the life cycle of the cuttlefish Sepia officinalis: Marine Ecology-Progress Series, v. 231, p. 167-177.

Callomon, J.H., 1968, The Kellaways Beds and the Oxford Clay: In: Sylvester Bradley, P.S. and Ford, T. D. (eds) The Geology of the East Midlands. Leicester, Leicester University Press, p. 264-290.

Caswell, B.A., Coe, A.L., and Cohen, A.S., 2009, New range data for marine invertebrate species across the early Toarcian (Early Jurassic) mass extinction: Journal of the Geological Society, v. 166, p. 859-872, doi: 10.1144/0016-76492008-0831.

Channell, J.E.T., Bralower, T.J., and Grandesso, P., 1987, Biostratigraphic Correlation of Mesozoic Polarity Chrons Cm1 to Cm23 at Capriolo and Xausa (Southern Alps, Italy): Earth and Planetary Science Letters, v. 85, p. 203-221.

Channell, J.E.T., and Erba, E., 1992, Early Cretaceous Polarity Chrons Cm0 to Cm11 Recorded in Northern Italian Land Sections near Brescia: Earth and Planetary Science Letters, v. 108, p. 161-179.

Channell, J.E.T., Erba, E., and Lini, A., 1993, Magnetostratigraphic calibration of the Late Valanginian carbon-isotope event in Pelagic Limestones from Northern Italy and Switerland: Earth and Planetary Science Letters, v. 118, p. 145-166, doi: 10.1016/0012-821x(93)90165-6.

Chave, K.E., 1954, Aspects of the Biogeochemistry of Magnesium: 1. Calcareous Marine Organisms: Journal of Geology, v. 62, p. 266-283.

Christensen, W.K., 1990, Upper cretaceous belemnite stratigraphy of Europe: Cretaceous Research, v. 11, p. 371-386.

Christensen, W.K., 1996, A review of the Upper Campanian and Maastrichtian belemnite biostratigraphy of Europe: Cretaceous Research, v. 17, p. 751-766.

Combémorel, R., 1997, Bélemnites. In: Cariou, E. & Hantzpergue, P. (eds): Biostratigraphie du Jurassique ouest-européen et méditerranéen: zonations parallèles et distribution des invertébrés et microfossiles: Bulletin du Centre Recherches Elf Exploration Production Mémoire, p. 157-168.

Delaney, M.L., and Boyle, E.A., 1983, Uranium and thorium isotope concentrations in foraminiferal calcite: Earth and Planetary Science Letters, v. 62, p. 258-262.

Denniston, R.F., Asmerom, Y., Polyalk, V.Y., McNeill, D.F., Klaus, J.S., Cole, P., and Budd, A.F., 2008, Caribbean chronostratigraphy refined with U-Pb dating of a Miocene coral: Geology, v. 36, p. 151-154, doi: Doi 10.1130/G24280a.1.

Dickin, A.P., 2005, Radiogenic isotope geology: Cambridge: Cambridge univeristy Press, 2005, p. 492p.

Djogic, R., Sipos, L., and Branica, M., 1986, Characterization of Uranium(Vi) in Seawater: Limnology and Oceanography, v. 31, p. 1122-1131.

Doyle, P., 1987, Lower Jurassic-Lower Cretaceous belemnite biogeography and the development of the Mesozoic Boreal Realm: Palaeogeography, Palaeoclimatology, Palaeoecology, v. 61, p. 237-254.

Doyle, P., 1990, The British Toarcian (Lower Jurassic) Belemnites, p. 1-49.

Doyle, P., 2003, Type belemnites of Simpson's Fossils of the Yorkshire Lias: Proceedings of the Yorkshire Geological Society, v. 54, p. 147-184.

Doyle, P., and Bennett, M.R., 1995, Belemnites in biostratigraphy: Palaeontology, v. 38, p. 815-829.

Duff, K.L., 1975, Paleo ecology of a bituminous shale - the Lower Oxford Clay of Central England: Palaeontology (Oxford), v. 18, p. 443-482.

Duff, K.L., 1978, Bivalvia from the English Lower Oxford Clay (Middle Jurassic). Monograph of the Palaeontographical Society, London.

Dunca, E., Doguzhaeva, L., Schone, B.R., and Van de Schootbrugge, B., 2006, Growth Patterns in Rostra of the Middle Jurassic Belemnite *Megateuthis Giganteus*: Controled by the Moon?: Acta Universitatis Carolinae - Geologica, v. 49, p. 107-117.

Dunk, R.M., Mills, R.A., and Jenkins, W.J., 2002, A re-evaluation of the oceanic uranium budget for the Holocene: Chemical Geology, v. 190, p. 45-67, doi: Pii S0009-2541(02)00110-9.

Dutton, A., Huber, B.T., Lohmann, K.C., and Zinsmeister, W.J., 2007, High-resolution stable isotope profiles of a dimitobelid belemnite: Implications for

paleodepth habitat and late Maastrichtian climate seasonality: Palaios, v. 22, p. 642-650.

Eggins, S.M., Sadekov, A., and De Deckker, P., 2004, Modulation and daily banding of Mg/Ca in Orbulina universa tests by symbiont photosynthesis and respiration: a complication for seawater thermometry?: Earth and Planetary Science Letters, v. 225, p. 411-419, doi: 10.1016/j.epsl.2004.06.019.

Emery, W.J., and Dewar, J.S., 1982, Mean temperature-salinity, salinity-depth and temperature-depth curves for the North-Atlantic and the North Pacific: Progress in Oceanography, v. 11, p. 219-305.

Erba, E., Bartolini, A., and Larson, R.L., 2004, Valanginian Weissert oceanic anoxic event: Geology, v. 32, p. 149-152, doi: 10.1130/g20008.1.

Faure, G., and Mensing, T.M., 2005, Isotopes: Principles and Applications: Hoboken, N.J.: Wiley, c2005, p. 897p.

Frimmel, A., Oschmann, W., and Schwark, L., 2004, Chemostratigraphy of the posidonia Black Shale, SW Germany I. Influence of sea-level variation on organic facies evolution: Chemical Geology, v. 206, p. 199-230, doi: DOI 10.1016/j.chemgeo.2003.12.007.

Getty, S.R., Asmerom, Y., Quinn, T.M., and Budd, A.F., 2001, Accelerated Pleistocene coral extinctions in the Caribbean Basin shown by uranium-lead (U-Pb) dating: Geology, v. 29, p. 639-642.

Gradstein, F.M., Ogg, J.G., and Smith, A.G., 2004, A geologic time scale 2004 Cambridge : Cambridge University Press, p. 589p.

Grocke, D.R., Price, G.D., Robinson, S.A., Baraboshkin, E.Y., Mutterlose, J., and Ruffell, A.H., 2005, The Upper Valanginian (Early Cretaceous) positive carbon-isotope event recorded in terrestrial plants: Earth and Planetary Science Letters, v. 240, p. 495-509.

Gröcke, D.R., Price, G.D., Robinson, S.A., Baraboshkin, E.Y., Mutterlose, J., and Ruffell, A.H., 2005, The Upper Valanginian (Early Cretaceous) positive carbon-isotope event recorded in terrestrial plants: Earth and Planetary Science Letters, v. 240, p. 495-509.

Gröcke, D.R., Price, G.D., Ruffell, A.H., Mutterlose, J., and Baraboshkin, E., 2003, Isotopic evidence for Late Jurassic-Early Cretaceous climate change: Palaeogeography, Palaeoclimatology, Palaeoecology, v. 202, p. 97-118.

Guerra, A., 2006, Ecology of Sepia officinalis: Vie Et Milieu-Life and Environment, v. 56, p. 97-107.

Hamilton, C.P., Spero, H.J., Bijma, J., and Lea, D.W., 2008, Geochemical investigation of gametogenic calcite addition in the planktonic foraminifera

Orbulina universa: Marine Micropaleontology, v. 68, p. 256-267, doi: 10.1016/j.marmicro.2008.04.003.

Haq, B.U., and Al-Qahtani, A.M., 2005, Phanerozoic cycles of sea-level change on the Arabian Platform: Geoarabia, v. 10, p. 127-160.

Harding, D.J., Arden, J.W., and Rickaby, R.E.M., 2006, A method for precise analysis of trace element/calcium ratios in carbonate samples using quadrupole inductively coupled plasma mass spectrometry: Geochemistry Geophysics Geosystems, v. 7, p. -, doi: Artn Q06003 Doi 10.1029/2005gc001093.

Harries, P.J., and Little, C.T.S., 1999, The early Toarcian (Early Jurassic) and the Cenomanian-Turonian (Late Cretaceous) mass extinctions: similarities and contrasts: Palaeogeography Palaeoclimatology Palaeoecology, v. 154, p. 39-66.

Hays, P.D., and Grossman, E.L., 1991, Oxygen Isotopes in Meteoric Calcite Cements as Indicators of Continental Paleoclimate: Geology, v. 19, p. 441-444.

Hennig, S., Weissert, H., and Bulot, L., 1999, C-isotope stratigraphy, a calibration tool between ammonite and magnetostratigraphy: The Valanginian-Hauterivian transition: Geologica Carpathica, v. 50, p. 91-95.

Hesselbo, S.P., and Jenkyns, H.C., 1995, A comparison of the Hettangian to Bajocian successions of Dorset and Yorkshire: Field Geology of the British Jurassic. Geological Society, London, p. 105-150.

Hoedemaeker, P.J., and Herngreen, G.F.W., 2003, Correlation of Tethyan and Boreal Berriasian - Barremian strata with emphasis on strata in the subsurface of the Netherlands: Cretaceous Research, v. 24, p. 253-275, doi: Doi 10.1016/S0195-6671(03)00044-2.

Hoefs, J., 2009, Stable isotope geochemistry: Berlin: Springer, 6th ed., p. 285.

Howarth, M.K., 1963, The Jet Rock series and the Alum Shales series of the Yorkshire coast: Proceedings of the Yorkshire Geological Society, v. 30, part 4, No.18, p. 381-422.

Howarth, M.K., 1973, The stratigraphy and ammonite fauna of the upper Liassic Grey Shales of the Yorkshire coast: Bull.Br.Mus. (Nat. Hist.) Geology, v. 24, p. 235-277.

Huber, M., 2008, A hotter greenhouse?: Science, v. 321, p. 353-354, doi: 10.1126/science.1161170.

Hudson, J.D., 1978, Concretions, Isotopes, and Diagenetic History of Oxford Clay (Jurassic) of Central England: Sedimentology, v. 25, p. 339-369.

Hudson, J.D., 1994, Oxford Clay studies: Journal of the Geological Society, v. 151, p. 111-112.

Hudson, J.D., and Martill, D.M., 1991, The Lower Oxford Clay: Production and Perservation of Organic Matter in the Callovian (Jurassic) of Central England. In: Tyson, R. V. and Person, T. H. (eds): Modern and Ancient Continental Shelf Anoxia. Geological Society, London, Special Publications, v. 58, p. 363-379.

Hudson, J.D., and Martill, D.M., 1994, The Peterborough Member (Callovian, Middle Jurassic) of the Oxford Clay Formation at Peterborough, Uk: Journal of the Geological Society, v. 151, p. 113-124.

Israelson, C., Halliday, A.N., and Buchardt, B., 1996, U-Pb dating of calcite concretions from Cambrian black shales and the Phanerozoic time scale: Earth and Planetary Science Letters, v. 141, p. 153-159.

Jaffey, A.H., Flynn, K.F., Glendeni.Le, Bentley, W.C., and Essling, A.M., 1971, Precision measurement of half-lives and specific activities of ^{235}U and ^{238}U: Physical Review C, v. 4, p. 1889-1906.

Jenkyns, H.C., and Clayton, C.J., 1997, Lower Jurassic epicontinental carbonates and mudstones from England and Wales: chemostratigraphic signals and the early Toarcian anoxic event: Sedimentology, v. 44, p. 687-706.

Jones, C.E., Halliday, A.N., and Lohmann, K.C., 1995, The Impact of Diagenesis on High-Precision U-Pb Dating of Ancient Carbonates - an Example from the Late Permian of New-Mexico: Earth and Planetary Science Letters, v. 134, p. 409-423.

Jones, C.E., Jenkyns, H.C., Coe, A.L., and Hesselbo, S.P., 1994b, Strontium Isotopic Variations in Jurassic and Cretaceous Seawater: Geochimica Et Cosmochimica Acta, v. 58, p. 3061-3074.

Jones, C.E., Jenkyns, H.C., and Hesselbo, S.P., 1994a, Strontium Isotopes in Early Jurassic Seawater: Geochimica Et Cosmochimica Acta, v. 58, p. 1285-1301.

Kenig, F., Hayes, J.M., Popp, B.N., and Summons, R.E., 1994, Isotoic biogeochemistry of the Oxford Clay Formation (Jurassic), UK: Journal of the Geological Society, v. 151, p. 139-152.

Ku, T.L., Knauss, K.G., and Mathieu, G.G., 1977, Uranium in Open Ocean - Concentration and Isotopic Composition: Deep-Sea Research, v. 24, p. 1005-1017.

Kuiper, K.F., Deino, A., Hilgen, F.J., Krijgsman, W., Renne, P.R., and Wijbrans, J.R., 2008, Synchronizing rock clocks of Earth history: Science, v. 320, p. 500-504, doi: 10.1126/science.1154339.

Kumar, S.A., Shenoy, N.S., Pandey, S., Sounderajan, S., and Venkateswaran, G., 2008, Direct determination of uranium in seawater by laser fluorimetry: Talanta, v. 77, p. 422-426, doi: DOI 10.1016/j.talanta.2008.07.002.

Kump, L.R., and Arthur, M.A., 1999, Interpreting carbon-isotope excursions: carbonates and organic matter: Chemical Geology, v. 161, p. 181-198.

Küspert, W., 1982, Environmental changes during oil shale deposition as deduced from stable isotope ratios: Cyclic and Event Stratification, Einsele, G. and Seilacher, A. (Ed), Springer, Berlin, p. 482-501.

Lang, W.D., Spath, L.F., Cox, L.R., and Muir-Wood, H.M., 1928, The Belemnite Marls of Charmouth, a Series in the Lias of the Dorset Coast: Quarterly Journal of the Geological Society, v. 84, p. 179-222.

Lea, D.W., Mashiotta, T.A., and Spero, H.J., 1999, Controls on magnesium and strontium uptake in planktonic foraminifera determined by live culturing: Geochimica Et Cosmochimica Acta, v. 63, p. 2369-2379, doi: 10.1016/s0016-7037(99)00197-0.

Li, Q., McArthur, J.M., and Atkinson, T.C., 2011, Jurassic belemnites as indicators of palaeotemperature: Palaeogeography, Palaeoclimatology, Palaeoecology. In Review.

Lini, A., Weissert, H., and Erba, E., 1992, The Valanginian Carbon Isotope Event - a 1st Episode of Greenhouse Climate Conditions during the Cretaceous: Terra Nova, v. 4, p. 374-384.

Little, C.T.S., and Benton, M.J., 1995, Early Jurassic mass extinction - a global long-term event: Geology, v. 23, p. 495-498.

Longerich, H.P., Gunther, D., and Jackson, S.E., 1996, Elemental fractionation in laser ablation inductively coupled plasma mass spectrometry: Fresenius Journal of Analytical Chemistry, v. 355, p. 538-542.

Ludwig, K.R., 2003, User's Manual for Isoplot 3.00 a Geochronological Toolkit for Microsoft Excel.

Macquaker, J.H.S., 1994, A Lithofacies Study of the Peterborough Member, Oxford Clay Formation (Jurassic), Uk - an Example of Sediment Bypass in a Mudstone Succession: Journal of the Geological Society, v. 151, p. 161-172.

Martill, D.M., and Hudson, J.D., 1991, Fossils of the Oxford Clay: The Palaeontological Association, Field Guides to Fossils, v. 4.

McArthur, J.M., Algeo, T.J., van de Schootbrugge, B., Li, Q., and Howarth, R.J., 2008, Basinal restriction, black shales, Re-Os dating, and the Early Toarcian (Jurassic) oceanic anoxic event: Paleoceanography, v. 23, doi: Artn Pa4217, Doi 10.1029/2008pa001607.

McArthur, J.M., Donovan, D.T., Thirlwall, M.F., Fouke, B.W., and Mattey, D., 2000, Strontium isotope profile of the early Toarcian (Jurassic) oceanic anoxic event, the duration of ammonite biozones, and belemnite palaeotemperatures: Earth and Planetary Science Letters, v. 179, p. 269-285.

McArthur, J.M., Doyle, P., Leng, M.J., Reeves, K., Williams, C.T., Garcia-Sanchez, R., and Howarth, R.J., 2007b, Testing palaeo-environmental proxies in Jurassic

belemnites: Mg/Ca, Sr/Ca, Na/Ca, [delta]18O and [delta]13C: Palaeogeography, Palaeoclimatology, Palaeoecology, v. 252, p. 464-480.

McArthur, J.M., Doyle, P., Leng, M.J., Reeves, K., Williams, C.T., Garcia-Sanchez, R., and Howarth, R.J., 2007b, Testing palaeo-environmental proxies in jurassic belemnites: Mg/Ca, Sr/Ca, Na/Ca, delta O-18 and delta C-13: Palaeogeography Palaeoclimatology Palaeoecology, v. 252, p. 464-480, doi: DOI 10.1016/j.palaeo.2007.05.006.

McArthur, J.M., Janssen, N.M.M., Reboulet, S., Leng, M.J., Thirlwall, M.F., and van de Schootbrugge, B., 2007a, Palaeotemperatures, polar ice-volume, and isotope stratigraphy (Mg/Ca, [delta]18O, [delta]13C, 87Sr/86Sr): The Early Cretaceous (Berriasian, Valanginian, Hauterivian): Palaeogeography, Palaeoclimatology, Palaeoecology, v. 248, p. 391-430.

McArthur, J.M., Janssen, N.M.M., Reboulet, S., Leng, M.J., Thirlwall, M.F., and van de Schootbrugge, B., 2007a, Palaeotemperatures, polar ice-volume, and isotope stratigraphy (Mg/Ca, delta O-18, delta C-13, Sr-87/Sr-86): The Early Cretaceous (Berriasian, Valanginian, Hauterivian): Palaeogeography Palaeoclimatology Palaeoecology, v. 248, p. 391-+, doi: DOI 10.1016/j.palaeo.2006.12.015.

McCall, K., Lanzirotti, A., and Rasbury, E.T., 2001, Uranium (VI) Incorporation in Paleosol Calcite: Evidence for Sequestration of U on Geologic Time Scales: Geolocical and Environmental Sciences, NSLS Activity Report 2001, v. 2, p. 93-96.

McConnaughey, T., 1989a, C-13 and O-18 Isotopic Disequilibrium in Biological Carbonates .1. Patterns: Geochimica Et Cosmochimica Acta, v. 53, p. 151-162.

McConnaughey, T., 1989b, C-13 and O-18 Isotopic Disequilibrium in Biological Carbonates .2. Invitro Simulation of Kinetic Isotope Effects: Geochimica Et Cosmochimica Acta, v. 53, p. 163-171.

McConnaughey, T.A., Burdett, J., Whelan, J.F., and Paull, C.K., 1997, Carbon isotopes in biological carbonates: Respiration and photosynthesis: Geochimica Et Cosmochimica Acta, v. 61, p. 611-622.

McConnaughey, T.A., and Gillikin, D.P., 2008, Carbon isotopes in mollusk shell carbonates: Geo-Marine Letters, v. 28, p. 287-299, doi: DOI 10.1007/s00367-008-0116-4.

Miller, K.G., Wright, J.D., and Browning, J.V., 2005, Visions of ice sheets in a greenhouse world: Marine Geology, v. 217, p. 215-231, doi: DOI 10.1016/j.margeo.2005.02.007.

Miramand, P., and Bentley, D., 1992, Concentration and Distribution of Heavy-Metals in Tissues of 2 Cephalopods, Eledone-Cirrhosa and Sepia-Officinalis, from the French Coast of the English-Channel: Marine Biology, v. 114, p. 407-414.

Miramand, P., and Bentley, D., 1992, Heavy-Metal Concentrations in 2 Biological Indicators (Patella-Vulgata and Fucus-Serratus) Collected near the French Nuclear-Fuel Reprocessing Plant of La-Hague: Science of the Total Environment, v. 111, p. 135-149.

Miramand, P., Bustamante, P., Bentley, D., and Koueta, N., 2006, Variation of heavy metal concentrations (Ag, Cd, Co, Cu, Fe, Pb, V, and Zn) during the life cycle of the common cuttlefish Sepia officinalis: Science of the Total Environment, v. 361, p. 132-143, doi: DOI 10.1016/j.scitotenv.2005.10.018.

Misra, N.L., Dhara, S., and Mudher, K.D.S., 2006, Uranium determination in seawater by total reflection X-ray fluorescence spectrometry: Spectrochimica Acta Part B - Atomic Spectroscopy, v. 61, p. 1166-1169.

Murray, J.W., 2004, What controls the composition of riverwater and seawater: Equilibrium versus kinetic ocean: Oceanography 400 - Autumn 2006, Chemical Oceanography Lecture Notes. E-publishing Inc., University of Washington.

Mutterlose, J., 1990, A belemnite scale for the Lower Cretaceous: Cretaceous Research, v. 11, p. 1-15.

Mutterlose, J., 1992, Migration and Evolution Patterns of Floras and Faunas in Marine Early Cretaceous Sediments of Nw Europe: Palaeogeography Palaeoclimatology Palaeoecology, v. 94, p. 261-282.

Mutterlose, J., Malkoc, M., Schouten, S., Damste, J.S.S., and Forster, A., 2010, TEX86 and stable delta O-18 paleothermometry of early Cretaceous sediments: Implications for belemnite ecology and paleotemperature proxy application: Earth and Planetary Science Letters, v. 298, p. 286-298, doi: DOI 10.1016/j.epsl.2010.07.043.

Mutterlose, J., Malkoc, M., Schouten, S., Damste, J.S.S., and Forster, A., 2010, TEX(86) and stable delta(18)O paleothermometry of early Cretaceous sediments: Implications for belemnite ecology and paleotemperature proxy application: Earth and Planetary Science Letters, v. 298, p. 286-298, doi: 10.1016/j.epsl.2010.07.043.

Nunn, E.V., and Price, G.D., 2010, Late Jurassic (Kimmeridgian-Tithonian) stable isotopes (delta O-18, delta C-13) and Mg/Ca ratios: New palaeoclimate data from Helmsdale, northeast Scotland: Palaeogeography Palaeoclimatology Palaeoecology, v. 292, p. 325-335, doi: 10.1016/j.palaeo.2010.04.015.

Page, K.N., 2004, A sequence of biohorizons for the subboreal province Lower Toarcian in Northern Britain and their correlation with a submediterranean standard: Rivista Italiana Di Paleontologia E Stratigrafia, v. 110, p. 109-114.

Palfy, J., Parrish, R.R., and Smith, P.L., 1997, A U-Pb age from the Toarcian (Lower Jurassic) and its use for time scale calibration through error analysis of biochronologic dating: Earth and Planetary Science Letters, v. 146, p. 659-675.

Pearce, C.R., Cohen, A.S., Coe, A.L., and Burton, K.W., 2008, Molybdenum isotope evidence for global ocean anoxia coupled with perturbations to the carbon cycle during the early Jurassic: Geology, v. 36, p. 231-234, doi: Doi 10.1130/G24446a.1.

Phillips, J., 1865, A monograph of British Jurassic Belemnitidae: Monograph of the Palaeontographical Society, London, p. 1-28.

Pirrie, D., and Marshall, J.D., 1990a, High-Paleolatitude Late Cretaceous Paleotemperatures - New Data from James Ross Island, Antarctica: Geology, v. 18, p. 31-34.

Podlaha, O.G., Mutterlose, J., and Veizer, J., 1998, Preservation of delta O-18 and delta C-13 in belemnite rostra from the Jurassic Early Cretaceous successions: American Journal of Science, v. 298, p. 324-347.

Powell, J.H., 1984, Lithostratigraphical nomenclature of the Liass Group in the Yorkshire Basin: Proceedings of Yorkshire Geological society, v. 45, p. 51-57.

Price, G.D., 1999, The evidence and implications of polar ice during the Mesozoic: Earth-Science Reviews, v. 48, p. 183-210.

Price, G.D., and Mutterlose, J., 2004, Isotopic signals from late Jurassic-early Cretaceous (Volgian-Valanginian) sub-Arctic belemnites, Yatria River, Western Siberia: Journal of the Geological Society, v. 161, p. 959-968.

Price, G.D., Ruffell, A.H., Jones, C.E., Kalin, R.M., and Mutterlose, J., 2000, Isotopic evidence for temperature variation during the early Cretaceous (late Ryazanian-mid-Hauterivian): Journal of the Geological Society, v. 157, p. 335-343.

Price, G.D., and Sellwood, B.W., 1997, "Warm" palaeotemperatures from high Late Jurassic palaeolatitudes (Falkland Plateau): Ecological, environmental or diagenetic controls?: Palaeogeography Palaeoclimatology Palaeoecology, v. 129, p. 315-327.

Raiswell, R., and Berner, R.A., 1985, Pyrite Formation in Euxinic and Semi-Euxinic Sediments: American Journal of Science, v. 285, p. 710-724.

Ramezani, J., Davydow, V.I., and Northrup, C.J., 2003, Volcanic ashes in the Upper Paleozoic of the Southern Urals: opportunities for high-precision calibration of the Upper Carboniferous Cisuralian Interval.: Abstract of the International Congress on Carboniferous and Permian Stratigraphy, p. 431-432.

Rasbury, E.T., and Cole, J.M., 2009, Directly Dating Geologic Events: U-Pb Dating of Carbonates: Reviews of Geophysics, v. 47, p. -, doi: Artn Rg3001 Doi 10.1029/2007rg000246.

Rasbury, E.T., Ward, W.B., Hemming, N.G., Li, H., Dickson, J.A.D., Hanson, G.N., and Major, R.P., 2004, Concurrent U-Pb age and seawater Sr-87/Sr-86 value of a

marine cement: Earth and Planetary Science Letters, v. 221, p. 355-371, doi: Doi 10.1016/S0012-821x(03)00105-0.

Reboulet, S., Hoedemaeker, P.J., Aguirre-Urreta, M.B., Alsen, P., Atrops, F., Baraboshkin, E.Y., Company, M., Delanoy, G., Dutour, Y., Klein, J., Latil, J.L., Lukeneder, A., Mitta, V., Mourgues, F.A., Ploch, I., Raisossadat, N., Ropolo, P., Sandoval, J., Tavera, J.M., Vasicek, Z., Vermeulen, J., Arnaud, H., Granier, B., and Premoli-Silva, I., 2006, Report on the 2nd international meeting of the IUGS lower Cretaceous ammonite working group, the "Kilian Group" (Neuchatel, Switzerland, 8 September 2005): Cretaceous Research, v. 27, p. 712-715, doi: DOI 10.1016/j.cretres.2006.03.006.

Reboulet, S., Mattioli, E., Pittet, B., Baudin, F., Olivero, D., and Proux, O., 2003, Ammonoid and nannoplankton abundance in Valanginian (early Cretaceous) limestone-marl successions from the southeast France Basin: carbonate dilution or productivity?: Palaeogeography Palaeoclimatology Palaeoecology, v. 201, p. 113-139, doi: Doi 10.1016/S0031-0182(03)00541-8.

Rexfort, A., and Mutterlose, J., 2006, Stable isotope records from Sepia officinalis - a key to understanding the ecology of belemnites?: Earth and Planetary Science Letters, v. 247, p. 212-221, doi: DOI 10.1016/j.epsl.2006.04.025.

Rink, S., Kuhl, M., Bijma, J., and Spero, H.J., 1998, Microsensor studies of photosynthesis and respiration in the symbiotic foraminifer Orbulina universa: Marine Biology, v. 131, p. 583-595, doi: 10.1007/s002270050350.

Rohl, H.J., Schmid-Rohl, A., Oschmann, W., Frimmel, A., and Schwark, L., 2001, The Posidonia Shale (Lower Toarcian) of SW-Germany: an oxygen-depleted ecosystem controlled by sea level and palaeoclimate (vol 165, pg 27, 2001): Palaeogeography Palaeoclimatology Palaeoecology, v. 169, p. 271-299.

Rosales, I., Quesada, S., and Robles, S., 2001, Primary and diagenetic isotopic signals in fossils and hemipelagic carbonates: the Lower Jurassic of northern Spain: Sedimentology, v. 48, p. 1149-1169.

Rosales, I., Quesada, S., and Robles, S., 2004a, Paleotemperature variations of Early Jurassic seawater recorded in geochemical trends of belemnites from the Basque-Cantabrian basin, northern Spain: Palaeogeography Palaeoclimatology Palaeoecology, v. 203, p. 253-275, doi: Doi 10.1016/S0031-0182(03)00686-2.

Rosales, I., Robles, S., and Quesada, S., 2004b, Elemental and oxygen isotope composition of early Jurassic belemnites: Salinity vs. temperature signals: Journal of Sedimentary Research, v. 74, p. 342-354.

Russell, A.D., Emerson, S., Mix, A.C., and Peterson, L.C., 1996, The use of foraminiferal uranium/calcium ratios as an indicator of changes in seawater uranium content: Paleoceanography, v. 11, p. 649-663.

Russell, A.D., Emerson, S., Nelson, B.K., Erez, J., and Lea, D.W., 1994, Uranium in foraminiferal calcite as a recorder of seawater uranium concentrations: Geochimica Et Cosmochimica Acta, v. 58, p. 671-681.

Russell, A.D., Honisch, B., Spero, H.J., and Lea, D.W., 2004, Effects of seawater carbonate ion concentration and temperature on shell U, Mg, and Sr in cultured planktonic foraminifera: Geochimica Et Cosmochimica Acta, v. 68, p. 4347-4361, doi: 10.1016/j.gca.2004.03.013.

Saelen, G., 1989, Diagenesis and construction of the belemnite rostrum: Palaeontology, v. 32, p. 765-797.

Saelen, G., Doyle, P., and Talbot, M.R., 1996, Stable-isotope analyses of Belemnite rostra from the Whitby Mudstone Fm, England: Surface water conditions during deposition of a marine black shale: Palaios, v. 11, p. 97-117.

Saelen, G., Tyson, R.V., Talbot, M.R., and Telnaes, N., 1998, Evidence of recycling of isotopically light CO2 (aq) in stratified black shale basins: Contrasts between the Whitby Mudstone and Kimmeridge Clay formations, United Kingdom: Geology, v. 26, p. 747-750.

Saelen, G., Tyson, R.V., Telnaes, N., and Talbot, M.R., 2000, Contrasting watermass conditions during deposition of the Whitby Mudstone (Lower Jurassic) and Kimmeridge Clay (Upper Jurassic) formations, UK: Palaeogeography Palaeoclimatology Palaeoecology, v. 163, p. 163-196.

Schmid-Rohl, A., and Rohl, H.J., 2003, Overgrowth on ammonite conchs: Environmental implications for the Lower Toarcian Posidonia Shale: Palaeontology, v. 46, p. 339-352.

Schmid-Rohl, A., Rohl, H.J., Oschmann, W., Frimmel, A., and Schwark, L., 2002, Palaeoenvironmental reconstruction of Lower Toarcian epicontinental black shales (Posidonia Shale, SW Germany): global versus regional control: Geobios, v. 35, p. 13-20, doi: Pii S0016-6995(02)000050-.

Schmitz, M.D., and Schoene, B., 2007, Derivation of isotope ratios, errors, and error correlations for U-Pb geochronology using Pb-205-U-235-(U-233)-spiked isotope dilution thermal ionization mass spectrometric data: Geochemistry Geophysics Geosystems, v. 8, p. 1-20, doi: Artn 8 Doi 10.1029/2006gc001492.

Scholle, P.A., and Ulmer-Scholle, D.S., 2003, A color guide to the petrography of carbonate rocks: grains, textures, porosity, diagenesis: Tulsa, OK, The American Association of Petroleum Geologists Memoir 77, 474p.

Schone, B.R., Dunca, E., Fiebig, J., and Pfeiffer, M., 2005, Mutvei's solution: An ideal agent for resolving microgrowth structures of biogenic carbonates: Palaeogeography Palaeoclimatology Palaeoecology, v. 228, p. 149-166, doi: DOI 10.1016/j.palaeo.2005.03.054.

Schwark, L., and Frimmel, A., 2004, Chemostratigraphy of the Posidonia Black Shale, SW-Germany II. Assessment of extent and persistence of photic-zone anoxia using aryl isoprenoid distributions: Chemical Geology, v. 206, p. 231-248, doi: DOI 10.1016/j.chemgeo.2003.12.008.

Shackleton, N.J., and Kennet, D.J., 1975, Paleotemperature history of the Cenozoic and initiation of Antarctic flaciation: Oxygen and carbon isotope analyses in DSDP sites 277,279 and 289.: Initial Reports of the Deep Sea Drilling Project, v. 29, p. 743-755.

Shen, C.C., Lin, H.T., Chu, M.F., Yu, E.F., Wang, X.F., and Dorale, J.A., 2006, Measurements of natural uranium concentration and isotopic composition with permil-level precision by inductively coupled plasma-quadrupole mass spectrometry: Geochemistry Geophysics Geosystems, v. 7, doi: Artn Q09005 Doi 10.1029/2006gc001303.

Simms, M.J., Chidlaw, N., Morton, N., and Page, K.N., 2004, British Lower Jurassic stratigraphy: Geological Conservation Review Series, No. 30, Joint Nature Conservation Committee, Peterborough, p. 458 pp.

Smith, P.E., and Farquhar, R.M., 1989, Direct dating of Phanerozoic sediments by the ^{238}U-^{206}Pb method: Nature, v. 341, p. 518-521.

Smith, P.E., Farquhar, R.M., and Hancock, R.G., 1991, Direct radiometric age-determination of carbonate diagenesis using U-Pb in secondary calcite: Earth and Planetary Science Letters, v. 105, p. 474-491.

Spaeth, C., Hoefs, J., and Vetter, U., 1971, Some aspects of isotopic composition of belemnites and related paleotemperatures: Geological Society of America Bulletin, v. 82, p. 3139-3150.

Spence, R., 1968, Uranium content of sea-water: Talanta, v. 15, p. 1307-1309.

Spero, H.J., 1988, Ultrastructural examination of chamber morphogenesis and biomineralization in the planktonic foraminifer *Orbulina universa*: Marine Biology, v. 99, p. 9-20, doi: 10.1007/bf00644972.

Steiger, R.H., and Jager, E., 1977, Subcommission on Geochronology - Convention on Use of Decay Constants in Geochronology and Cosmochronology: Earth and Planetary Science Letters, v. 36, p. 359-362.

Stevens, G.R., and Clayton, R.N., 1971, Oxygen isotope studies on Jurassic and Cretaceous belemnites from New-Zealand and their biogeographic significance: New Zealand Journal of Geology and Geophysics, v. 14, p. 829-897.

Stoyanova-Vergilova, M., 1977, An attempt for belemnite zonal subdivision of the Lower Jurassic sediments in Bulgaria: Annuaire de l'Universite de Sofia. Faculte de Geologie et Geographie, p. 161-192.

Urey, H.C., Lowenstam, H.A., Epstein, S., and Mckinney, C.R., 1951, Measurement of Paleotemperatures and Temperatures of the Upper Cretaceous of England, Denmark, and the Southeastern United-States: Geological Society of America Bulletin, v. 62, p. 399-416.

van de Schootbrugge, B., Föllmi, K.B., Bulot, L.G., and Burns, S.J., 2000, Paleoceanographic changes during the early Cretaceous (Valanginian-Hauterivian): evidence from oxygen and carbon stable isotopes: Earth and Planetary Science Letters, v. 181, p. 15-31.

van de Schootbrugge, B., McArthur, J.M., Bailey, T.R., Rosenthal, Y., Wright, J.D., and Miller, K.G., 2005, Toarcian oceanic anoxic event: An assessment of global causes using belemnite C isotope records: Paleoceanography, v. 20, p. 1-10, doi: Artn Pa3008, Doi 10.1029/2004pa001102.

Veizer, J., 1974, Chemical diagenesis of belemnite shells and possible consequences for paleotemperature determinations: Neues Jahrbuch Fur Geologie Und Palaontologie-Abhandlungen, v. 147, p. 91-111.

Veizer, J., Ala, D., Azmy, K., Bruckschen, P., Buhl, D., Bruhn, F., Carden, G.A.F., Diener, A., Ebneth, S., Godderis, Y., Jasper, T., Korte, C., Pawellek, F., Podlaha, O.G., and Strauss, H., 1999, Sr-87/Sr-86, delta C-13 and delta O-18 evolution of Phanerozoic seawater: Chemical Geology, v. 161, p. 59-88.

Wang, Z.S., Rasbury, E.T., Hanson, G.N., and Meyers, W.J., 1998, Using the U-Pb system of calcretes to date the time of sedimentation of elastic sedimentary rocks: Geochimica Et Cosmochimica Acta, v. 62, p. 2823-2835.

Weissert, H., Lini, A., Follmi, K.B., and Kuhn, O., 1998, Correlation of Early Cretaceous carbon isotope stratigraphy and platform drowning events: a possible link?: Palaeogeography Palaeoclimatology Palaeoecology, v. 137, p. 189-203, doi: 10.1016/s0031-0182(97)00109-0.

Westermann, S., Follmi, K.B., Adatte, T., Matera, V., Schnyder, J., Fleitmann, D., Fiet, N., Ploch, I., and Duchamp-Alphonse, S., 2010, The Valanginian delta(13)C excursion may not be an expression of a global oceanic anoxic event: Earth and Planetary Science Letters, v. 290, p. 118-131, doi: 10.1016/j.epsl.2009.12.011.

Wierzbowski, H., 2002, Detailed oxygen and carbon isotope stratigraphy of the Oxfordian in Central Poland: International Journal of Earth Sciences, v. 91, p. 304-314, doi: 10.1007/s005310100217.

Wierzbowski, H., 2004, Carbon and oxygen isotope composition of Oxfordian-Early Kimmeridgian belemnite rostra: palaeoenvironmental implications for Late Jurassic seas: Palaeogeography Palaeoclimatology Palaeoecology, v. 203, p. 153-168, doi: Doi 10.1016/S0031-0182(03)00673-4.

Wierzbowski, H., and Joachimski, M.M., 2009, Stable isotopes, elemental distribution, and growth rings of Belemnopsid Belemnite rostra: proxies for

belemnite life habitat: Palaios, v. 25, p. 377-386, doi: DOI 10.2110/palo.2008.p08-101r.

Wierzbowski, H., and Rogov, M., 2010, Reconstructing the palaeoenvironment of the Middle Russian Sea during the Middle-Late Jurassic transition using stable isotope ratios of cephalopod shells and variations in faunal assemblages: Palaeogreography, Palaeoclimatology, Palaeoecology, doi: 10.1016/j.palaeo.2010.11.006.

Wignall, P.B., Newton, R.J., and Little, C.T.S., 2005, The timing of paleoenvironmental change and cause-and-effect relationships during the Early Jurassic mass extinction in Europe: American Journal of Science, v. 305, p. 1014 -1032.

Williams, A.C., 1988, Palaeoecological and Palaeoenvironmentle Variations in the Callovian, Oxfordian and Kimmeridgian (Jurassic) of Britian: PhD theis, University of Leicester.

Wilson, V., Welch, F.B.A., Robbie, J.A., and Green, G.W., 1958, The Geology of the Country around Bridport and Yeovil: Memoir of the Geological Survey of Great Britain, sheets 327 and 312 (England and Wales), HMSO, London, p. 239.

Wolf-Gladrow, D.A., Bijma, J., and Zeebe, R.E., 1999, Model simulation of the carbonate chemistry in the microenvironment of symbiont bearing foraminifera: Marine Chemistry, v. 64, p. 181-198, doi: 10.1016/s0304-4203(98)00074-7.

Yasamanov, N.A., 1981, Paleothermometry of Jurassic, Cretaceous, and Paleogene periods of some regions of the USSR.: International Geological Review, v. 23, p. 700-706.

Yu, J.M., Day, J., Greaves, M., and Elderfield, H., 2005, Determination of multiple element/calcium ratios in foraminiferal calcite by quadrupole ICP-MS: Geochemistry Geophysics Geosystems, v. 6, doi: Artn Q08p01 Doi 10.1029/2005gc000964.

Yu, J.M., Elderfield, H., Jin, Z.D., and Booth, L., 2008, A strong temperature effect on U/Ca in planktonic foraminiferal carbonates: Geochimica Et Cosmochimica Acta, v. 72, p. 4988-5000, doi: DOI 10.1016/j.gca.2008.07.011.